ΠΑΝΕΠΙΣΤΗΜΙΟ ΘΕΣΣΑΛΙΑΣ
ΠΟΛΥΤΕΧΝΙΚΗ ΣΧΟΛΗ
ΤΜΗΜΑ ΜΗΧΑΝΟΛΟΓΩΝ ΜΗΧΑΝΙΚΩΝ

ΕΡΓΑΣΤΗΡΙΟ ΔΥΝΑΜΙΚΗΣ ΣΥΣΤΗΜΑΤΩΝ

ΔΙΑΧΕΙΡΙΣΗ ΤΩΝ ΑΒΕΒΑΙΟΤΗΤΩΝ ΣΕ ΠΡΟΣΟΜΟΙΩΣΕΙΣ ΑΠΟΚΡΙΣΗΣ ΚΑΙ ΑΞΙΟΠΙΣΤΙΑΣ ΚΑΤΑΣΚΕΥΩΝ ΑΞΙΟΠΟΙΩΝΤΑΣ ΔΕΔΟΜΕΝΑ ΜΕΤΡΗΣΕΩΝ

Διδακτορική Διατριβή

ΔΗΜΗΤΡΑ-ΧΡΙΣΤΙΝΑ ΠΑΠΑΔΙΩΤΗ

Διπλωματούχου Πολιτικού Μηχανικού, Π.Θ., 2009
Μ.Δ.Ε. Μηχανολόγου Μηχανικού, Π.Θ., 2011

Υπεβλήθη για την εκπλήρωση μέρους των
απαιτήσεων για την απόκτηση του
Διδακτορικού Διπλώματος

2015

UNIVERSITY OF THESSALY
SCHOOL OF ENGINEERING
DEPARTMENT OF MECHANICAL ENGINEERING

SYSTEM DYNAMICS LABORATORY

MANAGEMENT OF UNCERTAINTIES IN STRUCTURAL RESPONSE AND RELIABILITY SIMULATIONS USING MEASURED DATA

Thesis by

DIMITRA-CHRISTINA PAPADIOTI

Diploma in Civil Engineering, University of Thessaly, 2009
M.Sc. in Mechanical Engineering, University of Thessaly, 2011

In partial fulfillment of the requirements
for the degree of
Doctor of Philosophy

2015

Η παρούσα έρευνα έχει συγχρηματοδοτηθεί από την Ευρωπαϊκή Ένωση (Ευρωπαϊκό Κοινωνικό Ταμείο - ΕΚΤ) και από εθνικούς πόρους μέσω του Επιχειρησιακού Προγράμματος «Εκπαίδευση και Δια Βίου Μάθηση» του Εθνικού Στρατηγικού Πλαισίου Αναφοράς (ΕΣΠΑ) – Ερευνητικό Χρηματοδοτούμενο Έργο: Ηράκλειτος ΙΙ . Επένδυση στην κοινωνία της γνώσης μέσω του Ευρωπαϊκού Κοινωνικού Ταμείου.

This research has been co-financed by the European Union (European Social Fund – ESF) and Greek national funds through the Operational Program "Education and Lifelong Learning" of the National Strategic Reference Framework (NSRF) - Research Funding Program: Heracleitus II. Investing in knowledge society through the European Social Fund.

Διαχείριση των Αβεβαιοτήτων σε Προσομοιώσεις Απόκρισης και Αξιοπιστίας Κατασκευών Αξιοποιώντας Δεδομένα Μετρήσεων

ISBN

Η έγκριση της παρούσας διδακτορικής διατριβής από το Τμήμα Μηχανολόγων Μηχανικών της Πολυτεχνικής Σχολής του Πανεπιστημίου Θεσσαλίας δεν υποδηλώνει αποδοχή των απόψεων του συγγραφέα (Ν. 5343/32 αρ. 202 παρ. 2).

Εγκρίθηκε από τα Μέλη της Επταμελούς Εξεταστικής Επιτροπής:

Πρώτος Εξεταστής (Επιβλέπων)
Δρ. Κώστας Παπαδημητρίου
Καθηγητής, Τμήμα Μηχανολόγων Μηχανικών
Πανεπιστήμιο Θεσσαλίας

Δεύτερος Εξεταστής
Δρ. Σωτήριος Νατσιάβας
Καθηγητής, Τμήμα Μηχανολόγων Μηχανικών,
Αριστοτέλειο Πανεπιστήμιο Θεσσαλονίκης

Τρίτος Εξεταστής
Dr. Lambros Katafygiotis
Professor, Department of Civil Engineering
Hong Kong University of Science and Technology

Τέταρτος Εξεταστής
Δρ. Δημήτριος Γιαγκόπουλος
Επίκουρος Καθηγητής, Τμήμα Μηχανολόγων Μηχανικών,
Πανεπιστήμιο Δυτικής Μακεδονίας

Πέμπτος Εξεταστής
Δρ. Αλέξης Κερμανίδης
Επίκουρος Καθηγητής, Τμήμα Μηχανολόγων Μηχανικών,
Πανεπιστήμιο Θεσσαλίας

Έκτος Εξεταστής
Δρ. Παναγιώτης Τσόπελας
Αναπληρωτής Καθηγητής, Σχολή Εφαρμοσμένων
Μαθηματικών και Φυσικών Επιστημών,
Εθνικό Μετσόβιο Πολυτεχνείο.

Έβδομος Εξεταστής
Dr. Eleni Chatzi
Assistant Professor, Institute of Structural Engineering
ETH-Zurich.

Ευχαριστίες

Η παρούσα διδακτορική διατριβή εκπονήθηκε στο Εργαστήριο Δυναμικής Συστημάτων του τμήματος Μηχανολόγων Μηχανικών στο Πανεπιστήμιο Θεσσαλίας.

Φτάνοντας στο τέλος αυτής της προσπάθειας, πρώτα απ' όλα, θα ήθελα να ευχαριστήσω τον επιβλέποντα της διδακτορικής εργασίας μου, Καθηγητή κ. Κώστα Παπαδημητρίου, για την ενθάρρυνση, πολύτιμη βοήθεια και καθοδήγησή του καθόλη τη διάρκεια της συνεργασίας μας αλλά και για τη διαρκή του προσπάθεια να με μυήσει στις αρχές και αξίες που επικρατούν στην διεθνή επιστημονική κοινότητα. Επίσης, ευχαριστώ τα υπόλοιπα μέλη της τριμελούς συμβουλευτικής επιτροπής της διδακτορικής διατριβής μου, Καθηγητές κ. Σωτήριο Νατσιάβα και Λάμπρο Καταφυγιώτη, καθώς και τα υπόλοιπα μέλη της επταμελούς επιτροπής για την προσεκτική ανάγνωση της εργασίας μου και για τις πολύτιμες υποδείξεις τους. Ευχαριστίες οφείλω επίσης στον κ. Τσόπελα καθώς ήταν ο πρώτος που με δίδαξε τις βασικές αρχές της Δυναμικής ως προπτυχιακή φοιτήτρια και η διδασκαλία του αποτέλεσε καταλυτικό παράγοντα για την μετέπειτα επιλογή μου. Ιδιαίτερες ευχαριστίες οφείλω επίσης στον κ. Γιαγκόπουλο Δημήτρη για την πολύτιμη βοήθεια του κατά την διάρκεια εκπόνησης της διδακτορικής διατριβής και την άψογη συνεργασία μας.Τέλος, ευχαριστίες οφείλω στους μεταδιδακτορικούς φοιτητές του Εργαστηρίου Δυναμικής Συστημάτων Ντότσιο Βαγγέλη, Πέρρο Κυριάκο και Saeed Eftekhar Azam για την άριστη συνεργασία που είχαμε κατά τη διάρκεια της εκπόνησης της παρούσας διδακτορικής διατριβής.

Πάνω απ' όλα, είμαι ευγνώμων στο σύζυγο μου Μιχάλη, για την αγάπη και ολόψυχη υποστήριξή του, στον οποίον αφιερώνω αυτή την διατριβή.

Δήμητρα-Χριστίνα Παπαδιώτη

Ιούλιος 2015, Βόλος.

ΠΕΡΙΛΗΨΗ

Αντικείμενο της παρούσας Διατριβής αποτελεί η ανάπτυξη μεθόδων μοντελοποίησης και διαχείρισης των αβεβαιοτήτων στην διαδικασία της προσομοίωσης κατασκευών. Έμφαση δίνεται στην ανάπτυξη ενός πιθανοτικού-στατιστικού πλαισίου για (α) την ποσοτικοποίηση των αβεβαιοτήτων που υπεισέρχονται στην επιλογή παραμετρικών μαθηματικών μοντέλων προσομοίωσης μηχανικών συστημάτων και εξωτερικών δυναμικών διεγέρσεων, (β) την διάδοση των αβεβαιοτήτων αυτών μέσω των υπολογιστικών μοντέλων πεπερασμένων στοιχείων στην πρόβλεψη των αβεβαιοτήτων μεγεθών απόκρισης και αξιοπιστίας έναντι διαφόρων οριακών καταστάσεων ασφάλειας και λειτουργικότητας μηχανικών συστημάτων. Πιθανοτικά/στοχαστικά μοντέλα χρησιμοποιούνται για την ποσοτικοποίηση των αβεβαιοτήτων, ενώ εξελιγμένες μεθοδολογίες στοχαστικής προσομοίωσης αποτελούν το βασικό εργαλείο διάδοσης των αβεβαιοτήτων μέσω των προσομοιωμάτων. Ένα ιδιαίτερα καινοτόμο στοιχείο της έρευνας αποτελεί η αξιοποίηση μετρήσεων για την βελτίωση των μαθηματικών μοντέλων περιγραφής του μηχανικού συστήματος, των διεγέρσεων και των αβεβαιοτήτων με βάση τη στατιστική μεθοδολογία Bayes. Οι εφαρμογές επίδειξης εστιάζουν (α) στην πιστοποίηση των μοντέλων, πρόβλεψη της αξιοπιστίας και διερεύνηση της επιρροής των αβεβαιοτήτων για κατασκευές μεγάλης κλίμακας, και (β) στην πρόβλεψη κόπωσης σε ολόκληρο τον φορέα μεταλλικών κατασκευών βάσει περιορισμένου αριθμού λειτουργικών μετρήσεων ταλάντωσης.

Η παρούσα Διατριβή δομείται από τρία συσχετιζόμενα μέρη.

Μέρος Α: Από την αρχή εκπόνησης της Διδακτορικής Διατριβής έγινε σαφές ότι για να καταστεί δυνατή η ανάλυση και διαχείριση των αβεβαιοτήτων σε πολύπλοκα μοντέλα κατασκευών όπως μοντέλα με υψηλό αριθμό βαθμών ελευθερίας της τάξης των πολλών χιλιάδων, εκατοντάδων χιλιάδων ή ακόμα και εκατομμυρίων βαθμών ελευθερίας, καθώς και μοντέλα που παρουσιάζουν τοπικές μη-γραμμικότητες στην συμπεριφορά των δομικών στοιχείων, ήταν απαραίτητη η ενσωμάτωση έξυπνων τεχνικών μείωσης των επαναλαμβανόμενων χρονοβόρων διαδικασιών υπολογισμού της απόκρισης. Για τον σκοπό αυτό μεγάλο μέρος της ερευνητικής δραστηριότητας εστίασε στην ανάπτυξη αποτελεσματικών τεχνικών μείωσης των βαθμών ελευθερίας του μοντέλου του συστήματος. Είναι γνωστό ότι για γραμμικά μοντέλα η μέθοδος σύνθεσης των κατασκευαστικών συνιστωσών (Component Mode Synthesis - CMS) μπορεί να προσφέρει τα ζητούμενα πλεονεκτήματα. Όμως ο χρόνος που απαιτείται για την επίτευξη της μείωσης είναι σχετικά μεγάλος και ουσιαστικά η απ' ευθείας εφαρμογή αναιρεί τα

πλεονεκτήματα της μεθόδου σύνθεσης των κατασκευαστικών συνιστωσών. Για τον σκοπό αυτό αναπτύχθηκε καινοτόμος μέθοδος για την επίτευξη της μείωσης των βαθμών ελευθερίας για τον πολύ μεγάλο αριθμό εναλλακτικών μοντέλων με βάση την ανάλυση των κατασκευαστικών συνιστωσών ενός μόνο ονομαστικού μοντέλου του συστήματος. Η προτεινόμενη μεθοδολογία είναι εφαρμόσιμη για τις περιπτώσεις που οι κατασκευαστικές συνιστώσες επιλέγονται με βάση τη παραμετροποίηση του μοντέλου. Η μεθοδολογία αποδείχθηκε ιδιαίτερα αποτελεσματική για την διαχείριση αβεβαιοτήτων σε δυναμικές αναλύσεις κατασκευών μεγάλης κλίμακας καθώς οδηγεί σε σημαντική μείωση των βαθμών ελευθερίας αλλά και του χρόνου διαχείρισης των αβεβαιοτήτων κατά τρεις και περισσότερες τάξεις μεγέθους. Συγκεκριμένα παραδείγματα σε μοντέλα πολύπλοκων κατασκευών εκατοντάδων χιλιάδων βαθμών ελευθερίας, όπως είναι το γραμμικό μοντέλο της γέφυρας του Μετσόβου, έδειξαν ότι ο χρόνος ανάλυσης των αβεβαιοτήτων μειώνεται από τάξη ημερών σε τάξη λίγων μόνο δευτερολέπτων, το οποίο αποτελεί δραστική μείωση του χρόνου και επιτρέπει για πρώτη φορά την διαχείριση και εφαρμογή μεθόδων διαχείρισης, ποσοτικοποίησης και διάδοσης αβεβαιοτήτων σε πολύπλοκες κατασκευές.

Η παραπάνω τεχνική μείωσης των βαθμών ελευθερίας αποτελεί πολύ σημαντικό εργαλείο για την εκπόνηση της παρούσας Διδακτορικής Διατριβής καθώς μειώνει σημαντικά το υπολογιστικό κόστος για την διαχείριση ενός μεγάλου σχετικά αριθμού επαναληπτικών αναλύσεων που απαιτούνται σε αλγορίθμους βελτιστοποίησης και σε αλγορίθμους στοχαστικής προσομοίωσης που χρησιμοποιούνται κατά την διαχείριση των αβεβαιοτήτων σε μοντέλα πεπερασμένων στοιχείων. Επίσης οι παραπάνω τεχνικές αποτέλεσαν πολύ σημαντικό εργαλείο για την ανάπτυξη των μεθόδων διαχείρισης των αβεβαιοτήτων στις τεχνικές διάγνωσης της δομικής ακεραιότητας των κατασκευών .

Μέρος Β: Στα πλαίσια εκπόνησης της παρούσας Διατριβής αναπτύχθηκε το στατιστικό πλαίσιο Bayes για την επιλογή και αναγνώριση μοντέλων πεπερασμένων στοιχείων με βάση την πληροφορία που προέρχεται από τις μετρήσεις. Συγκεκριμένα, ολοκληρώθηκε η θεωρητική διατύπωση του προβλήματος εκτίμησης των παραμέτρων γραμμικών μοντέλων κατασκευής με τη μέθοδο Bayes για την περίπτωση που οι διαθέσιμες μετρήσεις είναι τα ιδιομορφικά χαρακτηριστικά της κατασκευής (ιδιοσυχνότητες και ιδιομορφές). Επίσης η παραπάνω μεθοδολογία υλοποιήθηκε σε λογισμικό και η εφαρμογή της σε γραμμικά μοντέλα πεπερασμένων στοιχείων με πολλούς βαθμούς ελευθερίας έδωσε πολύ ικανοποιητικά αποτελέσματα υψηλής ακρίβειας. Υλοποιήθηκαν επίσης σε λογισμικό διαθέσιμες από την βιβλιογραφία εναλλακτικές διατυπώσεις Bayes και μελετήθηκε η αποτελεσματικότητάς τους σε σχέση με την προτεινόμενη μεθοδολογία. Επίσης, η παρούσα Διατριβή επικεντρώθηκε στην ανάπτυξη αποτελεσματικών υπολογιστικών εργαλείων για την περιγραφή των αβεβαιοτήτων των παραμέτρων ενός μοντέλου που παρουσιάζει μη γραμμικότητες με βάση τη μέθοδο Bayes αλλά και την διαχείριση των

αβεβαιοτήτων στον υπολογισμό των αβεβαιοτήτων απόκρισης χρησιμοποιώντας ασυμπτωτικές μεθόδους και μεθόδους στοχαστικής προσομοίωσης. Από τις διαθέσιμες στοχαστικές μεθόδους για την περιγραφή των αβεβαιοτήτων των παραμέτρων, χρησιμοποιήθηκε η μέθοδος Transitional MCMC. Η Transitional MCMC είναι γενική και εφαρμόσιμη σε γραμμικά και μη-γραμμικά μοντέλα, όπως αποδείχθηκε και από την εφαρμογή της για την αναθεώρηση των τιμών των παραμέτρων των συστημάτων έδρασης σκάφους οχήματος μικρής κλίμακας.

Στην συγκεκριμένη περίπτωση έγινε γενίκευση της θεωρητικής διατύπωσης έτσι ώστε η μέθοδος Bayes να λαμβάνει υπόψη ότι οι μετρήσεις είναι οι χρονοιστορίες απόκρισης αντί των ιδιομορφικών χαρακτηριστικών και επίσης τα φάσματα απόκρισης προκειμένου να γίνει η εκτίμηση των παραμέτρων των μη γραμμικών μοντέλων ανάρτησης του οχήματος. Για την περίπτωση των χρονοϊστοριών απόκρισης υλοποιήθηκε σε λογισμικό μεθοδολογία η οποία λαμβάνει υπόψη εναλλακτικά μαθηματικά μοντέλα πρόβλεψης σφάλματος στην διατύπωση της μεθόδου του Bayes. Συγκεκριμένα χρησιμοποιήθηκαν μοντέλα πρόβλεψης σφάλματος με χωρο-χρονικές συσχετίσεις, σε αντίθεση με τα υπάρχοντα μοντέλα τα οποία θεωρούν ασυσχέτιστα τα σφάλματα στο χώρο και τον χρόνο. Πραγματοποιήθηκε λοιπόν με επιτυχία η διαχείριση των αβεβαιοτήτων (αναγνώριση και διάδοση) σε πειραματικό σκάφος οχήματος με συνδυασμό γραμμικών και μη γραμμικών συνιστωσών. Η διαχείριση των χρονοβόρων επαναληπτικών αναλύσεων του μοντέλου του συστήματος αντιμετωπίστηκε με την ενσωμάτωση της τεχνικής σύνθεσης κατασκευαστικών συνιστωσών, που αναπτύχθηκαν στο πρώτο μέρος εκπόνησης της Διατριβής, για τις γραμμικές συνιστώσες του συστήματος όπως είναι τα επιμέρους κατασκευαστικά στοιχεία του σκάφους του οχήματος. και προέκυψε το μειωμένο μη-γραμμικό μοντέλο που μειώνει σημαντικά τον υπολογιστικό χρόνο που απαιτείται καθώς υπήρξε σημαντική μείωση των βαθμών ελευθερίας από 50,000 σε λιγότερους από 100. Τέλος, με βάση την αξιοποίηση των πειραματικών μετρήσεων από τις επιμέρους συνιστώσες (σκάφος και αναρτήσεις) του πειραματικού οχήματος μπόρεσαν να εξαχθούν χρήσιμα συμπεράσματα σχετικά με την δυνατότητα διαχείρισης των αβεβαιοτήτων στο όχημα με βάση την αναγνώριση τους και την βαθμονόμηση τους από επιμέρους συνιστώσες.

Μέρος Γ: Μια ιδιαίτερα καινοτόμος μεθοδολογία για την πρόβλεψη της συσσώρευσης βλαβών λόγω κόπωσης σε ολόκληρο το φορέα μεταλλικών κατασκευών με αξιοποίηση πληροφοριών από μετρήσεις της ταλαντωτικής τους απόκρισης σε περιορισμένο αριθμό θέσεων στην κατασκευή προτείνεται στα πλαίσια της παρούσας Διατριβής. Συγκεκριμένα, χρησιμοποιήθηκαν μέθοδοι τύπου Kalman και μέθοδοι Modal Expansion για την πρόγνωση των χρονοιστοριών των παραμορφώσεων σε ολόκληρο τον φορέα τόσο απλών όσο και πολύπλοκων

κατασκευών από περιορισμένο αριθμό μετρήσεων, αποφεύγοντας την αναγνώριση των πραγματικών διεγέρσεων. Με χρήση του κανόνα Palmgren-Miner και των S-N καμπύλως κόπωσης, έγινε η πρόβλεψη της βλάβης λόγω κόπωσης και του εναπομείναντα χρόνου ζωής τως κατασκευών. Η απόδοση και ακρίβεια της προτεινόμενης μεθοδολογίας παρουσιάζεται τόσο με ένα απλοικό σύστημα λίγων μόνων βαθμών ελευθερίας με μη γραμμικότητα σε μία υποκατασκευή, όσο και μέσα από την εφαρμογή της μεθόδου στο στο όχημα μικρής κλίμακας που μελετήθηκε στο δεύτερο μέρος της Διατριβής, μερικών δεκάδων χιλιάδων βαθμών ελευθερίας, που περιλαμβάνει το γραμμικό σκάφος οχήματος και τα τέσσερα μη γραμμικά υποσυστήματα των τροχών-αναρτήσεων.Τέλος, οι χρονοιστορίες των προβλεπόμενων παραμορφώσεων χρησιμοποιήθηκαν με αξιοπιστία για την πρόβλεψη της κόπωσης του οχήματος και για την δημιουργία χαρτών κόπωσης και χαρτών του εναπομείναντος χρόνος ζωής της κατασκευής.

SUMMARY

The subject of current PhD thesis is the development of methods for the modeling and management of uncertainties in structural simulations. Emphasis is given on developing the probabilistic-statistical framework that is used for (a) quantifying and calibrating uncertainty models of mechanical systems and external excitation forces, in structural dynamics based on vibration measurements, as well as (b) propagating these modeling uncertainties in structural dynamics simulations to achieve updated robust predictions of system performance, reliability and safety. The tools for identifying system and uncertainty models as well as performing robust prediction analyses are the Bayesian Inference, Laplace methods of asymptotic approximation and more accurate stochastic simulation algorithms, such as Transitional Markov Chain Monte Carlo. These tools involve solving optimization problems, generating samples for tracing and then populating the important uncertainty region in the parameter space, as well as evaluating integrals over high-dimensional spaces of the uncertain model parameters. A moderate to very large number of repeated system analyses are required to be performed over the space of uncertain parameters. Consequently, the computational demands depend highly on the number of system analyses and the time required for performing a system analysis. For such large-order finite element models the computational demands in implementing asymptotic approximations as well as stochastic simulation techniques may be excessive. This study integrates an efficient Component Mode Synthesis technique that takes into account the FE model parameterization to substantially alleviate the computational burden associated with the Bayesian methodology. Another innovative aspect of this thesis is the use of measurements in order to improve the mathematical models that simulate the mechanical system, the excitation and the uncertainties that arise, based on the Bayesian Inference. Finally, the computational efficiency of the proposed techniques is demonstrated through applications (a) in structural health monitoring, damage identification and updating structural reliability of civil infrastructure, and (b) in predicting fatigue for metallic structures through a limited number of acceleration measurements.

Part A: From the beginning of the current PhD thesis it became clear that in order to perform the analysis and management of uncertainties for complex structural models such as large DOF models involving hundreds of thousands or even million DOF and models including localized nonlinearities, it was necessary the analysis to be integrated with smart techniques for reducing the time consuming analysis that appear in reliability simulations. For this reason, much effort of the research was devoted to investigate efficient techniques for reducing the number of degrees of freedom of the FE model simulating the structural system. Specifically, component mode synthesis (CMS) techniques are widely used to

carry out system analyses in a significantly reduced space of generalized coordinates, thus alleviating the computational burden involved in the implementation of methods for management of uncertainties. In this work, a novel framework is presented for integrating the Craig-Bampton technique into existing FE model updating formulations in order to reduce the time consuming operations involved in reanalyses of large-order models of hundreds of thousands or even millions degrees of freedom. The proposed method exploits the fact that in FE model parameterization schemes the stiffness matrix of the structure often depends linearly on the parameters of the model and also that a parameter usually represents a global property (e.g. the modulus of elasticity) of a substructure. The division of the structure into components is then guided by the FE parameterization scheme so that the stiffness matrix that arise for each one of the introduced components to depend linearly on only one of the parameters to be estimated. The methodology proved to be very effective for the management of uncertainties in the dynamic structural analysis of large-scale models, since it led to a significant reduction both of the degrees of freedom and of the time consumed for the management of uncertainties by three and more orders of magnitude. Through the implementation of the framework to large order models of structures involving hundreds of thousands of degrees of freedom, such as the linear model of Metsovo bridge, it was demonstrated that the computational effort was reduced drastically from days to a few seconds. This drastic reduction of the computational time without compromising the accuracy allowed for first time the uncertainty quantification and propagation of large order complex structures.

The above reduction techniques proved to be a very useful tool for the research conducted in the context of current thesis due to the reduction of the computational effort of reanalyses involved in stochastic optimizations and simulations algorithms implemented for performing management of uncertainties in structural response and reliability simulations the reduction of degrees of freedom is a very important tool for the preparation of this thesis as it significantly reduces the computational cost for the management of a large number of repeat analyzes required in optimization algorithms and stochastic simulation algorithms used in the management of uncertainties in finite element models. Finally the above techniques were very useful for the development of a framework for management of uncertainties that appear in structural health monitoring (SHM).

Part B: In the context of this thesis, a Bayesian framework for model parameter estimation and class selection, based on vibration measurements, was developed. Specifically, the theoretical framework for the parameter estimation problem for linear models using the modal characteristics (eigenfrequencies and modeshapes) was first formulated and then implemented in software. The results of the application of the proposed Bayesian Framework, implemented in the developed software, for linear large DOF models were of high accuracy.αποτελέσματα υψηλής ακρίβειας. Moreover, different approaches of the

Bayesian Framework, presented in relevant literature were implemented in software and tested for their accuracy. Another field of great interest of this thesis was the development of Bayesian tools, including asymptotic approximations and stochastic simulation algorithms, for the quantification and management of uncertainties in parameter estimation for both linear and nonlinear models. Among the stochastic simulation algorithms available Transitional MCMC is one of the most promising and for this reason it was chosen to be used. The Transitional MCMC is an algorithm of general use and can be applied to both linear and non-linear models, as it was demonstrated in this thesis through its application to a small scale experimental model of a vehicle with nonlinear wheel and suspension components review for the model updating of the parameters of the nonlinear.

In this case of this nonlinear model, the Bayesian framework was extended to cover the case that the measurements are taken to be either response time histories or response spectra functions instead of the modal characteristics that were used in case of linear models. For the case that measured data is response time histories, the proposed methodologies were implemented in software, taking into account different approaches for calculating the prediction error that appears according to Bayesian formulation. The Bayesian framework for uncertainty quantification, calibration and propagation was successfully implemented in the case of the experimental vehicle that was a combination of linear and nonlinear components. Drastic reduction in computational effort to manageable levels was achieved using component mode synthesis techniques that are presented in the context of this thesis, for the linear vehicle frame obtaining a drastic reduction in the DOFs from 50,000 to less than 100. Finally, based on the measured output quantities of interest of the components of the vehicle frame, interesting results were concluded about the methodology that the estimates of the model parameter values and their uncertainties for each component can be used to build the model for the combined wheel-suspension-frame structure.

Part C: A novel framework is proposed for estimating damage accumulation due to fatigue in the entire body of a metallic structure using vibration measurements from a limited number of sensors. Fatigue is estimated using Palmgren-Miner damage rule, S-N curves, rainflow cycle counting of the variable amplitude time histories of the stress components, or frequency domain stochastic fatigue methods based on PSD of the stress components. These methods can be applied to any point in the structure and construct the complete fatigue map of the entire structure, provided that the stress response characteristics (time histories or PSDs) at all desirable points are available. These stress response characteristics are predicted from limited number of vibration sensors using a high fidelity finite element model and different prediction methods, including Kalman filter type techniques, kriging approximations and modal expansion methods. The effectiveness of the proposed methods is demonstrated using simulated data from

a chain-like spring-mass model and a small-scale model of a vehicle structure. The proposed framework can be used to construct fatigue damage accumulation and lifetime prediction maps consistent with the actual operational conditions provided by a monitoring system. These maps are useful for designing optimal fatigue-based maintenance strategies for metallic structures taking into account all uncertainties in modeling and fatigue predictions.

LIST OF CONTENTS

LIST OF FIGURES

LIST OF TABLES

CHAPTER 1 Introduction

1.1 Research Context

1.1.1 Preface and Motivation

Structural dynamics plays an increasing role in the design and analysis of engineering systems. In modern analysis of structural dynamics, much effort is devoted to the derivation of accurate models of structures. Civil and mechanical engineering are some examples of engineering disciplines which have become more and more reliant on computational models and simulation results in order to predict the performance of the analyzed structural system. Today's computational resources make it more and more possible to analyze complex structures by sophisticated numerical models, which are usually Finite Element (FE) models (Bathe and Wilson, 1976; Bathe, 1996). Thus, the availability of an accurate dynamic finite element model of a structure is very important for engineers as it allows them to improve the dynamic design of the structure at computer level resulting in an optimized design apart from savings in terms of money and time.

However, there may be some inaccuracies or uncertainties that may be associated with a finite element model. Despite the available powerful computational tools, numerical models are subject to the limitation of available data, physical theory, mathematical representation and numerical solutions. First of all the discretization error, arising due to approximation of a continuous structure by a finite number of

individual elements, is inherent to the finite element technique. Other inaccuracies may be due to the assumptions and simplifications made by the analyst concerning the choice of elements, modelling of boundary conditions, joints, etc. These assumptions and simplifications have as a result that when tests are performed to validate the analytical model, inevitably their results, notably natural frequencies and modeshapes, do not coincide with the expected results from the theoretic model. Given the availability of an accurate data acquisition and measuring equipment the measured test data, though may not be precise, is generally considered to be more accurate than analytical model predictions.

This has led to the development of techniques for the modification or correction of a finite element model, based on the measured test data, also referred to as model updating or model calibration. Generally speaking, the aim of model updating is to use the modal properties, mainly identified modal frequencies and mode shapes, in order to validate a finite element model (FEM) as well as update the values of various properties of the FEM considered as unknown parameters, such as material properties, geometrical properties and boundary conditions, in order to obtain a reliable FEM model of the structure consistent with the measured data (Mottershead and Friswell, 1993; Katafygiotis et al., 1998; Bohle and Fritzen, 2003; Teughels, 2003; Christodoulou and Papadimitriou, 2007).

Finite Element model updating serves a wide array of purposes; this updated FE model for instance can be used to carry out updated response predictions consistent with the test data, or simply to identify unknown system parameters. One of the most promising application areas of FE model updating is structural health monitoring (SHM). By calibrating stiffness parameters of FE models, based on observed modal characteristics, damage can be identified, quantified and located. Here damage is defined as changes to the material and/or geometric properties of these systems, including changes to the boundary conditions and system connectivity, which adversely affect the system's performance. In this context, FE model updating is also used to improve predictions of structural response and reliability.

1.1.2 Management of Uncertainties

FE model updating aims to modify or correct the initial FE model in order to become an accurate reflection of the observed structural behavior. However, it is always observed that even after the process of performing model updating, a comparison between the output of the FE model and the respective results of the experimental tests always reveals some discrepancies. These differences are due

to uncertainties that arise from the simplified assumptions and idealizations used for developing models for simulating the behaviour of engineering structures, as well as models for simulating the loads (mechanical, thermal, etc.) that are applied on the structures. These uncertainties include:

Modelling uncertainties: arising in modelling the constitute behaviour of materials, the damage mechanisms (e.g. due to fatigue, corrosion), the support conditions of structures and their interaction with their environment, the connection between structural members (fixity conditions, friction mechanisms, impact phenomena), the geometric variability due to manufacturing processes.

Loading uncertainties: arising from the lack of detailed knowledge of the spatial and temporal variation of the forces (mechanical, thermal, etc) applied to engineering structures. Examples include spatial variability of road roughness affecting the dynamics of vehicles, spatial and temporal variability of earthquake-induced excitations on civil engineering structures, turbulent wind loads affecting the design of aircrafts, variability of thermal loads affecting the design of a large class of mechanical and aerospace structures.

Numerical uncertainties: stemming from PDE spatial discretization using finite element methods, temporal discretization used in numerical time integration schemes, rounding-off errors in numerical solutions due to computer inaccuracies.

The uncertainties may affect considerably the prediction of performance and safety of the analyzed systems. Modeling tools and techniques are necessary for identifying accurate mechanical models taking into account all uncertain factors, properly quantify uncertainties for the purpose of integrating them with the mechanical models, as well as analyze through model simulation the effect of uncertainties on the performance of engineering structures.

In the context of this thesis, emphasis is given on model uncertainties. Over the last decades, several approaches have been proposed for taking model uncertainties into consideration. These approaches have been formulated in the framework of the parametric, the non-parametric and the Bayesian approach.

1.1.2.1 Model Uncertainties within the parametric approach

Parameter uncertainties relate to the parameters of the mathematical mechanical model; more specifically to material parameters, such as the elasticity modulus or the mass density, and to geometrical parameters, such as the cross-section dimensions of structural members. The uncertainty affecting these parameters, mostly due to natural variability, can be accounted for by modelling these as

random quantities, i.e. by constructing a so-called parametric model of uncertainties. Within this parametric approach, the uncertainty associated with each of the parameters of the models is accounted for explicitly. The uncertainty can thus be captured locally, down to a level corresponding to the degree of resolution of the mathematical-mechanical model.

The parametric approach is well established in structural and mechanical engineering; comprehensive reviews on stochastic mechanics can be found in the work of Schueller (Schueller, 2001 and 2006; Schueller and Pradlwarter, 2009). A wide array of methods exists to construct a stochastic representation of the random parameters. One of the most widely used parametric approaches in stochastic mechanics is the Stochastic Finite Element Method (SFEM), introduced by Ghanem and Spanos (1991), where the FE system matrices are expressed in terms of the underlying random FE model parameters.

This type of approach is suitable to quantify uncertainty that is due to the inherent variability in the system parameters. On the other hand, uncertainty that is due to the lack of knowledge regarding a system, does not explicitly depend on the system parameters. For example, there can be unquantified errors associated with the equation of motion (linear or nonlinear), in the damping model (viscous or non-viscous), in the model of structural joints, and also in the numerical methods (e.g. tolerances in the optimization and iterative algorithms, step sizes in the time-integration method.)

It is evident that the parametric approach is not suitable to quantify uncertainty that is due to the lack of knowledge regarding a system. As a result non-parametric approaches have been proposed for this purposes (Soize, 2000 and 2001 and 2005).

1.1.2.2 Model Uncertainties within the non-parametric approach

According to Soize (2008 and 2010 and 2013),model uncertainties cannot be taken into account by applying the parametric approach, which is underlined by case studies in which it is shown that the desired discrepancy tolerated between the output of the real system and the predicted output cannot be reached with the parametric approach. The non-parametric model of uncertainties has been proposed for structural dynamics problems, in order to capture model uncertainties in addition to the parametric uncertainties. This approach is based on the random matrix theory introduced in the 1930ies in the field of mathematical statistics (Metha, 2004). The non-parametric approach has been developed by

introducing a new ensemble of random matrices, which differs from other known ensembles of the random matrix theory.

The non-parametric method makes use of random matrix theory to construct a probabilistic model of the prediction model, resulting in random mass, stiffness and damping matrices, thus avoiding the need for explicit mapping of model parameters to the system matrices. More specifically, within this approach, the relaxation of the topological connectivity of the structural matrices aims at a consideration of the uncertainties in processes that are not modeled explicitly by structural parameters. Then the probability model model for the random matrices is constructed by using the principle of maximum entropy (Shannon, 1948). This method makes it possible to construct directly the probabilistic model of the generalized mass, damping and stiffness matrices which is proposed as an approach for considering the whole spectrum of uncertainties.

By combining the parametric and non-parametric methods, model parameter uncertainty as well as model structure uncertainty can be included. This generalized approach allows to model the individual errors seperately, depending on the type and amount of information, that is available. For more details on this method and its applications, the reader is referred to Soize (2010) and Batou et al. (2011), respectively.

1.1.2.3 Model Uncertainties within the Bayesian approach

The Bayesian interpretation of probability does not distinguish between the above discussed two categories of uncertainties since all uncertainties are seen as uncertainties that is due to the lack of knowledge regarding a system and not due to the inherent variability in the system parameters. Probability is not interpreted as the relative occurrence of a random event in the long run, but as the plausibility of a hypothesis. The notation of an uncertain-valued parameter as a random variable, as used in the parametric approach, is a characteristic of the so-called frequentist interpretation of probability. On the other hand, the Bayesian intepretation of probability quantifies the uncertainty about propositions and therefore its domain contains both physical variables and models by themselves. The wider scope of the interpretation of probability in the Bayesian sense leads to the fact that the reason of uncertainty of both parameters and models is seen in the incomplete available information. Hence, also in the Bayesian framework, it refers to all kinds of uncertainties since also the unceratinties about parameter values are intepreted as lack of knowledge rather than as an intrinsic property of the real structure.

The Bayesian inference framework complements the probabilistic model description with a probabilistic model for the prediction error. The prediction error represents the difference between the model and the system output. It consists of two parts, the measurement error and also the fact that there are discrepancies between the model and the real system. Each probability model in the chosen model class is described by probability distributions of the unknown parameters and the prediction error. Based on the available data, the initial knowledge of the range of the unknown parameters is updated, making some parameter ranges more plausible if the data provide the necessary information. Therefore, the values of the model parameters are updated in order to better predict the output of the system, but due to the fact that there is no true value of the parameters, there is a gap between model output and measurement, which is bridged by the prediction error. Hence, the prediction error provides a means for considering those uncertainties that cause the remaining lack of knowledge which prohibits a perfect matching between model and real system.

The Bayesian statistical framework represents a general, rational and powerful tool for model updating that is capable of handling the above stated difficulties (Beck and Katafygiotis, 1998; Katafygiotis and Beck, 1998). The Bayesian approach updates the relative plausibility of each model within a set of candidate models, which is quantified by the posterior probability distribution. Therefore, probability in the Bayesian sense is interpreted as the degree of plausibility of a hypothesis based on the conditioning information (Cox, 1946; Jaynes, 2003), where the hypothesis may refer to the structural parameters but also to the model itself. This interpretation makes it possible to extend the application of probability theory to fields where the frequentist interpretation may not be directly intuitive, as it is the case for one-of-a-kind structures, where no ensemble exists, and also in the case of limited data, where classical statistics is of limited applicability. Therefore, Bayesian statistics makes it possible to deal with the usual situation in industry, where a large amount of experimental data is infeasible due to high costs associated with test campaigns, and it provides a means for making decisions based on limited, incomplete information.

1.1.3 Incorporation of Measured Data in Structural Response Simulations

Methods for reducing the uncertainty about some unknown structural parameters expressed by the probability distributions assigned to them aim at an increase of the above mentioned level of information in order to further increase the credibility of the established model. This task can be accomplished by using

measured data into the analysis. The measured data can be either modal data or response time histories.

The measured data used for FE model updating purposes can be obtained during forced, ambient or hybrid vibration testing (Peeters and De Roeck, 2001; Reynders and De Roeck, 2008). In cases where the input excitation is known, the response time histories, e.g accelerations measured at certain locations along the structure can be used directly by solving the equation of motion. However, since this condition is very rare for dynamic systems, in most cases of linear dynamic systems we use modal data that are identified by the measured response time histories using experimental (EMA) (Ntotsios, 2009), operational (OMA) (Felber, 1993; Beck et al., 1994; Peeters and De Roeck, 1999; Verboten, 2002) or combined (OMAX) modal analysis methods (Reynders, 2009). An additional advantage of using modal characteristics is that they are relatively few in number but provide a comprehensive description of the overall dynamical behavior of a structure. However, in cases that nonlinearities are imposed on the structure, the response time histories are used instead of the modal data.

The experimental activities serve the purpose of both improving the numerical model and they are also a means for determining the accuracy with respect to the intended use of the model. The enhancement of a numerical model based on experimental data is denoted as model updating and the subsequent process of determining the degree of accuracy of the established model is referred to as model validation. A model which meets the requirements in terms of accuracy is referred to as validated model. In the present thesis particular weight is attached to the dynamic behavior of structures, hence the above mentioned comparison is based on properties of the natural modes of the structure such as natural frequencies and mode shapes for linear structures. The combined use of frequencies and mode shapes serves an important goal: even though natural frequencies cn be measured relatively accurately and are generally quite sensitive to changes in structural stiffness, they provide only global information about the structure. Therefore, mode shape components are capable of providing localized information along the structure. For example, in the problem of locating damage the mode shape displacements are essential. In most cases, however, the mode shape components are less sensitive to changes in structure stiffness and are more difficult to measure accurately.

1.2 Organization of this Thesis

The research work presented in the thesis contributes to three interrelated research areas of structural response and reliability simulations using vibration measurements:

(1) Development of component mode synthesis techniques that are integrated with model updating methods and with Bayesian uncertainty and quantification framework for reducing the computation effort without sacrificing the accuracy presented in Chapters 2 and 3,

(2) Development of Bayesian uncertainty and quantification framework for nonlinear systems, presented in Chapter 4, and

(3) Development of methods for predicting the fatigue damage accumulation in the entire body of metallic structures exploiting vibration measurements from a limited number of sensors, presented in Chapter 5.

In the first research area, for the analyzed structures in FE model parameterization schemes the stiffness matrix of the structures is assumed to depend linearly on only one of the parameters of the model. In the second research area , time histories are used to integrate the information contained in vibration measurements for making informed response predictions using the identified mechanical models. In the third research area, a problem that is formulated and solved for the first time is related to the estimation of fatigue damage accumulation in the entire body of a metallic structure using ambient vibration measurements collected from a limited number of sensors placed on the structure. The application areas of this research are mainly related to ground/air vehicle and civil structures. Emphasis though is given to applications on ground vehicles.

A more detailed overview of the contents of this thesis is given in the following.

Chapter 1: The research context and the general motivation of this PhD thesis is given.This chapter acts as a prologue to this work, by presenting in detail the meaning of "*management of uncertainties*" and "*using measured data*" that appear in the title of this thesis.

Chapter 2: The widely used deterministic finite element model updating methods are reviewed in this chapter and the Bayesian framework for parameter estimation and model class selection is presented. The Bayesian tools for identifying system and uncertainty models as well as performing model class selection are Laplace methods of asymptotic approximation and stochastic simulation algorithms such as Markov Chain Monte Carlo (MCMC) and Transitional MCMC. Both tools are

used to represent the posterior distribution of the parameters of a model class introduced to simulate the behavior of the engineering system, as well as compute multidimensional integrals over high-dimensional spaces of the uncertain model parameters, manifested in the formulations for model class selection. The asymptotic approximations involve solving optimization problems as well as computing the Hessian of certain functions in a small number of points in the parameter space. The stochastic simulation tools involve generating samples for tracing and then populating the important uncertainty region in the parameter space, as well as evaluating integrals over high-dimensional spaces of the uncertain model parameters. These tools require a moderate to very large number of system re-analyses to be performed over the space of uncertain parameters. Consequently, the computational demands depend highly on the number of system analyses and the time required for performing a system analysis. For complex models of engineering systems, one simulation may require a significant amount of time and the overall computational demands involved in the Bayesian tools may be substantial, or even excessive for stochastic simulation algorithms. This chapter proposes methods for drastically reducing the computational demands at the system, algorithm and hardware levels involved in the implementation of Bayesian tools.

Chapter 3: A framework is presented for integrating the Craig-Bampton CMS technique into existing FE model updating formulations in order to reduce the time consuming operations involved in reanalyses of large-order models of hundreds of thousands or millions degrees of freedom. The proposed method exploits the fact that in FE model parameterization schemes the stiffness matrix of the structure often depends linearly on the parameters of the model and also that a parameter usually represents a global property (e.g. the modulus of elasticity) of a substructure. The division of the structure into components is then guided by the FE parameterization scheme so that the stiffness matrix that arise for each one of the introduced components to depend linearly on only one of the parameters to be estimated. In this case the fixed-interface and constraint modes of the components for any value of the model parameters can be obtained exactly from the fixed-interface and constraint modes corresponding to a single reference FE model, avoiding re-analyses at component level. Additional substantial reductions in computational effort are also proposed by reducing the number of interface DOF using characteristic interface modes through a Ritz coordinate transformation. The repeated solutions of the component and interface eigen-problems are avoided, reducing drastically the computational demands in FE formulations, without compromising the solution accuracy. It is also shown that the linear expansions of

the original mass and stiffness matrices in terms of the structural parameters are preserved for the reduced mass and stiffness matrices. Thus, the reassembling of the reduced system matrices from the original matrices is also avoided in the execution of the system re-analyses. The only time consuming operation left is the re-analysis of the eigenproblem of the reduced-order model. It is finally demonstrated that the new developments are readily accommodated in existing FE model updating formulations and software with minimal modifications. Moreover, in this chapter, Bayesian estimators are proposed for damage identification (localization and quantification) of civil infrastructure using vibration measurements. The structural damage identification is accomplished by associating a FE model class to a damage location pattern in the structure, indicative of the location of damage. The effectiveness of the damage identification methodology is illustrated using simulated vibration data from a real bridge. It can be concluded that the proposed methodology, illustrated in this work using computationally efficient stochastic simulation algorithms, correctly identifies the location and the magnitude of damage. Surrogate models are also incorporated in the formulation to further alleviate the computational burden. Finally, parallel computing algorithms are combined with the proposed method to efficiently distribute the computations in available GPUs and multi-core CPUs.

Chapter 4: A Bayesian uncertainty quantification and propagation (UQ&P) framework is presented for identifying nonlinear models of dynamic systems using vibration measurements of their components. The measurements are taken to be either response time histories or frequency response functions of linear and nonlinear components of the system. For such nonlinear models, stochastic simulation algorithms are suitable Bayesian tools to be used for identifying system and uncertainty models as well as perform robust prediction analyses. At the system level, efficient computing techniques are integrated with Bayesian techniques to efficiently handle large order models of hundreds of thousands or millions degrees of freedom (DOF) and localized nonlinear actions activated during system operation. Specifically, fast and accurate component mode synthesis (CMS) techniques that have been proposed in Chapter 3 are used, consistent with the FE model parameterization, to achieve drastic reductions in computational effort. The UQ&P framework is applied to a small scale experimental model of a vehicle with nonlinear wheel and suspension components. Uncertainty models of the nonlinear wheel and suspension components are identified using the experimentally obtained response spectra for each of the components tested separately. These uncertainties, integrated with uncertainties in the body of the experimental vehicle, are propagated to estimate

the uncertainties of output quantities of interest for the combined wheel-suspension-frame system. The computational challenges are outlined and the effectiveness of the Bayesian UQ&P framework on the specific example structure is demonstrated.

Chapter 5: A novel framework for estimating damage accumulation due to fatigue in the entire body of a metallic structure using vibration measurements from a limited number of sensors is presented. Fatigue is estimated using the Palmgren-Miner damage rule, S-N curves and rainflow cycle counting methods of the variable amplitude time histories of the stress components. These methods can be applied to any point in the structure and construct the complete fatigue map of the entire structure, provided that the stress response characteristics (time histories or PSDs) at all desirable points are available. These stress response characteristics are predicted from limited number of vibration sensors using a high fidelity finite element model and different prediction methods, including Kalman filter type techniques, kriging approximations and modal expansion methods. The effectiveness of the proposed methods is demonstrated using simulated data from a chain-like spring-mass model and a small-scale model of a vehicle structure. The proposed framework can be used to construct fatigue damage accumulation and lifetime prediction maps consistent with the actual operational conditions provided by a monitoring system. These maps are useful for designing optimal fatigue-based maintenance strategies for metallic structures taking into account all uncertainties in modeling and fatigue predictions.

Chapter 6: Summarizes the conclusions and the novel contributions of this work. Also it presents suggestions for future research on issues related to this thesis.

CHAPTER 2 Finite Element Model Updating Methods in System Dynamics

2.1 Introduction

Finite element (FE) models are widely used to predict the dynamic characteristics of systems. These models often give results that differ from the measured results and therefore need to be updated to match the measured data. FE model updating entails tuning the model so that it can better reflect the measured data from the physical structure being modeled. One fundamental characteristic of a FE model is that it can never be a true reflection of the physical structure but it will forever be an approximation. The aim of FE model updating is the identification of a better approximation model of the physical structure than the original model.

Structural model updating methods (Mottershead and Friswell, 1993; Marwala, 2010; Yuen and Kuok, 2011) are used to reconcile mathematical models, usually discretized finite element (FE) models, with experimental data. Structural model parameter estimation problems based on identified modal characteristics (modal frequencies and mode shapes), are often formulated as weighted least-squares problems (Mottershead and Friswell, 1993; Fritzen et al., 1998; Katafygiotis et al., 1998; Yuen et al., 2006; Christodoulou and Papadimitriou, 2007; Moaveni et al., 2008) in which metrics, measuring the residuals between measured and model

predicted modal characteristics, are build up into a single weighted residuals metric formed as a weighted average of the multiple individual metrics using weighting factors. Standard optimization techniques are then used to find the optimal values of the structural parameters that minimize the single weighted residuals metric. Due to model error and measurement noise, the results of the optimization are affected by the values assumed for the weighting factors. The model updating problem has also been formulated as a multi-objective optimization problem (Haralampidis et al., 2005; Christodoulou et al., 2008), that allows the simultaneous minimization of the multiple metrics, eliminating the need for using arbitrary weighting factors for weighting the relative importance of each metric in the overall measure of fit. The multi-objective parameter estimation methodology provides multiple Pareto optimal structural models in the sense that the fit each Pareto optimal model provides in a group of measured modal properties cannot be improved without deteriorating the fit in at least one other modal group. The Normal Boundary Intersection algorithm (Das et al., 1998) is used to compute the Pareto optimal solutions.

In addition, a Bayesian statistical framework (Beck , 1989; Sohn and Law, 1997; Beck and Katafygiotis, 1998), for structural model parameter identification is used to identify the values of the weights. Using Bayes theorem, the probability distribution of the weight values based on the data is formulated as a probability integral over the structural model parameters (Christodoulou and Papadimitriou, 2007). An asymptotic approximation is presented to analytical approximate this probability distribution. The best values of the weights are selected as the ones that maximize the probability distribution of the weights.

Bayesian techniques have also been proposed to quantify the uncertainty in the parameters of a FE model, select the best model class from a family of competitive model classes (Beck and Yuen, 2004; Yuen , 2010),, as well as propagate uncertainties for robust response and reliability predictions (Papadimitriou et al., 2001). Posterior probability density functions (PDFs) are derived that quantify the uncertainty in the model parameters based on the data. These PDFs are formulated in terms of the modal residuals involved in the aforementioned single and multi-objectives deterministic methods. The Bayesian tools for identifying uncertainty models as well as performing robust prediction analyses are Laplace methods of asymptotic approximation and more accurate stochastic simulation algorithms (SSA) such as Markov Chain Monte Carlo (MCMC) (Metropolis et al., 1953), Transitional MCMC (Ching and Chen, 2007) and Delayed Rejection Adaptive Metropolis (Haario et al., 2006). Similar to the

deterministic FE model updating techniques, the asymptotic approximations in the Bayesian framework involve solving an optimization problem for finding the most probable model, as well as estimating the Hessian of the logarithm of the posterior PDF at the most probable model for describing the uncertainty in the model parameters. The SSA algorithms involve generating samples for tracing and then populating the important uncertainty region in the parameter space, as well as evaluating integrals over high-dimensional spaces of the uncertain model parameters.

The optimal structural models and their uncertainties resulting from model updating methods can be used for improving the model response and reliability predictions (Papadimitriou et al., 2001; Beck and Au, 2002), for assessing structural health and identifying structural damage (Fritzen et al., 1998; Katafygiotis et al., 1998; Yuen et al., 2006; Christodoulou and Papadimitriou, 2007; Metropolis et al., 1953, Vanik et al., 2000; Papadimitriou et al., 2001; Beck and Au, 2002; Beck and Yuen, 2004; Haario et al., 2006; Ching and Chen, 2007; Yuen, 2010) and for improving effectiveness of structural control devices (Ntotsios et al., 2009).

This Chapter is organised as follows. The finite element model parameterization for both linear and nonlinear formulations is presented in Section 2.2. Deterministic FE model updating formulations using modal characteristics are reviewed in Section 2.3. The framework for Bayesian model parameter estimation and model class selection is outlined in Sections 2.4 and 2.5. The Bayesian tools are given in detail in Section 2.6. In Section 2.7, the computational aspects that arise from for finite element models with large number of DOFs are discussed and methods for reducing the computational effort are proposed in Section 2.8. Finally, conclusions are summarized in Section 2.9.

2.2 Finite Element Model Parameterization

Consider a parameterized class of linear structural models (e.g. a class of finite element models) used to model the dynamic behaviour of the structure. The structural model class, denoted by M, involves a set of model parameters $\underline{\theta} \in R^{N_\theta}$. The equation of motion of such systems is

$$M(\underline{\theta})\ddot{\underline{u}}(t) + C(\underline{\theta})\dot{\underline{u}}(t) + K(\underline{\theta})\underline{u}(t) = f(t) \tag{2.1}$$

where $K(\underline{\theta}) \in \mathbb{R}^{n\times n}$, $M(\underline{\theta}) \in \mathbb{R}^{n\times n}$ and $C(\underline{\theta}) \in \mathbb{R}^{n\times n}$ are the global model stiffness , mass, and damping matrices respectively, $\underline{u}(t)$ is the displacement vector of the

model DOFs, $f(t)$ is the vector of forces at the model DOFs, n is the number of model DOFs.

The parameter set $\underline{\theta}$ is the set of free model parameters to be estimated using the measured data. The parameter set is usually associated with geometrical, material, stiffness or mass properties and boundary conditions. Examples of finite element properties that can be included in the parameter set are: modulus of elasticity, cross-sectional area, thickness, moment of inertia and mass density of the finite elements comprising the model, as well as spring (translational or rotational) stiffnesses used to model fixity conditions at joints or boundaries.

Using finite element model analysis, one derives the element stiffness and the mass matrices, the stiffness and the mass matrices of the substructures formed by a group of elements, and finally the global stiffness and the mass matrices. These matrices depend on the properties of the structure, like modulus of elasticity, mass density and the geometrical characteristics (e.g. cross-sectional area, thickness, length and moments of inertia). Usually, a subgroup of these properties is selected for updating. The properties that are updated are included in the parameter set $\underline{\theta}$.

For the case of linear relation between the stiffness and mass matrices of the structural model and the parameters set $\underline{\theta}$ one has that

$$K(\underline{\theta}) = K_0 + \sum_{i=1}^{N_\theta} K_{,j}\theta_j$$
$$M(\underline{\theta}) = M_0 + \sum_{j=1}^{N_\theta} M_{,j}\theta_j \qquad (2.2)$$

where N_θ is the number of parameters used to parameterize the structural model, K_0 and M_0 are assembled from element stiffness and mass matrices that do not depend on $\underline{\theta}$, and the $K_{,j}$ and $M_{,j}$ are assembled from element stiffness and mass matrices that depend linearly on $\underline{\theta}$. Once the parameterization has been done and the matrices K_0, M_0, $K_{,j}$ and have been calculated and stored in computer's memory, global stiffness and mass matrices are easily calculated for each value of the parameters $\underline{\theta}$ using the parameterization (2.2). That parameterization is computationally attractive since the model updating process requires the repeated computation of global matrices for different values of the parameters $\underline{\theta}$.

In the general case where the relation between model stiffness and mass matrices, and the parameters set $\underline{\theta}$ is nonlinear, the global stiffness and mass matrices are given by the following expressions

$$K(\underline{\theta}) = K_0 + \sum_{j=1}^{N_\theta} K_{,j}\theta_j + \sum_{i=1}^{N_\theta} K_{,i} f(\theta_j)$$
$$M(\underline{\theta}) = M_0 + \sum_{j=1}^{N_\theta} M_{,j}\theta_j + \sum_{i=1}^{N_\theta} M_{,i} g(\theta_j) \tag{2.3}$$

where $f(\theta_j)$ and $g(\theta_j)$ are nonlinear functions of the parameter θ_j. For each value of the parameter set $\underline{\theta}$, the evaluation of the global matrices should be repeated only for the elements that have non-linear relation between the element matrices and the parameters . Then these matrices are composed in order to form the non-linear part of the global matrices. This parameterization scheme is computationally efficient, if there is only a small number of elements that have non-linear relation between the stiffness and mass matrices and the parameters set $\underline{\theta}$.

In this chapter, we limit to the formulation to the case for which the stiffness and mass matrices depend linearly on the model parameters $\underline{\theta}$, as presented in (2.2) .

2.3 Deterministic FE Model Updating using Modal Characteristics

Consider a parameterized linear FE model class M of a structure and let $\underline{\theta} \in R^{N_\theta}$ be a vector of free structural model parameters to be estimated using a set of modal properties identified from vibration measurements. The identified modal properties consist of the square of the modal frequencies, $\hat{\lambda}_r = \hat{\omega}_r^2$ and the mode shape components $\underline{\hat{\phi}}_r \in \mathbb{R}^{N_0}$ at N_0 measured DOFs, for $r = 1, \cdots, m$, where m is the number of observed modes. The values of the parameter vector $\underline{\theta}$ are estimated so that the modal frequencies $\lambda_r(\underline{\theta}) = \omega_r^2(\underline{\theta})$ and modeshapes $\underline{\phi}_r(\underline{\theta}) \in \mathbb{R}^{N_0}$ predicted by the FE model, best matches the experimentally obtained modal data D. For this, the following modal frequency and mode shape residuals

$$J_{\omega_r}(\underline{\theta}) = \sum_{r=1}^{m} \varepsilon_{\lambda r}^2(\underline{\theta}) = \sum_{r=1}^{m} \frac{[\lambda_r(\underline{\theta}) - \hat{\lambda}_r]^2}{\hat{\lambda}_r^2} \tag{2.4}$$

and

$$J_{\underline{\phi}_r}(\underline{\theta}) = \sum_{r=1}^{m} \varepsilon_{\underline{\phi}_r}^2(\underline{\theta}) = \sum_{r=1}^{m} \frac{\left\| \beta_r(\underline{\theta})\underline{\phi}_r(\underline{\theta}) - \underline{\hat{\phi}}_r \right\|^2}{\left\| \underline{\hat{\phi}}_r \right\|^2} = \sum_{r=1}^{m} [1 - MAC_r^2(\underline{\theta})] \tag{2.5}$$

are introduced to measure the difference between the identified modal data and the model predicted modal data for the modal frequency and modeshape components, respectively, where $\beta_r(\underline{\theta}) = \underline{\hat{\phi}}_r^T \underline{\phi}_r(\underline{\theta}) / \left\| \underline{\phi}_r(\underline{\theta}) \right\|^2$ is a normalization constant that guaranties that the measured mode shape $\underline{\hat{\phi}}_r$ at the measured DOFs is closest to the model mode shape $\beta_r(\underline{\theta})\underline{\phi}_r(\underline{\theta})$ predicted by the particular value of $\underline{\theta}$, $MAC_r = \underline{\phi}_r^T \underline{\hat{\phi}}_r / (\| \underline{\phi}_r \| \| \underline{\hat{\phi}}_r \|)$ is the modal assurance criterion between the experimentally identified and model predicted mode shapes for the r - th mode, and $\| \underline{z} \|^2 = \underline{z}^{\mathrm{T}} \underline{z}$ is the usual Euclidian norm.

The mode shape components $\underline{\phi}_r(\underline{\theta}) = L\underline{\varphi}_r(\underline{\theta}) \in R^{N_0}$ at the N_0 measured DOFs involved in (2.2) are computed from the complete mode shapes $\underline{\varphi}_r(\underline{\theta}) \in R^N$ that satisfy the eigenvalue problem

$$[K(\underline{\theta}) - \lambda_r(\underline{\theta}) M(\underline{\theta})] \underline{\varphi}_r(\underline{\theta}) = \underline{0} \tag{2.6}$$

where $K(\underline{\theta}) \in \mathbb{R}^{n \times n}$ and $M(\underline{\theta}) \in R^{N \times N}$ are respectively the stiffness and mass matrices of the finite element model of the structure, N is the number of model degrees of freedom (DOF), and $L \in R^{N_0 \times N}$ is an observation matrix, usually comprised of zeros and ones, that maps the N model DOFs to the N_0 observed DOFs. For a model with large number of DOFs, N , the number of measurement locations N_0 is a very small fraction of the model DOFs ($N_0 \ll N$).

2.3.1 Modal Grouping Schemes

The grouping of the modal properties $\{\omega_r(\underline{\theta}), \underline{\phi}_r(\underline{\theta}), r = 1, \cdots, m\}$ into n groups and the selection of the measures of fit $J_1(\underline{\theta}), \cdots, J_n(\underline{\theta})$ are usually based on user preference.

The number and type of modal properties involved in the i th group as well as the particular form of $J_i(\underline{\theta})$ may depend on the modal characteristics (mode type, modal frequencies and/or modeshapes), their expected uncertainties, and their significance of each modal property on the model identification. The modal properties assigned to each group are selected by the user according to their type and the purpose of the analysis. Among the various grouping schemes available, the following are considered for illustration purposes.

A grouping scheme is defined so that each group contains one modal property, the modal frequency or the modeshape for each mode. In this case, there are $n = 2m$ measures of fit given by $J_i(\underline{\theta}) = J_{\omega_i}(\underline{\theta})$ and $J_{m+1}(\underline{\theta}) = J_{\underline{\phi}_i}(\underline{\theta}), i = 1, \cdots, m$. This

grouping scheme, allows one to estimate all optimal models that trade-off the fit in various modal frequencies and modeshapes. A special case of grouping is to consider only the first m groups measuring the fit between the modal frequencies, ignoring the fit in the modeshapes.

A second grouping scheme may be defined by grouping the modal properties into two groups as follows. The first group contains all modal frequencies with the measure of fit $J_1(\underline{\theta})$ selected to represent the difference between the measured and the model predicted frequencies for all modes, while the second group contains the modeshape components for all modes with the measure of fit $J_2(\underline{\theta})$ selected to represents the difference between the measured and the model predicted modeshape components for all modes. Specifically, the two measures of fit are given by

$$J_1(\underline{\theta}) = \frac{1}{m}\sum_{r=1}^{m} J_{\omega_r}(\underline{\theta}) \tag{2.7}$$

and

$$J_2(\underline{\theta}) = \frac{1}{m}\sum_{r=1}^{m} J_{\underline{\phi}_r}(\underline{\theta}) \tag{2.8}$$

This selection allows one to estimate models that trade-off the overall fit in modal frequencies with the overall fit in the modeshapes.

Finally, a third grouping scheme, may be selected so that a group contains the modal frequency and all modeshape components at the measured DOFs for a particular observed mode. In this case the number of groups equals the number of observed modes $n = m$. The i th measure of fit $J_i(\underline{\theta})$ accounts for the mismatch between the measured and the model predicted frequencies and modeshape components for the i th measured mode. Specifically, can be given in the form

$$J_i(\underline{\theta}) = \frac{J_{\omega_i}(\underline{\theta}) + J_{\underline{\phi}_i}(\underline{\theta})}{2} \tag{2.9}$$

This grouping scheme is appropriate when the objective of the identification is to estimate all optimal models that trade-off the fit between different modes.

In the context of this thesis, the second grouping scheme, with the measures of fit $J_1(\underline{\theta})$ and $J_2(\underline{\theta})$, is preferred for model updating purposes.

2.3.2 Formulation as single-objective optimization problem

The estimation of the model parameters is traditionally formulated as a minimization of the weighted residuals

$$J(\underline{\theta};\underline{w}) = w_1 J_1(\underline{\theta}) + w_2 J_2(\underline{\theta}) \tag{2.10}$$

where $w_i \propto [0,\infty)$, $i = 1,2$ and $\sum_{i=1}^{2} w_i = 1$.The relative importance of the residual errors in the selection of the optimal model is reflected in the choice of the weights. The results of the identification depend on the weight values used. The weight values depend on the adequacy of the model class used to represent structural behaviour and the accuracy with which the measured modal data are obtained. However, the choice of weight values is arbitrary since the modelling error and the uncertainty in the measured data are usually not known apriori. The single objective formulation is computationally attractive since conventional minimization algorithms, such as Quasi-Newton algorithm, can be applied to solve the problem. The objective function $J(\underline{\theta};\underline{w})$ represents an overall measure of fit between the measured and the model predicted characteristics. Conventional weighted least squares methods assume equal weight values, $w_1 = w_2 = 1/2$. This conventional method is referred as the equally weighted modal residuals method.

2.3.3 Formulation as multi-objective optimization problem

The parameter estimation problem can be formulated as a multi-objective optimization problem (Haralampidis et al., 2005; Christodoulou et al., 2008), of finding the values of $\underline{\theta}$ that simultaneously minimize the objectives

$$J(\underline{\theta}) = (J_1(\underline{\theta}), J_2(\underline{\theta})) \tag{2.11}$$

where $\underline{J}(\underline{\theta})$ is the objective vector defined over the two-dimensional objective space. For conflicting objectives $J_1(\underline{\theta})$ and $J_2(\underline{\theta})$, there is no single optimal solution, but rather a set of alternative solutions, known as Pareto optimal solutions, that are optimal in the sense that no other solutions in the parameter space are superior to them when both objectives are considered.

Using multi-objective terminology, the Pareto optimal solutions are the non-dominating vectors in the parameter space Θ, defined mathematically as follows. A vector $\underline{\theta} \in \Theta$ is said to be non-dominated regarding the set Θ if and only if there is no vector in Θ which dominates $\underline{\theta}$. A vector $\underline{\theta}$ is said to dominate a vector $\underline{\theta}'$ if and only if

$$J_i(\underline{\theta}) \le J_i(\underline{\theta}') \quad \forall i \in \{1,\cdots,n\} \quad \text{and} \quad \exists\ j \in \{1,\cdots,n\} \ :\ J_j(\underline{\theta}) < J_j(\underline{\theta}') \tag{2.12}$$

The set of objective vectors $\underline{J}(\underline{\theta})$ corresponding to the set of Pareto optimal solutions $\underline{\theta}$ is called Pareto optimal front. The characteristics of the Pareto solutions are that the modal residuals cannot be improved in any modal group without deteriorating the modal residuals in at least one other modal group. Specifically, using the objective functions in (2.7) and (2.8), all optimal models that trade-off the overall fit in modal frequencies with the overall fit in the modeshapes are estimated.

The multiple Pareto optimal solutions are due to modelling and measurement errors. The level of modelling and measurement errors affect the size and the distance from the origin of the Pareto front in the objective space, as well as the variability of the Pareto optimal solutions in the parameter space. The variability of the Pareto optimal solutions also depends on the overall sensitivity of the objective functions or, equivalently, the sensitivity of the modal properties, to model parameter values $\underline{\theta}$. Such variabilities were demonstrated for the case of two-dimensional objective space and one-dimensional parameter space in the work by Christodoulou and Papadimitriou (2007). It should be noted that in the absence of modelling and measurement errors, there is an optimal value $\underline{\hat{\theta}}$ of the parameter set $\underline{\theta}$ for which the model based modal frequencies and modeshape components match exactly the corresponding measured modal properties. In this case, all objective functions $J_1(\underline{\hat{\theta}}), J_2(\underline{\hat{\theta}})$ take the value of zero and, consequently, the Pareto front consists of a single point at the origin of the objective space

The solution obtained by optimizing (2.10) for any weight value is a Pareto optimal solution [10]. However, in order to adequately describe the Pareto optimal solutions by uniformly spaced points along the solution manifold in the parameter space, the multi-objective optimization problem is preferred since varying the weight value in (2.10) may miss significant portions of the Pareto optimal solutions in the objective and parameter space. An advantage of the multi-objective identification methodology is that all admissible solutions in the parameter space are obtained. However, this is a time consuming task, it requires that multi-objective optimization algorithms are available and that the number of objectives remain small in order to limit the number of solutions required to fully represent the multi-dimensional Pareto front.

2.4 Bayesian FE Model Updating using Modal Characteristics

Consider a parameterized class M_i of structural dynamics models used to predict various output quantities of interest of a system. Let $\underline{\theta}_i \in R^{N_i}$ be a set of

parameters in this model class that need to be estimated using experimental data. Also, let $\Pi(\underline{\theta}_i;\mathsf{M}_i) = \omega_r(\underline{\theta}_i;\mathsf{M}_i), \underline{\phi}_r(\underline{\theta}_i;\mathsf{M}_i) \in R^{N_o}$ $, r = 1,\ldots,m$ be the predictions of the modal frequencies and modeshapes predicted by a model in the model class M_i given a value of the parameter set $\underline{\theta}_i$

$$\underline{\phi}_r(\underline{\theta}_i;\mathsf{M}_i) = L\underline{\varphi}_r(\underline{\theta}_i;\mathsf{M}_i) \tag{2.13}$$

where $\underline{\phi}_r(\underline{\theta}_i;\mathsf{M}_i)$ is the complete modeshape and $L \in R^{N_o \times N}$ selects the N_0 measured DOFs from the N DOFs of the FE model.

The values of the model parameters $\underline{\theta}_i$ are considered to be uncertain. Probability distributions are convenient mathematical tools to quantify the uncertainty in these parameters. Specifically, the probability distribution of the parameter set $\underline{\theta}_i$ quantifies how plausible is each possible value of the model parameters. The user may assign a prior probability distribution $\pi_i(\underline{\theta}_i)$ to the model parameters to incorporate prior information on the values of the model parameters. The structural model and uncertainty propagation algorithms can be used to identify the uncertainty in the prediction of the output quantities of interest. However, the probability distribution $\pi_i(\underline{\theta}_i)$ is subjective based on previous knowledge and user experience.

In Bayesian inference, the interest lies in updating the probability distribution of the model parameters $\underline{\theta}_i$ based on measurements and then propagate these uncertainties through the structural dynamics model to quantify the uncertainty in the output quantities of interest.

For this, let $D = \hat{\omega}_r, \hat{\underline{\phi}}_r \in R^{N_o}$ $, r = 1,\ldots,m$ be the available measured modal frequencies $\hat{\omega}_r$ and modeshape components $\hat{\underline{\phi}}_r$ at N_0 measured DOFs, where m is the number of observed modes. The Bayesian formulation starts by building a probabilistic model that characterizes the discrepancy between the model predictions $\omega_r(\underline{\theta}_i;\mathsf{M}_i)$, $\underline{\phi}_r(\underline{\theta}_i;\mathsf{M}_i)$ obtained from a particular value of the model parameters $\underline{\theta}_i$ and the corresponding data D that are available from experiments. This discrepancy always exists due to measurement and model errors. An error term $\underline{e}$ is introduced to denote this discrepancy. The vector of prediction errors $\underline{e}^{(i)} = [\underline{e}_1^{(i)},\cdots,\underline{e}_m^{(i)}]$ is defined as the difference between the measured modal properties involved in D for all modes $r = 1,\cdots,m$ and the corresponding modal

properties predicted by a model in the model class M_i. Specifically, $\underline{e}_r^{(i)} = [e_{\omega_r}^{(i)} \;\; \underline{e}_{\phi_r}^{(i)}]$ is given as:

$$\hat{\omega}_r = \omega_r(\underline{\theta}_i;\mathsf{M}_i) + \hat{\omega}_r e_{\omega_r}^{(i)} \qquad r = 1,\ldots,m \tag{2.14}$$

$$\underline{\hat{\phi}}_r = \beta_r^{(i)} \underline{\phi}_r(\underline{\theta}_i;\mathsf{M}_i) + \left\|\underline{\hat{\phi}}_r\right\| \underline{e}_{\phi_r}^{(i)} \qquad r = 1,\ldots,m \tag{2.15}$$

where $\beta_r^{(i)} = \underline{\hat{\phi}}_r^T \underline{\phi}_r^{(i)} / \underline{\hat{\phi}}_r^T \underline{\phi}_r^{(i)}$ is a normalization constant that accounts for the different scaling between the measured and the predicted modeshape. The model prediction errors are due to modeling error and measurement noise. A probabilistic structure for the prediction error needs to be defined in order to proceed with the Bayesian calibration. Let M_e be a family of probability model classes for the error term $\underline{e}$. This model class depend on a set of prediction error parameters $\underline{\theta}_e$ to be determined using the experimental data. Similarly to the structural model parameters $\underline{\theta}_i$, probability distribution $\pi_e(\underline{\theta}_e)$ is also assigned to quantify the possible values of the prediction error parameters.

The Bayesian approach (Beck ,1989; Beck and Katafygiotis, 1998) to model calibration is used for updating the values of the combined set $\underline{\theta} = (\underline{\theta}_i, \underline{\theta}_e)$ associated with the structural and the prediction error parameters. The parameters $\underline{\theta}_i$ and $\underline{\theta}_e$ can be considered to be independent with prior probability distribution for the combined set given by $\pi(\underline{\theta}\,|\,\mathsf{M}) = \pi_i(\underline{\theta}_i\,|\,\mathsf{M}_i)\;\pi_e(\underline{\theta}_e\,|\,\mathsf{M}_e)$, where $\mathsf{M} = \{\mathsf{M}_i, \mathsf{M}_e\}$ includes the structural and prediction error model classes. The updated distribution $p(\underline{\theta}\,|\,D,\mathsf{M})$ of the parameters $\underline{\theta}$, given the data D and the model class M, results from the application of the Bayes theorem

$$p(\underline{\theta}\,|\,D,\mathsf{M}) = \frac{p(D\,|\,\underline{\theta},\mathsf{M})\;\pi(\underline{\theta}\,|\,\mathsf{M})}{p(D\,|\,\mathsf{M})} \tag{2.16}$$

where $p(D\,|\,\underline{\theta},\mathsf{M})$ is the likelihood of observing the data from the model class and $p(D\,|\,\mathsf{M})$ is the evidence of the model, given by the multi-dimensional integral over the space of the uncertain model parameters.

$$p(D\,|\,\mathsf{M}) = \int_{\Theta} p(D\,|\,\underline{\theta},\mathsf{M})\;\pi(\underline{\theta}\,|\,\mathsf{M})\;d\underline{\theta} \tag{2.17}$$

The updated probability distribution of the model parameters depends on the selection of the prediction error $\underline{e}$. Assuming that the prediction error model class postulates zero-mean Gaussian models for the modal frequency and mode shape

error terms $\underline{e}_{\omega_r}$ and $\underline{e}_{\phi_r}$, respectively, with equal variances σ^2 for all modal frequency errors $\underline{e}_{\omega_r}$ and equal variances σ^2 / w_2 for all mode shape errors $\underline{e}_{\phi_r}$. Using probability density functions (PDF) to quantify uncertainty and following the Bayesian formulation described in (Christodoulou and Papadimitriou, 2007; Beck and Katafygiotis,1998; Vanik et al., 2000), the posterior PDF $p(\underline{\theta} \mid D, \mathsf{M})$ of the structural model parameters $\underline{\theta}$ and the prediction error parameter σ given the data D and the model class M can be obtained in the form

$$p(\underline{\theta} \mid D, \mathsf{M}) = \frac{[p(D \mid \mathsf{M})]^{-1}}{\left(\sqrt{2\pi}\sigma\right)^{m(N_0+1)}} \exp\left[-\frac{1}{2\sigma^2} J(\underline{\theta}; w)\right] \pi(\underline{\theta} \mid \mathsf{M}) \tag{2.18}$$

where

$$J(\underline{\theta}; w) = w_1 \sum_{r=1}^{m} \frac{[\lambda_r(\underline{\theta}) - \hat{\lambda}_r]^2}{\hat{\lambda}_r^2} + w_2 \sum_{r=1}^{m} \frac{\left\| \beta_r(\underline{\theta}) \underline{\phi}_r(\underline{\theta}) - \hat{\underline{\phi}}_r \right\|^2}{\left\| \hat{\underline{\phi}}_r \right\|^2} \tag{2.19}$$

represents the measure of fit between the experimentally obtained modal data and the modal data predicted by a particular model in the class M, and $\| \ \|$ is the usual Euclidian norm.

In particular, the optimal value $\hat{\underline{\theta}}$ of the model parameters corresponds to the most probable value that is obtained by maximizing the posterior probability distribution $p(\underline{\theta} \mid D, \mathsf{M})$ or, equivalently, minimizing the function

$$\begin{aligned} g(\underline{\theta}; \mathsf{M}) &= -\ln p(\underline{\theta} \mid D, \mathsf{M}) \\ &= [m(N_0 + 1)/2)][\sigma^{-2} J(\underline{\theta}; w) + \ln \sigma^2] - \ln \pi(\underline{\theta} \mid \mathsf{M}) \end{aligned} \tag{2.20}$$

For the case for which analytical expressions for $\Pi(\underline{\theta}; \mathsf{M}_i)$ are available, computationally efficient gradient-based optimization algorithms can be used to obtain the optimal value of the model parameters by minimizing the function $g(\underline{\theta}; \mathsf{M})$ with covariance equal to the inverse of the Hessian $h(\theta) = \underline{\nabla} \underline{\nabla}^T g(\underline{\theta}, \mathsf{M})$ of the function $g(\underline{\theta}; \mathsf{M})$ evaluated at the most probable value. For a uniform prior distribution, the most probable value of the FE model parameters $\underline{\theta}$ coincides with the estimate obtained by minimizing the weighted residuals in (2.10).

2.5 Bayesian Model Selection

The Bayesian probabilistic framework can also be used to compare two or more competing model classes and select the optimal model class based on the available

data. Consider a family $\mathsf{M}_{Fam} = \{\mathsf{M}_i \; i = 1, \cdots, k\}$, of k alternative, competing, parameterized FE and prediction error model classes, and let $\underline{\theta}_i \in R^{N_{\theta_i}}$ be the free parameters of the model class M_i. The posterior probabilities $P(\mathsf{M}_i \mid D)$ of the various model classes given the data D is [16]

$$P(\mathsf{M}_i \mid D) = \frac{p(D \mid \mathsf{M}_i)\; P(\mathsf{M}_i)}{p(D \mid \mathsf{M}_{Fam})} \tag{2.21}$$

where $P(\mathsf{M}_i)$ is the prior probability and $p(D \mid \mathsf{M}_i)$ is the evidence of the model class M_i. The optimal model class M_{best} is selected as the one that maximizes $P(\mathsf{M}_i \mid D)$ given by (2.21) . Model class selection is used to compare between alternative model classes and select the best model class (Muto and Beck, 2008), as well as for structural damage identification (Ntotsios et al., 2009).

2.6 Bayesian Uncertainty Propagation

Let q be an output quantity of interest in structural dynamics simulations. Posterior robust predictions of q are obtained by taking into account the updated uncertainties in the model parameters given the measurements D. Let $p(q \mid \underline{\theta}, \mathsf{M})$ be the conditional probability distribution of q given the values of the parameters. Using the total probability theorem, the posterior robust probability distribution $p(q \mid D, \mathsf{M})$ of q, taking into account the model M and the data D, is given by (Papadimitriou et al., 2001).

$$p(q \mid D, \mathsf{M}) = \int p(q \mid \underline{\theta}, \mathsf{M})\; p(\underline{\theta} \mid D, \mathsf{M})\; d\underline{\theta} \tag{2.22}$$

as an average of the conditional probability distribution $p(q \mid \underline{\theta}, \mathsf{M})$ weighting by the posterior probability distribution $p(\underline{\theta} \mid D, \mathsf{M})$ of the model parameters. Let $G(q; \underline{\theta})$ be a function of a deterministic output quantity of interest $q(\underline{\theta})$. A posterior robust performance measure of the system given the data D is (Papadimitriou et al., 2001).

$$E[G(q; \underline{\theta}) \mid D, \mathsf{M})] = \int G(q; \underline{\theta})\; p(\underline{\theta} \mid D, \mathsf{M})\; d\underline{\theta} \tag{2.23}$$

For $G(q; \underline{\theta}) = q(\underline{\theta})$ and $G(q; \underline{\theta}) = (q(\underline{\theta}) - E[q(\underline{\theta}) \mid D, \mathsf{M}])^2$, the measure (2.23) is the robust mean and the variance of the output quantity of interest q taking into account the model parameter uncertainties that are estimated by the data D.

2.7 Bayesian Tools

The Bayesian tools for identifying uncertainty models and performing robust prediction analyses are Laplace methods of asymptotic approximation and stochastic simulation algorithms.

2.7.1 Asymptotic Approximation

2.7.1.1 Parameter Estimation

For large enough number of measured data, the posterior distribution of the model parameters in (2.18) can be asymptotically approximated by a Gaussian distribution (Beck and Katafygiotis, 1998).

$$p(\underline{\theta} \mid D, \mathsf{M}) \approx \frac{|h(\underline{\hat{\theta}})|^{1/2}}{(2\pi)^{N_\theta/2}} \exp\left[-\frac{1}{2}(\underline{\theta}-\underline{\hat{\theta}})^T h(\underline{\hat{\theta}})(\underline{\theta}-\underline{\hat{\theta}})\right] \tag{2.24}$$

centered at the most probable value $\underline{\hat{\theta}}$ of the model parameters with covariance matrix equal to the inverse of the Hessian $h(\theta) = \underline{\nabla}\underline{\nabla}^T g(\underline{\theta}, \mathsf{M})$ of the function $g(\underline{\theta}; \mathsf{M})$ in (2.20) evaluated at the most probable value $\underline{\hat{\theta}}$. This approximation is also known as the Bayesian central limit theorem. The asymptotic expression (2.24), although approximate, provides a good representation of the posterior PDF for a number of applications involving even a relatively small number of data. Given the Gaussian approximation (2.24), the marginal distributions of the parameters are readily obtained to be Gaussian distributions with means and variances equal to the individual means appearing in the mean vector $\underline{\hat{\theta}}$ and the variances appearing in the diagonal elements of the covariance matrix $h^{-1}(\underline{\hat{\theta}})$

The asymptotic approximation (2.24) fails to provide an adequate representation of the posterior probability distribution in the case of multimodal distributions. To improve on the asymptotic approximation, one needs to identify all modes of the posterior PDF and consider them in the asymptotic expression by considering a weighted contribution of each mode with weights based on the probability volume of the PDF in the neighborhood of each mode (Beck and Katafygiotis, 1998). The weighted estimate is reasonable, provided that the modes are separable. For interacting modes or closely spaced modes, this estimate is inaccurate due to overlapping of the regions of high probability volume involved in the interaction. Numerical implementation problems arise in multi-modal cases, associated with the inconvenience in estimating all modes of the distribution (Metropolis et al., 1953). The asymptotic approximation fails to provide acceptable estimates for un-

identifiable cases (Katafygiotis and Lam, 2002), manifested for relatively large number of model parameters in relation to the information contained in the data.

The results from the asymptotic estimate are also useful for efficiently populating the posterior PDF with samples generating from MCMC algorithms. For uni-modal posterior PDFs, the asymptotic estimate can be performed as a first step in a Bayesian analysis to obtain information and identify the importance region in the parameter space of high posterior probability volume. Then the mode of the distribution can be used as a starting point of a stochastic simulation algorithm for exploring the support of the posterior PDF, while the Hessian at the mode provides valuable information for selecting the proposal PDF in MCMC algorithms. For multi-modal posterior PDFs with disjoint supports, the information from an asymptotic approximation may be misleading since other important regions in the parameter space may be easily missed. As a result, the stochastic simulation algorithms starting from the mode provided by the asymptotic estimate will usually fail to adequately explore the parameter space and identify the domains with high probability volume.

2.7.1.2 Model Selection

For model selection, an asymptotic approximation (Papadimitriou and Katafygiotis, 2001; Beck and Yuen, 2004; Yuen, 2010) based on Laplace's method can also be used to give an estimate of the evidence integral in (2.17) that appears in the model selection equation (2.21). Substituting this estimate in (2.21), the final asymptotic estimate for $P(\mathsf{M}_i \mid D)$ is given in the form

$$P(\mathsf{M}_i \mid D) = \frac{\sqrt{2\pi}^{\,n_i}\, p(D \mid \underline{\hat{\theta}}_i, \mathsf{M}_i)\; \pi(\underline{\hat{\theta}}_i \mid \mathsf{M}_i)}{p(D \mid \mathsf{M}_{Fam}) \det\left[h_i(\underline{\hat{\theta}}_i, \mathsf{M}_i)\right]} P(\mathsf{M}_i) \tag{2.25}$$

where $\underline{\hat{\theta}}_i$ is the most probable value of the parameters of the model class M_i and $h_i(\theta) = \nabla\nabla^T g_i(\underline{\theta}, \mathsf{M})$ is the Hessian of the function $g_i(\underline{\theta}_i; \mathsf{M}_i)$ given in (2.20) for the model class M_i. It should be noted that the asymptotic estimate for the probability of a model class M_i can readily be obtained given the most probable value and the Hessian of the particular mode. For the multi modal case the expression (2.25) can be generalized by adding the contributions from all modes.

2.7.1.3 Uncertainty Propagation

For the robust prediction integrals such as (2.22) or (2.23) a similar asymptotic approximation can be applied to simplify the integrals. Specifically, substituting

the posterior PDF $p(\underline{\theta} \mid D, \mathsf{M})$ from (2.16) into (2.23), one obtains that the robust prediction integral is given by (Papadimitriou et al., 2001).

$$E[G(q;\underline{\theta}) \mid D, \mathsf{M})] = \frac{\int G(\underline{\theta};\mathsf{M})\, p(D \mid \underline{\theta}, \mathsf{M})\, \pi(\underline{\theta} \mid \mathsf{M})\, d\underline{\theta}}{p(D \mid \mathsf{M})} \tag{2.26}$$

Introducing the function

$$r_G(\underline{\theta};\mathsf{M}) = -\ln[G(\underline{\theta};\mathsf{M})\, p(D \mid \underline{\theta}, \mathsf{M})\, \pi(\underline{\theta} \mid \mathsf{M})] \tag{2.27}$$

the integral in (2.26) takes the form of Laplace integral which can be approximated as before in the form:

$$\int \exp[-r_G(\underline{\theta})]\, d\underline{\theta} = \frac{\exp[-r_G(\tilde{\underline{\theta}})]\left[\sqrt{2\pi}\right]^m}{\det\left[H_G(\tilde{\underline{\theta}})\right]} \tag{2.28}$$

where $\tilde{\underline{\theta}}$ is the value of $\underline{\theta}$ that minimizes the function $r_G(\underline{\theta};\mathsf{M})$, and $H_G(\tilde{\underline{\theta}}, \mathsf{M})$ is the Hessian of the function $r_G(\underline{\theta};\mathsf{M})$ evaluated at $\tilde{\underline{\theta}}$. Substituting in (2.26), using (2.25) to asymptotically approximate the term $p(D \mid \mathsf{M})$ and replacing $r_G(\underline{\theta})$ by (2.27), it can be readily derived that $E[G(q;\underline{\theta}) \mid D, \mathsf{M})]$ is given by the asymptotic approximation (Tierney and. Kadane, 1986)

$$E[G(q) \mid D, \mathsf{M})] = G(\tilde{\underline{\theta}};\mathsf{M})\ \frac{p(D \mid \tilde{\underline{\theta}}, \mathsf{M})\pi(\tilde{\underline{\theta}} \mid \mathsf{M}) \det\left[h(\hat{\underline{\theta}}, \mathsf{M})\right]}{p(D \mid \hat{\underline{\theta}}, \mathsf{M})\pi(\hat{\underline{\theta}} \mid \mathsf{M}) \det\left[H(\tilde{\underline{\theta}}, \mathsf{M})\right]} \tag{2.29}$$

The error in the asymptotic estimate is of order N^{-2}. However, the asymptotic estimate requires solving two extra optimization problems, one for the mean and one for the variance of $G(q;\underline{\theta})$. In general, one needs to carry out N_G extra optimization problems, where $2N_G$ is the number of output quantities of interest. Such optimization problems are independent and can be performed in parallel. Similarly, the asymptotic approximation for the posterior robust probability distribution $p(q \mid D, \mathsf{M})$ of q is given by

$$p(q \mid D, \mathsf{M}) = p(q(\tilde{\underline{\theta}}(q));\mathsf{M})\ \frac{p(D \mid \tilde{\underline{\theta}}, \mathsf{M})\pi(\tilde{\underline{\theta}} \mid \mathsf{M}) \det\left[h(\hat{\underline{\theta}}, \mathsf{M})\right]}{p(D \mid \hat{\underline{\theta}}, \mathsf{M})\pi(\hat{\underline{\theta}} \mid \mathsf{M}) \det\left[H(\tilde{\underline{\theta}}, \mathsf{M})\right]} \tag{2.30}$$

where $\tilde{\underline{\theta}}(q)$ is the value of $\underline{\theta}$ that minimizes the function

$$r_p(\underline{\theta};\mathsf{M}) = -\ln[\, p(q \mid \underline{\theta},\mathsf{M})\; p(D \mid \underline{\theta},\mathsf{M})\; \pi(\underline{\theta} \mid \mathsf{M})] \tag{2.31}$$

and $H_p(\tilde{\underline{\theta}}(q),\mathsf{M})$ is the Hessian of the function $r_G(\underline{\theta};\mathsf{M})$ evaluated at $\tilde{\underline{\theta}}$. The estimate of the robust posterior probability distribution of q using (2.30) can be implemented efficiently in a parallel computer cluster, carrying out simultaneously the optimization problems for a range of q values.

2.7.1.4 Gradient-Based Optimization Algorithms

The optimization problems that arise in the asymptotic approximations are solved using available single objective optimization algorithms. The optimization of $g(\underline{\theta};\mathsf{M})$ given in (2.20), with respect to $\underline{\theta}$ can readily be carried out numerically using any available algorithm for optimizing a nonlinear function of several variables. In particular, iterative gradient-based optimization algorithms can be conveniently used to achieve fast convergence to the optimum. However, to guarantee the convergence of the gradient-based algorithms for models involving a relatively large number of DOFs, the gradient of the objective function with respect to the parameter set $\underline{\theta}$ has to be estimated with sufficient accuracy. It has been observed that numerical algorithms such as finite difference methods for gradient evaluation do not converge due to the fact that the errors in the numerical estimation may provide the wrong directions in the search space, especially for intermediate parameter values in the vicinity of a local/global optimum. The remedy is to provide analytical expressions for the gradients of the objective function. This, however, requires the development of the analytical equations for the gradients of the response quantities of interest involved in the objective function $g(\underline{\theta};\mathsf{M})$ which, for complex models of systems, might not be convenient or it may be impossible to accomplish for non-smooth systems.

Adjoint methods, if applicable for a system, provide a fast estimate of the gradients of the objective function with respect to all parameters, which is computationally very effective since it requires the solution of a single adjoint problem for finding the gradients, independently of the number of variables in the set $\underline{\theta}$. Example of adjoint methods for Bayesian parameter estimation can be found in (Ntotsios and Papadimitriou, 2008) for linear structural dynamics applications of the Bayesian framework based on modal frequencies and mode shapes. In particular, for linear representation of the stiffness and mass matrices with respect to the model parameters, adjoint methods can be made model non-intrusive. For nonlinear models of structures, the adjoint techniques are model intrusive, requiring tedious algorithmic and software development that in most cases are not easily integrated within the commercial software packages. Selected

examples of model intrusiveness includes the sensitivity formulation for hysteretic-type nonlinearities in structural dynamics and earthquake engineering [Barbato and Conte, 2005; Barbato et al., 2007) and the adjoint formulation for certain classes of turbulence models in computational fluid dynamics applications (Papadimitriou and Papadimitriou, 2013)

Independent of the computer resources available, a drawback of the gradient-based optimization algorithms is that they may convergence to a local optimum, failing to estimate the global optimum for the cases where multiple local/global optima exist.

2.7.1.5 Stochastic Optimization Algorithms

Evolution strategies are more appropriate and effective to use in cases of multiple local/global optima. Evolution strategies are random search algorithms that explore better the parameter space for detecting the neighborhood of the global optimum, avoiding premature convergence to a local optimum. A disadvantage of evolution strategies is their slow convergence at the neighborhood of an optimum since they do not exploit the gradient information. However, evolutionary strategies are highly parallelizable so the time to solution in a HPC environment is often comparable to conventional gradient based optimization methods, with the extra advantages that evolutionary stategies will have a better chance of finding the global optimum. In addition, stochastic optimization algorithms do not require the evaluation of the gradient of the objective function with respect to the parameters. Thus, they are model non-intrusive since there is no need to formulate the adjoint problem. In some cases the adjoint formulation requires considerable algorithmic development time to set up the equations for the adjoint problem and implement this formulation in software. In other cases (e.g. contact and impact problems) the development of an adjoint formulation or analytical equations for the sensitivity of objective functions to parameters is not possible.

Stochastic optimization algorithms can be used with parallel computing environments to find the optimum for non-smooth functions or for models that an adjoint formulation is not possible to develop. Examples include hysteretic models of structural components, as well as problems involving contact and impact. In the absence of a HPC environment, the disadvantage of the stochastic optimization algorithms arises from the high number of system re-analyses which may make the computational effort excessive for real world problems for which a simulation may take minutes, hours or even days to complete.

The covariance matrix adaptation (CMA) algorithm (Hansen et al., 2003) exhibits fast convergence properties among several classes of evolutionary algorithms, especially when searching for a single global optimum. The Hessian estimation required in Bayesian asymptotic approximations can be computed using the Romberg method (Lyness and Moler, 1969). This procedure is based on a number of system re-analyses at the neighborhood of the optimum, which can all be performed independently for problems involving either calibration or propagation, and are thus highly parallelizable.

Note that an alternative way for uncertainty propagation that can substantially expedite the propagation process as well as improve the accuracy of the estimates in a HPC environment is to draw samples from the asymptotic Gaussian posterior PDF and then provide a sampling estimate of the robust propagation integral. The sample generation from the Gaussian posterior PDF and the propagation to provide robust estimate of the uncertainties of a number of important quantities of interest are fully parallelized processes.

2.7.2 Stochastic Simulation Algorithms

It should be noted that the asymptotic approximation is valid if the optimal $\hat{\underline{\theta}}$ belongs to the domain $\underline{\Theta}$ of integration in (2.17). For the cases for which this condition is violated or for the case for which more accurate estimates of the integral are required, one should use stochastic simulation methods to evaluate the integral (2.17). The focus has thereby been put onto Markov Chain Monte Carlo methods (MCMC) which reveal to be very efficient and which can tackle all possible shapes of posterior pdfs. The basic principle of these methods is the use of Markov Chains which will be addressed in the following. Markov Chain Monte Carlo (MCMC) algorithms are used to efficiently draw samples from the posterior distribution. MCMC variants such as Differential Evolution MC (Braak et al. 2006) or Differential Evolution Random Subsampling MC (DREAM) (Braak et al. 2008) were introduced to improve parallel efficiency. These methods consist of a population of chains that interact by exchanging information but at the same time preserve the MCMC convergence characteristics at the individual chain level. Another MCMC method which can be categorized in the framework of Evolutionary Strategy MCMC methods (Drugan and Thierens 2010) is the TMCMC (Ching and Chen, 2007). This method is a generalization of the method proposed by Au and Beck (2002).extended by notions inherent to simulated annealing algorithms.

2.7.2.1 Metropolis Hasting Algorithm

The Metropolis algorithm (Metropolis et al., 1953) and its generalization to non-symmetric proposal densities denoted by Metropolis Hasting algorithm (Hastings, 1970) constitute the basis for Markov Chain Monte Carlo methods. Starting from any point $\underline{\theta}^{(0)}$ the algorithm generates a chain of length N , $\underline{\theta}^{(i)}, i=1,\cdots,N$ with stationary distribution $p(\underline{\theta})$ by using a transition kernel (namely the probability for a state to change its value). The scheme of the Metropolis Hasting algorithm is as follows:

1. Start with a value $\underline{\theta}^{(0)}$.
2. Using the current value, sample a candidate point $\xi^{(i+1)}$ from the proposal density $q(\xi|\underline{\theta}^{(i)})$ where q is an output quantity of interest in dynamic simulations.
3. Take $\underline{\theta}^{(i+1)}=\xi^{(i+1)}$ with probability $p(\xi^{(i+1)},\underline{\theta}^{(i)})$ or $\underline{\theta}^{(i+1)}=\underline{\theta}^{(i)}$ with probability $1-p(\xi^{(i+1)},\underline{\theta}^{(i)})$, where

$$p(\xi^{(i+1)},\underline{\theta}^{(i)})=\min(1,\frac{p(\xi^{(i+1)})q(\underline{\theta}^{(i)}|\xi^{(i+1)})}{p(\underline{\theta}^{(i)})q(\xi^{(i+1)}|\underline{\theta}^{(i)})} \tag{2.32}$$

4. Go to step no.2

The direct application of the Metropolis Hasting algorithm to sample from the posterior PDF in Bayesian updating reveals several difficulties. First, the shape of the posterior distribution is not known apriori which might lead to the situation that the starting sample is too far away from the target region. In addition, in case of a peaked posterior PDF, a large step size (i.e. a proposal density with a large standard deviation), the probability of reaching the area with high probability mass is very low. On the other hand, if the step size is small, the convergence might be too slow. Furthermore, the Markov Chain might get stuck in isolated modes of a multi-modal PDF, i.e. there is a very small chance to move out, because the sample will be rejected whenever it leaves this domain.

Hence, it is highly desirable to have an approach for stochastic simulation that is effective in all possible cases of the type of posterior PDF since its properties are not unknown beforehand. In the following, a frequently applied algorithms are presented.

2.7.2.2 Transitional Markov Chain Monte Carlo Algorithm

Among the stochastic simulation algorithms available, the transitional MCMC algorithm (Ching and Chen, 2007) which is a generalization of the MCMC

algorithm proposed by Beck is one of the most promising algorithms for selecting the most probable model as well as finding and populating with samples the importance region of interest of the posterior pdf in (2.18), even in the unidentifiable cases and multi-modal pdfs. The main idea of Transitional Markov Chain Monte Carlo (TMCMC) algorithm is to iteratively proceed from the prior to the posterior distribution. It starts with the generation of samples from the prior PDF in order to populate the space in which also the most probable regions of the posterior distribution lie. Then, some intermediate PDFs are defined, where the shape does not change remarkably from the intermediate PDF $p[j]$ to the next $p[j+1]$. The small change of the shape makes it possible to efficiently sample according to $p[j+1]$ if samples according to $p[j]$ have been generated. The intermediate distributions are defined by

$$p[j+1] \propto p(D|\underline{\theta},\mathsf{M})^{\beta_j} p(\underline{\theta},|\mathsf{M}) \tag{2.33}$$

with $j=0,\cdots,m$ as the step index and $0=\beta_0<\beta_1<\cdots,<\beta_m=1$ Hence, the exponent β_i can be interpreted as the percentage of the total information provided by the experimental data which is incorporated in the jth iteration of the updating procedure $\beta_0=0$ corresponds to the prior distribution and for $\beta_m=1$ the samples are generated from the posterior distribution.

Samples of the subsequent intermediate distribution $p[j+1]$ are obtained by generating Markov chains where the lead samples are selected from the distribution $p[j]$ by computing their probability weights with respect to $p[j+1]$, which are given by

$$w(\underline{\theta}_j^{(l)}) = \frac{p(D|\underline{\theta}^{(l)},\mathsf{M})^{\beta_{j+1}} p(\underline{\theta}^{(l)}|\mathsf{M})}{p(D|\underline{\theta}^{(l)},\mathsf{M})^{\beta_j} p(\underline{\theta}^{(l)}|\mathsf{M})} = p(D|\underline{\theta}^{(l)},\mathsf{M})^{\beta_{j+1}-\beta_j} \tag{2.34}$$

where the upper index $l=1,\cdots,N_j$ denotes the sample number in the jth iteration step. Each sample of the current step is generated using the Metropolis-Hastings algorithm: The starting point of a Markov chain is a sample from the previous step that is selected according to the probability equal to its normalized weight

$$\overline{w}(\underline{\theta}_j^{(l)}) = \frac{w(\underline{\theta}_j^{(l)})}{\sum_{i=1}^{Nj} w(\underline{\theta}_j^{(l)})} \tag{2.35}$$

and the proposal density for the Metropolis-Hastings algorithm is a Gaussian distribution centered at the preceding sample of the chain and with a covariance

matrix $\underline{\underline{\Sigma}}_0$ which is equal to the scaled version of the estimated covariance matrix of the current intermediate PDF:

$$\underline{\underline{\Sigma}}_0 = c^2 \sum_{l=1}^{Nj} \overline{w}(\underline{\theta}_j^{(l)})(\underline{\theta}_j^{(l)} - \overline{\underline{\theta}}_j^{(l)})(\underline{\theta}_j^{(l)} - \overline{\underline{\theta}}_j^{(l)})^T \tag{2.36}$$

Where

$$\overline{\underline{\theta}}_j = \sum_{l=1}^{N_j} \overline{w}(\underline{\theta}_j^{(l)})\underline{\theta}_j^{(l)} \tag{2.37}$$

The parameter c is a scaling parameter that is used to control the rejection rate of the Metropolis-Hastings algorithm at each step. The iterations are repeated until $\beta_j = 1$ is reached, i.e. until the samples are generated from the posterior distribution. Due to the repeated execution of the normal mode analysis of the FE-model, the computational effort of the Bayesian updating method might become infeasible for large FE-models. Hence, in order to reduce the wall clock time, i.e. the time between submitting the updating analysis and its completion, a parallelized version of this algorithm is presented in Section 2.8.2.

2.8 Computational aspects for linear FE models with large number of DOF

The computational demands in the aforementioned FE model updating methodologies depend highly on the number of FE analyses and the time required for performing a FE analysis. The optimal model in the proposed single optimization and the Pareto models in the multi-objective optimization can be estimated using available optimization algorithms. In particular, the optimization of $J(\underline{\theta};\underline{w})$ in (2.10) or $g(\underline{\theta};\mathbb{M})$ in (2.20) can readily be carried out numerically using any available gradient-based algorithm for optimizing a nonlinear function of several variables. In addition, the set of Pareto optimal solutions can be obtained using the Normal-Boundary Intersection (NBI) method [Das and Dennis, 1998), which is a very efficient algorithm for solving the multi-objective optimization problem defined in (Christodoulou and Papadimitriou, 2007). Each Pareto optimal solution is obtained by solving a single-objective optimization problem using gradient-based constrained optimization algorithms (Christodoulou et al., 2008). The computational time is of the order of the number of points used to represent the Pareto front multiplied by the computational time required to solve a single-objective optimization problem for computing each point on the front.

The gradient-based optimization algorithms require the estimation of the gradients of the residuals $J_1(\underline{\theta})$ and $J_2(\underline{\theta})$ defined in (2.7) and (2.8). This also contributes significantly to the time required to complete an iteration. Herein, Nelson method [Pradlwarter et al., 2002) is used to compute the gradients of the modal frequencies and mode shapes. The advantage of the Nelson's method compared to other methods (Hinke et al., 2009) is that the gradients of the modal frequency and mode shape of a mode are computed from the modal frequency and mode shape of the same mode and there is no need to compute the modal frequencies and mode shapes from other modes. Using adjoint formulations (Mace and Shorter, 2001), the computational demands for estimating the gradients of $J_1(\underline{\theta})$ and $J_2(\underline{\theta})$ are independent of the number of parameters involved in the vector $\underline{\theta}$. The most time consuming operation arises from the solution of a linear system with the matrix of coefficients to be a slightly modified version of the symmetric, non-positive definite, matrix $K-\lambda_r M$. This requires the factorization for the modified $K-\lambda_r M$ matrices of the lowest $r=1,\cdots,m$ modes involved in the residuals, contributing significantly to the overall computational effort at each iteration.

For objective functions in (2.4) involving multiple local/global optima, gradient based optimization algorithms may fail to converge to the global optimum. Stochastic optimization algorithms (Goller et al., 2011; Goller, 2011) are convenient tools for estimating the global optimum, avoiding premature convergence to a local one. These non-gradient based stochastic optimization algorithms require a significantly larger number of FE model re-analyses to be performed compared to the FE model analyses involved in gradient-based optimization algorithms, substantially increasing the computational demands.

The objective of this work is to examine the conditions under which substantial reductions in the computational effort can be achieved by integrating dynamic reduction techniques into the FE formulations, aiming at reducing the sizes of the stiffness and mass matrices and eliminating the expensive re-analyses of components eigenvalue problems due to the variations of the system parameters, without compromising the solution accuracy.

Furthermore, Bayesian FE model updating techniques, based on SSA such as the efficient TMCMC algorithm, involve drawing a large number of samples for tracing and then populating the important region in the uncertain parameter space. Compared to the previous algorithms, TMCMC require a substantially larger number of FE model analyses since one FE analysis is required for each sample generated in the TMCMC algorithm. Consequently, the computational demands

can become excessive when the computational time for performing a FE analysis is not negligible. The proposed Bayesian estimators requires a large number of FE model simulations to be carried out which imposes severe computational limitations on the application of the damage identification technique. For FE models involving hundreds of thousands or even million degrees of freedom and localized nonlinear actions activated during system operation these computational demands for repeatedly solving the large-scale eigen-problems and the gradient of the eigensolutions may be excessive.

2.9 Computational Challenges

For large order finite element models with hundreds of thousands or even million DOFs encountered in structural dynamics, the computational demands involved may be excessive, especially when a model simulation takes several minutes, hours or even days to complete. Drastic reductions in the time to solution are achieved by integrating surrogate models to reduce the number of full model simulations within certain classes of stochastic simulation algorithms such as TMCMC presented in Section 2.8.1, parallelization techniques to efficiently distribute the computations in available multi-core CPUs presented in Section 2.8.2 and model reduction techniques to substantially reduce the order of high fidelity large order finite element models presented in Section 2.8.3.

2.9.1 Surrogate Models

Surrogate models are used to reduce the computational time at the level of the algorithm. The objective is to avoid the full structural dynamics model runs at a sampling point in the parameters space by exploiting the function evaluations that are available at the neighbour (design) points in order to generate an approximate estimate. Surrogate models are well-suited to be used with the TMCMC method. Details of the implementation of surrogate models with TMCMC algorithm are given in Angelikopoulos et al. (2012). Specifically, following (Angelikopoulos et al., 2012), a kriging technique (Lophaven et al., 2002) is used to approximate the function evaluation at a new sampling point at a TMCMC stage using the function evaluations at neighbour points in the parameter space available from previous TMCMC stages. To ensure a high quality approximation, a surrogate estimate is accepted only if it satisfies certain conditions as follows.

The surrogate estimate is based on a user-defined number of support points which are in the neighbour of the surrogate point. The minimum number of support points depends on the dimension of the uncertain parameter space and the order of

the kriging interpolation. The surrogate point belongs to the convex hull of the design points so that an interpolation is performed, while extrapolations are prohibited. The design points correspond to actual system simulations and not other surrogate estimates from previous stages, avoiding error propagation and subsequent deterioration of the surrogate quality. The design point are kept the same when generating the surrogate estimates within a chain of the TMCMC stage, avoiding discontinuities in the estimates of the sampling points in a chain caused by changing the design points. The surrogate estimate is checked whether its predicted value is within the lower 95% quantile of all the design point's likelihood values accounted so far. The purpose of the threshold is to prevent overshooting surrogate estimates as this will quickly lead to the breakdown of the sampling procedure due to the concentration of most points around this overshooting estimate. The surrogate estimate is accepted if the prediction error is smaller than a user specified tolerance value.

It has been demonstrated that the proposed adaptive kriging method can achieve up to one order of magnitude reduction in computational effort.

2.9.2 Parallel TMCMC Algorithm

At the computer hardware level, high performance computing techniques can be used to reduce the computational time. Most MCMC algorithms involve a single Markov chain and are thus not parallelizable. In contrast, the TMCMC algorithm involves a large number of independent Markov chains that can run in parallel. Thus, the TMCMC algorithm is very-well suited for parallel implementation in a computer cluster. Specifically, parallelization is activated at every stage of the TMCMC algorithm exploiting the large number of short, variable length, chains that need to be generated starting from the leader samples determined from the TMCMC algorithm at the particular stage. Static and dynamic scheduling schemes can be conveniently used to optimally distribute these chains in a multi-host configuration of complete heterogeneous computer workers. The static scheduling scheme distributes the chains in the workers using a weighted round-robin algorithm so that the number of likelihood evaluations is arranged to be the same for each computer worker. The static scheduling scheme is computational efficient when the computational time for a likelihood evaluation is the same independently of the location of sample in the parameter space as well as when surrogate estimates are not activated. The dynamic scheduling scheme is more general, ensuring a more efficient balancing of the loads per computer worker in the case of variable run time of likelihood function evaluations and unknown number of surrogates activated during estimation. Specifically, each worker is

periodically interrogated at regular time intervals by the master computer about its availability and samples from TMCMC chains are submitted to the workers on a first come first serve basis to perform the likelihood function evaluations so that the idle time of the multiple workers is minimized. Details of the parallel implementation of the TMCMC algorithm are given in Angelikopoulos et al. (2012). (Haralampidis et al., 2005).

The highest computational efforts are associated to the solution of the eigenvalue problem which is required for the evaluation of the likelihood function. Hence, the parallelization strategy exploits the parallelism of those parts of the code where eigensolutions are performed.

The simulation algorithm starts with the generation of samples from the prior distribution and the evaluation of the probability weights $\overline{w}(\underline{\theta}_j^{(l)})$ according to (2.35) with $j=0$. This step can be scheduled completely in parallel since the samples are independent.

At the iteration steps $j=1,\cdots,m$ the lead samples are selected according to their probabilities given by (2.34) and then Markov chains are generated with the lengths equal to the number of times the respective lead samples are selected. Samples forming a Markov chain depend on the previous sample, which implies inherent dependence and which excludes therefore parallelization. However, the chains themselves are independent from each other, which means that the generation of different chains can be performed concurrently. The length of a chain, which is equal to the number of eigenvalue solutions and therefore proportional to the computational effort, is determined by the number of times the lead sample is selected and differs for each chain. In order to obtain an optimal work balance of each cluster node, the number of chains generated by each node is determined such that the total number of function evaluations is on average the same for each node.

Hence, the parallelized code works such that the master node determines the lead samples according to (2.34) and sends matrices with the parameter values of the lead samples together with the information about the length of the respective chains to the slaves. The generation of the Markov chains is performed in parallel. The matrices with the samples according to $p[j+1]$ are then sent back to the master node. After receiving all samples of this iteration step, the master node evaluates the probability weights needed for the next iteration. These iteration steps are repeated until samples of the posterior PDF are generated, i.e. until $j=m$

In the context of this thesis, only the so-called high-level parallelism associated with the consecutive execution of full FE-analysis, is exploited.

2.9.3 Model Reduction Techniques

Model reduction techniques can be applied at the system level to reduce the order of the model selected to simulate the behavior of the system. The objective is to obtain reduced models that run significantly faster than the original high-fidelity models, incorporating the important dynamics of the system analyzed so that the simulations from the reduced model are sufficiently accurate.

In structural dynamics, dynamic reduction techniques have been integrated with Bayesian techniques to carry out system analyses in a significantly reduced space of generalized coordinates and thus efficiently handle large-order models of hundreds of thousands or millions degrees of freedom and localized nonlinear actions activated during system operation. Specifically, component mode synthesis (CMS) techniques (Hurty, 1965; Craig and Bampton, 1968) can be used to alleviate the computational burden associated with each model run in the re-analyses required in the asymptotic and stochastic simulation methods. CMS techniques divide the structure into components with mass and stiffness matrices that are reduced using fixed-interface and constrained modes. Dividing the structure into components and reducing the number of physical coordinates to a much smaller number of generalized coordinates certainly alleviates part of the computational effort. However, at each iteration or TMCMC sampling point one needs to re-compute the eigen-problem and the interface constrained modes for each component. This procedure is usually a very time consuming operation and computationally more expensive that solving directly the original matrices for the eigenvalues and the eigenvectors, due to the substantial computational overhead that arises at component level.

The main objective in methods involving re-analyses of models with varying properties is to avoid, to the extent possible, the re-computation of the eigenproperties at the component or system level. Such techniques have been incorporated in methods for uncertainty management in structural dynamics to efficiently handle the computational effort in system re-analyses that arise from FE model variations caused by variations in the values of the uncertain parameters (Balmes, 1996; Mace and Shorter, 2001; Pradlwarter et al., 2002). In particular, perturbation techniques (Pradlwarter et al., 2002) provide accurate results locally for small variations of the model parameters about a reference structure. To improve the accuracy of the approximations for large variation of the model

parameters, methods have been proposed to approximate the modes at the component or system level in terms of the modes of a family of structures corresponding to support points in the parameter space (Hong, 2011). In Goller et al. (2011), linear and quadratic interpolations of the structural mass and stiffness matrix and the matrix of eigenvectors at the component and/or system level using support points in the larger region in the parameter space have been proposed. Such methods have been successfully used for model updating of large-order models of structures (Goller et al., (2011) and for damage detection at component level (Goller et al., (2011). These techniques proved to be quite effective in substantially reducing the computational demands in problems requiring system re-analyses. Fast and accurate CMS techniques, consistent with the finite element (FE) model parameterization, will be proposed in Chapter 3 of current thesis to achieve drastic reductions in computational effort.

2.10 Conclusions

The widely used deterministic finite element model updating methods are reviewed in this chapter and the Bayesian framework for parameter estimation and model class selection is presented. The Bayesian tools for identifying system and uncertainty models as well as performing model class selection are Laplace methods of asymptotic approximation and stochastic simulation algorithms such as Markov Chain Monte Carlo (MCMC) and Transitional MCMC. Both tools are used to represent the posterior distribution of the parameters of a model class introduced to simulate the behavior of the engineering system, as well as compute multidimensional integrals over high-dimensional spaces of the uncertain model parameters, manifested in the formulations for model class selection. The asymptotic approximations involve solving optimization problems as well as computing the Hessian of certain functions in a small number of points in the parameter space. The stochastic simulation tools involve generating samples for tracing and then populating the important uncertainty region in the parameter space, as well as evaluating integrals over high-dimensional spaces of the uncertain model parameters. These tools require a moderate to very large number of system re-analyses to be performed over the space of uncertain parameters. Consequently, the computational demands depend highly on the number of system analyses and the time required for performing a system analysis. For complex models of engineering systems, one simulation may require a significant amount of time and the overall computational demands involved in the Bayesian tools may be substantial, or even excessive for stochastic simulation algorithms.

This chapter proposes methods for drastically reducing the computational demands at the system, algorithm and hardware levels involved in the implementation of Bayesian tools.

CHAPTER 3 Component Mode Synthesis Techniques for FE Model Updating

3.1 Introduction

The optimization algorithms mentioned in Chapter 2 require a moderate to very large number of FE reanalyses to be performed over the space of model parameters. Consequently, the computational demands depend highly on the number of FE re-analyses and the time required for performing a FE analysis. In addition, gradient-based optimization algorithms require the estimation of the gradients of the residuals which may also add substantially to the computational effort. For high fidelity FE models involving hundreds of thousands or even million DOF, the computational demands may be large or even excessive. The present work proposes efficient methods based on dynamic reduction techniques to alleviate the computational burden involved in the implementation of deterministic and probabilistic (Bayesian) techniques for FE model updating.

Specifically, component mode synthesis (CMS) techniques (Hurty, 1965; Craig et al., 1965; Craig, 1981) are widely used to carry out system analyses in a significantly reduced space of generalized coordinates. Such techniques have been incorporated in methods for uncertainty management in structural dynamics to efficiently handle the computational effort in system re-analyses that arise from

FE model variations caused by variations in the values of the uncertain parameters (Balmes, 1996; Pradlwarter et al., 2002). Such variations in the values of the model parameters require that the computation of the component and/or system modes be repeated in each re-analysis. As a result, a computational overhead arises at component level which may be substantial. The main objective in methods involving re-analyses of models with varying properties is to avoid, to the extent possible, the recomputation of the eigenproperties at the component or system level. Perturbation techniques (Hinke et al., 2009; Mace and Shorter, 2001) provide accurate results locally for small variations of the model parameters about a reference structure. To improve the accuracy of the approximations for large variation of the model parameters, most efforts has been concentrated in approximating the modes at the component or system level in terms of the modes of a family of structures corresponding to support points in the parameter space (Balmes, 1996). Linear and quadratic interpolations of the structural mass and stiffness matrix and the matrix of eigenvectors at the component and/or system level using support points in the larger region in the parameter space have been proposed in (Goller et al., 2011). Such methods have been successfully used for model updating of large-order models of structures (Goller et al., 2011; Goller, 2011), while similar methods have been developed for damage detection at component level (Hong et al., 2011). Such techniques proved to be quite effective in substantially reducing the computational demands in problems requiring system re-analyses.

In this work, a framework is presented for integrating the Craig-Bampton CMS technique (Craig and Bampton, 1965; Craig, 1981) into existing FE model updating formulations in order to reduce the time consuming operations involved in reanalyses of large-order models of hundreds of thousands or millions degrees of freedom. The proposed method exploits the fact that in FE model parameterization schemes the stiffness matrix of the structure often depends linearly on the parameters of the model and also that a parameter usually represents a global property (e.g. the modulus of elasticity) of a substructure. The division of the structure into components is then guided by the FE parameterization scheme so that the stiffness matrix that arise for each one of the introduced components to depend linearly on only one of the parameters to be estimated. In this case the fixed-interface and constraint modes of the components for any value of the model parameters can be obtained exactly from the fixed-interface and constraint modes corresponding to a single reference FE model, avoiding re-analyses at component level. Additional substantial reductions in computational effort are also proposed by reducing the number of interface DOF

using characteristic interface modes through a Ritz coordinate transformation. The repeated solutions of the component and interface eigen-problems are avoided, reducing drastically the computational demands in FE formulations, without compromising the solution accuracy. It is also shown that the linear expansions of the original mass and stiffness matrices in terms of the structural parameters are preserved for the reduced mass and stiffness matrices. Thus, the reassembling of the reduced system matrices from the original matrices is also avoided in the execution of the system re-analyses. The only time consuming operation left is the re-analysis of the eigenproblem of the reduced-order model. It is finally demonstrated that the new developments are readily accommodated in existing FE model updating formulations and software with minimal modifications.

Moreover, in this chapter, Bayesian estimators (Christodoulou et al., 2008) are proposed for damage identification (localization and quantification) of civil infrastructure using vibration measurements. The structural damage identification is accomplished by associating a FE model class to a damage location pattern in the structure, indicative of the location of damage. Damage occurring at one or more structural components can be monitored by updating an appropriately parameterized FE model with parameters associated with the properties of the monitored structural components. The actual damage occurring in the structure is predicted by Bayesian model selection and updating of a family of parameterized model classes with the members in the model class family introduced to monitor the large number of potential damage scenarios covering most critical parts of the structure. Bayesian inference ranks the plausible damage scenarios according to the posterior probability of the corresponding parameterized FE model classes to fit the measurements. The most probable FE model class is indicative of the location of damage, while the severity of damage is inferred from the posterior probability of the model parameters of the most probable model class.

This Chapter is organised as follows. The mathematical background for the Craig-Bampton CMS technique and a technique to reduce the DOF in the interface between components using characteristic interface modes, is outlined in Section 3.2. The integration of the CMS technique with model updating formulations is given in Section 3.3. In Section 3.4 the effectiveness of the proposed algorithms, in terms of computational efficiency and accuracy, is demonstrated with application on model updating and damage identification of a bridge using simulated data and a high fidelity model with hundreds of thousands of DOF. Conclusions are summarized in Section 3.5.

3.2 Component Mode Synthesis

3.2.1 Formulation using fixed-interface modes

In CMS techniques (Craig and Bampton, 1965; Craig, 1981), a structure is divided into several components. For each component, the unconstrained DOF are partitioned into the boundary DOF, denoted by the subscript b and the internal DOF, denoted by the subscript i . The boundary DOF of a component include only those that are common with the boundary DOF of adjacent components, while the internal DOF of a component are not shared with any adjacent component. The stiffness and mass matrices K and M of a component s are partitioned to blocks related to the internal and boundary DOF as follows

$$M^{(s)} = \begin{bmatrix} M_{ii}^{(s)} & M_{ib}^{(s)} \\ M_{bi}^{(s)} & M_{bb}^{(s)} \end{bmatrix} \qquad K^{(s)} = \begin{bmatrix} K_{ii}^{(s)} & K_{ib}^{(s)} \\ K_{bi}^{(s)} & K_{bb}^{(s)} \end{bmatrix} \tag{3.1}$$

where the indices i and b are sets containing the internal and boundary DOF of the component. According to the Craig-Bampton fixed-interface mode method, the Ritz coordinate transformation $\underline{u}^{(s)} = [\underline{u}_i^{(s)T}, \underline{u}_b^{(s)T}]^T = \Psi^{(s)} \underline{p}^{(s)}$, where

$$\Psi^{(s)} = \begin{bmatrix} \Phi_{ik}^{(s)} & \Psi_{ib}^{(s)} \\ 0_{bk}^{(s)} & I_{bb}^{(s)} \end{bmatrix} \tag{3.2}$$

is used to relate the physical displacement coordinates $\underline{u}^{(s)} \in \mathbb{R}^{n^{(s)}}$ of the component to the generalized coordinates $\underline{p}^{(s)} = [\underline{p}_k^{(s)T}, \underline{p}_b^{(s)T}]^T \in \mathbb{R}^{\hat{n}^{(s)}}, \hat{n}^{(s)} = \hat{n}_k^{(s)} + \hat{n}_b^{(s)}$, using the kept fixed-interface normal modes $\Phi_{ik}^{(s)} \in \mathbb{R}^{n_i^{(s)} \times n_k^{(s)}}$ satisfying the eigen-problem

$$K_{ii}^{(s)} \Phi_{ik}^{(s)} = M_{ii}^{(s)} \Phi_{ik}^{(s)} \Lambda_{kk}^{(s)} \tag{3.3}$$

and the interface constrained modes $\Psi_{ib}^{(s)} \in \mathbb{R}^{n_i^{(s)} \times n_b^{(s)}}$ given by $\Psi_{ib}^{(s)} = -\left[K_{ii}^{(s)}\right]^{-1} K_{ib}^{(s)}$ .The matrix $\Lambda_{kk}^{(s)} = diag(\lambda_1^{(s)}, \cdots, \lambda_{\hat{n}_k^{(s)}}^{(s)}) \in \mathbb{R}^{\hat{n}_k^{(s)} \times \hat{n}_k^{(s)}}$ is diagonal containing the eigenvalues $\lambda_j^{(s)}$, $j = 1, \cdots, \hat{n}_k^{(s)}$, of the kept fixed-interface normal modes. The fixed-interface modes $\Phi_{ik}^{(s)}$ are considered to be mass normalized, satisfying $\Phi_{ik}^{(s)T} M_{ii}^{(s)} \Phi_{ik}^{(s)} = I_{kk}^{(s)}$ and $\Phi_{ik}^{(s)T} K_{ii}^{(s)} \Phi_{ik}^{(s)} = \Lambda_{kk}^{(s)}$

The component's mass and stiffness matrices $\hat{M}^{(s)} \in \mathbb{R}^{\hat{n}^{(s)} \times \hat{n}^{(s)}}$ and $\hat{K}^{(s)} \in \mathbb{R}^{\hat{n}^{(s)} \times \hat{n}^{(s)}}$ in the new reduced set of generalized coordinates $\underline{p}^{(s)}$ are transformed as follows

$$\hat{M}^{(s)} = \Psi^{(s)T} M^{(s)} \Psi^{(s)}, \qquad \hat{K}^{(s)} = \Psi^{(s)T} K^{(s)} \Psi^{(s)} \tag{3.4}$$

with the partitions for the component mass matrices $\hat{M}_{kk}^{(s)} \in \mathbb{R}^{\hat{n}_k^{(s)} \times \hat{n}_k^{(s)}}$, $\hat{M}_{kb}^{(s)} \in \mathbb{R}^{\hat{n}_k^{(s)} \times n_b^{(s)}}$, $\hat{M}_{bb}^{(s)} \in \mathbb{R}^{n_b^{(s)} \times n_b^{(s)}}$ and stiffness matrices $\hat{K}_{kk}^{(s)} \in \mathbb{R}^{\hat{n}_k^{(s)} \times \hat{n}_k^{(s)}}$, $\hat{K}_{kb}^{(s)} \in \mathbb{R}^{\hat{n}_k^{(s)} \times n_b^{(s)}}$ and $\hat{K}_{bb}^{(s)} \in \mathbb{R}^{n_b^{(s)} \times n_b^{(s)}}$ given respectively by

$$\begin{aligned} \hat{M}_{kk}^{(s)} &= I_{kk}^{(s)} \\ \hat{M}_{kb}^{(s)} &= \hat{M}_{bk}^{(s)T} = \Phi_{ik}^{(s)T} M_{ii}^{(s)} \Psi_{ib}^{(s)} + \Phi_{ik}^{(s)T} M_{ib}^{(s)} \\ \hat{M}_{bb}^{(s)} &= (\Psi_{ib}^{(s)T} M_{ii}^{(s)} + M_{bi}^{(s)}) \Psi_{ib}^{(s)} + \Psi_{ib}^{(s)T} M_{ib}^{(s)} + M_{bb}^{(s)} \end{aligned} \tag{3.5}$$

and

$$\begin{aligned} \hat{K}_{kk}^{(s)} &= \Lambda_{kk}^{(s)} \\ \hat{K}_{kb}^{(s)} &= \hat{K}_{bk}^{(s)T} = 0_{kb}^{(s)} \\ \hat{K}_{bb}^{(s)} &= K_{bb}^{(s)} - K_{bi}^{(s)} [K_{ii}^{(s)}]^{-1} K_{ib}^{(s)} = K_{bb}^{(s)} + \Psi_{ib}^{(s)T} K_{ib}^{(s)} \end{aligned} \tag{3.6}$$

For convenience, the relationships (3.5) and (3.6) between the reduced and the original stiffness and mass matrices of a component, with $\Lambda_{kk}^{(s)}$ and $\Phi_{ik}^{(s)}$ given by (3.3), can be written in compact form as $[\hat{K}^{(s)}, \hat{M}^{(s)}] = \mathbb{G}[K^{(s)}, M^{(s)}]$ using the operator $\mathbb{G}$

In the substructure assembly process, the vector $\underline{p} = [\underline{p}^{(1)T}, \cdots, \underline{p}^{(N_c)T}]^T \in \mathbb{R}^{n_p}$ of all generalized coordinates for each components is introduced. Letting $\underline{q} = [\underline{p}_k^{(1)T}, \cdots, \underline{p}_k^{(N_c)T}, \underline{u}_b^T]^T \in \mathbb{R}^{n_q}$ be the vector of independent generalized coordinates formed from the generalized coordinates (fixed-interface modal and boundary coordinates) of all components, where $\underline{u}_b^T = [\underline{u}_b^{(1)T}, \cdots, \underline{u}_b^{(N_b)T}]^T$ and N_b is the number of interfaces/boundaries, the following transformation is introduced

$$\begin{aligned} \hat{K}_{kk}^{(s)} &= \Lambda_{kk}^{(s)} \\ \hat{K}_{kb}^{(s)} &= \hat{K}_{bk}^{(s)T} = 0_{kb}^{(s)} \\ \hat{K}_{bb}^{(s)} &= K_{bb}^{(s)} - K_{bi}^{(s)} [K_{ii}^{(s)}]^{-1} K_{ib}^{(s)} = K_{bb}^{(s)} + \Psi_{ib}^{(s)T} K_{ib}^{(s)} \end{aligned} \tag{3.7}$$

where the component coupling matrix $S \in \mathbb{R}^{n_p \times n_q}$ couples the independent generalized coordinates with the generalized coordinates of each component.

The assembled Craig-Bampton stiffness matrix $\hat{K}^{CB} \in \mathbb{R}^{n_q \times n_q}$ and mass matrix $\hat{M}^{CB} \in \mathbb{R}^{n_q \times n_q}$ for the reduced vector $\underline{q}$ of generalized coordinates are given by

$$\hat{K}^{CB} = S^T \begin{bmatrix} \hat{K}^{(1)} & 0 & 0 \\ 0 & \ddots & 0 \\ 0 & 0 & \hat{K}^{(N_s)} \end{bmatrix} S = \sum_{s=1}^{N_s} \mathbb{F}_s[\hat{K}^{(s)}] \tag{3.8}$$

and

$$\hat{M}^{CB} = S^T \begin{bmatrix} \hat{M}^{(1)} & 0 & 0 \\ 0 & \ddots & 0 \\ 0 & 0 & \hat{M}^{(N_s)} \end{bmatrix} S = \sum_{s=1}^{N_s} \mathbb{F}_s[\hat{M}^{(s)}] \tag{3.9}$$

where the new mathematical operator $\mathbb{F}_s[\hat{K}^{(s)}]$ is conveniently introduced by the second part of equation (2.14) as

$$\mathbb{F}_s[\hat{K}^{(s)}] = S^T blockdiag(0_{\hat{n}^{(1)}\hat{n}^{(1)}}, \cdots, 0_{\hat{n}^{(s-1)}\hat{n}^{(s-1)}}, \hat{K}^{(s)}, 0_{\hat{n}^{(s+1)}\hat{n}^{(s+1)}}, \cdots, 0_{\hat{n}^{(Nc)}\hat{n}^{(Nc)}}) S \tag{3.10}$$

where $0_{ij} \in \mathbb{R}^{i \times j}$ denotes a matrix of zeroes, and $blockdiag[\hat{K}^{(1)}, \cdots, \hat{K}^{(N_c)}] \in \mathbb{R}^{n_p \times n_p}$ denotes a block diagonal matrix having as diagonal blocks the matrices $\hat{K}^{(s)}, s = 1, \cdots, N_c$. The operator $\mathbb{F}_s$ will be used later to simplify the integration of the CMS into the FE formulation.

Solving the reduced eigen-problem

$$\hat{K}^{CB} Q = \hat{M}^{CB} Q \, \Lambda \tag{3.11}$$

associated with the reduced mass and stiffness matrices $\hat{M}^{CB}$ and $\hat{K}^{CB}$, respectively, one obtains the modal frequencies in $\Lambda = diag(\omega_i^2) \in \mathbb{R}^{N_q \times N_q}$ and the corresponding mode shapes $Q = [\hat{q}_1, \cdots, \hat{q}_{n_q}] \in \mathbb{R}^{n_q \times n_q}$ of the reduced system.

Introducing the constant matrix $\hat{S} \in \mathbb{R}^{N_0 \times n_p}$ to map the vector $[\underline{u}^{(1)T}, \cdots, \underline{u}^{(N_c)T}]$ of the physical coordinates of each structural component to the physical coordinates $\underline{u}$ of the structure at N_0 measured DOF such that $\underline{u} = \hat{S}\underline{p}$ and using (3.7), the physical mode shapes $\underline{\phi}_r \in \mathbb{R}^{N_0}$ r of the original structure at the N_0 measured DOF are recovered from the mode shapes $\hat{q}_r \in \mathbb{R}^{n_q}$ of the reduced system as follows

$$\underline{\phi}_r = \hat{S} \Psi S \hat{q}_r = \hat{L} \hat{q}_r \tag{3.12}$$

where $\hat{L} = \hat{S}\Psi S \in \mathbb{R}^{N_0 \times n_q}$ and $\Psi = blockdiag[\Psi^{(1)}, \cdots, \Psi^{(N_c)}] \in \mathbb{R}^{n_p \times n_p}$

3.2.2 Reduction of the interface DOF using characteristic interface modes

Further reduction in the generalized coordinates can be achieved by replacing the interface DOFs by a reduced number of constraint interface modes (Castanier et al., 2001). For this, the physical displacement coordinates $\underline{u}_b^{\{l\}} \in \mathbb{R}^{m_b^{(l)}}$ at a boundary/interface between two or more components are represented in terms of the generalized coordinates $\underline{\zeta}^{\{l\}} \in \mathbb{R}^{m_k^{(l)}}$ of the interface by the Ritz coordinate transformation

$$\underline{u}_b^{\{l\}} = V^{\{l\}} \underline{\zeta}^{\{l\}} \tag{3.13}$$

$i = 1, \cdots, N_b$, where the columns of $V^{(l)} \in \mathbb{R}^{m_b^{(l)} \times m_k^{(l)}}$ form the reduced basis of the $m_b^{(l)}$-dimensional space.and $m_k^{(l)}$ is the number of elements in the basis.

The following transformation from the CMS generalized coordinates $\underline{q}$ to the reduced order model generalized coordinates $\underline{\upsilon} = [\underline{p}_k^{(1)T}, \cdots, \underline{p}_k^{(N_S)T}, \zeta^{\{1\}T}, \cdots, \zeta^{\{N_b\}T}]^T \in \mathbb{R}^{n_r}$, $n_r = \sum_{s=1}^{N_c} \hat{n}_k^{(s)} + \sum_{l=1}^{N_b} m_b^{(l)}$, that contains the kept fixed interface modes and the kept constraint interface modes, is introduced as

$$\underline{q} = V \underline{\upsilon} \tag{3.14}$$

where $V = blockdiag(I_{\hat{n}_k^{(1)}}, \cdots, I_{\hat{n}_k^{(N_c)}}, V^{\{1\}}, \cdots, V^{\{N_b\}}) \in \mathbb{R}^{n_q \times n_r}$ and I_n is the identity matrix of dimension n. Using (3.14), the reduced mass and stiffness matrices take the form $\hat{K} = V^T \hat{K}^{CB} V$ and $\hat{M} = V^T \hat{M}^{CB} V$ and the resulting eigenvalue problem at the reduced system level becomes

$$\hat{K} \Gamma = \hat{M} \Gamma \Lambda \tag{3.15}$$

where the diagonal matrix Λ contains the modal frequencies and the matrix $\Gamma \in \mathbb{R}^{n_r \times n_r}$ contains the corresponding n_r mode shapes of the reduced system.

The kept characteristic interface modes of the matrix $V^{\{l\}}$ satisfy the eigen-problem

$$\hat{K}_{\hat{b}_l \hat{b}_l}^{CB} V^{\{l\}} = \hat{M}_{\hat{b}_l \hat{b}_l}^{CB} V^{\{l\}} \Omega^{\{l\}} \tag{3.16}$$

where $\hat{b}_l$ is the index set denoting the positions of the generalized coordinates $\underline{u}_b^{\{l\}} \in \mathbb{R}^{m_b^{(l)}}$ in the vector $\underline{q}$ corresponding to the interface l, while the stiffness and mass matrices $\hat{K}_{\hat{b}_l \hat{b}_l}^{CB} \in \mathbb{R}^{m_b^{(l)} \times m_b^{(l)}}$ and $\hat{M}_{\hat{b}_l \hat{b}_l}^{CB} \in \mathbb{R}^{m_b^{(l)} \times m_b^{(l)}}$ in (3.16) are the partitions

of the reduced stiffness and mass matrices $\hat{K}^{CB}_{\hat{b}_l\hat{b}_l} \in \mathbb{R}^{m_b^{(l)}\times m_b^{(l)}}$ and $\hat{M}^{CB}_{\hat{b}_l\hat{b}_l} \in \mathbb{R}^{m_b^{(l)}\times m_b^{(l)}}$ associated with the coordinates $\underline{u}_b^{\{l\}} \in \mathbb{R}^{m_b^{(l)}}$ at the l-th interface. These partitions are readily obtained from the corresponding partitions of the stiffness and mass matrices of the components connecting to the interface l in the form

$$\hat{K}^{CB}_{\hat{b}_l\hat{b}_l} = \sum_{s\in C_l} \hat{K}^{(s)}_{b_lb_l} \tag{3.17}$$

and

$$\hat{M}^{CB}_{\hat{b}_l\hat{b}_l} = \sum_{s\in C_l} \hat{M}^{(s)}_{b_lb_l} \tag{3.18}$$

where C_l is the integer set that contains the components that connect to the interface l, and b_l is the index set corresponding to the interface l in the vector $\underline{u}^{\{s\}}$ of the component s. Note that the stiffness matrix $\hat{K}$ of the reduced system is diagonal, given by $\hat{K} = diag(\Lambda^{(1)}_{kk},\cdots,\Lambda^{(N_c)}_{kk},\Omega^{(1)}_{kk},\cdots,\Omega^{(N_B)}_{kk})$, with diagonal elements the eigenvalues of each fixed interface and constraint interface mode.

The components of the mode shape matrix $Q=[\underline{\hat{q}}_1,\cdots,\underline{\hat{q}}_{n_k}]\in\mathbb{R}^{n_q\times n_q}$ of the eigenvalue problem (3.11) are related to the components of the mode shape matrix $\Gamma=[\underline{\gamma}_1,\cdots,\underline{\gamma}_{n_r}]\in\mathbb{R}^{n_r\times n_r}$ of the eigenvalue problem (3.15) through the relationship $\underline{\hat{q}}_r = V\underline{\gamma}_r$. Specifically, using (3.12), the mode shapes $\underline{\phi}_r$ of the original structure at the N_0 measured DOF are recovered from the mode shapes $\underline{\gamma}_r$ of the reduced system as follows

$$\underline{\phi}_r = \hat{S}\Psi SV\underline{\gamma}_r = \hat{L}V\underline{\gamma}_r = \tilde{L}\underline{\gamma}_r \tag{3.19}$$

where $\tilde{L} = \hat{L}V = \hat{S}\Psi SV \in \mathbb{R}^{N_0\times n_r}$

3.3 Model Updating using CMS

The component mode synthesis procedure is next integrated into the finite element model updating formulation. The linear dependence of the mass and stiffness matrices on the parameter set $\underline{\theta}$ implies that at the component level the mass and stiffness matrices as well as their partitions admit a similar representation, that is

$$K^{(s)} = K_0^{(s)} + \sum_{i=1}^{N_\theta} K_{,j}^{(s)} \theta_j$$
$$M^{(s)} = M_0^{(s)} + \sum_{j=1}^{N_\theta} M_{,j}^{(s)} \theta_j \tag{3.20}$$

Attention is focused on two special cases of the parameterization (3.20) for a component s .In the first case (3.3.1) it is assumed that the mass and stiffness matrix of a component s do not depend on the model parameters in $\underline{\theta}$. In the second case (3.3.2) the stiffness matrix of a component s depends linearly only on one model parameter, say θ_j , in the parameter vector $\underline{\theta}$, while the mass matrix $M^{(s)} = M_0^{(s)}$ is constant independent of $\underline{\theta}$.

3.3.1 Component stiffness and mass matrix is constant

In this case one has that $K^{(s)} = K_0^{(s)}$ and $M^{(s)} = M_0^{(s)}$ The component fixed-interface and constrained modes are independent of the parameter values. Only a single analysis is required to estimate the fixed-interface and constrained modes for the particular component s . Within the model updating iteration scheme, these component modes are computed once and are then used in the iterations involved. The computational saving in the iterative process of model updating arises from the fact that the eigenvalue problem to compute the eigenvalues and mode shapes of the kept interface modes as well as the solution of the linear system to compute the constrained interface modes are not repeated at each iteration.

$$K^{(s)} = K_0^{(s)} + \sum_{i=1}^{N_\theta} K_{,j}^{(s)} \theta_j$$
$$M^{(s)} = M_0^{(s)} + \sum_{j=1}^{N_\theta} M_{,j}^{(s)} \theta_j \tag{3.21}$$

3.3.2 Component stiffness matrix is proportional to model parameters

This case is enforced by dividing the structure into components based on the parameters introduced in the FE model for each physical substructure. Let Δ_j be the set of components that depend on the j –th variable θ_j . The stiffness matrix of a component s takes the form

$$K^{(s)} = \bar{K}^{(s)} \theta_j \tag{3.22}$$

Equivalently, the relation (3.21) holds also for the partitions of the stiffness matrix. Substituting the partitions $K_{ii}^{(s)} = \bar{K}_{ii}^{(s)} \theta_j$ and $\mathrm{M}_{ii}^{(s)} = \bar{M}_{ii}^{(s)} \theta_j$ in (3.3), it is

readily derived that the matrix of the kept eigenvalues and eigenvectors of the component fixed-interface modes are given with respect to the parameter θ_j in the form

$$\Lambda^{(s)} = \bar{\Lambda}^{(s)}\theta_j \qquad \text{and} \qquad \Phi_{ik} = \bar{\Phi}_{ik}^{(s)} \tag{3.23}$$

where the matrices $\bar{\Lambda}^{(s)}$ and $\bar{\Phi}_{ik}^{(s)}$ are solutions of the following eigen-problem

$$\bar{K}_{ii}^{(s)}\bar{\Phi}_{ik}^{(s)} = \bar{M}_{ii}^{(s)}\bar{\Phi}_{ik}^{(s)}\bar{\Lambda}_{kk}^{(s)} \tag{3.24}$$

and thus they are independent of the values of θ_j or the FE model variations at the component level due to changes in the model parameter. Also using the stiffness matrix partitions $K_{ii}^{(s)} = \bar{K}_{ii}^{(s)}\theta_j$ and $K_{ib}^{(s)} = \bar{K}_{ib}^{(s)}\theta_j$, the constrained modes are given by the constant matrix

$$\Psi_{ib}^{(s)} = -[K_{ii}^{(s)}]^{-1}K_{ib}^{(s)} = -[\bar{K}_{ii}^{(s)}]^{-1}\bar{K}_{ib}^{(s)} \tag{3.25}$$

also independent of the values of the parameter θ_j or FE model variations at component level. Thus, a single component analysis is required to provide the exact estimate of the fixed-interface modes from (3.22) and the constrained modes from (3.24) for any value of the model parameter θ_j .

Substituting into the reduced mass and stiffness matrices (3.5) and (3.6) the partitions of the stiffness matrix (3.21), the eigenproperties (3.22) and the interface constraint modes (3.24) of the component s , it is straightforward to verify that the reduced stiffness matrix of component *s* takes the form

$$\hat{K}^{(s)} = \hat{\bar{K}}^{(s)}\theta_j \tag{3.26}$$

where the reduced matrix $\hat{\bar{K}}^{(s)}$ and the reduced mass matrix $\hat{M}^{(s)}$ are constant matrices given by $[\hat{\bar{K}}^{(s)}, \hat{M}^{(s)}] = \mathbb{G}[\bar{K}^{(s)}, M_0^{(s)}]$, independent of the values of the model parameters $\underline{\theta}$.

Introduce next the index set Σ to contain the structural components s that depend on a parameter in the vector $\underline{\theta}$. Then the set $\bar{\Sigma} = \{1, \cdots, N_s\} - \Sigma$ contains the component numbers for which their properties are constant and independent on the values of the parameter vector $\underline{\theta}$. Substituting (3.21) into (3.8), the stiffness matrix of the Craig-Bampton reduced system admits the representation

$$\hat{K}^{(s)} = \hat{\bar{K}}^{(s)}\theta_j \hat{K}^{CB} = \hat{K}_0^{CB} + \sum_{j=1}^{N_\theta} \hat{K}_{,j}^{CB}\theta_j \tag{3.27}$$

and the mass matrix is given by $\hat{M}^{CB} = \hat{M}_0^{CB}$, where the coefficient matrices $\hat{K}_0^{CB}$ and $\hat{K}_{,j}^{CB}$ in the expansion (3.26) are assembled from the component stiffness matrices, defined in (3.25), by

$$\hat{K}_0^{CB} = \sum_{s\in\bar{\Sigma}} \mathbb{F}_s[\hat{K}^{(s)}] \qquad \text{and} \qquad \hat{K}_{,j}^{CB} = \sum_{s_j\in\Delta_j} \mathbb{F}_s[\hat{\bar{K}}^{(s)}] \tag{3.28}$$

The sum in the second of (3.27) takes into account that more than one components $s \in \Delta_j$ may depend on the parameter θ_j.

It is important to note that the assembled matrices $\hat{K}_0^{CB}$ and $\hat{K}_{,j}^{CB}$ of the Craig-Bampton reduced system in the expansion (3.26) are independent of the values of $\underline{\theta}$. In order to save computational time, these constant matrices are computed and assembled once and, therefore, there is no need this computation to be repeated during the iterations involved in optimization due to the changes in the values of the parameter vector $\underline{\theta}$. This aforementioned procedure results in substantial computational savings since it avoids (a) re-computing the fixed-interface and constrained modes for each component, and (b) assembling the reduced matrices from these components. The formulation guarantees that the reduced system is based on the exact component modes for all values of the model parameters. In addition, using (3.19) and the fact that $\Psi^{(s)}$ and thus Ψ are independent of $\underline{\theta}$, the observation matrix $\hat{L} = \hat{S}\Psi S$ in (3.19) is constant, independent of the parameter vector $\underline{\theta}$.

The modal frequency and mode shape residuals involved in the objective $J(\underline{\theta};\underline{w})$ have the same exactly form as in finite element model updating without using CMS, with $\underline{\phi}_r(\underline{\theta})$ and the constant matrix L in $\underline{\phi}_r(\underline{\theta}) = L\underline{\varphi}_r(\underline{\theta})$ be replaced by $\underline{\hat{q}}_r(\underline{\theta})$ and the constant matrix $\hat{L} = \hat{S}\Psi S$, respectively. Available model updating formulations and software can thus be readily used to handle the parameter estimation by just replacing the eigenvalue problem of the original mass and stiffness matrices with the eigenvalue problem (3.11) of the reduced system matrices with $\hat{K}^{CB}(\underline{\theta})$ given by (3.26) and $\hat{\mathrm{M}}^{CB}(\underline{\theta}) = \hat{\mathrm{M}}_0^{CB}$, as well as replacing the constant matrix L of zeros and ones by the constant matrix $\hat{L} = \hat{S}\Psi S$.

Special attention should be given when the size of the reduced mass and stiffness matrices are dominated by a large number of interface DOF. In this case, the

coordinate transformation (3.13) can be used to further reduce the number of interface DOF for one or more interfaces. Using (3.18), it is clear that the stiffness matrix of the eigenvalue problem involved in (3.16) depends on the parameters associated with the components that connect to the interface l. The variability of these parameters affects the characteristic interface modes V_l which are functions of these parameters. Exact estimates of the characteristic interface modes in iterative algorithms can only be obtained by repeatedly solving (3.16) for each different value of the respective parameters. For large number of DOF at the interface, such re-analyses at the interface level may increase substantially the computational demands. Interpolation schemes (Teughels et al., 2003) can be used to approximate the characteristic interface modes at the interface level in terms of the characteristic interface modes at a number of support points in a significantly reduced space of model parameters associated with the components that connect to the interface.

Alternatively, selecting V_l in (3.13) to be constant, independent of , the formulation significantly simplifies, with the reduced stiffness matrix to be given by

$$\hat{K} = \hat{K} + \sum_{j=1}^{N_\theta} \hat{K}_{,j}\theta_j \tag{3.29}$$

where $\hat{K}_0 = V^T \hat{K}_0^{CB} V$ and $\hat{K}_{,j} = V^T \hat{K}_{,j}^{CB} V$ are constant matrices, while the reduced mass matrix be given by the constant matrix $\hat{M}_0 = V^T \hat{M}_0^{CB} V$. The modal frequency and mode shape residuals involved in the objective function $J(\underline{\theta}; \underline{w})$ in the model updating formulations have exactly the same form as in finite element model updating without using CMS with $\underline{\phi}_r(\underline{\theta})$ and the constant matrix L in $\underline{\phi}_r(\underline{\theta}) = L\underline{\varphi}_r(\underline{\theta})$ be replaced by $\underline{\gamma}_r(\theta)$ defined in (3.15) and the constant matrix $\hat{L} = \hat{S}\Psi SV$ defined in (3.19), respectively. The choice of constant V_l is critical in order to get accurate results with the least number of characteristic interface modes over the region of variation of the model parameters associated with the interface l. In FE model updating, the V_l can be chosen as the eigenvectors of the lowest modes of the eigenvalue problem (3.16) corresponding to a reference model of the structure, avoiding the computational cost involved with the repetitive solution of (3.16) at each iteration. This, however, may deteriorate the accuracy of the predictions for large variations of the model parameters. To improve convergence and maintain the accuracy of the final optimal estimate in iterative optimization algorithms, the reduced basis forming V_l can be updated

every few iterations The computational efficiency and accuracy of reducing the interface DOF using constant V_l will be demonstrated in the application section.

It should be pointed out that the significant savings arising partly from the reduction of the size of the eigenvalue problem from n to n_r in the proposed model reduction technique and partly from the fact that the estimation of the the component fixed-interface modes and the characteristic interface modes need not to be repeated for each iteration involved in the algorithms. Moreover, for gradient-based optimization algorithms required in model updating schemes, further computational savings are obtained due to the reduction of the size of the matrix of the linear system that needs to be factorized in the adjoint formulation (COMSOL AB COMSOL Multiphysics User's Guide, 2005), from the size n for the full matrices $K-\lambda_r M$ to the size n_r for the reduced-order matrices $\hat{K}-\lambda_r \hat{M}$.

Attention should also be paid on the optimal number of components that should be used to represent a substructure with stiffness that depends linearly on a single parameter. More components within such substructure introduce extra interface DOFs or characteristic interface modes which increase the size and affect the sparsity structure of the reduced matrices $\hat{K}$ and $\hat{M}$. The total size of the reduced matrices is also affected by the number of the fixed interface modes for all components introduced for the substructure. From the computational point of view, the optimal choice of components for such a substructure would be to select the number of components and the optimal spatial division which will result in a reduced system that requires the least computational time for analysis. However, as the number of interface DOFs or characteristic interface modes increases by the introduction of more components per substructure, it is unlikely that the resulting increase in the size of the reduced matrices be effectively compensated by a decrease in the total number of fixed interface modes arising from the multiple components that represent the single substructure. Thus, in case where detailed optimal component selection studies are not available, the wisest choice is to select a single component per substructure.

Following the formulation proposed, the aforementioned framework can be extended to handle the case for which the component stiffness and mass matrices depend nonlinearly on a single parameter θ_j of the system parameter set $\underline{\theta}$. This is the case for which the stiffness and mass matrices of a component $s \in \Delta_j$ depend nonlinearly on θ_j, i.e. $K^{(s)} = \bar{K}^{(s)} f^{(s)}(\theta_j)$ and $M^{(s)} = \bar{M}^{(s)} g^{(s)}(\theta_j)$, where $f^{(s)}(\theta_j)$ and $g^{(s)}(\theta_j)$ are nonlinear functions of the parameter θ_j. The

interface modes, the modal frequencies and the interface constrained modes of a component can readily be computed by the corresponding interface modes, modal frequencies and interface constrained modes of the same component for a reference structural configuration corresponding to a particular nominal value of the parameter set $\underline{\theta}$ as well as the current value of the parameter θ_j. In the nonlinear case, a representation similar to $\hat{K}^{CB} = \hat{K}_0^{CB} + \sum_{j=1}^{N_\theta} \hat{K}_{,j}^{CB} \theta_j$ and $\hat{\mathrm{M}}^{CB} = \hat{\mathrm{M}}_0^{CB}$ is no longer applicable and the reduced mass and stiffness matrices of the reduced structure should be re-assembled from the component mass and stiffness matrices for the new value of θ_j. This procedure also saves substantial computational effort since it avoids re-computing the fixed-interface and constrained modes for each component.

As a final note, it is worth mentioning the treatment of a component in the CMS process for the general case for which the component stiffness and mass matrices depends on two or more parameters in the vector $\underline{\theta}$. In these cases, in order to obtain exact estimates of the component modes, the solution of the eigenvalue problems for such a component is not avoided. The fixed-interface and characteristic interface modes have to be recomputed in each iteration involved in the model updating procedure and used to form the reduced stiffness and mass matrices of the components. This repeated computation, however, is usually confined to a small number of components. Interpolation schemes can also be adopted to avoid re-analyses at the component or interface level by approximating the fixed interface modes and/or the characteristic interface modes at various values of the model parameters in terms of the corresponding modes of a family of models defined at a number of support points in the parameter space (Teughels et al., 2003). However, it should be pointed out that the use of interpolating schemes for approximating the fixed interface and the characteristic interface modes is an open issue and further analyses are required to evaluate the effectiveness of such techniques in the general case.

3.4 Applications

The purpose of the application is to demonstrate the computational efficiency and accuracy of the proposed component mode synthesis technique for finite element model updating. For this, the method is applied to update a model of the Metsovo bridge of Egnatia Odos motorway, shown in Figure 3.1.

3.4.1 Description and FE Model of Metsovo Bridge

The Metsovo bridge is the highest reinforced concrete bridge of Egnatia Odos motorway located in Greece, with the height of the taller pier P2 equal to 110m. The total length of the bridge is 537m. The bridge has 4 spans, of length 44.78m, 117.87m, 235.00m, 140.00m and three piers of which pier P1, 45m high, supports the boxbeam superstructure through pot bearings (movable in both horizontal directions), while P2 and P3 piers (110 m and 35 m, respectively) connect monolithically to the superstructure. The total width of the deck is 13.95m. The superstructure is prestressed of single boxbeam section, of height varying from the maximum 13.5m in its support to pier P2 to the minimum 4.00m in key section. Piers P2 and P3 are founded on huge circular Ø12.0m rock sockets in the steep slopes of the Metsovitikos river, in a depth of 25m and 15m, respectively.

Figure 3.1: General View of Metsovo bridge.

The commercial software package COMSOL Multiphysics [36] is used for developing the FE model of the bridge. For this, the structure was first designed in CAD environment and then imported in COMSOL Multiphysics modelling

environment. The models were constructed based on the design plans, the geometric details and the material properties of the structure. The following nominal values of the material properties of the concrete deck, piers and foundations are considered. For the concrete deck, the nominal value of the Young's modulus is taken to be $E = 37Gpa$, the Poison's ratio $\nu = 0.2$ and the density $\rho = 2548kg/m^3$. For the piers and the foundation the nominal value of the Young's modulus is taken to be $E = 34Gpa$. A detailed FE model is created using three-dimensional tetrahedron quadratic Lagrange finite elements to model the whole bridge. An extra coarse mesh with quadratic Lagrange elements are chosen to predict the lowest 20 modal frequencies and mode shapes of the bridge. The selected model has 97,636 finite elements and 562,101 DOF.

3.4.2 Effectiveness of CMS technique

For demonstration purposes, the bridge is divided into nine physical components shown schematically in Figure 3.2.. Six components are related to the four spans of the bridge deck, while three components are related to the three piers. The eight interfaces between the components are also shown in Figure 3.2..

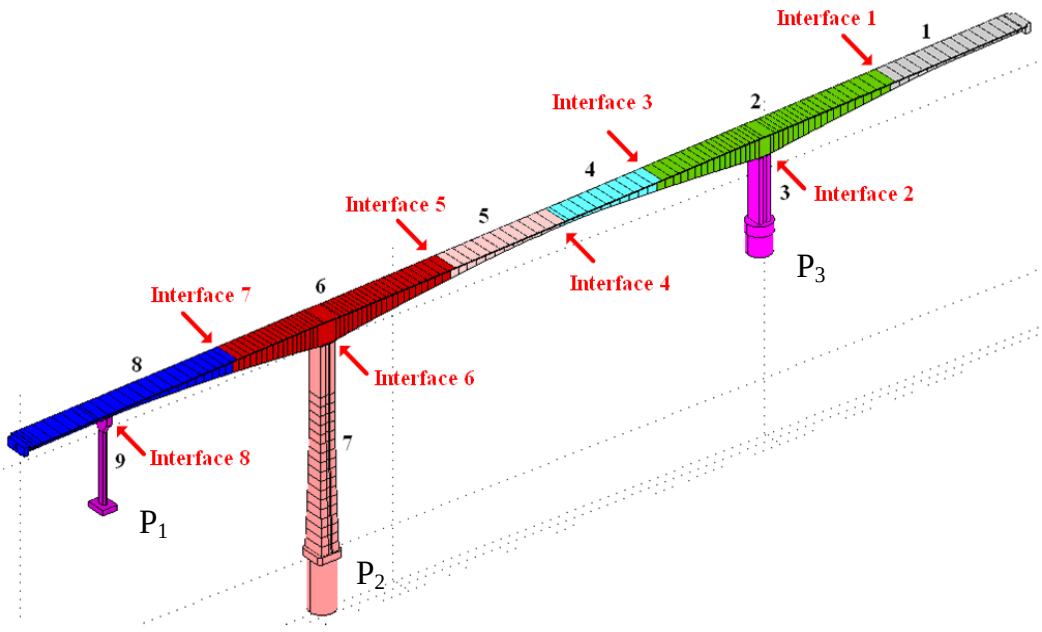

Figure 3.2: Components of FE model of Metsovo bridge

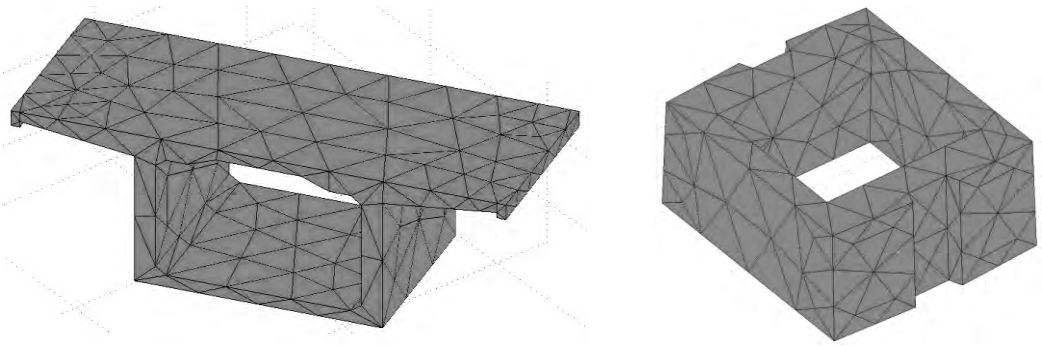

(a) (b)

Figure 3.3: (a) A typical 5m section of the deck with its FE mesh, (b) a typical 4m section of the tallest pier with its FE mesh.

Each deck component consists of several 4-5m deck sections. A typical 5m section is shown in Figure 3.3 (a) along with its FE mesh. The tallest pier also consists of several sections. A typical 4m pier section is also shown in Figure 3.3 (b) along with its FE mesh. It should be noted that the size of the elements in the FE mesh is the maximum possible one that can be considered, with typical element length of the order of the thickness of the deck cross-section. The entire simulation for assembling the mass and stiffness matrices of the structure or its components is performed within the COMSOL Multiphysics modelling environment and exported in Matlab environment for further processing using CMS techniques and FE model updating software.

The cut-off frequency ω_c is introduced to denote the highest modal frequency value that is of interest in FE model updating. In this study the cut-off frequency is selected to be equal to the 20th modal frequency of the nominal model. For the specific model, this frequency is obtained from modal analysis to be $\omega_c = 4.6$ Hz. The effectiveness of the CMS technique as a function of the number of modes retained for each component is next evaluated. For each component it is selected to retain all fixed interface modes that have frequency less than $\omega_{\max} = \rho\omega_c$, a multiple of the cut-off frequency ω_c , where the value of the multiplication factor ρ affects computational efficiency and accuracy of the model reduction technique. Representative values of ρ range from 2 to 10. The total number of internal DOF and retained modes for $\rho = 8$, $\rho = 5$ and $\rho = 2$ within all the components are reported in the second row of Table 3.1.

Table 3.1: Total number of internal and interface DOF for the full (unreduced) and reduced models.

Interfaces	Structure without Reduction	Retained modes $\rho=8$, $\nu=200$	Retained modes $\rho=5$, $\nu=200$	Retained modes $\rho=2$, $\nu=200$
Total Internal DOFs	558,801	286	100	31
Total Boundary DOFs	3.300	306	306	306
Total DOFs	562,101	592	406	337

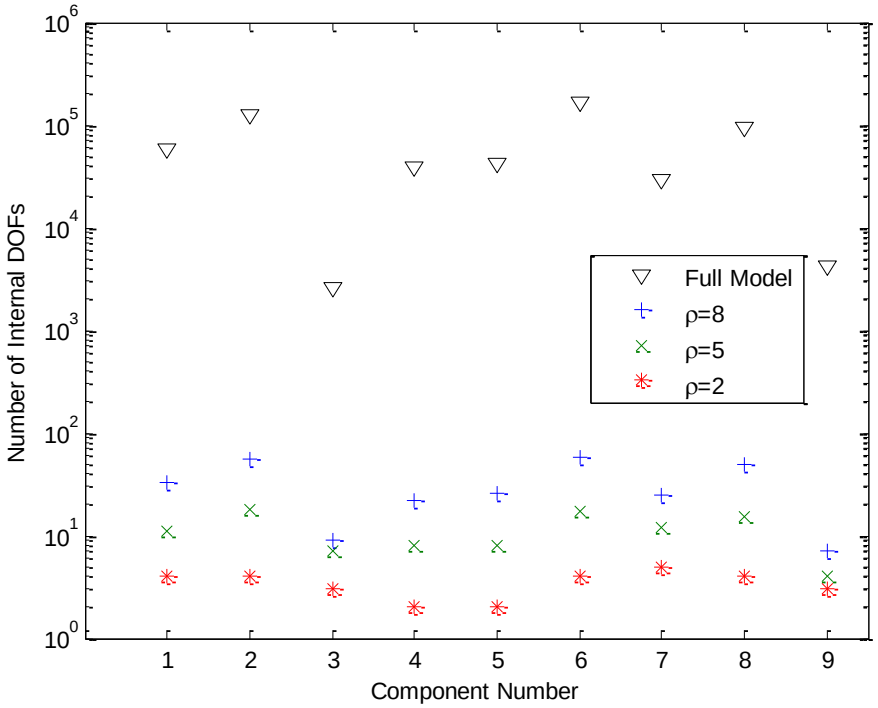

Figure 3.4: Number of DOF per component of the FE model of Metsovo bridge.

The total number of internal and boundary DOF of the unreduced model are reported in the second column of Table 3.1 based on the components and interfaces shown in Figure 3.2. The total number of internal DOF per component and the number of modes retained per component for different values is shown in Figure 3.4. It is clear from the results in Table 3.1 and Figure 3.4 that a more than three orders of magnitude reduction in the number of DOF per component is achieved using CMS. For the case $\rho = 8$, a total of 286 internal modes out of the 558,801 are retained for all 9 components. Figure 3.5 shows the fractional error between the modal frequencies computed using the complete FE model and the modal frequencies computed using the CMS technique as a function of the mode number for $\rho = 2$, $\rho = 5$ and $\rho = 8$. It can be seen that the fractional error for the lowest 20 modes fall below 10^{-4} for $\rho = 8$, 10^{-3} for $\rho = 5$ and 10^{-2} for $\rho = 2$, which ensures high levels of accuracy. The total number of DOF of the reduced model $\rho = 8$ is 3,586 which consist of 286 fixed interface generalized coordinates and 3,300 constraint interface DOF for all components.

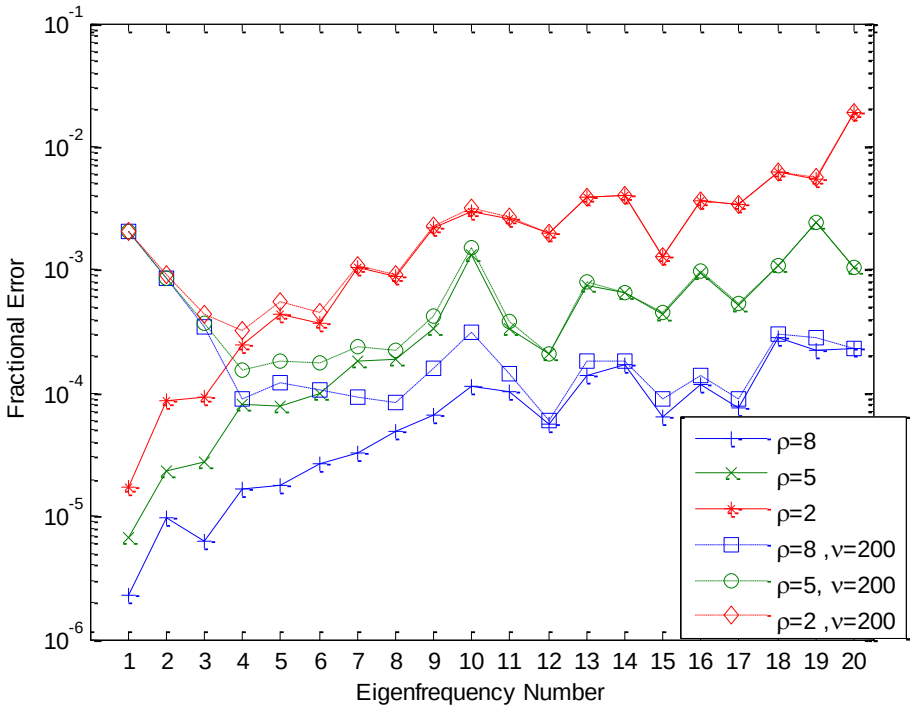

Figure 3.5: Fractional modal frequency error between the predictions of the full model and the reduced model as a function of eigenmode number and for different values of ρ and ν .

It is thus obvious that a large number of generalized coordinates for the reduced system arises from the interface DOF. A further reduction in the number of generalized coordinates for the reduced system can be achieved by retaining only a fraction of the constrained interface modes.

The number of DOF per interface is shown in the third column of Table 3.2. For each interface defined in Table 3.1, it is selected to retain all modes that have frequency less than $\omega_{\max}$, a multiple of the cutoff frequency ω_c , where the multiplication factor ρ is user and problem dependent. The number of modes retained per interface for $\nu = 200$ is given in the last column of Table 3.2. The number of retained interface modes is approximately 10% of the interface DOF for each interface. Figure 3.5 presents results for the fractional error between the modal frequencies computed using the CMS method with retained characteristic interface modes for $\nu = 200$ for each interface and the modal frequencies computed using the complete FE model as a function of the mode number. It can be seen that the fractional error for most of the lowest 20 modes of the structure fall well below 10^{-3} for $\nu = 200$ and ρ values as low as $\rho = 5$. Thus, the value of $\nu = 200$ gives accurate results in this case, while the number of retained interfaces modes for all interfaces is 306 which corresponds to 10% of the total number of interface DOF.

Table 3.2: Information for each interface involved in the modelling (with number of interface DOFs)

Interfaces	Adjacent Components	Interface DOFs	Retained modes $\nu = 200$
1	1-2	441	46
2	2-3	258	27
3	2-4	432	47
4	4-5	441	42
5	5-6	423	46
6	6-7	660	33
7	6-8	495	49
8	8-9	150	16
Total DOFs		3,300	306

The reduced system for $\rho = 5$ and $\nu = 200$ has 406 DOF from which 100 generalized coordinates are fixed-interface modes for all components and the rest 306 generalized coordinates are characteristic interface modes for all 8 interfaces. Obviously the number of generalized coordinates is drastically reduced by more than three orders of magnitude compared to the number of DOF of the original unreduced FE model. The significant reduction in number of generalized coordinates of the reduced system and the increased accuracy of the results are promising for using the proposed model reduction method in FE model updating.

3.4.3 FE model updating using sinle- and multi- objective formulation

For demonstration purposes, the FE model is parameterized using five parameters associated with the modulus of elasticity of one or more structural components shown in Figure 3.2. The parameterization is graphically depicted in Figure 3.6. Specifically, the first two parameters θ_1 and θ_2 account respectively for the modulus of elasticity of the pier components 3 and 7 of the bridge. The parameter θ_3 accounts for the modulus of elasticity of the components 1 and 2 of the deck,

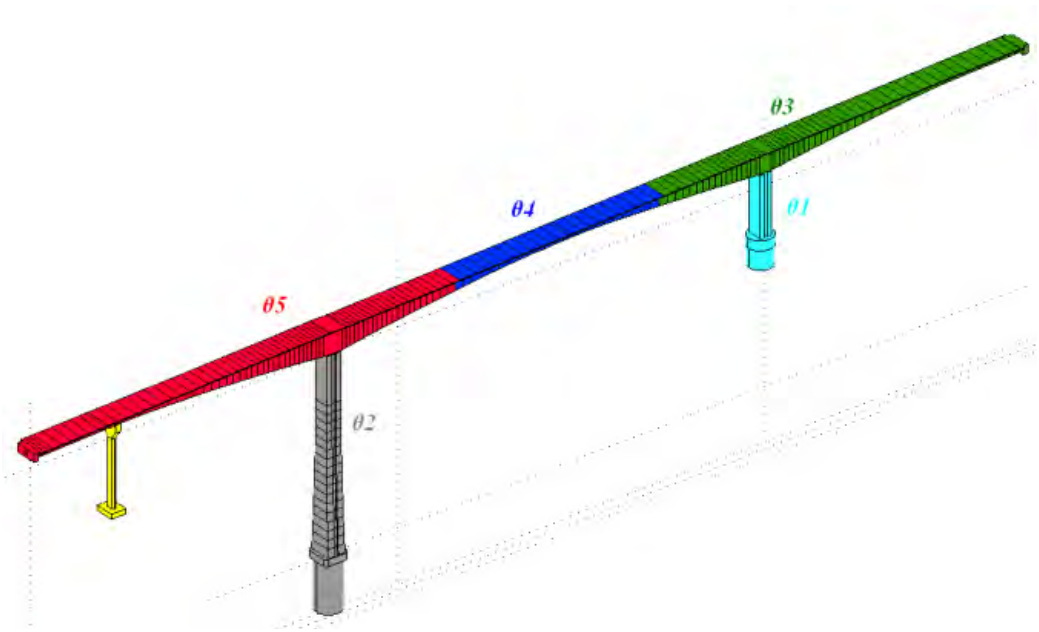

Figure 3.6: FE model parameterization based on 5 parameters.

the parameter θ_4 accounts for the components 4 and 5, while the parameter θ_5 accounts for the components 6 and 8. Note that for the three substructures

parameterized by a single parameter θ_3 , θ_4 or θ_5 , two components per substructure have been introduced, demonstrating the flexibility of the proposed methodology. The component 9 is not parameterized. The parameters are introduced to scale the nominal values of the properties that they model so that the value of the parameters equal to one correspond to the nominal value of the FE model. The nominal FE model corresponds to values of $\theta_1 = \cdots = \theta_5 = 1$.

For the purpose of the present analysis, simulated, noise contaminated, measured modal frequencies $\hat{\omega}_r^2$ and mode shapes $\hat{\underline{\phi}}_r$ are generated by perturbing the values of the modal properties $\omega_{0,r}$ and $\underline{\varphi}_{0,r}$, corresponding to the nominal FE model for $\underline{\theta} = 1$, according to the expressions $\hat{\omega}_r^2 = \omega_{0,r}(1+n_r)$ and $\hat{\underline{\phi}}_r = \underline{\varphi}_{0,r} + \|\underline{\varphi}_{0,r}\| \underline{e}_r$, where $n_r \sim N(0, s^2)$ are samples from a zero-mean normal distribution with variance s^2 , and $\underline{e}_r$ is a zero-mean normal random vector with diagonal covariance matrix $e^2 I$. The standard deviations s and e of the perturbed terms control mainly the size of the model and measurement errors for the modal frequencies and the mode shapes. The assumed constant noise level for the different modeshape components may not exactly reflect the actual differences

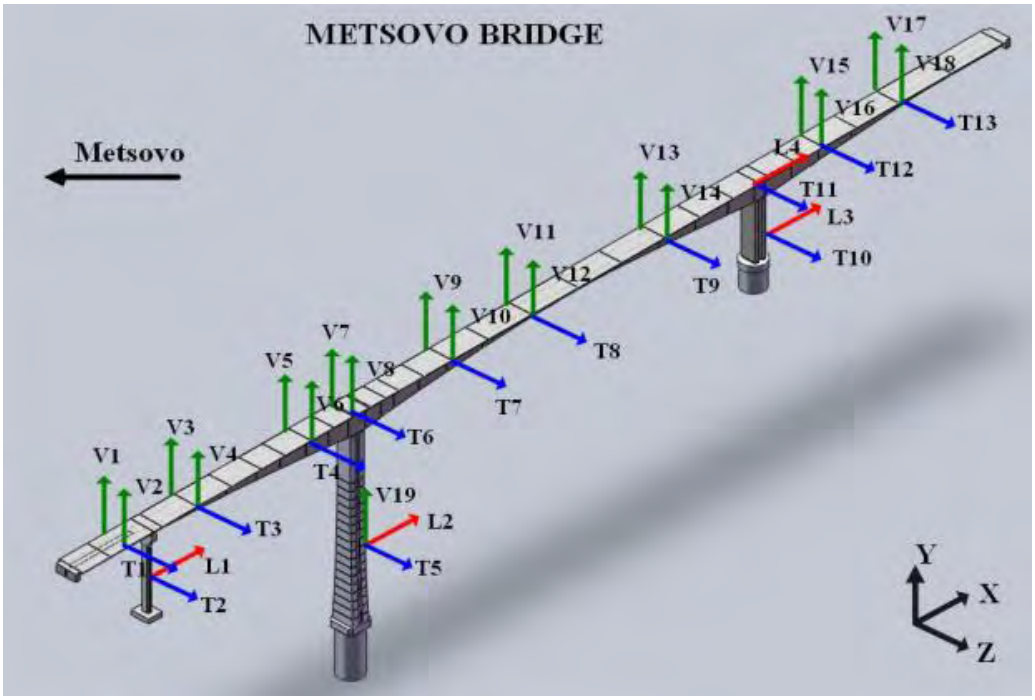

Figure 3.7: Sensor configuration involving 36 sensors.

observed in real applications between the predictions from a model and the actual behavior of the structure since model error will cause dissimilar noise levels at different modeshape components. However, for the purpose of this study, which is to demonstrate the efficiency of the proposed CMS scheme, the addition of constant noise level to different modeshape components is sufficient. Herein, the magnitudes of the error terms are chosen to be $s_r = 1\%$ and $e_r = 3\%$.

The FE model is updated using the simulated modal data for the lowest ten modes. A sensor configuration involving 36 sensors is considered. The sensors are placed along the deck and the piers at the locations and directions as shown in Figure 3.7, measuring along the longitudinal, transverse and vertical directions.

To investigate the accuracy and computational efficiency of the proposed CMS formulation, the FE model updating is first performed using the single objective optimization method by selecting the weight in (4) to be $w = 1$. Results for the accuracy of the model parameters and the computational effort are presented in Table 3.3 for the following six cases involving different reduction schemes in internal and boundary DOF: (a) $\rho = 8$, (b) $\rho = 5$, (c) $\rho = 2$, (d) $\rho = 8$ and $\nu = 200$, (e) $\rho = 5$ and $\nu = 200$, and (f) $\rho = 2$ and $\nu = 200$. The initial values of the parameters used to carry out the optimization are $\theta_i = 1.2$, $i = 1, \cdots, 5$. The errors in the fourth column of the table are defined by the norm $\sqrt{\left\| \underline{\theta}^{est} - \underline{\theta}^{full} / \underline{\theta}^{full} \right\|_2 / N_\theta} \times 100$ of the fractional errors of the optimal model parameter estimates $\underline{\theta}^{est}$ obtained from the CMS-reduced FE model and the optimal estimates $\underline{\theta}^{full}$ obtained from the full (non - reduced) FE model. The percentage difference of the optimal estimates for the full model from the values $\underline{\theta} = 1$ of the nominal model is $(\underline{\theta}^{full} - \underline{1})^T \times 100 = (0.57, 1.87, 1.09, 0.61, 1.21)^T$ and it is due to the noisy data considered. The results in Table 2.3 clearly suggest that the error in the estimates of the model parameters is very small for the case of reducing the internal DOF using $\rho = 8$, $\rho = 5$ and $\rho = 2$. The fluctuation in the ρ values of the parameters errors reported in Table 3.3 as a function of the values should not be surprising since, due to the noise added, the experimental modal data do not coincide with the modal data predicted by the unreduced model.

The number of function evaluations and the computational effort are also shown in Table 3.3. The computational time for carrying out the optimization for the reduced-order models is 5% of the time required for the full model. Consequently, significant gains in computational effort are achieved without sacrificing the accuracy in the model parameter estimates. A further reduction in the

Table 3.3: Accuracy and computational effort for FE model updating based on full and reduced ordermodels of Metsovo bridge.

FE Models	Total DOFs	Equally Weighted Method				Multi-objective Method Time (sec)
		Error (%) Max	Error (%) Mean	Function Evaluations	Time (sec)	
Full Model	562,101	0.00	0.00	8	14,251	321,352
$\rho = 8$	3,586	0.04	0.03	14	766	15,050
$\rho = 5$	3,400	0.69	0.43	13	677	12,282
$\rho = 2$	3,331	0.30	0.17	13	674	11,437
$\rho = 8, \nu = 200$	592	0.17	0.11	14	12	197
$\rho = 5, \nu = 200$	406	0.62	0.46	13	8	128
$\rho = 2, \nu = 200$	337	0.46	0.24	13	6	109

computational effort, close to two order of magnitude, is achieved by reducing the interface degrees of freedom using $\nu = 200$, while the accuracy is maintained to acceptable levels since the errors are smaller than 0.46%. Overall, for $\rho = 8$ and $\nu = 200$, the computational effort is drastically reduced by three to four orders of magnitude, without sacrificing in accuracy since the error norm is 0.11%.

Results are next presented for the multi-objective model updating framework. Figure 3.8 and Figure 3.9 present the Pareto front and the Pareto optimal models, respectively, computed using the full FE model and the six reduced-order models introduced before. The Pareto front and optimal solutions are represented by 20 points computed by the Normal Boundary Intersection algorithm [Das and Dennis, 1998). It is clear from Figure 3.8, that the quality of the estimates provided is excellent for the reduced-order models (a) and (d), very good for the reduced-order models (b) and (e), and acceptable for the reduced-order models (c) and (f). The computational effort for performing the FE model updating using the full and reduced-order models is reported in the last column of Table 3.3. The computational time required to carry out the multi-objective optimization for obtaining the Pareto optimal models using the full FE model is of the order of 89 hours (approximately four days).

Compared to the full model, the computational demands are substantially reduced by a factor of 20 for the reduced models (a) and (b), and by more than three orders of magnitude for the reduced models (d) and (e).Specifically, the computational time is 3-4 hours when only the internal DOF of each component are reduced and 2-3 minutes when both internal and interface DOF are reduced. A drastic reduction in computational effort is thus achieved by using the reduced-order models, without sacrificing in accuracy of the model parameter estimates as shown in Figure 3.8 and Figure 3.9

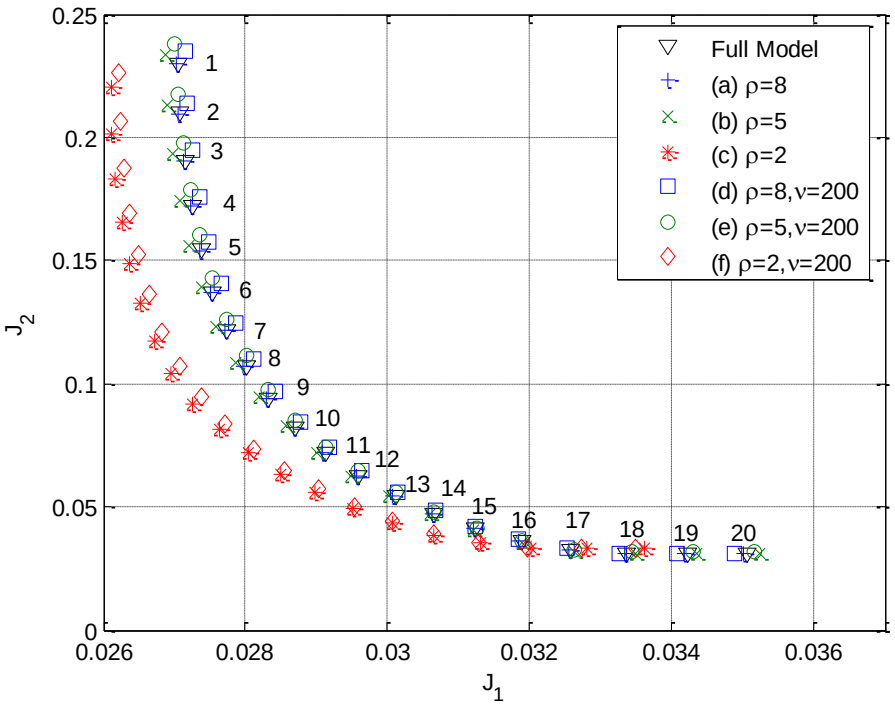

Figure 3.8: Comparison of Pareto fronts for the full and reduced-order FE models.

.

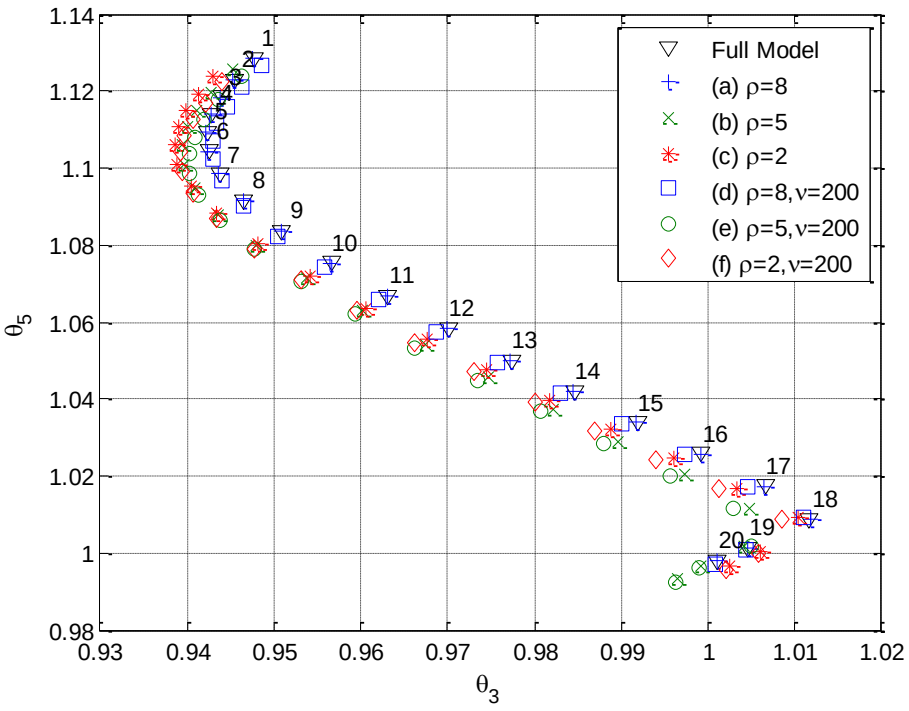

Figure 3.9: Comparison of Pareto models in the 2-d projection (θ_3, θ_5) of the 5-d parameter space for the full and reduced-order FE models.

3.4.4 Bayesian Model Updating Results using TMCMC

The finite element model is parameterized using five parameters associated with the modulus of elasticity of one or more structural components shown in Figure 3.2. The parameterization is graphically depicted in Figure 3.6.

Simulated, noise contaminated, measured modal frequencies and mode shapes are generated by adding a 1% and 3% Gaussian noise to the modal frequencies and modeshape components, predicted by the nominal non-reduced finite element models. The added Gaussian noise reflects the differences observed in real applications between the predictions from a model of a structure and the actual (measured) behavior of the structure. A sensor configuration involving 36 sensors is considered. The sensors are placed along the deck and the piers, measuring along the longitudinal, transverse and vertical directions. The finite element model is updated using simulated modal data for the lowest ten modes.

The Bayesian model updating is performed using the stochastic simulation algorithm TMCMC with 1000 samples per TMCMC stage (Ching and Chen, 2007). Results for the accuracy of the reduced-order models and the computational effort have been presented in Figure 3.5 for the following cases involving reduction in internal and boundary DOFs: (a) $\rho = 8$, (b) $\rho = 8$ and $\nu = 200$, (c) $\rho = 5$ and $\nu = 200$, and (d) $\rho = 2$ and $\nu = 200$. The results for the log evidence as well as the mean parameter values for the different reduced-order models are reported in Table 3.4. Comparing the log evidence of each reduced model and also the corresponding mean values of the model parameters it is evident that the various reduced-order models provide adequate accuracy,resulting number of finite element model runs and the computational demands in minutes for each reduced-order model are also is shown in Table 3.4.

The number of finite element model runs for each model depends on the number of TMCMC stages which vary for each model class from 19 to 20. The parallelization features of TMCMC (Angelikopoulos et al, 2015; Hadjidoukas et al., 2015) were exploited, taking advantage of the available 8 workers to simultaneously run eight TMCMC samples in parallel. For comparison purposes, the computational effort for solving the eigenvalue problem of the original unreduced finite element model is approximately 129 seconds. Multiplying this by the number of TMCMC samples shown in Table 3.4 and considering that 8 samples run in parallel , the total computational effort for each model class is expected to be of the order of 4 days. The results from the full finite element model are not shown due to the excessive computational time required to obtain results. In contrast, for the reduced-order model for $\rho = 8$, the computational demands are reduced to 16 hours (831 minutes as shown in Table 3.4), while for the reduced-order models for $\rho = 8$ and $\nu = 200$ these computational demands are drastically reduced to 14 minutes. It is thus evident from the results in Table 3.4 that a drastic reduction in computational effort for performing the structural identification based on a set of monitoring data is achieved from four days for the unreduced model classes to 14 minutes for the reduced model classes corresponding to $\rho = 8$ and $\nu = 200$ without compromising the accuracy of the proposed model updating methodology. This results in a drastic reduction in the number of the computational effort of almost three orders of magnitude. A large number of function evaluations, of the order of 70%, are also estimated using surrogate models, resulting in extra reduction in the computational time. The drastic reduction in computational time achieved for the present finite element model of approximately 560,000 DOFs is evident.

Table 3.4: Model updating results, model DOFs, number of FE simulations (NFES) and computational effort (CE) in minutes for each model class.

Cases	FE Reduced Order Models	Evidence (log)	Mean	Total DOFs	NFES	CE (Min)
Full	Full Model	–	–	562,101	20,000	6,000
(a)	$\rho = 8$	1666.5	1.005 1.019 1.011 1.006 1.012 1.008	3,586	20,000	831
(b)	$\rho = 8, \nu = 200$	1670.5	1.021 1.010 1.004 1.011 1.008	592	20,000	14
(c)	$\rho = 5, \nu = 200$	1672.6	1.022 1.007 1.012 1.007 1.007	406	20,000	9.5
(d)	$\rho = 2, \nu = 200$	1666.3	1.016 1.009 1.005 1.007	337	20,000	8.5

3.4.5 Damage Identification using the Bayesian Formulation

The proposed model reduction technique is well suited in damage identification applications that are based on FE model updating. This is illustrated next using the Bayesian method for structural damage identification proposed in Ntotsios et al. (Ntotsios et al., 2009). Specifically, a structure is divided into a number of substructures and it is assumed that damage in the structure is confined in one or more substructures, causing stiffness reduction in these damaged substructures. In order to identify which substructure contains the damage and predict the level of damage, a family of μ model classes $\mathrm{M}_1,\cdots,\mathrm{M}_\mu$, is introduced, and the damage identification is accomplished by associating each model class to damage contained within a substructure. For this, each model class M_i is parameterized by a number of structural model parameters $\underline{\theta}_i$ controlling the stiffness in the substructure i, while all other substructures are assumed to have fixed stiffness values equal to those corresponding to the undamaged structure. Damage in the substructure i will cause stiffness reduction which will alter the measured modal characteristics of the structure. The model class M_i that "contains" the damaged substructure i will be the most likely model class to observe the modal data since the parameter values i can adjust to the modified stiffness distribution of the substructure i, while the other modal classes that do not contain the substructure i are expected to provide a poor fit to the modal data.

Using the Bayesian model selection framework, the model classes are ranked according to the posterior probabilities based on the modal data identified from measurements. The most probable model class M_{best} that maximizes $P(\mathsf{M}_i \mid D)$, through its association with a damage scenario on a specific substructure, will be indicative of the substructure that is damaged, while the posterior PDF of the model parameters of the corresponding most probable model class M_{best}, compared to the parameter values of the undamaged structure, will be indicative ofthe severity of damage in the identified damaged substructure.

To demonstrate the methodology, the Metsovo bridge is divided into 15 substructures as shown in Figure 3.1. A number of competitive model classes $\mathrm{M}^{[i]}$ and $\mathrm{M}^{[i,j]}$ are introduced to monitor various probable damage scenarios for the bridge corresponding to single and multiple damages at different substructures. The model class $\mathrm{M}^{[i]}$ contains one parameter related to the stiffness (modulus of elasticity) of substructure i shown in Figure 3.10 . It can monitor damage

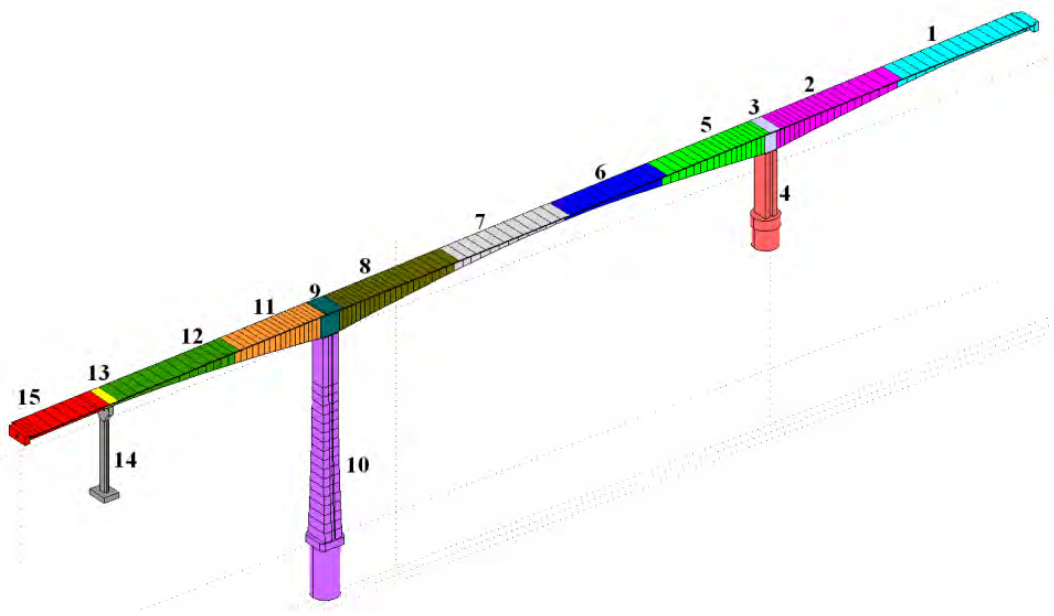

Figure 3.10: Substructures of FE model of Metsovo bridge used for damage identification.

associated with the stiffness reduction in the i substructure. The model class $\mathrm{M}^{[i,j]}$ contains two parameters related to the stiffness of substructures i and j in Figure 3.10. It can monitor damage associated with the stiffness reduction in either substructures i and j or simultaneously at both substructures. The five-parameter model shown in Figure 3.6 is also included in the family of model classes to monitor simultaneous damages at five different substructures. This five-parameter model class is denoted by $\mathrm{M}^{[5-par]}$. All model classes are generated from the updated FE model of the undamaged structure. For each model class, CMS techniques are used to alleviate the computational burden associated with the model updating problems that needs to be solved. For this, two different cases of reduced-order FE models are considered. The first case corresponds to models obtained by reducing the internal DOF using $\rho = 8$, while the second case corresponds to models obtained by reducing both the internal and interface DOF using $\rho = 8$ and $\nu = 200$. The Ritz basis for reducing the interface DOF were selected to be the characteristic interface modes obtained from equation (3.19) for the reference values

The number of components introduced for each model class depends on the parameterization. Specifically, the model class $\mathrm{M}^{[i]}$ is divided into two, three or four components. One component is selected to be the substructure i shown in

Figure 3.10, while the remaining components are selected to be the parts of the remaining structure that connect to the interfaces of component i . The model classes $\mathrm{M}^{[1]}$, $\mathrm{M}^{[10]}$, $\mathrm{M}^{[14]}$ and $\mathrm{M}^{[15]}$ have one interface, the model classes $\mathrm{M}^{[2]}, \mathrm{M}^{[5]}, \mathrm{M}^{[8]}, \mathrm{M}^{[11]}$ and $\mathrm{M}^{[12]}$ have two interfaces, while the model classes $\mathrm{M}^{[3]}$, $\mathrm{M}^{[9]}$ and $\mathrm{M}^{[13]}$ have three interfaces with the remaining structure. A similar division into components is introduced for the family of $\mathrm{M}^{[i,j]}$ model classes. For example, model class $\mathrm{M}^{[10,8]}$ is divided into four components, the first two components coincide with the physical substructures 10 and 8, the third includes the physical substructures 9, 11 to 15 and the fourth includes the substructures 1 to 7. The components in the $\mathrm{M}^{[5-par]}$ model class are kept the same as the ones used in Section 3.4.4. The reduced stiffness matrices $\hat{K}_0$ and $\hat{K}_j$ in the linear representation (3.28) and the mass matrix $\hat{M}_0$ are assembled once for each model class and are stored in a database of model classes.

For investigating the computational efficiency and accuracy of the reduced models, a simulated damage is introduced at the highest pier (substructure 10 in Figure 3.10), manifested as a stiffness reduction of 30% the nominal stiffness value. Simulated, noise contaminated, measured modal frequencies and mode shapes are generated for the damaged structure by adding a 1% and 3% Gaussian noise to the modal frequencies and modeshape components generated from the nominal non-reduced FE model with 30% reduction of the stiffness in the highest pier. It is expected that the proposed Bayesian damage identification methodology will promote $\mathrm{M}^{[10]}$ and $\mathrm{M}^{[10,i]}$ and $\mathrm{M}^{[5-par]}$ as the most probable model classes since these models classes monitor the stiffness of the component that contains the actual damage.

The model class selection and the model updating is performed using the stochastic simulation algorithm TMCMC with the following settings of the TMCMC parameters: tolCov 1.0 , 0.2 and 1000 samples per TMCMC stage (Ching and Chen, 2007). The results for the log evidence for representative model classes and the corresponding magnitude of damages i predicted by each model class are reported in Table 3.5 for the two cases of reduced-order models. Herein, for demonstration purposes, the percentage change $\Delta\underline{\theta}_i$ between the mean estimates $\underline{\overline{\theta}}^{[i]}$ (or $\underline{\overline{\theta}}^{[i,j]}$, $\underline{\overline{\theta}}^{[5-par]}$) of the model parameters of each model class and the corresponding values $\underline{\hat{\theta}}^{[i.und]}$ (or $\underline{\hat{\theta}}^{[i,j.und]}$, $\underline{\hat{\theta}}^{[5-par.und]}$) of the reference (undamaged) structure measures the severity (magnitude) of damage computed by each model class $\mathrm{M}^{[i]}$ (or $\mathrm{M}^{[i,j]}$, $\mathrm{M}^{[5-par]}$).

Table 3.5: Damage identification results, model DOF, number of FE simulations (NFES) and computational effort (CE) in minutes for each model class.

Model Class	Evidence $\rho=8$ (log)	Evidence $\rho=8$ $\nu=200$ (log)	$\Delta\theta_i$ $\rho=8$ (%)	$\Delta\theta_i$ $\rho=8$ $\nu=200$ (%)	DOF (NEFS) $\rho=8$	DOF (NEFS) $\rho=8$ $\nu=200$	CE $\rho=8$ (Min)	CE $\rho=8$ $\nu=200$ (Min)
$\mathbf{M}^{[2]}$	954.46	954.93	+27.9	+26.5	1,724(8000)	438(8000)	123	3.5
$\mathbf{M}^{[4]}$	954.99	955.08	-15.7	-15.2	989(8000)	381(8000)	42	3
$\mathbf{M}^{[6]}$	988.17	989.32	-47.8	-47.3	1,747(9000)	441(9000)	134	3.6
$\mathbf{M}^{[8]}$	1005.5	1006.4	-31.3	-30.8	1,824(9000)	408(9000)	170	0.5
$\mathbf{M}^{[10]}$	1723.1	1723.3	-29.2	-29.2	1,393(9000)	388(12000)	173	4.6
$\mathbf{M}^{[10,7]}$	1722.5	1723.1	-29.0 +4.0	-29.0 +3.9	1,829(12000)	425(13000)	245	5.4
$\mathbf{M}^{[10,8]}$	1718.7	1719.0	-29.0 +1.9	-29.0 +1.3	2,485(14000)	433(13000)	509	5.5
$\mathbf{M}^{[5-par]}$	1700.4	1698.2	-1.3 -28.3 +1.0 +2.3 +0.5	-0.5 -28.5 +0.9 +1.5 +0.5	3,586(19000)	592(19000)	759	14
Total							2155	40.1

Comparing the log evidence of each model class and also the corresponding magnitude of damages $\Delta\underline{\theta}_i$ predicted by each model class in Table 3.5 it is evident that the proposed methodology correctly predicts the location and magnitude of damage using the reduced-order model classes. Specifically, based on the reduced-order models for $\rho = 8$, the most probable model class is $\mathrm{M}^{[10]}$ which predicts a mean 29.2% reduction in stiffness which is very close to the inflicted 30%. Among all alternative model classes $\mathrm{M}^{[10]}$, $\mathrm{M}^{[10,7]}$, $\mathrm{M}^{[10,8]}$ and $\mathrm{M}^{[5-par]}$ that contain the actual damage, the proposed methodology favors the model class $\mathrm{M}^{[10]}$ with the least number of parameters and it predicts the five parameter model class $\mathrm{M}^{[5-par]}$ as the least probable model. This is consistent with theoretical results for model class penalization for over parameterization, available for Bayesian model class selection (Beck and Yuen, 2004). The model classes that do not contain the damage are not favored by the proposed methodology. Based on the reduced-order models for $\rho = 8$ and $\nu = 200$, the predictions of the location and severity of damage are very close to the ones obtained from the reduced-order models for $\rho = 8$ for most model classes included in Table 3.5. In particular, the most probable model class for $\rho = 8$ and $\nu = 200$ is also predicted to be $\mathrm{M}^{[10]}$, while the mean damage severity is predicted to correspond to 29.2% reduction in stiffness, exactly the same as the one predicted with the reduced-order models for $\rho = 8$.

The resulting number of FE model re-analyses and the computational demands in minutes for each model class are also is shown in Table 3.5. The number of FE model runs for each model class depends on the number of TMCMC stages which vary for each model class from 8 for the one-parameter model class to 19 for the five-parameter model class. The resulting variable number of stages per model class was automatically obtained from the TMCMC algorithm by keeping constant the value tolCov of the TMCMC parameter to tolCov 1.0 . This parameter controls the intermediate PDFs. For more details, the reader is referred to the original publication of the TMCMC algorithm (Ching and Chen, 2007).The parallelization features of TMCMC [38] were also exploited, taking advantage of the available four-core multi-threaded computer unit to simultaneously run eight TMCMC samples in parallel. For comparison purposes, the computational effort for solving the eigenvalue problem of the original unreduced FE model is approximately 139 seconds. Multiplying this by the number of TMCMC samples shown in Table 3.5 and considering parallel implementation in a four-core multi-threaded computer unit, the total computational effort for each mode class is expected to be of the order of 3 to 7 days for 8,000 to 19,000 samples,

respectively. The results from the full FE model are not shown due to the excessive computational time required to obtain results for the model classes in the database. For all eight model classes considered in Table 3.5, the total computational effort using the unreduced models is estimated to be approximately one month and seven 40 days. In contrast, for the reduced-order models for $\rho = 8$, the computational demands for running all model classes are reduced to 30 hours (2155 minutes as shown in the last row of Table 3.5), while for the reduced-order models for $\rho = 8$ and $\nu = 200$ these computational demands are drastically reduced to 40 minutes. It is thus evident that a drastic reduction in computational effort for performing the structural identification based on a set of monitoring data is achieved from approximately 37 days for the unreduced model classes to 40 minutes for the reduced model classes corresponding to 8 and 200, without compromising the predictive capabilities of the proposed damage identification methodology. This results in a drastic reduction in the computational effort of more than three orders of magnitude.

3.5 Conclusions

Iterative optimization algorithms and stochastic simulation algorithms involved in both deterministic and Bayesian FE model updating formulations require a moderate to large number of FE model re-analyses. For large size FE models with hundreds of thousands or even million DOF, the computational demands may be excessive. Exploiting certain stiffness-related parameterization schemes, often encountered in FE model updating formulations, to guide the division of the structure into components results in exact linear representations of the Craig-Bampton reduced stiffness matrix as a function of the model parameters with coefficient matrices computed and assembled once from a single CMS analysis of a reference structure. Further significant reductions in the size of the reduced system are shown to be possible using characteristic interface modes estimated for each interface between components. Re-analyses required in FE model updating formulations are associated with the solution of the eigenproblem of the reduced-order system, completely avoiding the re-analyses of the component fixed-interface and characteristic interface modes as well as the re-assembling of the reduced system matrices. FE model updating and damage identification results using a solid model of a bridge demonstrated the implementation, computational efficiency and accuracy of the proposed model reduction methodology. The computational effort was reduced drastically by more than three orders of magnitude. In particular, for the application in damage identification the

computational time was reduced from approximately one month to several minutes. Further computational savings can be obtained by adopting surrogate modes to drastically reduce the number of reduced-order system re-analyses and parallel computing algorithms to efficiently distribute the computations in available multi-core CPUs (Angelikopoulos et al, 2015; Hadjidoukas et al., 2015).

CHAPTER 4 Bayesian Uncertainty Quantification and Propagation Framework for Nonlinear Systems

4.1 Introduction

The type of nonlinearities encountered in structural dynamics include hysteretic nonlinearities as well as nonlinearities arising from contact and impact between surfaces, as well as from nonlinear isolation devices such as nonlinear dampers in civil infrastructure and nonlinear suspension models in vehicles. In a number of structural dynamics cases, the nonlinearities are localized in isolated parts of a structure, while the rest of the structure behaves linearly. Such localized nonlinearities can be found in vehicles where the frame usually behaves linearly and the nonlinearities are activated at the suspension mainly due to the dampers. In civil engineering structures the nonlinearities are at some cases localized at the various structural elements (dampers, etc) introduced to isolate the structure during system operation.

For nonlinear models of structures the quantification of the uncertainties in the model parameters depends on the measured quantities that are available. Depending on the type of application, two types of measured quantities are

usually available: full response time histories or frequency response functions. The likelihood formulation in the application of the Bayes theorem depends on the type of the measured quantities provided.

Details on the formulation of the likelihood for the case where full measured response time histories are available can be found in (Metallidis et al., 2003; Metallidis et al., 2008; Jensen et al., 2013). The formulation often depends on the user postulation of the prediction errors that represent the discrepancy that always appears between the model predictions obtained from a particular value of the model parameters and the corresponding data that are available from experiments. The likelihood and the posterior pdfs of the parameters of a finite element model are functions of the response time histories predicted by the finite element model. Each posterior evaluation requires the integration of the nonlinear set of equation of motion of the structure.

The formulation of the likelihood for the case where nonlinear frequency response spectra are available can be found in (Jensen et al., 2014; Natsiavas et al., 2013). The likelihood and the posterior pdf of the parameters of the nonlinear finite element model are functions of the frequency response spectra predicted by the finite element model. Each posterior evaluation requires the integration of the nonlinear set of equation of motion of the structure for as many different numbers of harmonic excitations as the number of frequency response spectra ordinates. This, however, increases substantially the computational effort.

At the model level, model reduction techniques based on CMS are readily applicable for special class of problems where the nonlinearities are localized at isolated parts of the structure. In such cases the structure can be decomposed into linear and nonlinear components and the dynamic behavior of the linear components be represented by reduced models. An implementation of such framework can be found in (Natsiavas et al., 2013) where it is demonstrated that substantial reductions in the DOFs of the model can be achieved which eventually yield to reduction in computational effort for performing a simulation run without sacrificing the accuracy.

For Bayesian asymptotic approximations, analytical approximations of the gradients of objective functions are not readily available. The development time and software implementation may be substantial. For certain classes of hysteretic nonlinearities, formulations for the sensitivities of the response quantities to parameter uncertainties have been developed (Barbato et al., 2007) and can be used within the Bayesian framework. However, it should be pointed out that such

formulation are model intrusive and are not easily integrated to commercial computer software packages available for simulating nonlinear structural dynamics problems. For the model cases where adjoint techniques can be applied, the development time may be substantial. However, for a number of important nonlinear class of models (e.g. impact, hysteretic) or output quantities of interests (e.g. frequency response spectra), adjoint methods are not applicable. The absence of adjoint formulation may substantially increase the computational cost and/or render gradient-based optimization algorithms unreliable for use with Bayesian asymptotic approximation tools. Stochastic optimization and stochastic simulations algorithms within a HPC environment are respectively the preferred algorithms to be used with Bayesian asymptotic and stochastic simulation tools.

At the algorithmic level, surrogate estimates are also applicable. For the case where the measurements are given as full response time histories, the surrogate estimates are applied to approximate the value of the log posterior PDF. For the case where the measurements consist of nonlinear frequency response spectra, it is more convenient computationally to apply the surrogate estimates for each spectral ordinate of the spectrum (Natsiavas et al., 2013). In addition, in the latter case, it should be pointed out that the frequency response spectral values can run in parallel, taking advantage of HPC environments to speed up computations.

A Bayesian uncertainty quantification and propagation (UQ&P) framework is presented for identifying nonlinear models of dynamic systems using vibration measurements of their components. The measurements are taken to be either response time histories or frequency response functions of linear and nonlinear components of the system. For such nonlinear models, stochastic simulation algorithms are suitable Bayesian tools to be used for identifying system and uncertainty models as well as perform robust prediction analyses. The UQ&P framework is applied to a small scale experimental model of a vehicle with nonlinear wheel and suspension components. Uncertainty models of the nonlinear wheel and suspension components are identified using the experimentally obtained response spectra for each of the components tested separately. These uncertainties, integrated with uncertainties in the body of the experimental vehicle, are propagated to estimate the uncertainties of output quantities of interest for the combined wheel-suspension-frame system. The computational challenges are outlined and the effectiveness of the Bayesian UQ&P framework on the specific example structure is demonstrated.

This chapter is organized as follows. In Section 4.2, the Bayesian framework for uncertainty quantification, calibration and propagation is presented for the case

that the measured response quantities are full response time histories. Moreover, the Bayesian framework for the case that response spectra are utilized, is presented in Section 4.3.The suitable Bayesian tools that are used for identifying system and uncertainty models as well as perform robust prediction analyses are also discussed in this section. In Section 4.4, the identification of the uncertainty models of the nonlinear wheel and suspension components is investigated using the experimentally obtained response spectra. The uncertainty models for the vehicle frame are also obtained using experimental data. The uncertainty is propagated to output quantities of interest for the combined wheel-suspension-frame system. In Section 4.5, the computational challenges are outlined and the effectiveness of the Bayesian UQ&P framework on the specific example structure is demonstrated. Finally, the conclusions are summarized in Section 4.6.

4.2 Bayesian Framework using Response Time Histories

4.2.1 Parameter Estimation

Consider a parameterized FE model class M of a nonlinear structure and let $\underline{\theta} \in R^{N_\theta}$ be the parameter set to be estimated using a set of measured response quantities. In nonlinear structural dynamics, the measured quantities may consist of full response time histories $D = \hat{y}_j(k) \in R^{N_o}, j = 1,\cdots N_o \,\&\, k = 1,\cdots, N_D$ at N_o DOF and at different time instants $t = k\Delta t$, where k is the time index and N_D is the number of sampled data with sampling period Δt, or response spectra $D = \hat{\underline{y}}_k \in R^{N_o}, k = 1,\cdots, N$ at different frequencies ω_k, where k is a frequency domain index. In the context of this Section of Chapter 4, in order to apply the Bayesian formulation for parameter calibration of non-linear models, we consider that the data consists of measured time histories.

In addition, let $y_j(k;\underline{\theta}_m) \in R^{N_o}, j = 1\cdots, N_o \,\&\, k = 1,\cdots, N_D$ be the predictions of the response time histories for the same quantities (displacements, accelerations and forces) and points in the structure, from the non-linear model corresponding to a particular value of the parameter set $\underline{\theta} \in R^{N_\theta}$. The prediction error equation between the sampled response time history of the quantity of interest at time $t = k\Delta t$ and the corresponding response time history predicted from the model for a particular value of the parameter set $\underline{\theta} \in R^{N_\theta}$ can now take the form

$$\hat{y}_j(k) = y_j(k;\underline{\theta} \,|\, \mathrm{M}) + e_j(k) \tag{4.1}$$

where $j = 1, \cdots N_o$ and $k = 1, \cdots, N_D$.

Prediction errors, measuring the fit between the measured and the model predicted response time histories, are modeled by Gaussian distributions. The difference between the measured and model predicted response is attributed to both experimental errors and modeling error. The prediction errors of a response time history at different time instants are assumed to be independent zero-mean Gaussian variables with equal variances for all sampling data of a response time history, but each time history is allowed to have a different prediction error associated with it. This formulation takes into account the fact that each measured time history is generally obtained from a different sensor (displacement, acceleration or force sensor) with a different accuracy and noise level, and this results in a number of prediction errors equal to the number of measured time histories.

Under the zero-mean Gaussian assumption for the prediction error, the error term $\underline{e}_k \sim N(\underline{\mu}, \Sigma(\underline{\theta}_e))$ is a Gaussian vector with mean zero $\underline{\mu} = 0$ and covariance $\Sigma(\underline{\theta}_e)$. It is assumed that the error terms $\underline{e}_k, k = 1, \cdots, N_D$ are independent. This assumption may be reasonable for the case where the measured quantities are the response spectra. However, for measured response time histories this assumption is expected to be violated for small sampling periods. The effect of correlation in the prediction error models is not considered in this study. The notation $\Sigma(\underline{\theta}_e)$ is used to denote that a model is postulated for the prediction error covariance matrix that depends on the parameter set $\underline{\theta}_e$. The measured quantity $\hat{y}_j(k)$ also follows a Gaussian distribution with mean $y_j(k;\underline{\theta})$ and covariance $\Sigma(\underline{\theta}_e)$, $\hat{y}_j(k) \sim N\left(y_j(k;\underline{\theta}), \sigma_j^2\right)$. A diagonal matrix is a reasonable choice for the covariance matrix, that is, $\Sigma(\underline{\theta}_e) = diag(\sigma_j^2 \hat{y}_j^2)$, where σ_j^2 are the variance

The prediction error e_j provides a measure of the discrepancy between the measured and model predicted quantities. As already stated in Chapter 2, this generally breaks down to two terms for the prediction error, one for the experimental error and one for the model error. In this study such a distinction is not made, and the prediction error is thought of as a measure of the total discrepancy between measurements and the model predictions without being able to distinguish how much is due to experimental or modeling error. Depending on the problem, and more specifically on the way the data was collected, $\underline{\sigma}$ might be considered known or unknown. In the most general case it is considered unknown and therefore is included in the parameters for calibration, along with the

structural model parameters. Herein, the prediction error parameters are considered unknown and from now on are included in the parameters to be calibrated given the data, along with the structural model parameters in the set $\underline{\theta}$.

The Bayesian method is used to quantify the uncertainty in the model parameters as well as select the most probable FE model class among a family of competitive model classes based on the measured data. The structural model class M is augmented to include the prediction error model class that postulates zero-mean Gaussian models. As a result, the parameter set is augmented to include the prediction error parameters $\underline{\theta}_e$. Using PDFs to quantify uncertainty and following the Bayesian formulation (Beck and Katafygiotis, 2009; Christodoulou and Papadimitriou, 2007; Yuen, 2010), the posterior PDF $p(\underline{\theta}|D,\mathsf{M})$ of the structural model and the prediction error parameters $\underline{\theta}=(\underline{\theta}_m,\underline{\theta}_e)$ given the data D and the model class M can be obtained in the form

$$p(\underline{\theta}|D,\mathsf{M})=\frac{\left[p(D|\mathsf{M})\right]^{-1}}{(2\pi\det\Sigma(\underline{\theta}_e))^{N_D N_o/2}}\exp\left[-\frac{1}{2}J(\underline{\theta})\right]\pi(\underline{\theta}|\mathsf{M}) \tag{4.2}$$

where

$$J(\underline{\theta})=\sum_{r=1}^{m}\left[\underline{y}(\underline{\theta}_m)-\underline{\hat{y}}\right]^T\Sigma^{-1}(\underline{\theta}_e)\left[\underline{y}(\underline{\theta}_m)-\underline{\hat{y}}\right] \tag{4.3}$$

is the weighted measure of fit between the measured and model predicted quantities, $\pi(\underline{\theta}|\mathsf{M})$ is the prior PDF of the model parameters $\underline{\theta}$ and $p(D|\mathsf{M})$ is the evidence of the model class M.

For a large enough number of experimental data, and assuming for simplicity a single dominant most probable model, the posterior distribution of the model parameters can be asymptotically approximated by the multi-dimensional Gaussian distribution (Beck and Katafygiotis, 2009; Christodoulou and Papadimitriou, 2007; Yuen, 2010) centered at the most probable value $\underline{\hat{\theta}}$ of the model parameters that minimizes the function $\mathrm{g}(\underline{\theta};\mathsf{M})=-\ln p(\underline{\theta}|D,\mathsf{M})$ with covariance equal to the inverse of the Hessian $h(\underline{\theta})$ of the function $\mathrm{g}(\underline{\theta};\mathsf{M})$ evaluated at the most probable value. For a uniform prior distribution, the most probable value of the FE model parameters $\underline{\theta}$ coincides with the estimate obtained by minimizing the weighted residuals. An asymptotic approximation based on Laplace's method is also available to give an estimate of the model

evidence $p(D|\mathsf{M})$ (Yuen, 2010). The estimate is also based on the most probable value of the model parameters and the value of the Hessian $h(\underline{\theta})$.

The asymptotic approximations may fail to give a good representation of the posterior PDF in the case of multimodal distributions or for unidentifiable cases manifested for relatively large number of model parameters in relation to the information contained in the data. For more accurate estimates, one should use SSA to generate samples that populate the posterior PDF in (4.2). Among the SSA available, the TMCMC algorithm (Beck and Katafygiotis, 2009) is one of the most promising algorithms for selecting the most probable model class among competitive ones, as well as finding and populating with samples the importance region of interest of the posterior PDF, even in the unidentifiable cases and multi-modal posterior probability distributions. In addition, the TMCMC samples $\underline{\theta}^{(i)}, i=1,\cdots,N_s$, drawn from the posterior distribution can be used to yield an estimate of the evidence $p(D|\mathrm{M}_i)$ required for model class selection (Beck and Katafygiotis, 2009; Christodoulou and Papadimitriou., 2007; Ching and Chen ,2007) . The TMCMC samples can further be used for estimating the probability integrals encountered in robust prediction of various performance quantities of interest (Papadimitriou et al., 2001).

4.2.2 Model Selection

The Bayesian probabilistic framework is also used to compare two or more competing model classes and select the optimal model class based on the available data. Consider a family $\mathsf{M} = \mathsf{M}_i, i=1,\cdots,\mu$, of μ alternative, competing, parameterized FE and prediction error model classes and let $\underline{\theta}_i \in \boldsymbol{R}^{N_{\theta_i}}$ be the free parameters of the model class M_i . The posterior probabilities $p(\mathrm{M}_i|D)$ of the various model classes given the data D is (Beck and Au, 2002)

$$p(\mathrm{M}_i|D)=\frac{p(D|\mathrm{M}_i)P(\mathrm{M}_i)}{p(D|\mathrm{M}_{Fam})} \tag{4.4}$$

where $P(\mathrm{M}_i)$ is the prior probability and $p(D|\mathrm{M}_i)$ is the evidence of the model class M_i . The optimal model class M_{best} is selected as the one that maximizes $p(\mathrm{M}_i|D)$ given by (4.4). For the case where no prior information is available, the prior probabilities are assumed to be $P(\mathrm{M}_i)=1/\mu$, so the model class selection is based solely on the evidence values.

For model selection, an asymptotic approximation (Papadimitriou et al., 2001; Beck and Yuen, 2004; Yuen, 2010) based on Laplace's method can also be used to give an estimate of the evidence integral in that appears in the model selection equation (4.4). Substituting this estimate in (4.4) the final asymptotic estimate for $p(\mathrm{M}_i|D)$ is given in the form

$$P(\mathsf{M}_i \mid D) = \frac{\sqrt{2\pi}^{\,n_i}}{\left[p(D \mid \mathsf{M}_{Fam})\right]} \frac{p(D \mid \underline{\hat{\theta}}_i, \mathsf{M}_i)\ \pi(\underline{\hat{\theta}}_i \mid \mathsf{M}_i)}{\det\left[h_i(\underline{\hat{\theta}}_i, \mathsf{M}_i)\right]} P(\mathsf{M}_i) \tag{4.5}$$

where $\underline{\hat{\theta}}_i$ is the most probable value of the parameters of the model class M_i and $h_i(\theta) = \underline{\nabla}\underline{\nabla}^T g_i(\underline{\theta}, \mathsf{M})$ is the Hessian of the function $g_i(\underline{\theta}_i; \mathsf{M}_i)$ for the model class M_i. It should be noted that the asymptotic estimate for the probability of a model class M_i can readily be obtained given the most probable value and the Hessian of the particular mode. For the multi modal case the expression (4.5) can be generalized by adding the contributions from all modes.

4.3 Bayesian Formulation for Parameter Estimation based on Frequency Response Spectra

To apply the Bayesian formulation for parameter estimation of non-linear models based on frequency response spectra (Yuen and Katafygiotis, 2003; Jensen et al., 2014; Natsiavas et al., 2013), we consider that the data consists of measured response spectra $D = \underline{\hat{s}}_k \in R^{N_o}, k = 1, \cdots, N$ at N_o DOF and at different frequencies ω_k, where k is a frequency domain index and N is the number of sampled data in the frequency domain. In addition, let $\underline{s}_k(\underline{\theta}_m) \in R^{N_o}, k = 1 \cdots, N$ be the model response predictions of response spectra, corresponding to the DOFs where measurements are available, given the model class M and the parameter set $\underline{\theta}_m \in R^{N_\theta}$. It is assumed that the observation data and the model predictions satisfy the prediction error equation

$$\underline{\hat{s}}_k = \underline{s}_k(\underline{\theta}_m \mid \mathrm{M}) + \underline{e}_k \tag{4.6}$$

where $k = 1 \cdots, N$. The error term $\underline{e}_k \sim N(\underline{\mu}, \Sigma(\underline{\theta}_e))$ is a Gaussian vector with mean zero $\underline{\mu} = 0$ and covariance $\Sigma(\underline{\theta}_e)$. It is assumed that the error terms $\underline{e}_k$, $k = 1 \cdots, N$ are independent, an assumption that is very reasonable for the case that the measured data consists of response spectra. The measured quantity $\underline{\hat{s}}_k$

also follows a Gaussian distribution with mean $\underline{s}_k(\underline{\theta}_m)$ and covariance $\Sigma(\underline{\theta}_e)$, $\underline{\hat{s}}_k \sim N\left(\underline{s}_k(\underline{\theta}_m), \Sigma(\underline{\theta}_e)\right)$.

The likelihood function $p(D|\underline{\theta},\underline{\sigma})$, which quantifies the probability of obtaining the data given a specific set of structural parameters and prediction error parameters, is derived by noting that the measured response spectra $\underline{\hat{s}}_k$ are implied from (4.6) to be independent Gaussian variables with mean $\underline{s}_k(\underline{\theta}_m)$ and variance $\underline{\sigma}^2$. Taking advantage of the independence of the measured quantities both at different frequencies of the same response spectra as well as between response spectra measured at different locations, the likelihood is formulated as follows.

$$p\left(D \mid \underline{\theta},\underline{\sigma}\right) = \prod_{j=1}^{N_0}\prod_{k=1}^{N} p\left(\hat{s}_j(k) \mid \underline{\theta},\underline{\sigma}\right) \tag{4.7}$$

Substituting with the formula for the Gaussian probability density function and rearranging terms one obtains that

$$p\left(D \mid \underline{\theta},\underline{\sigma}\right) = \frac{1}{\left(\sqrt{2\pi}\right)^{NN_0}\prod_{j=1}^{N_0}\sigma_j^N} \exp\left\{-\frac{1}{2}\sum_{j=1}^{N_0}\frac{1}{\sigma_j^2}\sum_{k=1}^{N}\left[\hat{s}_j(k) - s_j(k;\underline{\theta})\right]^2\right\} \tag{4.8}$$

Introducing the overall fit function

$$J\left(\underline{\theta};\underline{\sigma}\right) = \frac{1}{N_0}\sum_{j=1}^{N_0}\frac{1}{\sigma_j^2} J_j\left(\underline{\theta}\right) \tag{4.9}$$

where

$$J_j\left(\underline{\theta}\right) = \frac{1}{N}\sum_{k=1}^{N}\left[\hat{s}_j(k) - s_j(k;\underline{\theta})\right]^2 \tag{4.10}$$

represents the measure of fit between the measured and the model predicted response spectra, the likelihood function can be compactly written in the form

$$p\left(D \mid \underline{\theta},\underline{\sigma}\right) = \frac{1}{\left(\sqrt{2\pi}\right)^{NN_0}\prod_{j=1}^{N_0}\sigma_j^N} \exp\left\{-\frac{NN_0}{2} J\left(\underline{\theta};\underline{\sigma}\right)\right\} \tag{4.11}$$

Substituting (4.11) in (2.16) one derives the posterior probability distribution of the parameters in the form

$$p\left(\underline{\theta},\underline{\sigma}\,|\,D\right)=\frac{\pi\left(\underline{\theta},\underline{\sigma}\right)}{p(D)\left(\sqrt{2\pi}\right)^{N\,N_0}\prod_{j=1}^{N_0}\sigma_j^N}\exp\left\{-\frac{N\,N_0}{2}J\left(\underline{\theta};\underline{\sigma}\right)\right\} \qquad (4.12)$$

It is clear from (4.11) and (4.12) that the likelihood and the posterior of the parameters of the nonlinear finite element model are functions of the frequency response spectra predicted by the finite element model. Each posterior evaluation requires the integration of the nonlinear set of equation of motion of the structure for as many different number of harmonic excitations as the number of frequency response spectra ordinates. This, however, increases substantially the computational effort.

4.4 Application to a Small Scale Laboratory Vehicle

4.4.1 Description of the laboratory vehicle structure

In order to simulate the response of a ground vehicle an experimental device was selected and set up (Giagopoulos et al., 2001). More specifically, the selected frame structure comprises a frame substructure with predominantly linear response and high modal density plus four supporting substructures with strongly nonlinear action. First, Figure 4.1(a) shows a picture with an overview of the experimental set up. In particular, the mechanical system tested consists of a frame substructure (parts with red, gray and black color), simulating the frame of a vehicle, supported on four identical substructures. These supporting substructures consist of a lower set of discrete spring and damper units, connected to a concentrated (yellow color) mass, simulating the wheel subsystems, as well as of an upper set of a discrete spring and damper units connected to the frame and simulating the action of the vehicle suspension.

(a)

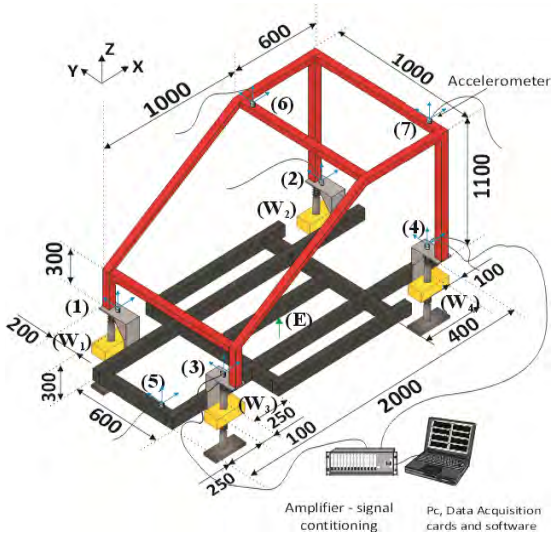

(b)

Figure 4.1: (a) Experimental set up of the structure tested, (b) Dimensions of the frame substructure and measurement points.

Also, Figure 4.1(b) presents more details and the geometrical dimensions of the frame subsystem. Moreover, the measurement points indicated by 1-4 correspond to connection points between the frame and its supporting structures, while the other measurement points shown coincide with characteristic points of the frame. Finally, point E denotes the point where the electromagnetic shaker is applied.

4.4.2 Experimental Set Up

In order to identify the parameters of the four supporting subsystems, which exhibit strongly nonlinear characteristics, a series of tests was performed. To investigate this further, the elements of the supporting units were disassembled and tested separately. First, Figure 4.2 shows a picture of the experimental setup and presents graphically the necessary details of the experimental device that was set up for measuring the stiffness and damping properties of the supports.

The experimental process was applied separately to both the lower and the upper spring and damper units of the supporting substructures and can be briefly described as follows. First, the system shown in Figure 4.2 is excited by harmonic forcing through the electromagnetic shaker up until it reaches a periodic steady state response. When this happens, both the history of the acceleration and the forcing signals are recorded at each forcing frequency. Some characteristic results obtained in this manner are presented in the following sequence of graphs. Next, Figure 4.3 presents the transmissibility function of the system tested, obtained experimentally for three different forcing levels while Figure 4.5 presents the transmissibility function of a wheel DOF of the vehicle, obtained experimentally for two different forcing levels.

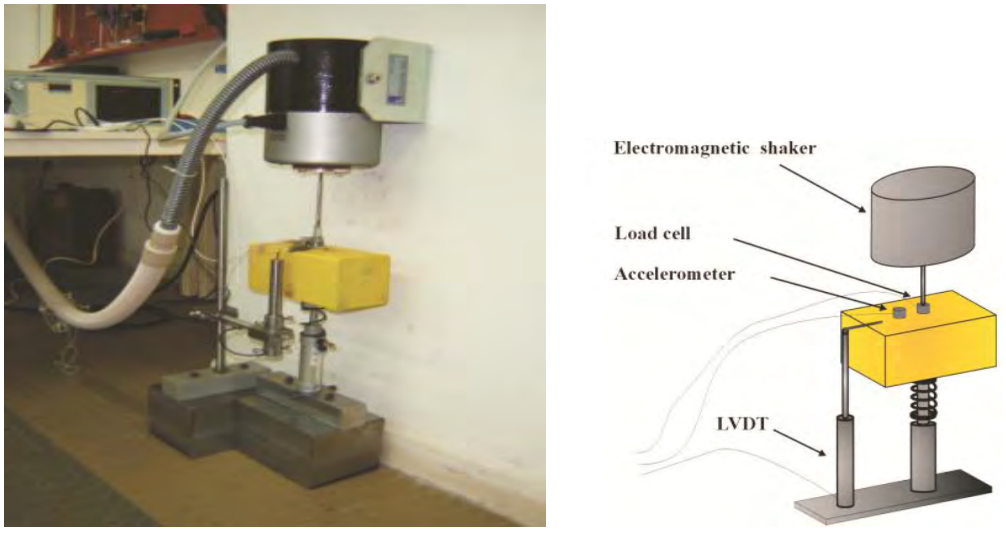

Figure 4.2: Experimental set up for measuring the support stiffness and damping parameters.

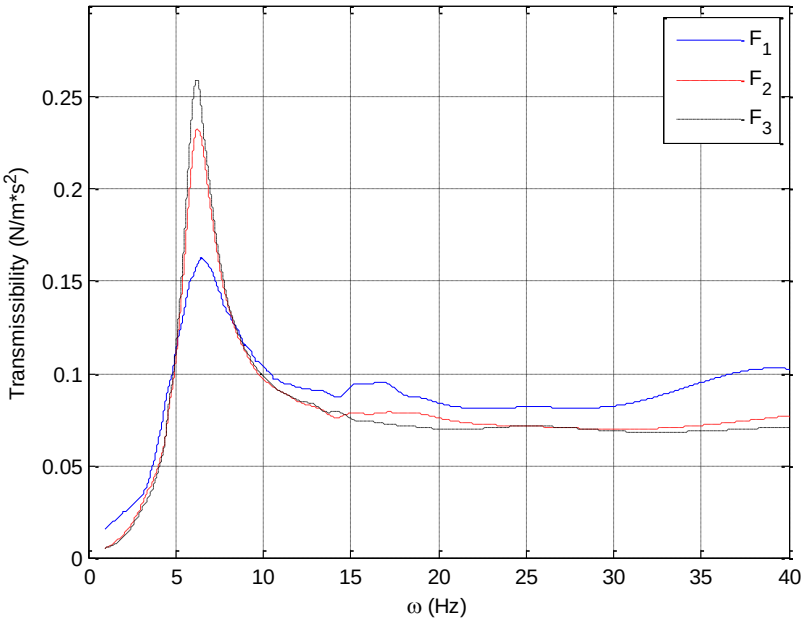

Figure 4.3: Transmissibility function of the support system for three different forcing levels.

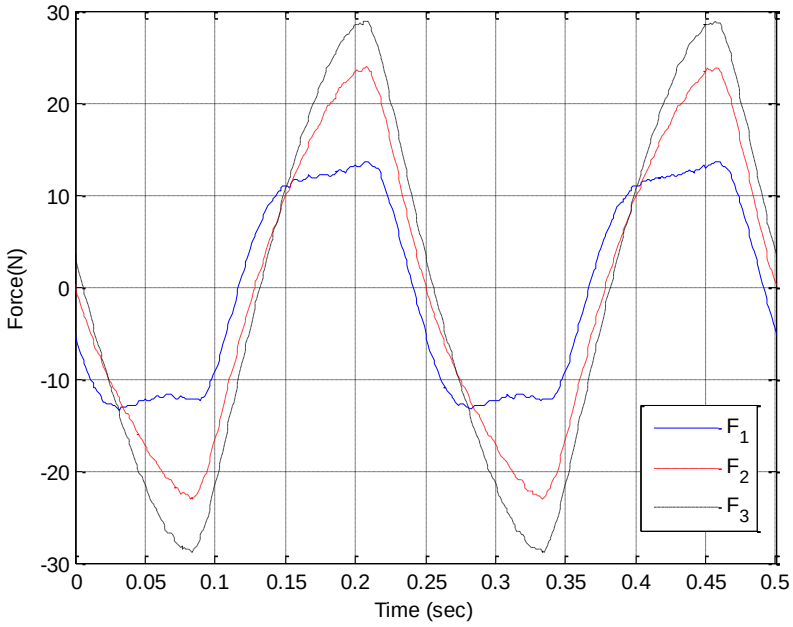

Figure 4.4: History of the external force applied with a fundamental harmonic frequency $\omega = 4Hz$.

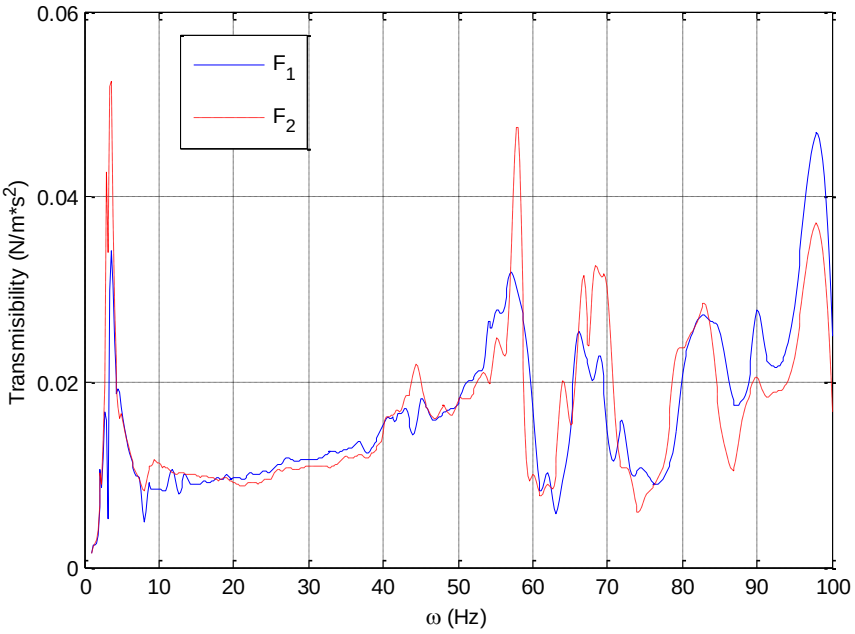

Figure 4.5: Transmissibility function of a wheel DOF of the vehicle for two different forcing levels.

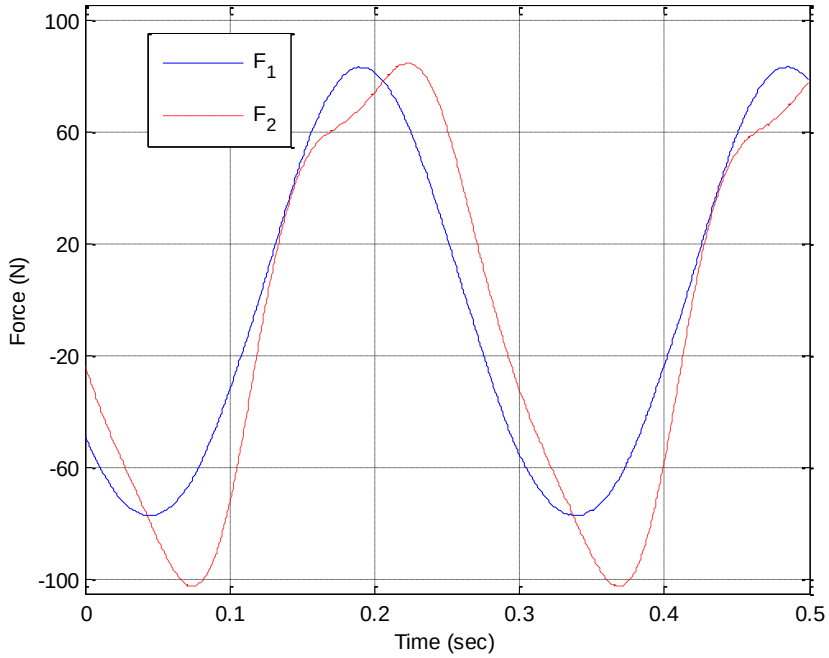

Figure 4.6: History of the external force applied with a fundamental harmonic frequency $\omega = 3.4Hz$.

Specifically, transmissibility function is defined as the ratio of the root mean square value of the acceleration to the root mean square value of the forcing signal measured at each forcing frequency. The blue, red and black lines correspond to the smallest, intermediate and largest forcing amplitude, respectively. Clearly, the deviations observed between the forcing levels indicate that the system examined possesses nonlinear properties. Moreover, neither the applied forcing is harmonic, especially within the frequency range below $\omega = 10Hz$. To illustrate this, Figure 4.4 shows two periods of the actual excitation force applied for the same three excitation levels in obtaining the results of Figure 4.3, which were recorded at a fundamental forcing frequency of $\omega = 4Hz$. Moreover, Figure 4.6 shows two periods of the actual excitation force applied to the vehicle for the two excitation levels in obtaining the results of Figure 4.5, which were recorded at a fundamental forcing frequency of $\omega = 3.4Hz$.

A number of models of the restoring and damping forces, say f_r and f_d respectively, and shown in Figure 4.7 were tried for modeling the action of the supports and compared with the experimental results.

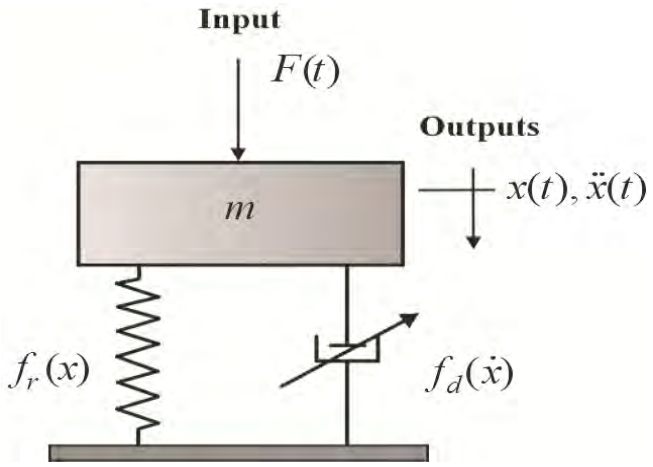

Figure 4.7: Mathematical model of the experimental set up for measuring the support stiffness and damping parameters

The classic linear dependence of the restoring force on the displacement and of the damping forces on the velocity of the support unit was first assumed. However, critical comparison with the experimental results using the Bayesian model selection framework demonstrated that the outcome was unacceptable in terms of accuracy. Eventually it was found that an acceptable form of the

restoring forces is the one where they remain virtually in a linear relation with the extension of the spring, namely

$$f_r(x) = k\,x \tag{4.13}$$

while the damping force was best approximated by the following formula

$$f_d(\dot{x}) = c_1\,\dot{x} + \frac{c_2\,\dot{x}}{c_3 + |\,\dot{x}\,|} \tag{4.14}$$

As usual, the linear term in the last expression is related to internal friction at the support, while the nonlinear part is related to the existence and activation of dry friction. More specifically, in the limit $c_3 \to 0$ the second term in the right hand side of (4.14) represents energy dissipation action corresponding to dry friction. On the other side, in the limit $c_3 \to \infty$, this term represents classical viscous action and can actually be absorbed in the first term.

4.4.3 Model Reduction of the Vehicle Frame

Detailed finite element models were created that correspond to the model used for the design of the experimental vehicle. The structure was first designed in CAD environment and then imported in COMSOL Multiphysics finite element modelling environment (COMSOL AB COMSOL Multiphysics User's Guide, 2005). The models were constructed based on the geometric details and the material properties of the structure. The finite element models for the vehicle were created using three-dimensional triangular shell finite elements to model the whole structure. A model of 15,202 finite elements having 45,564 DOF was chosen for the adequate modelling of the experimental vehicle. This model is shown in Figure 4.8. It should be noted that the size of the elements in the FE mesh is the maximum possible one that can be considered, with typical element length of the order of the thickness of the deck cross-section. The entire simulation for assembling the mass and stiffness matrices of the structure or its components is performed within the COMSOL Multiphysics modelling environment and exported in Matlab environment for further processing using CMS techniques and FE model updating methods.

Component mode synthesis methods (CMS) are implemented to substantially reduce the computational effort and save significant computational time. The hundreds of thousands of degrees of freedom (45,564 DOFs) of finite element model of the vehicle are drastically reduced to a much smaller number (668 DOFs), by implementing CMS technique.

The cut-off frequency ω_c is introduced to be the highest modal frequency that is of interest in FE model updating. In this study the cut-off frequency is selected to be equal to the 20th modal frequency of the nominal model. i.e. $\omega_c = 160.8531$ Hz. The first twenty modes of the vehicle frame are presented in Table 4.1.

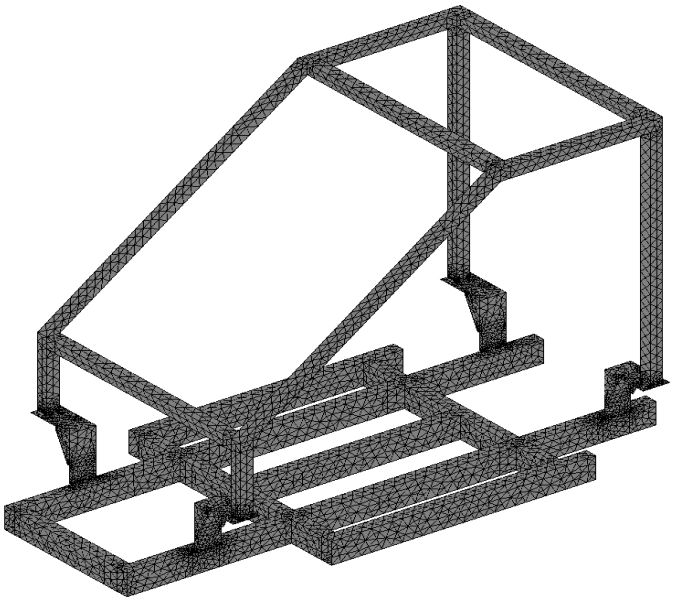

Figure 4.8: Vehicle structure with its FE mesh

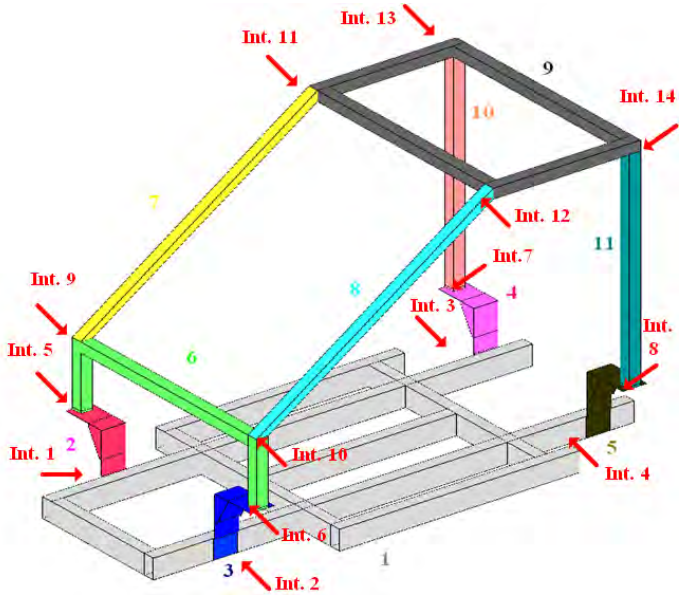

Figure 4.9: Components of FE model of vehicle structure.

Table 4. 1: The first twenty identified and predicted modes of the vehicle frame

Mode	Identified Modal Frequency (Hz)	Nominal FEM Predicted Frequency (Hz)	Difference between Identified and FE Predicted Modal Frequencies (%)
1	23.2139	23.2348	0.0902
2	42.1225	39.1265	-7.1126
3	42.5020	41.6084	-2.1024
4	48.2753	47.2930	-2.0349
5	58.1552	57.5692	-1.0077
6	69.0429	66.2020	0.0151
7	69.4700	69.0533	-4.7042
8	80.0413	80.4391	0.4969
9	86.1449	83.2491	-3.3615
10	100.2428	101.6080	1.3619
11	102.5815	105.9357	3.2701
12	110.4424	106.6243	-3.4572
13	115.1205	112.5407	-2.2409
14	123.6425	129.0741	4.3930
15	127.6472	121.7747	-4.6006
16	132.4204	131.7794	-0.4841
17	134.9544	133.8787	-0.7970
18	138.9425	137.3287	-1.1615
19	148.6929	146.5237	-1.4590
20	164.3888	160.8531	-2.1497

For demonstration purposes, the vehicle is divided into eleven physical components shown schematically in Figure 4.9. The first component is related to the floor of the vehicle, while the rest ten components are related to the frame of the structure. The thirteen interfaces between the components are also shown in Figure 4.9.

The effectiveness of the CMS technique as a function of the number of modes retained for each component is next evaluated. For each component it is selected

to retain all modes that have frequency less than $\omega_{\max} = \rho\omega_c$, where the ρ values affect computational efficiency and accuracy of the CMS technique. Representative ρ values range from 2 to 10. The total number of internal DOFs per component before the model reduction is applied are shown in Figure 4.10. The number of modes retained per components for various ρ values is also given in Figure 4.10. For the case $\rho = 8$, a total of 65 internal modes are retained for all 11 components. The total number of DOFs of the reduced model is 1,253 which consist of 65 fixed interface generalized coordinates and 1,188 constraint interface DOFs for all components. It is clear that a one order of magnitude reduction in the number of DOFs is achieved using CMS. The total number of internal DOF and retained modes for $\rho = 8$, $\rho = 5$ and $\rho = 2$ within all the components are reported in the second row of Table 4.1. The total number of internal and boundary DOF of the unreduced model are reported in the second

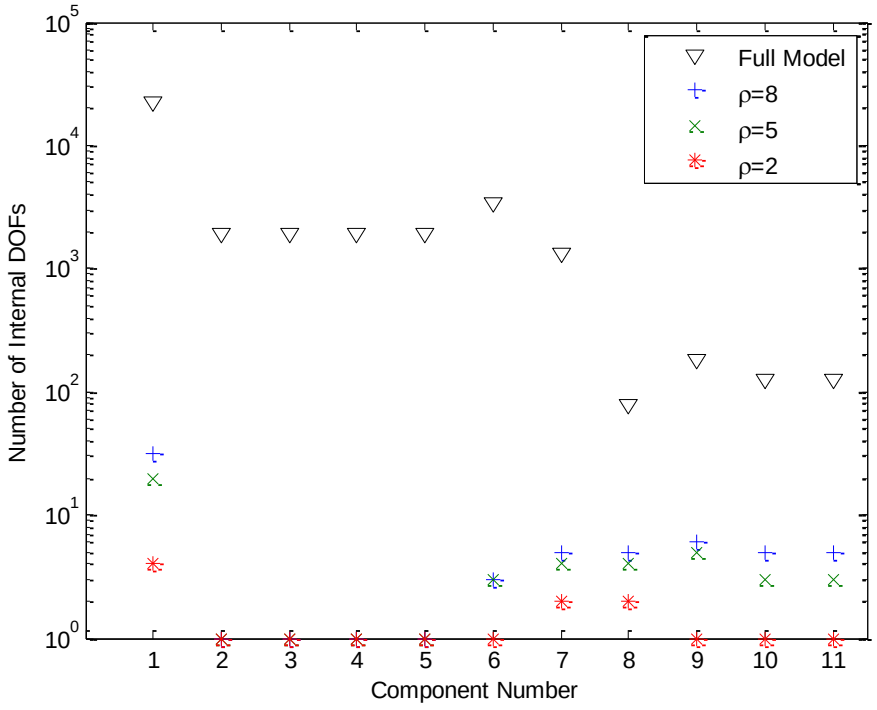

Figure 4.10: Number of DOF per component of the FE model of vehicle structure.

column of Table 4.2 based on the components and interfaces shown in Figure 4.9. It is clear from the results in Table 2.1 and Figure 4.10 that a more than two orders of magnitude reduction in the number of DOF per component is achieved using CMS.

Figure 4.11 shows the fractional error between the modal frequencies computed using the complete FE model and the modal frequencies computed using the CMS technique as a function of the mode number for $\rho = 2$, 5 and 8. It can be seen that the error for the lowest 20 modes fall below 10^{-5} for $\rho = 8$, 10^{-4} for $\rho = 5$ and 10^{-3} for $\rho = 2$. A very good accuracy is achieved even for the case of $\rho = 2$. The significant reduction in number of generalized coordinates of the reduced system and the increased accuracy of the results are promising for using the proposed model reduction method in FE model updating.

It is thus obvious that a large number of generalized coordinates for the reduced system arises from the interface DOF. A further reduction in the number of generalized coordinates for the reduced system can be achieved by retaining only a fraction of the constrained interface modes.

The number of DOF per interface is shown in the third column of Table 4.2. For each interface defined in Table 4.1, it is selected to retain all modes that have frequency less than $\omega_{\max}$, a multiple of the cutoff frequency ω_c , where the multiplication factor ρ is user and problem dependent. The number of modes retained per interface for $\nu = 200$ is given in the last column of Table 4.2. The number of retained interface modes is approximately 10% of the interface DOF for each interface. Figure 4.11 presents results for the fractional error between the modal frequencies computed using the CMS method with retained characteristic interface modes for $\nu = 200$ for each interface and the modal frequencies computed using the complete FE model as a function of the mode number. It can be seen that the fractional error for most of the lowest 20 modes of the structure fall well below 10^{-3} for $\nu = 200$ and ρ values as low as $\rho = 5$. Thus, the value of $\nu = 200$ gives accurate results in this case, while the number of retained interfaces modes for all interfaces is 652 which corresponds to half of the total number of interface DOF.

Table 4.2: Total number of internal and interface DOF for the full (unreduced) and reduced models.

Interfaces	Structure without Reduction	Retained modes $\rho = 8$, $\nu = 200$	Retained modes $\rho = 5$, $\nu = 200$	Retained modes $\rho = 2$, $\nu = 200$
Total Internal DOFs	44,376	65	46	16
Total Boundary DOFs	1,188	652	652	652
Total DOFs	45,564	717	698	668

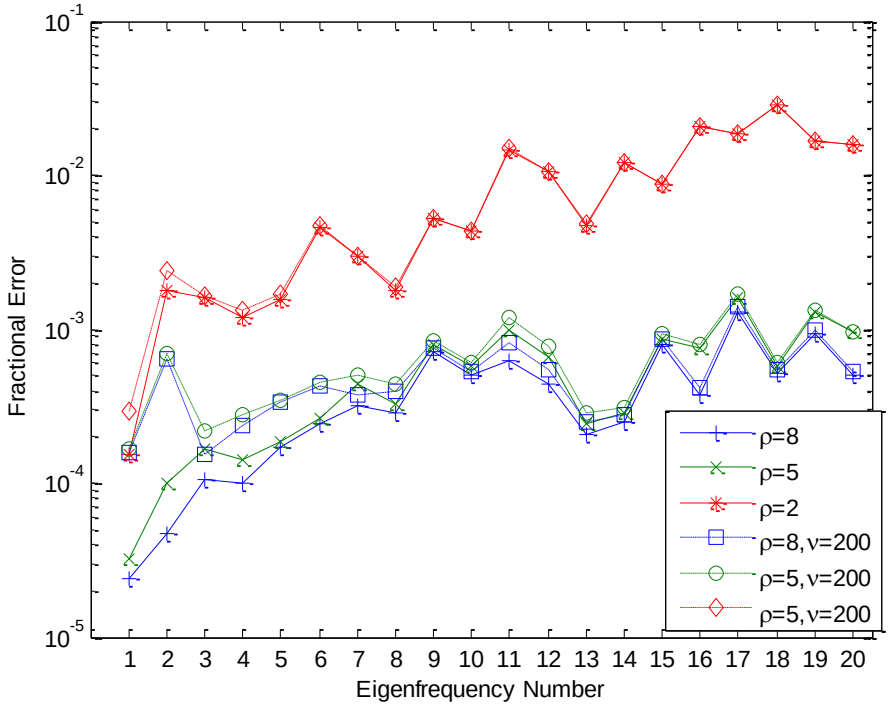

Figure 4.11: Fractional modal frequency error between the predictions of the full model and the reduced model as a function of eigenmode number and for different values of ρ and ν .

4.4.4 Model Updating of the Vehicle Frame

For demonstration purposes, the FE model is parameterized using six parameters associated with the modulus of elasticity of one or more structural components shown in Figure 4.9. The parameterization is graphically depicted in Figure 4.12. Specifically, the first parameter θ_1 accounts for the modulus of elasticity of the lower part of the experimental vehicle, the second parameter θ_2 accounts for the modulus of elasticity of the parts (joints) that connect the lower part with the upper part of the experimental vehicle, while the other four parameters θ_3, θ_4, θ_5 and θ_6 account for the modulus of elasticity of the different components of the upper part of the experimental vehicle Note that for substructures parameterized by a single parameter, two or more components per substructure have been introduced, demonstrating the flexibility of the proposed methodology. The parameters are introduced to scale the nominal values of the properties that they model so that the value of the parameters equal to one corresponds to the nominal value of the FE model. The nominal FE model corresponds to values of $\theta_1 = \cdots = \theta_6 = 1$.

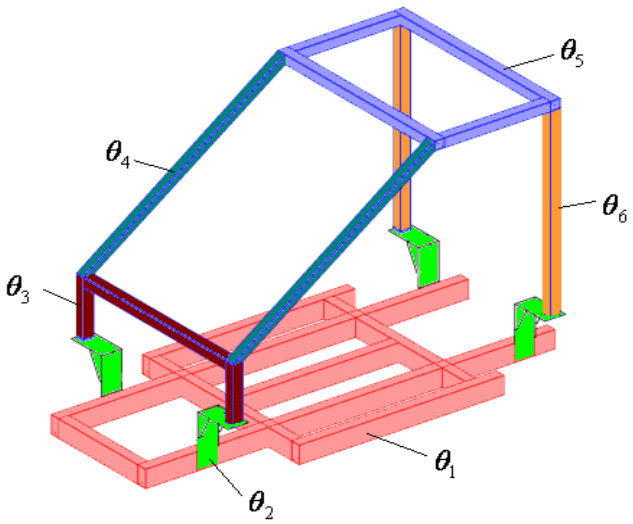

Figure 4.12: FE model parameterization based on 6 parameters

The FE model is updated using the simulated modal data for the lowest ten modes. The first ten modeshapes of the vehicle frame predicted by the FE model, created in Comsol, are graphically illustrated in Figures 4.13-4.22.

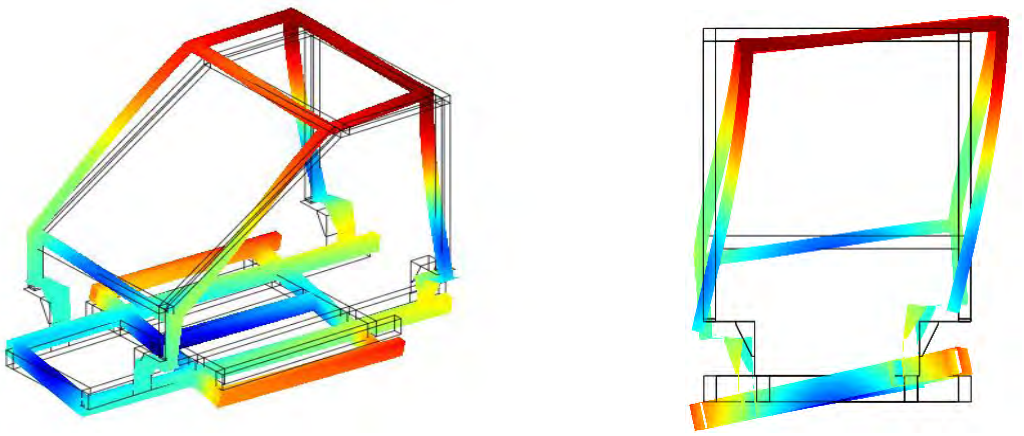

Figure 4.13: Modeshape predicted by the finite element model for the first mode at 23.23 Hz

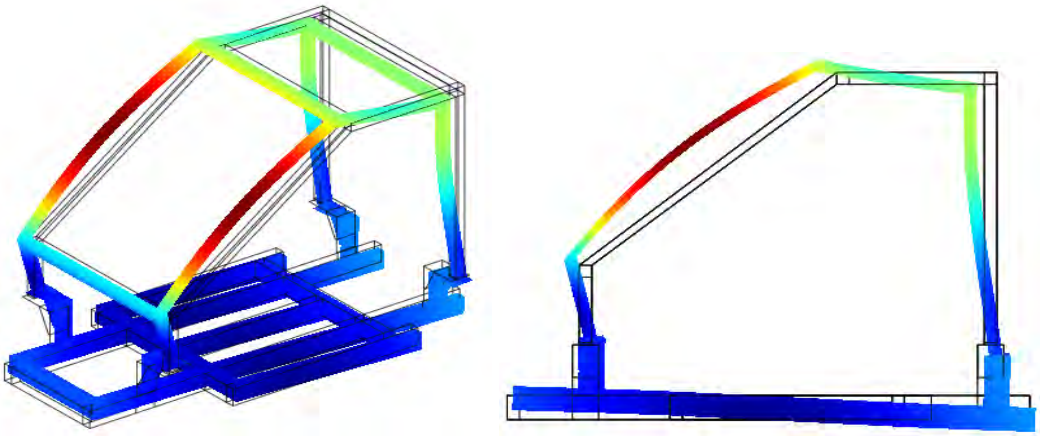

Figure 4.14: Modeshape predicted by the finite element model for the second mode at 39.13 Hz.

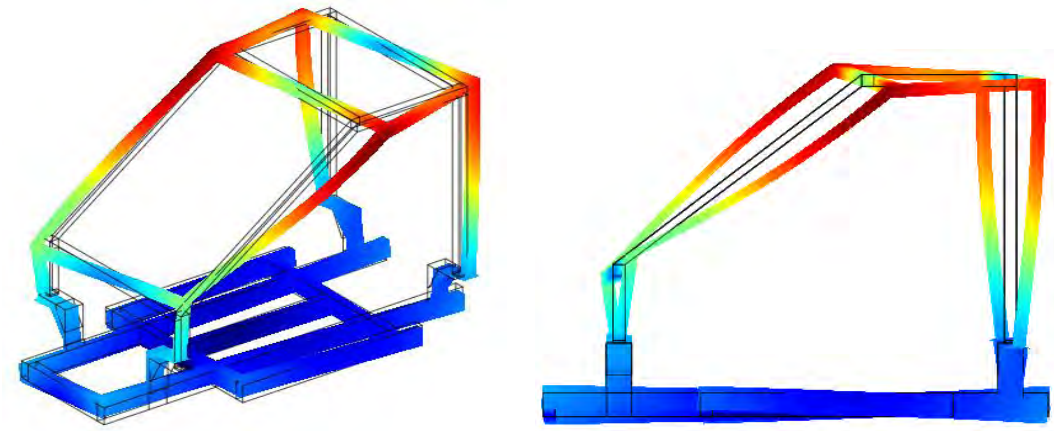

Figure 4.15: Modeshape predicted by the finite element model for the third mode at 41.61 Hz.

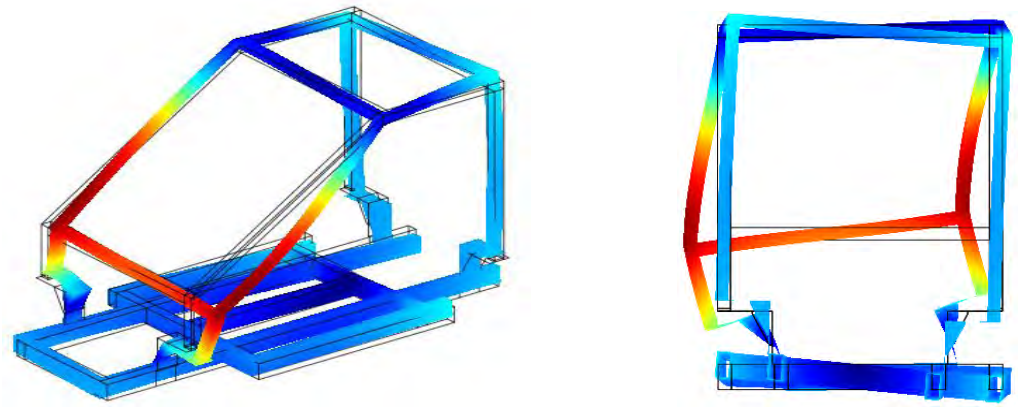

Figure 4.16: Modeshape predicted by the finite element model for the fourth mode at 47.29 Hz.

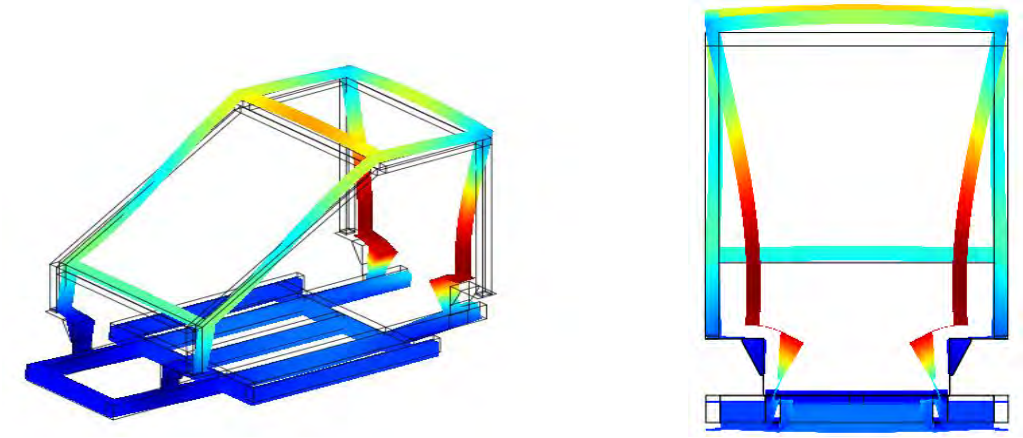

Figure 4.17: :Modeshape predicted by the finite element model for the fifth mode at 57.57 Hz.

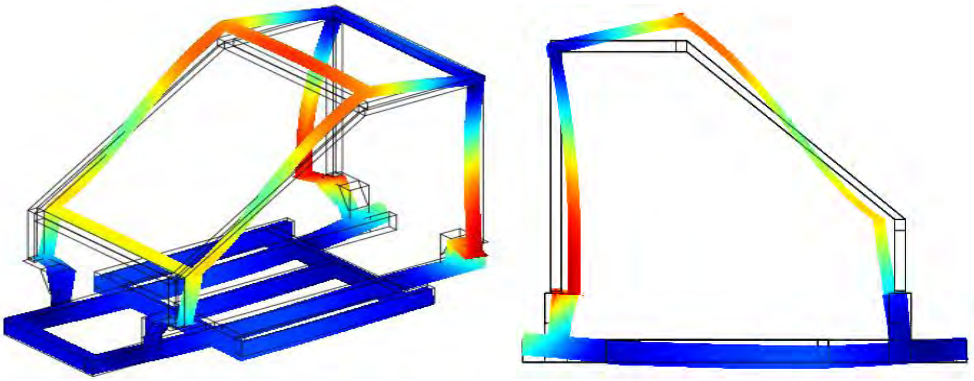

Figure 4.18: Modeshape predicted by the finite element model for the sixth mode at 66.20 Hz.

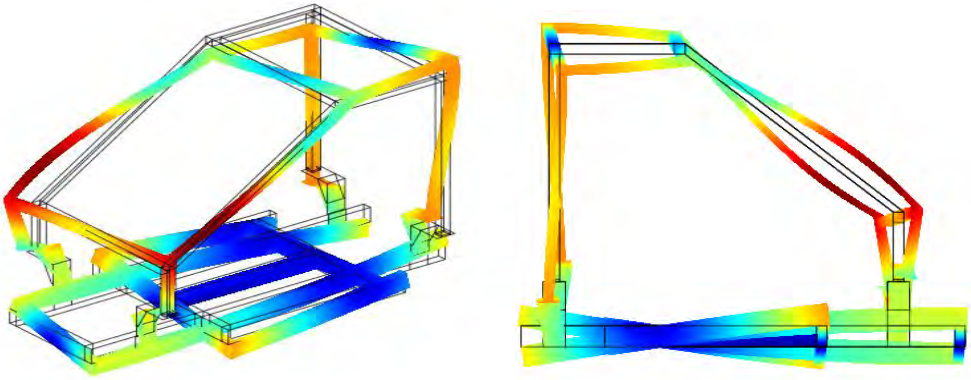

Figure 4.19: Modeshape predicted by the finite element model for the seventh mode at 69.05 Hz.

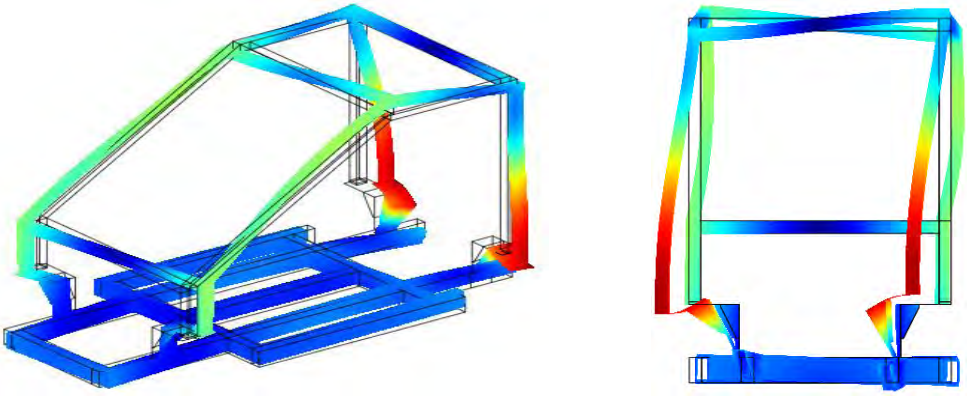

Figure 4.20: Modeshape predicted by the finite element model for the eight mode at 80.44 Hz.

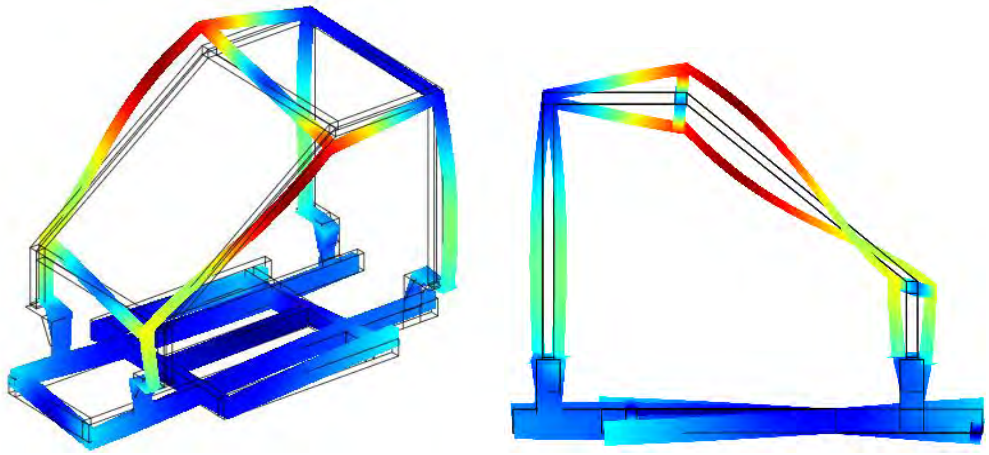

Figure 4.21: Modeshape predicted by the finite element model for the ninth mode at 83.25 Hz.

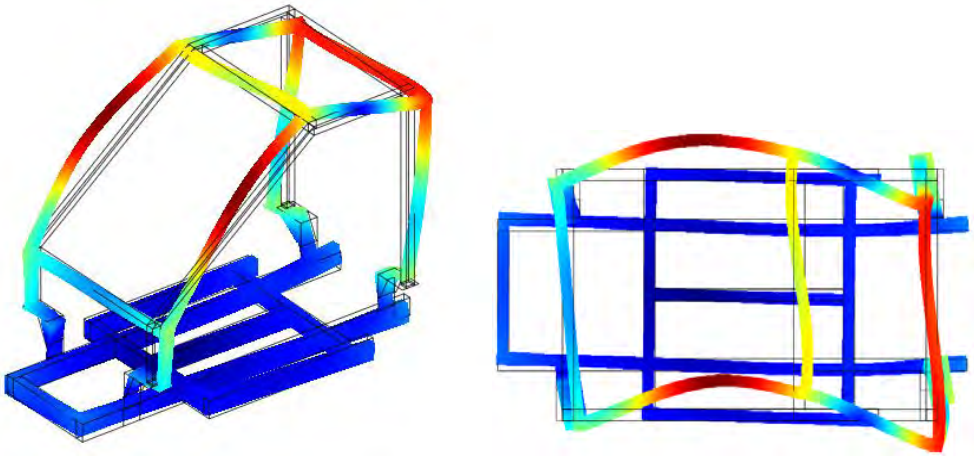

Figure 4.22: Modeshape predicted by the finite element model for the tenth mode at 101.60 Hz.

A sensor configuration involving 24 sensors is considered. The sensors are placed along the frame at the locations and directions as shown in Figure 4.23, measuring along the longitudinal, transverse and vertical directions. To investigate the accuracy and computational efficiency of the proposed CMS formulation, the FE model updating is first performed using the single objective optimization method by selecting the weight in (4) to be $w=1$. Results for the accuracy of the model

parameters and the computational effort are presented in Table 4.2 for the following six cases involving different reduction schemes in internal and boundary DOF: (a) $\rho = 8$, (b) $\rho = 5$, (c) $\rho = 2$, (d) $\rho = 8$ and $\nu = 200$, (e) $\rho = 5$ and $\nu = 200$, and (f) $\rho = 2$ and $\nu = 200$.

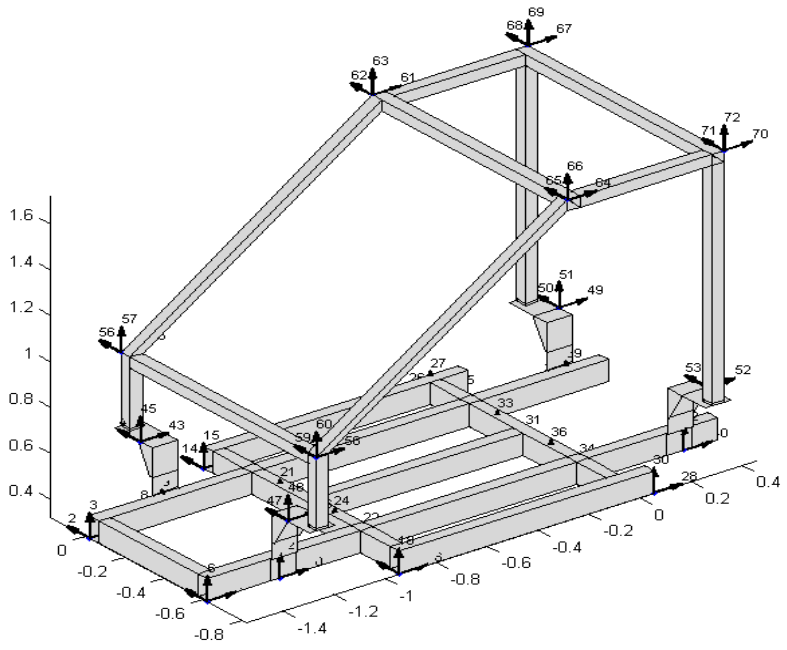

Figure 4.23: Sensor configuration involving 24 sensors

Table 4.3: Accuracy and computational effort for FE model updating based on full and reduced order models of vehicle.

FE Models	Total DOFs	Equally Weighted Method				Multi-objective Method Time (sec)
		Error (%) Max	Error (%) Mean	Function Evaluations	Time (sec)	
Full Model	45,564	0.00	0.00	16	1,262	13,177
$\rho = 8$	1,252	0.34	0.15	18	106	1,666
$\rho = 5$	1,234	0.26	0.13	18	103	1,610
$\rho = 2$	1,204	5.05	2.26	17	96	1,467
$\rho = 8, \nu = 200$	717	0.41	0.18	18	25	394
$\rho = 5, \nu = 200$	698	0.32	0.15	18	25	384
$\rho = 2, \nu = 200$	668	5.09	2.39	17	23	348

The initial values of the parameters used to carry out the optimization are $\theta_i = 1.2$, $i = 1, \cdots, 6$. The errors in the fourth column of the table are defined by the norm $\sqrt{\left\| (\underline{\theta}^{est} - \underline{\theta}^{full}) / \underline{\theta}^{full} \right\|_2 / N_\theta} \times 100$ of the fractional errors of the optimal model parameter estimates $\underline{\theta}^{est}$ obtained from the CMS-reduced FE model and the optimal estimates $\underline{\theta}^{full}$ obtained from the full (non - reduced) FE model.

The number of function evaluations and the computational effort are also shown in Table 4.2. The computational time for carrying out the optimization for the reduced-order models is 5% of the time required for the full model. Consequently, significant gains in computational effort are achieved without sacrificing the accuracy in the model parameter estimates. A further reduction in the computational effort, close to two order of magnitude, is achieved by reducing the interface degrees of freedom using $\nu = 200$, while the accuracy is maintained to acceptable levels .Overall, for $\rho = 8$ and $\nu = 200$, the computational effort is drastically reduced by two to three orders of magnitude, without sacrificing in accuracy since the error is smaller than 0.41%.

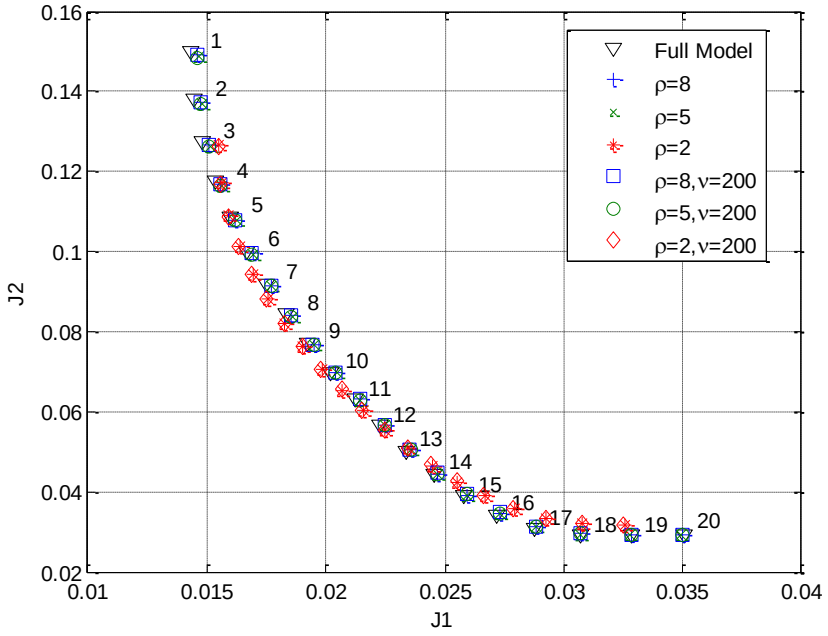

Figure 4.24: Comparison of Pareto fronts for the full and reduced-order FE models

Results are next presented for the multi-objective model updating framework. Figure 4.24 and Figure 4.25 present the Pareto front and the Pareto optimal models, respectively, computed using the full FE model and the six reduced-order models introduced before. The Pareto front and optimal solutions are represented by 20 points computed by the Normal Boundary Intersection algorithm (Das and Dennis, 1998). It is clear from Figure 4.25, that the quality of the estimates provided is excellent for the reduced-order models with $\rho = 8$, $\rho = 5$, $\rho = 8$ & $\nu = 200$ and $\rho = 5$ & $\nu = 200$ and very good for the reduced-order models with $\rho = 2$ and $\rho = 2$ & $\nu = 200$. The computational effort for performing the FE model updating using the full and reduced-order models is reported in the last column of Table 4.3. The computational time required to carry out the multi-objective optimization for obtaining the Pareto optimal models using the full FE model is of the order of 4 hours. Compared to the full model, the computational demands are substantially reduced by a factor of 10 for the reduced models with $\rho = 8$, $\rho = 5$ and $\rho = 2$ and by more than two orders of magnitude for the reduced models with $\rho = 8$ & $\nu = 200$, $\rho = 5$ & $\nu = 200$ and $\rho = 2$ & $\nu = 200$. Specifically, the computational time is almost half an hour when only the internal DOF of each component are reduced and 5 minutes when both internal and interface DOF are reduced.

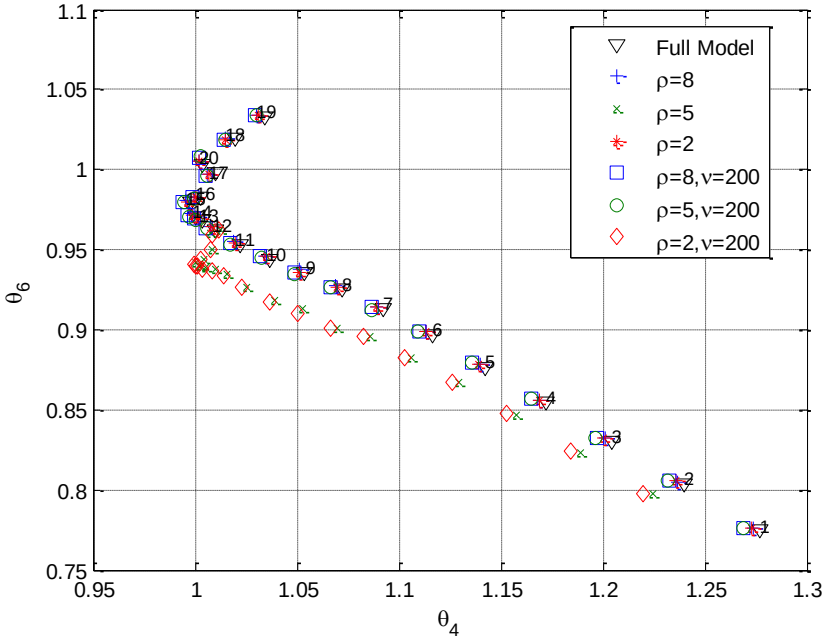

Figure 4.25: Comparison of Pareto models in the 2-d projection (θ_4, θ_6) of the 6-d parameter space for the full and reduced-order FE models.

A drastic reduction in computational effort is thus achieved by using the reduced-order models, without sacrificing in accuracy of the model parameter estimates as shown in Figure 4.24 and Figure 4.25.

4.5 Bayesian Uncertainty Estimation and Propagation of the Vehicle Structure

The value of the parameters appearing in the assumed models of the restoring and damping forces of the supports, like the coefficients k, c_1, c_2 and c_3 in (4.13) and (4.14) are determined by applying the Bayesian uncertainty quantification and calibration methodology. Results are obtained based on experimental response spectra values for both the displacement and acceleration of either the wheel or the suspension component. It is assumed that the prediction errors in the Bayesian formulation are uncorrelated with prediction error variance $\Sigma = diag(\Sigma_1, \Sigma_2) = diag(\sigma_1^2 I, \sigma_2^2 I)$, where $\Sigma_1 = \sigma_1^2 I$ and $\Sigma_2 = \sigma_2^2 I$ are the covariance matrices for the prediction errors corresponding to the displacements and accelerations, respectively. The parameter space is six dimensional and includes $\underline{\theta} = (k, c_1, c_2, c_3, \sigma_1, \sigma_2)$. Parameter estimation results are obtained using the parallelized and surrogate-based version (Angelikopoulos et al., 2012) of the TMCMC algorithm (Ching and Chen, 2007), with 500 samples per stage. Eight computer workers were used to perform in parallel the computations involved in the TMCMC algorithm. The computational time required to run all 5500 samples for the 11 TMCMC stages, without surrogate approximation, for the SDOF model is approximately 7 hours. Surrogate modeling (Angelikopoulos et al., 2012) reduces further this time by approximately one order of magnitude. For illustration purposes, results for the TMCMC samples projected in the two-dimensional parameter spaces (k, c_1), $(k, c_2), (k, c_3), (k, \sigma_1), (k, \sigma_2), (c_1, c_3)$, and (c_2, c_3) are shown from Figure 4.26 to Figure 4.33 for the SDOF system, corresponding to the suspension component.

It is clear that the uncertainties in the damping parameters c_1 and c_2 are relatively high and c_1 and c_2 are highly correlated along certain directions in the parameter space.

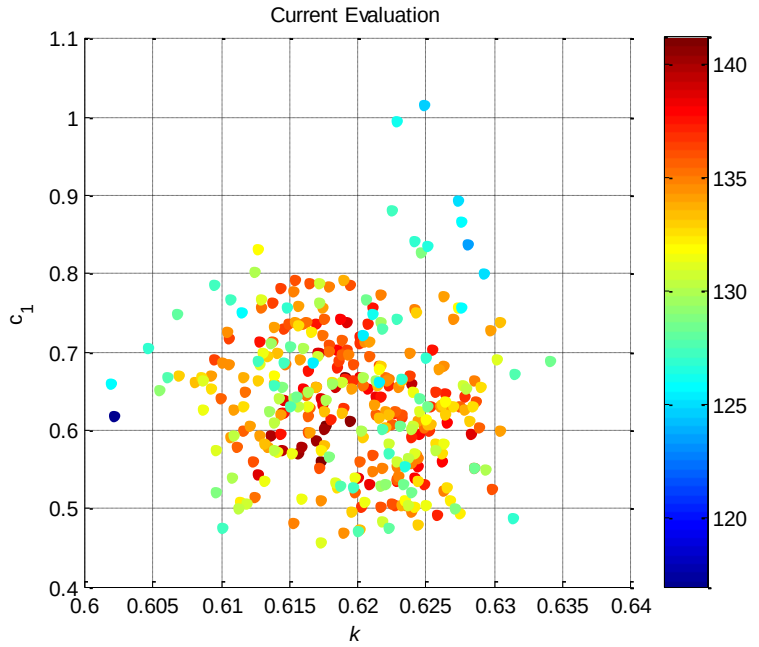

Figure 4.26: Model parameter uncertainty: projection of TMCMC samples in the two dimensional parameter space (k, c_1)

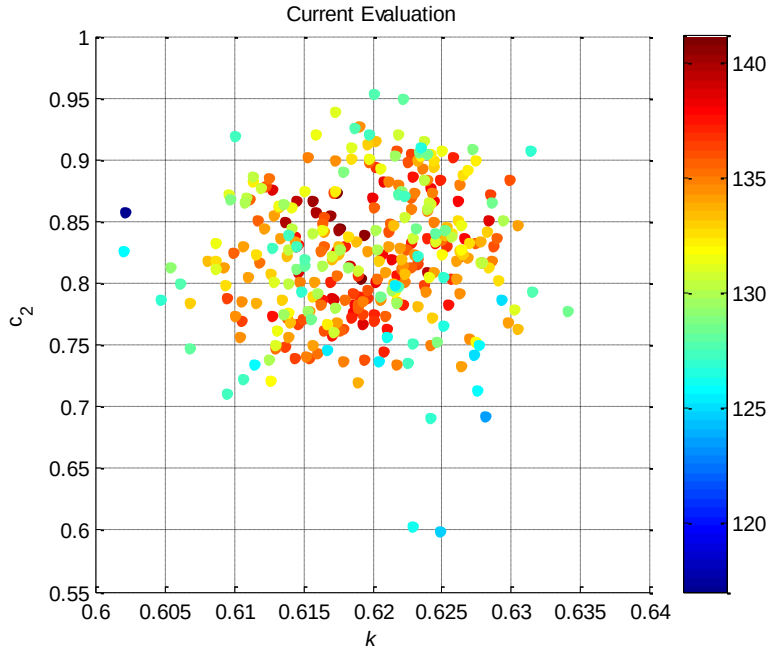

Figure 4.27: Model parameter uncertainty: projection of TMCMC samples in the two dimensional parameter space (k, c_2)

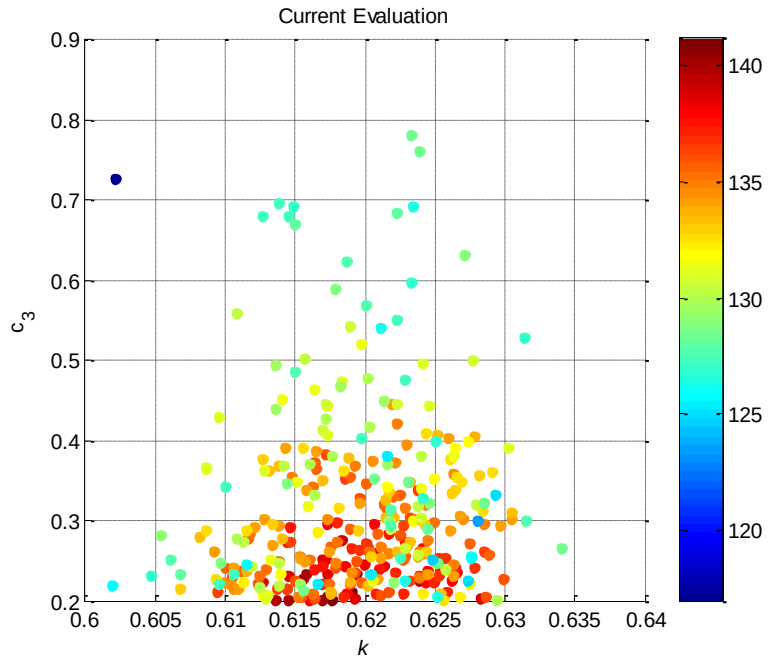

Figure 4.28: Model parameter uncertainty: projection of TMCMC samples in the two dimensional parameter space (k, c_3)

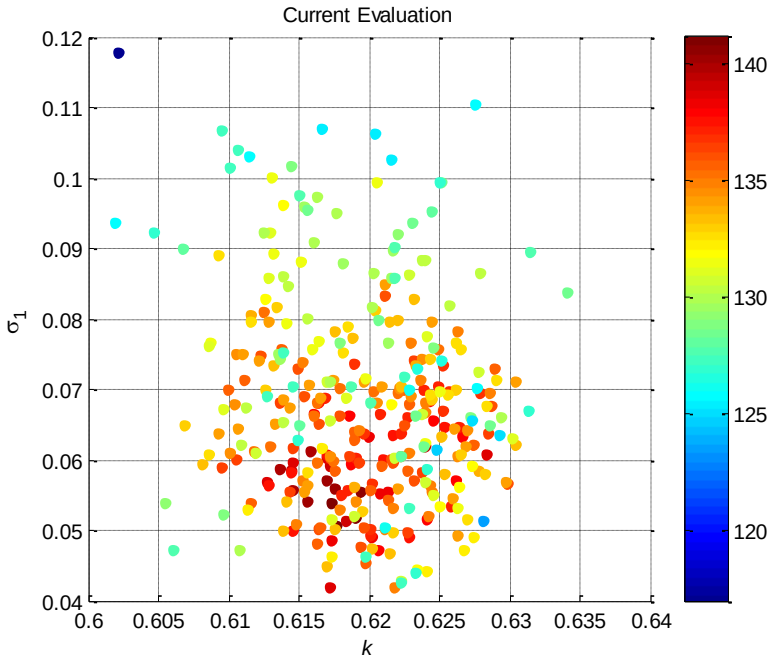

Figure 4.29: Model parameter uncertainty: projection of TMCMC samples in the two dimensional parameter space (k, σ_1)

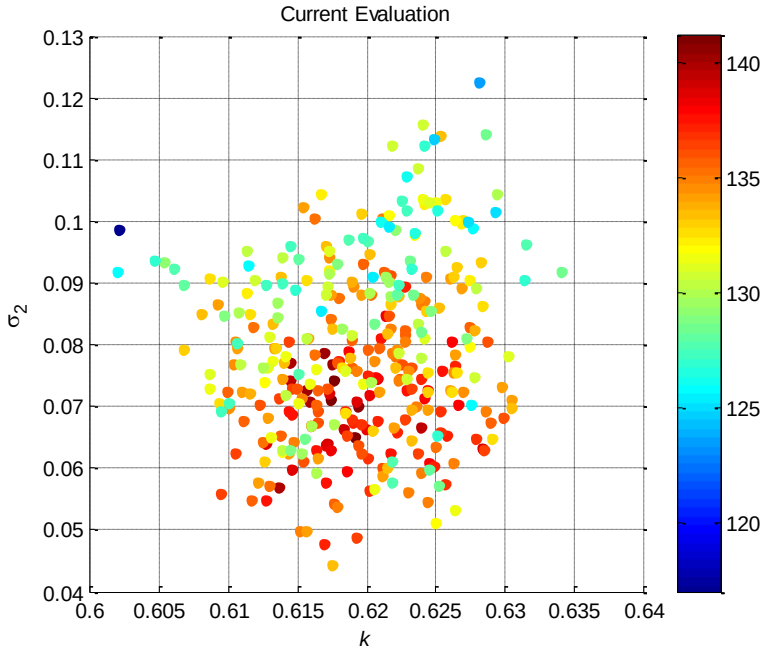

Figure 4.30: Model parameter uncertainty: projection of TMCMC samples in the two dimensional parameter space (k, σ_2)

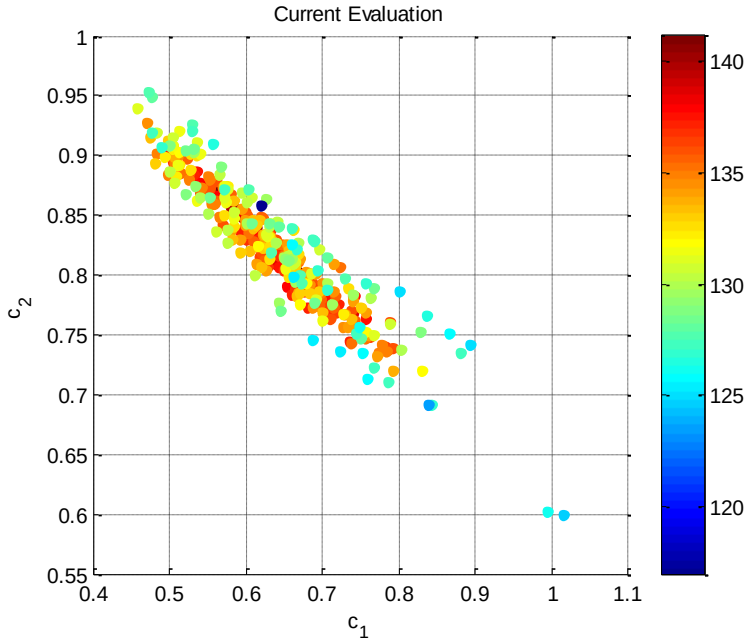

Figure 4.31: Model parameter uncertainty: projection of TMCMC samples in the two dimensional parameter space (c_1, c_2)

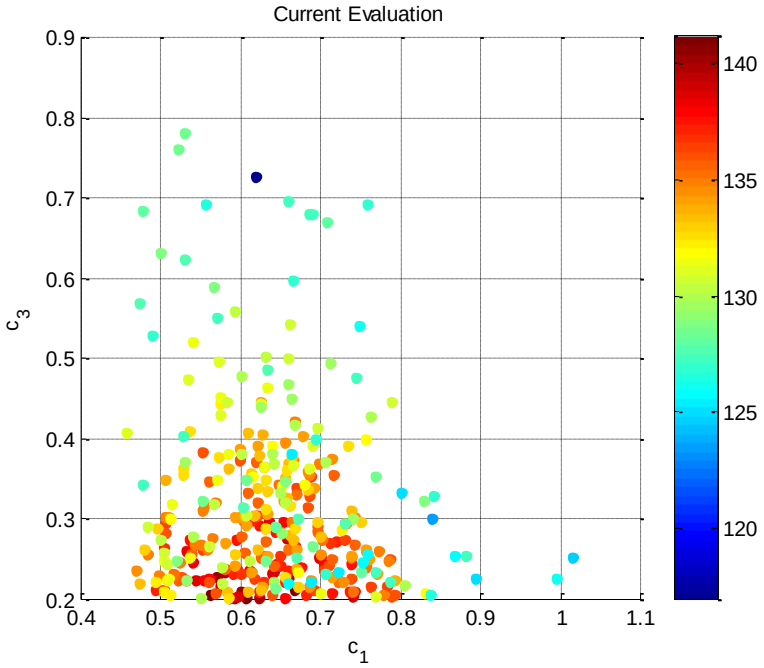

Figure 4.32: Model parameter uncertainty: projection of TMCMC samples in the two dimensional parameter space (c_1, c_3)

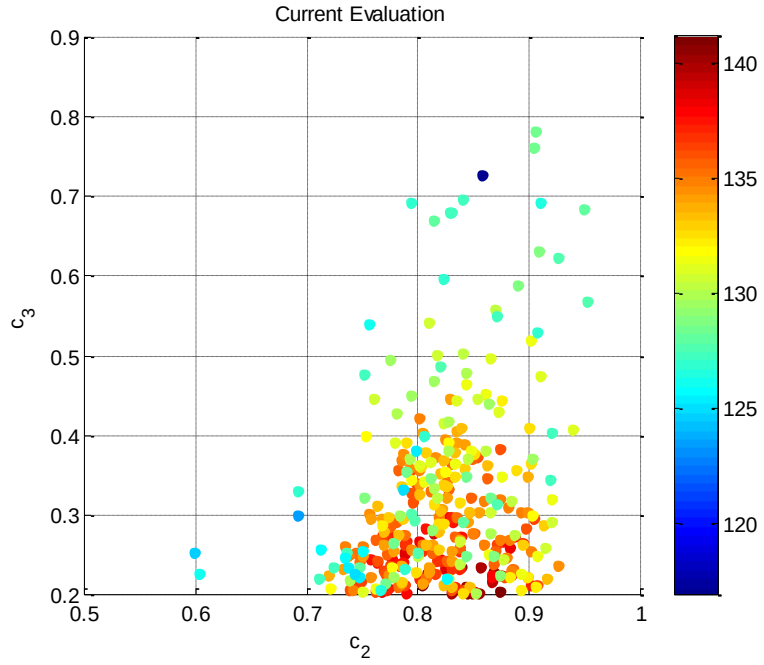

Figure 4.33: Model parameter uncertainty: projection of TMCMC samples in the two dimensional parameter space (c_2, c_3)

The parameter uncertainties are propagated through the SDOF model to estimate the uncertainties in the displacement and acceleration response spectra. The results are shown in Figure 4.34 and Figure 4.35 for the displacement for moderate and strong excitation level respectively and in Figure 4.36 and Figure 4.37 for the acceleration response spectra for moderate and strong excitation level respectively, and are compared to the experimental values of the response spectra. An adequate fit is observed. Discrepancies between the model predictions and the experimental measurements are mainly due to the model errors related to the selection of the particular forms of the restoring force curves in (4.13) and (4.14). The Bayesian model selection strategy based on equation (4.5) can be used to select among alternative restoring force models in an effort to improve the observed fit.

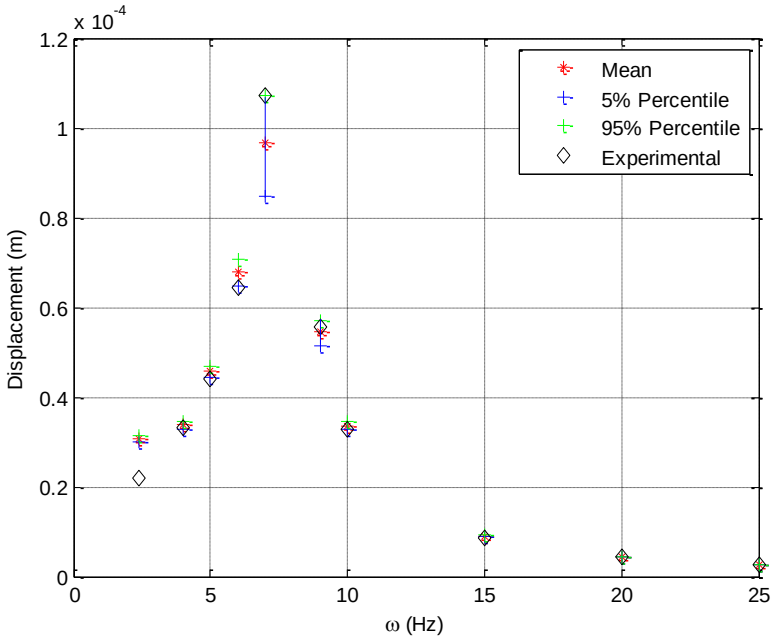

Figure 4.34: Uncertainty propagation: displacement response spectra uncertainty along with comparisons with the experimental data for the suspension component for moderate excitation level.

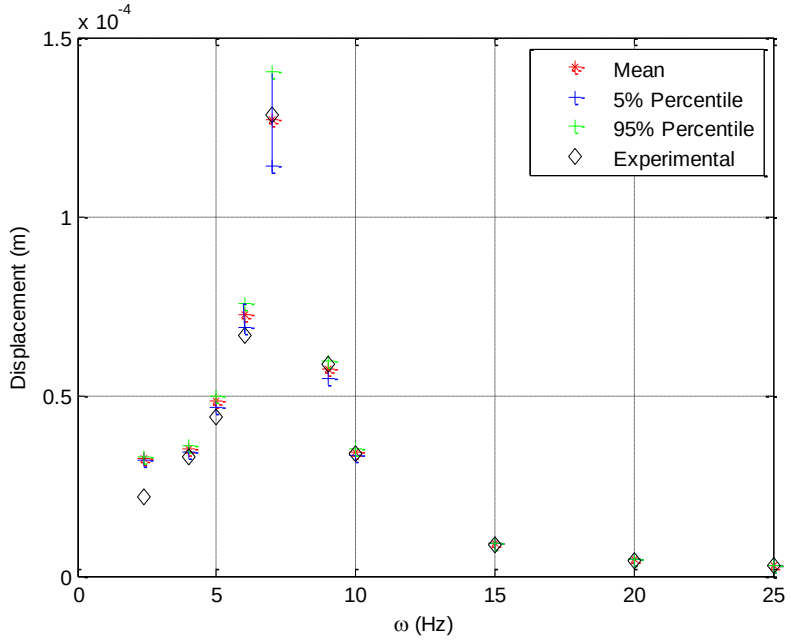

Figure 4.35: Uncertainty propagation: displacement response spectra uncertainty along with comparisons with the experimental data for the suspension component for strong excitation level.

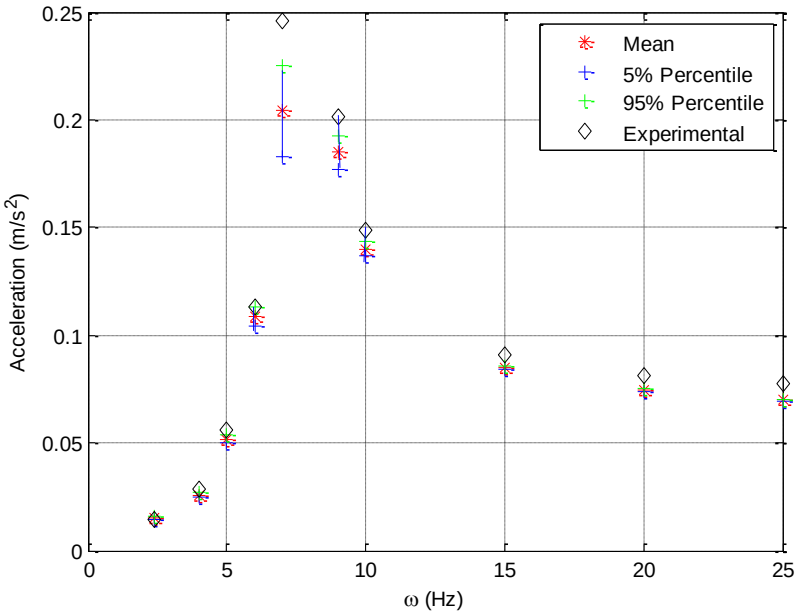

Figure 4.36: Uncertainty propagation: acceleration response spectra uncertainty along with comparisons with the experimental data for the suspension component for moderate excitation level.

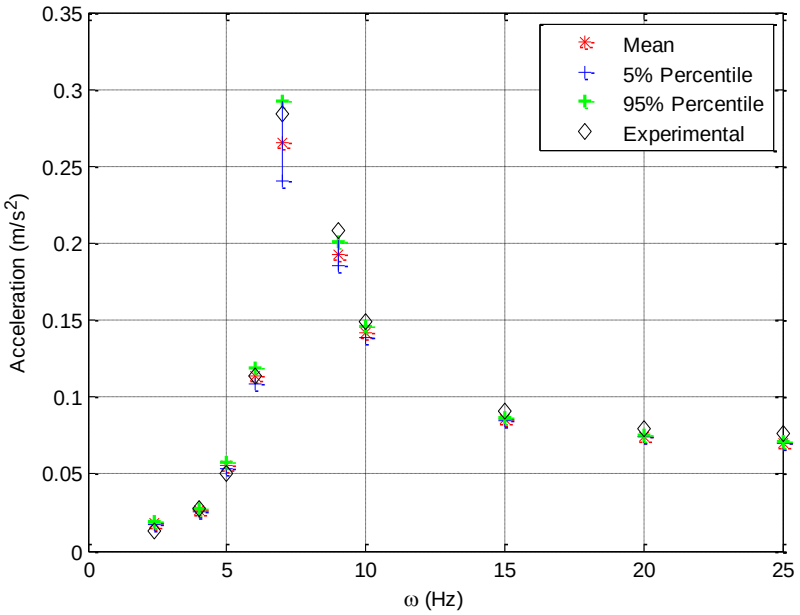

Figure 4.37: Uncertainty propagation: acceleration response spectra uncertainty along with comparisons with the experimental data for the suspension component for strong excitation level.

The above procedure has been repeated for the wheel component to identify the uncertainties in the linear stiffness and nonlinear damping model. The parameter uncertainties are again propagated through the SDOF model of the wheel to estimate the uncertainties in the displacement and acceleration response spectra. The results are shown in Figure 4.38 and Figure 4.39 for the displacement for moderate and strong excitation level respectively and in Figure 4.40 and Figure 4.41 for the acceleration response spectra for moderate and strong excitation level respectively, and are compared to the experimental values of the response spectra. An adequate fit is observed and for the case of the wheel component, while the discrepancies between the model predictions and the experimental measurements are again mainly due to the model errors related to the selection of the particular forms of the restoring force curves in (4.13) and (4.14).

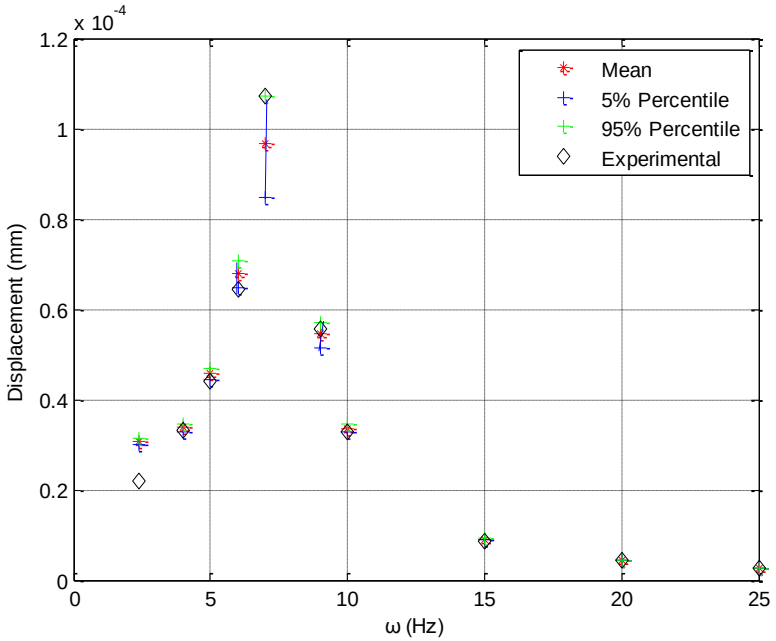

Figure 4.38: Uncertainty propagation: displacement response spectra uncertainty along with comparisons with the experimental data for the wheel component for moderate excitation level.

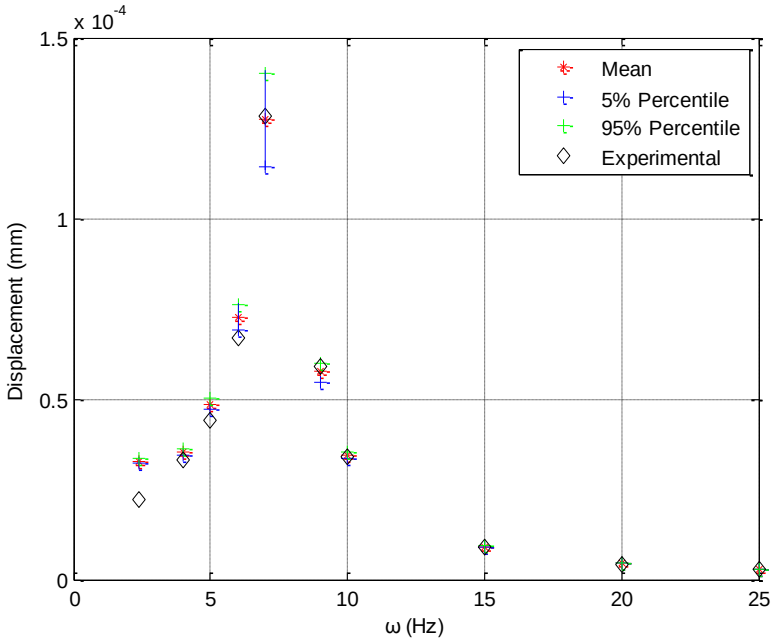

Figure 4.39: Uncertainty propagation: displacement response spectra uncertainty along with comparisons with the experimental data for the wheel component for strong excitation level.

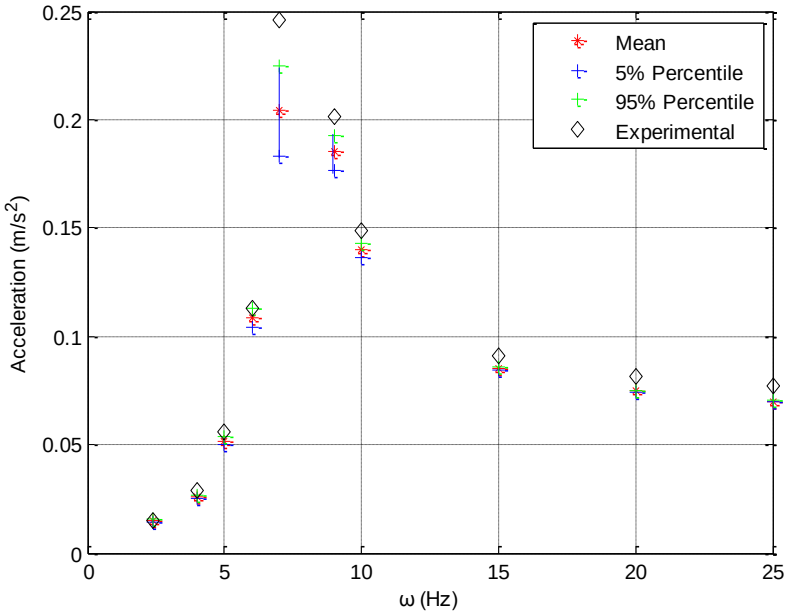

Figure 4.40: Uncertainty propagation: acceleration response spectra uncertainty along with comparisons with the experimental data for the wheel component for moderate excitation level.

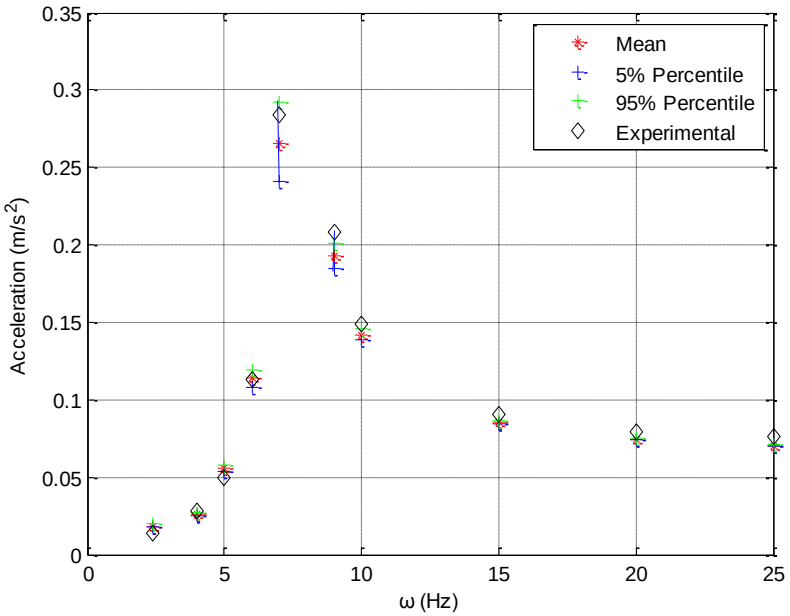

Figure 4.41: Uncertainty propagation: acceleration response spectra uncertainty along with comparisons with the experimental data for the wheel component for strong excitation level.

In addition, the uncertainties in nine stiffness-related parameters of the frame component were also estimated using the Bayesian methodology and the experimental values for the first ten modal frequencies and the mode shape components at 72 locations of the frame (Papadimitriou et al., 2011). The linear finite element model has 45564 DOFs. Due to excessive computational cost arising in stochastic simulation algorithms, the model was further reduced, retaining only the first 30 modes of the frame. using the CMS method for FE model updating ,presented in Chapter 3 The reduced model has 30 DOFs, resulting in substantial computational savings of more than two orders of magnitude.

The estimates of the model parameter values and their uncertainties for each component are used to build the model for the combined wheel-suspension-frame structure. The number of DOFs of the nonlinear model of the combined structure is 45568. The parametric uncertainties are then propagated to uncertainties in the response of the combined structure. The CMS was again used to reduce the number of DOFs to 34 and thus drastically reduce the computational effort that arises from the re-analyses due to the large number of TMCMC samples and the nonlinearity of the combined system.

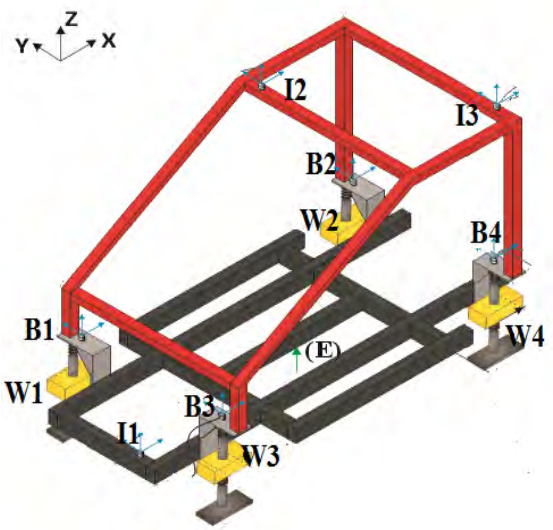

Figure 4.42: Points of the vehicle that uncertainties are propagated to theirs uncertainties for the acceleration transmissibility function.

Selected uncertainty propagation results are next presented. Specifically, the parameters of the wheel model and the model of the frame structure are kept to their mean values and only the uncertainties in the model parameters of the

suspension components are considered. Such uncertainties are propagated to uncertainties for the acceleration transmissibility function at some internal, boundary and wheel points of the vehicle that are shown in Figure 4.42.

Specifically, uncertainties are propagated to uncertainties for the acceleration transmissibility function at a point on the wheel W2 at the back left side of the vehicle as shown in Figure 4.41, a point on the wheel W3 at the front right side of the vehicle as shown in Figure 4.42, the connection of the wheel with the frame B2 at the back left side of the vehicle as shown in Figure 4.43, the connection of the wheel with the frame B3 at the front right side of the vehicle as shown in Figure 4.44,and for three internal points on the frame I1, I2, I3 as shown in Figure 4.47, Figure 4.48 and Figure 4.49 respectively.

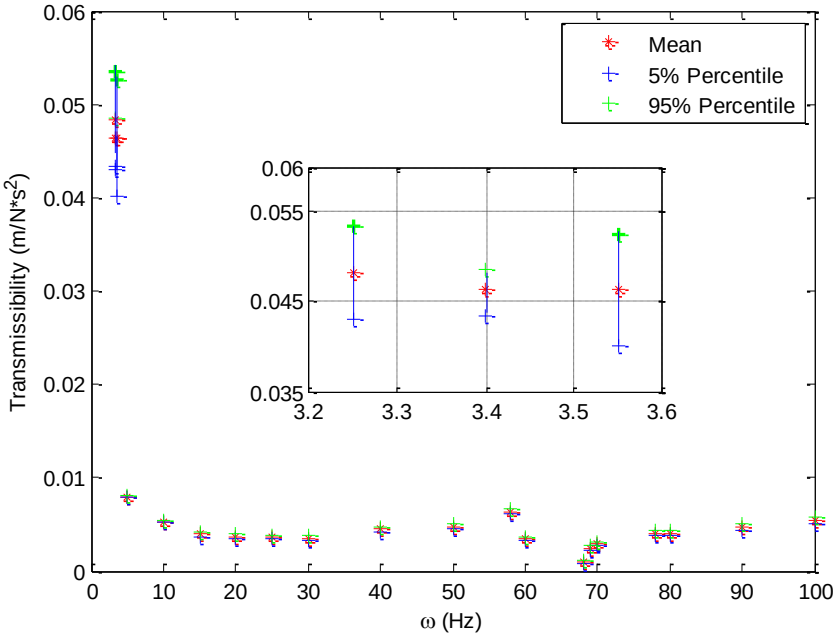

Figure 4.43: Uncertainty propagation: acceleration transmissibility function uncertainty for combined system for the wheel DOF W2

It is observed that a large uncertainty in the response spectra is obtained at the resonance region close to 3.4 Hz, which is dominated by local wheel body deflections. The response in the resonance regions close to 58 Hz and 68 Hz is mainly dominated by deflection of the frame structure.

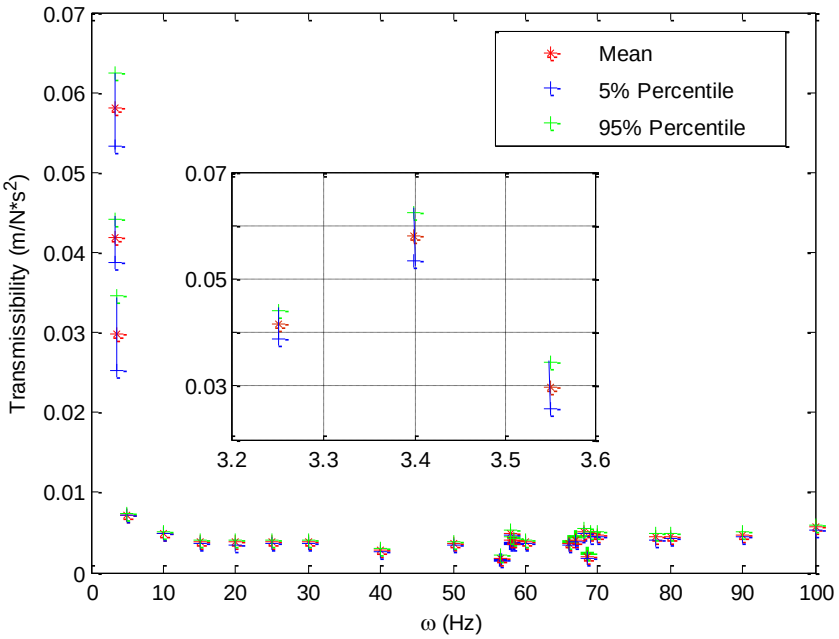

Figure 4.44: Uncertainty propagation: acceleration transmissibility function uncertainty for combined system for the wheel DOF W3

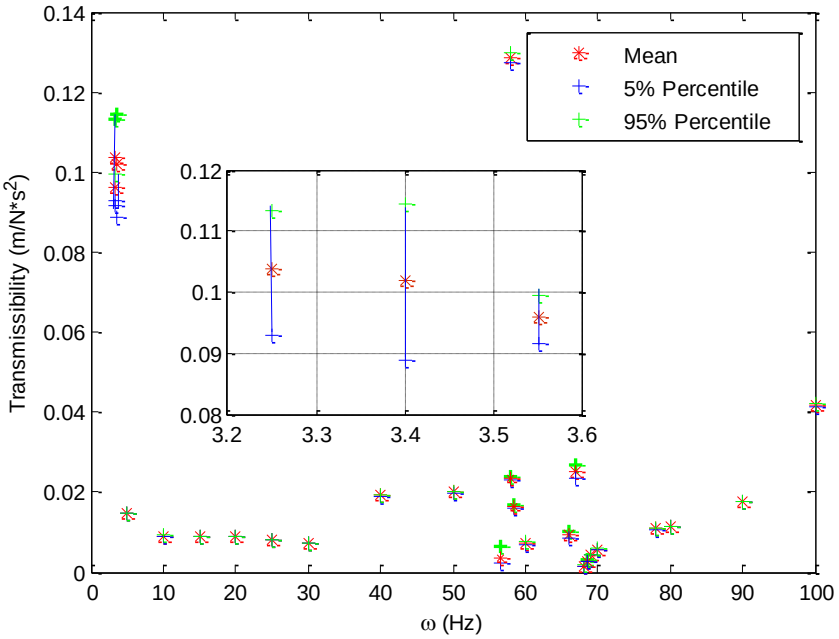

Figure 4.45: Uncertainty propagation: acceleration transmissibility function uncertainty for combined system for DOF B2 at connection between suspension and frame

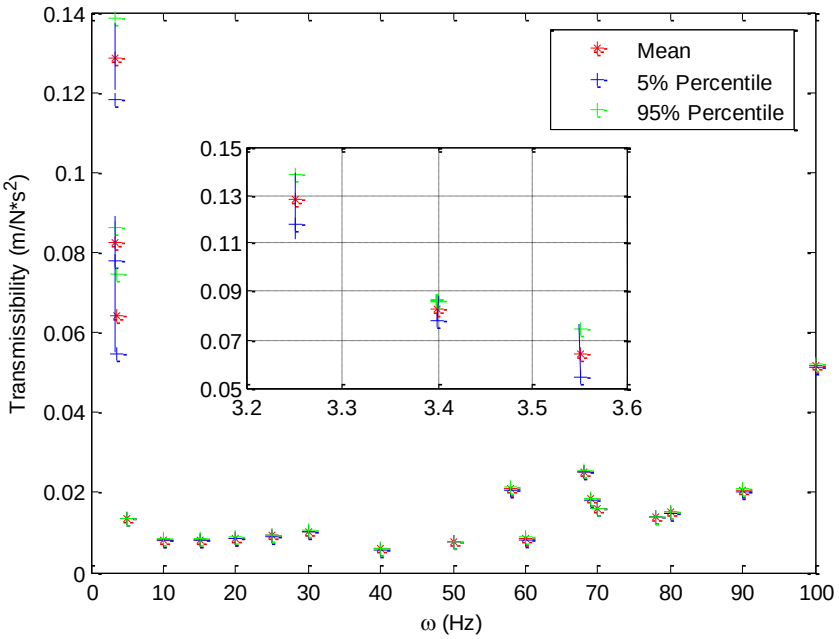

Figure 4.46: Uncertainty propagation: acceleration transmissibility function uncertainty for combined system for DOF B3 at connection between suspension and frame.

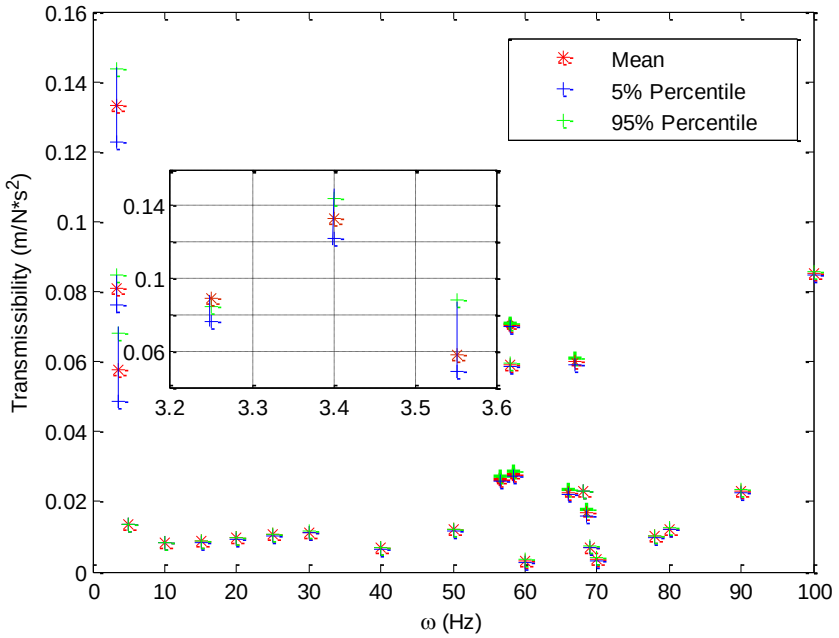

Figure 4.47: Uncertainty propagation: acceleration transmissibility function uncertainty for combined system for frame DOF I1.

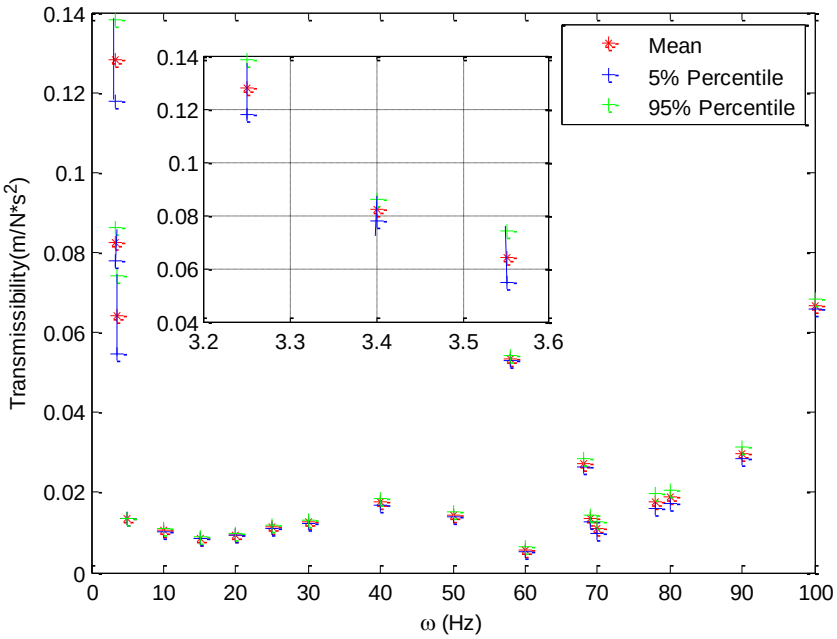

Figure 4.48: Uncertainty propagation: acceleration transmissibility function uncertainty for combined system for frame DOF I2.

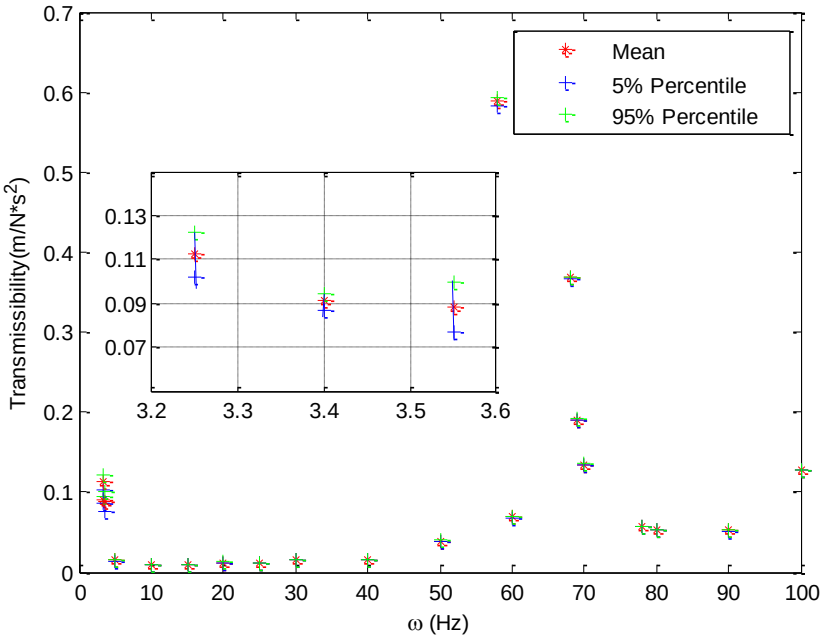

Figure 4.49: Uncertainty propagation: acceleration transmissibility function uncertainty for combined system for frame DOF I3.

It is observed that the uncertainties in the suspension parameters do not significantly affect the response spectra at the resonance regions. As a result, response spectra obtained experimentally in these resonance regions for the complete vehicle model are not expected to be adequate to identify uncertainties in the parameters of the suspension model.

4.6 Conclusions

A Bayesian UQ&P framework was presented for identifying nonlinear models of dynamic systems using vibration measurements of their components. The use of Bayesian tools, such as stochastic simulation algorithms (e.g., TMCMC algorithm), may often result in excessive computational demands. Drastic reduction in computational effort to manageable levels is achieved using component mode synthesis, surrogate models and parallel computing algorithms. The framework was demonstrated by identifying the linear and nonlinear components of a small-scale laboratory vehicle model using experimental response spectra available separately for each component. Such model uncertainty analyses for each component resulted in building a high fidelity model for the combined system to be used for performing reliable robust response predictions that properly take into account model uncertainties. The theoretical and computational developments in this work can be used to identify and propagate uncertainties in large order nonlinear dynamic systems that consist of a number of linear and nonlinear components.

CHAPTER 5 Fatigue Monitoring in Metallic Structures using Vibration Measurements from a Limited Number of Sensors

5.1 Introduction

A permanently installed network of sensors in a structure is often used to record output-only vibration measurements during operation. These vibration measurements provide valuable information for estimating important dynamic characteristics of the structures such as modal frequencies, modeshapes and modal damping ratios, updating finite element models, monitoring the health of the structure by identifying the location and severity of damage, identifying the temporal/spatial variation of the loads applied on the structure (Lourens et al., 2012), estimating the state (Ching et al., 2006; Wu and Smyth, 2007; Hernandez and Bernal, 2008; Chatzi and Smyth, 2009), and updating robust predictions of system performance (Papadimitriou et al., 2001; Beck, 2010). Recently, output-only vibration measurements were proposed to use for the estimation of fatigue damage accumulation in metallic components of structures (Papadimitriou, Fritzen et al., 2011). This is an important safety-related issue in metallic structures since information on fatigue damage accumulation is valuable for structural risk

assessment and for designing optimal, cost-effective maintenance strategies. Predictions of fatigue damage accumulation at a point of a structure can be estimated using available damage accumulation models that analyze the actual stress time histories developed during operation (Palmgren, 1924; Miner, 1945).

The stress response time histories can be readily inferred from strain response time histories directly measured using strain rosettes attached to the structure. However, such predictions are only applicable for the locations where measurements are available. A large number of strain sensors are therefore required to cover all hot spot locations in large structures encountered in engineering applications. Due to practical and economical considerations, the number of sensors placed in a structure during operation is very limited and in most cases they do not cover all critical locations. Moreover, there are locations in the structure that one cannot install sensors such as submerged structures, underwater locations in offshore structures (oil refinery structures, offshore wind turbines, offshore steel jackets, etc.), heated structural components, internal points in solid structures, and non-approachable areas of large extended structures. Available fatigue prediction methods based only on measurements cannot be used to predict fatigue damage accumulation at such locations where measurements are not available. In addition, in monitoring applications of a number of structures, acceleration measurements are conveniently used instead of strain measurements.

In order to proceed with fatigue predictions one has to infer the strain/stress response time histories characteristics based on the monitoring information contained in vibration measurements collected from a limited number of sensors attached to a structure. Such predictions are possible if one combines the information in the measurements with information obtained from a high fidelity finite element model of the structure. It is important to note that such estimations will reflect the actual strain time history characteristics developed on the structure during operation and thus the corresponding fatigue damage accumulation estimates will be more representative of the fatigue accumulated in the structure at the point under consideration. Repeating such estimates at all points in the structure, one is able to develop realistic fatigue damage accumulation maps that cover the entire structure.

These developments are very important for planning cost-effective maintenance strategies of number of structures that take into account the actual condition of the structure instead of being based on statistical models derived from data from a group of structures.

The work by Papadimitriou et al. (2011) was a first attempt along this direction. Prediction of fatigue accumulation was based solely on the spectral characteristics of the strain time histories, assuming that the time histories can be considered stationary over short enough time intervals. Specifically, the fatigue damage accumulation in critical locations of the entire structure was obtained by integrating (a) methods for predicting strain/stress response time histories and their correlation/spectral characteristics in the entire structure from output-only measured response time histories available at limited locations in the structure, and (b) frequency domain methods (Benasciutti and Tovo, 2006), for estimating fatigue damage accumulation using the spectral characteristics of the predicted strain/stress response time histories. In particular, Kalman filter methods were used to predict the spectral characteristics of the strain/stress response time history at various locations within structural components using measurements available at a limited number of locations. The main assumption was that the excitation or portions of the excitations can be approximated by a stationary stochastic process.

For a number of applications, however, the assumption of stationarity is either violated or is not representative of the actual excitation conditions. An obvious case in civil engineering where the non-stationarity of the excitation and response is pronounced includes the passage of trains or heavy trucks over metallic bridges. The fatigue under train or large truck loads is an important safety issue. However, the damage accumulation predictions proposed in Papadimitriou et al. (2011) are not applicable. Consequently, there is a need to use new estimation methods capable of predicting the full strain response time histories that are more appropriate in case of non-stationary excitations.

In this chapter, the problem of estimating the full strain time histories characteristics at critical locations of the structure using operational vibration measurements from a limited number of sensors is presented. The measurements may consist of response time histories such as e.g. strain, acceleration, velocity, displacement, etc. Moreover, this chapter deals with the use of such estimates to predict fatigue damage accumulation in the entire body of a metallic structure and lays out the formulation for estimating fatigue using output-only vibration measurements and outlines methods for estimating the stress response history characteristics required in deterministic and stochastic fatigue theories. Similar estimation techniques can be used to estimate other important response characteristics in the entire body of the structure, such as displacements, velocities, accelerations, etc. The analyses in this study are first implemented to the case of linear structures and then have been extended to cover nonlinear

models of structures. The stress response quantities are predicted at locations subjected to uni-axial stress states. The measured quantities are considered to be accelerations, displacements or strains or a combination of accelerations, displacements and strains.

The objective of this work is to formulate the fatigue prediction problem, illustrate the methodology and point out its use in evaluating the damage accumulation in the entire structure from a limited number of vibration measurements. For this, the analyses in this study are restricted to the case of stress response predictions at locations subjected to uni-axial stress states for both linear and nonlinear structures. The extension to multi-axial stress processes can be accomplished by using recent developments in frequency domain methods for stochastic fatigue based on spectral techniques (Preumont and Piefort, 1994; You and Lee, 1996; Pitoiset and Preumont, 2000). These methods reduce the multi-axial stress state to an equivalent uniaxial stress state that can be treated by available fatigue estimation techniques based on spectral methods.

This chapter is organized as follows. In Section 5.2, the deterministic and stochastic fatigue damage accumulation formulations are outlined. Section 5.3 presents the methods for estimating the strain response time history characteristics using operational vibration measurements, that are required in the fatigue formulations. In Section 5.4, state of the art algorithms for joint identification of state and input information are presented. Finally, Section 5.5 demonstrates the effectiveness of the proposed methodology using a chain-like mass-spring multi-degree-of-freedom (MDOF) structure and a small scale vehicle-like frame structure. Conclusions are summarized in Section 5.6.

5.2 Fatigue monitoring using operational vibrations

5.2.1 Deterministic Fatigue Damage Accumulation

The Palmgren-Miner rule (Palmgren, 1924; Miner, 1945) is commonly used to predict the damage accumulation due to fatigue. According to this rule, a linear damage accumulation law at a point in the structure subjected to variable amplitude stress time history is defined by the formula

$$D = \sum_{i}^{k} \frac{n_i}{N_i} \tag{5.1}$$

is n_i the number of cycles at a stress level σ_i, N_i is the number of cycles required for failure at a stress level σ_i, and k is the number of stress levels

identified in a stress time history at the corresponding structural point. S-N fatigue curves available from laboratory experiments on simple specimens subjected to constant amplitude loads, are used to describe the number of cycles N_i required for failure in terms of the stress level σ_i. The number of cycles n_i at a stress level σ_i is usually obtained by applying stress cycle counting methods, such as the rainflow cycle counting, on the stress time histories measured or estimated for the point under consideration. The fatigue damage accumulation at a point requires that the full stress time histories are available. The fatigue accumulation model can be revised to account for a non-zero mean stress according to the Goodman relationship (Tunna, 1986).

$$\Delta\sigma_{\mathrm{Rt}} = \Delta\sigma_{\mathrm{R}}\left(1-\frac{\sigma_{\mathrm{m}}}{\sigma_{\mathrm{u}}}\right) \tag{5.2}$$

where $\Delta\sigma_{\mathrm{Rt}}$ is the modified stress cycle range, $\Delta\sigma_{\mathrm{R}}$ is the original stress cycle range, σ_{m} is the mean stress, and σ_{u} is the static strength of the material.

Applying Miner's rule, the fatigue damage of a structural detail depends on the stress range spectrum (stress range $\Delta\sigma$ and number of stress cycles n) and the fatigue detail category classified in the Eurocode 3 (EN 1993-1-9 Eurocode 3, 2005) as follows:

$$D = \underbrace{\sum_{j=1}^{k_1}\frac{n_i}{5\times10^6}\left(\frac{\Delta\sigma_i}{\Delta\sigma_D}\right)^m}_{\Delta\sigma_{\mathrm{i}} \geq \Delta\sigma_D} + \underbrace{\sum_{j=1}^{k_2}\frac{n_j}{5\times10^6}\left(\frac{\Delta\sigma_j}{\Delta\sigma_D}\right)^{m+2}}_{\Delta\sigma_L \leq \Delta\sigma_j \leq \Delta\sigma_D} \tag{5.3}$$

where $\Delta\sigma_{\mathrm{D}}$ is the constant amplitude fatigue limit at 5×10^6 cycles; $\Delta\sigma_{\mathrm{L}}$ is the cut-off limit; $\Delta\sigma_{\mathrm{i}}$ and $\Delta\sigma_{\mathrm{j}}$ are the i^{th} and j^{th} stress ranges, n_i and n_j are the number of cycles in each $\Delta\sigma_{\mathrm{i}}$ and $\Delta\sigma_{\mathrm{j}}$ block, and k_1 and k_2 represent the number of different stress range blocks above or below the constant amplitude fatigue limit $\Delta\sigma_{\mathrm{D}}$.

In Eurocode 3, each fatigue detail category is designated by a number which represents, in N/mm^2, the reference value $\Delta\sigma_{\mathrm{C}}$ for the fatigue strength at 2 million cycles. As this study focuses on the accuracy of the fatigue damage predicted by the proposed method, the fatigue detail category 36 is adopted to illustrate the method. The following values of the parameters of the design S-N curves are recommended by Eurocode for detail category 36: $m=3$, $\Delta\sigma_{\mathrm{D}}=26.5\,\mathrm{MPa}$ and $\Delta\sigma_L=14.5$ MPa.

5.2.2 Estimation of strains at finite element level

The relation between the strain and the displacement at all DOFs depends on the type of the finite elements used. It can be readily obtained using the type of finite element used, the shape functions and the coordinates of the nodes of the elements and the strain points. Usually commercial finite element codes are not open to the user to implement such relationships. As a result, for applications where the mass, stiffness and modal properties are computed once in commercial finite element codes and then they are transferred in Matlab for further processing, such relations are not available and have to be build up. In the following, the procedure to build the expression that relates the strains at a finite element with the element nodal displacement is outlined.

Let $\varepsilon^{(e)}$ denote the strain at a point within the finite element e and let $\underline{u}^{(e)}$ be the vector of nodal displacements. Assuming a linear model and using the finite element formulation, the relation between the strain and the nodal displacement vector is given by

$$\varepsilon^{(e)} = \sum_{i=1}^{N_e} a_i^{(e)} u_i^{(e)} = \underline{a}^{(e)T} \underline{u}^{(e)} \tag{5.4}$$

where N_e is the number of element DOFs, and $a_i^{(e)}$ are constants that depend on the element type, location of nodal points in space, the element shape functions and the location of the strain point within the finite element. The relation between the strain $\varepsilon^{(e)}$ and the element nodal displacement vector $\underline{u}^{(e)}$ is completely defined by the coefficients $a_i^{(e)}$ which are independent of the loading type (static or dynamic) or the temporal-spatial variation of the excitations. The N_e unknown $a_i^{(e)}$, $i = 1, \cdots, N_e$, can then be computed from at least as many as N_e static finite element analyses as follows.

For this purpose, M $(M \geq N_e)$ static loading patterns corresponding to load vectors $\underline{p}_1, \cdots, \underline{p}_M$. Let $\varepsilon_j^{(e)}$ and $\underline{u}_j^{(e)}$ be the strain and nodal displacement vector, respectively, obtained at the element level for the loading case $\underline{p}_j$. These quantities are usually output quantities of a commercial finite element code and can be readily obtained from the output file. Then using (5.4), the following linear system of M equations holds:

$$\varepsilon_j^{(e)} = \underline{u}_j^{(e)T} \underline{a}^{(e)}, \qquad j = 1, \cdots, M \tag{5.5}$$

If we consider the matrix

$$\underline{\varepsilon}^{(e)} = \left[\varepsilon_1^{(e)} \cdots \varepsilon_M^{(e)} \right]^T \tag{5.6}$$

and the matrix

$$U^{(e)} = \left[\underline{u}_1^{(e)} \cdots \underline{u}_M^{(e)} \right]^T \tag{5.7}$$

the linear system (5.5) takes the matrix form

$$\underline{\varepsilon}^{(e)} = U^{(e)} \underline{a}^{(e)} \tag{5.8}$$

The solution of this linear system is given by

$$\underline{a}^{(e)} = \left[U^{(e)T} U^{(e)} \right]^{-1} U^{(e)T} \underline{\varepsilon}^{(e)} \tag{5.9}$$

We should note that $M \geq N_e$ and thus it is expected that at most N_e equation in (5.8) can be linearly independent. The number of M loading case should be selected to be higher than N_e and the corresponding loading patterns should be carefully selected in order to make sure that N_e lineally independent equations in (5.5) are generated so that the matrix $\left[U^{(e)T} U^{(e)} \right]$ in (5.9) is nonsingular. This step is important to guarantee the accuracy of the unknowns $\underline{a}^{(e)}$. Also, after the $\underline{a}^{(e)}$ are estimated, the estimate should be validated by computing the predictions $\hat{\underline{\varepsilon}}^{(e)}$ of the strains from (5.8) using the estimated $\underline{a}^{(e)}$ and comparing these predictions with the strain values $\varepsilon^{(e)}$ already obtained by the finite element model for each loading case.

The aforementioned procedure is repeated for all desirable strain points and the corresponding finite elements $\langle e \rangle$ on which these strain points belong. Once the relation between the strain $\varepsilon^{(e)}$ and the element nodal displacement $\underline{u}^{(e)}$ has been established, then the relation between the strain and the whole model displacement vector $\underline{u}$, containing the displacement at all DOFs, can be obtained by using the transformation

$$\varepsilon^{(e)} = L^{(e)} \underline{u} \tag{5.10}$$

where $L^{(e)}$ is a matrix of zeros and ones that relates the entries in the respective vectors $\underline{u}^{(e)}$ and $\underline{u}$. Finally, substituting (5.10) into (5.4), the relation between strains at element level and displacement vector $\underline{u}$ is given by

$$\varepsilon^{(e)} = \underline{a}^{(e)T} L^{(e)} \underline{u} \tag{5.11}$$

5.2.3 Stochastic Fatigue Damage Accumulation

Alternatively, for the cases where the full stress response time histories are not available from measurements, frequency domain methods based on spectral moments (Lutes and Larsen, 1990; Benasciutti and Tovo, 2006), can be used to predict the expected damage due to fatigue using the linear damage law (5.1). The methodology assumes that the stress is considered to be a stationary Gaussian stochastic process and that the power spectral density of the stress process at a structural location is available. For linear systems excited by time-varying loads that can be modeled by stationary stochastic processes, these power spectral densities can be straightforward computed using available random vibration results (Lutes and Sarkani, 2004).

Using frequency domain methods for fatigue estimation under stochastic excitations (Lutes and Larsen, 1990), and the continuous version of the damage accumulation law (5.1), the expected fatigue damage accumulation rate for a uni-axial stochastic stress process using the Dirlik formula (Dirlik, 1985), for the probability distribution of the stress levels for Gaussian stochastic stress processes, is given as a function of the spectral moments $\lambda_0, \lambda_1, \lambda_2, \lambda_4$ of the stress process (Benasciutti and Tovo, 2006), i.e.

$$\bar{D} \equiv \bar{D}(\lambda_0, \lambda_1, \lambda_2, \lambda_4) \tag{5.12}$$

where the form of $\bar{D} \equiv \bar{D}(\lambda_0, \lambda_1, \lambda_2, \lambda_4)$ can be found in (Benasciutti and Tovo, 2006). The expected time of failure due to fatigue (fatigue lifetime) is $T_{life} = 1/\bar{D}$, corresponding to a critical expected damage value $E[D] = D_{cr} = 1$. The aforementioned formulation assumes that the stress process at a point is uni-axial. For multi-axial stress states one can apply available methods (Pitoiset and Preumont , 2000), to extend the applicability of the present methodology. It is clear that the expected fatigue damage rate $\bar{D}$ at a point in the structure depends only on the spectral moments λ_i, $i = 0,1,2,4$, of the stress process $\sigma(t)$. Using the definition of the spectral moments $\lambda_j = \int_{-\infty}^{\infty} |\omega|^j S_\sigma(\omega) d\omega$, the spectral moments and the fatigue predictions at a point of a structure eventually depend only on the power spectral density $S_\sigma(\omega)$ of the stress process $\sigma(t)$. The power spectral densities of the stress response processes at a point can be calculated from measurements, provided that these measurements are long enough to be considered stationary. This issue of predicting the power spectral densities of the stress processes in the entire body of the structure using measurements at limited locations is addressed at the next Section 5.3.2.

5.3 Strain Monitoring using output only vibration measurements

The objective of this section is to predict the characteristics of strain responses, such as power spectral densities or full strain time histories, at all hot spot locations in a structure using output-only vibration measurements collected from a limited number of sensors attached to the structure. Such predictions are integrated with the fatigue damage accumulation laws to estimate the fatigue in the whole structure taking into account real measurements, instead of postulated excitation models that in most cases are not representative of the actual behavior of the structure.

5.3.1 Continuous-time state space formulation of equations of motion

It is assumed that the system can be represented by a linear model subjected to a number of excitations. The equations of motion are given by the following set of N second-order differential equations resulting from a spatial discretization (finite element analysis) of the structure The equations of motion are given by the following set of N second-order differential equations resulting from a spatial discretization of the structure, e.g. by finite element analysis

$$M\underline{\ddot{u}}(t)+C\underline{\dot{u}}(t)+K\underline{u}(t)=L_p\underline{p}(t) \tag{5.13}$$

where $\underline{u}(t)\in R^{N\times 1}$ is the displacement vector, M, C and $K\in R^{N\times N}$ are respectively the mass, damping and stiffness matrices, $\underline{p}(t)\in R^{N_{in}\times 1}$ is the applied excitation vector, and $L_p\in R^{N\times N_{in}}$ is a matrix comprised of zeros and ones that maps the N_{in} excitation loads to the N output DOFs. Throughout the analysis, it is assumed that the system matrices M, C and K are symmetric. Let $\underline{y}(t)\in R^{N_{meas}\times 1}$ be the vector that collects all N_{meas} measurements at different locations of the structure at time t. These measurements are expressed in terms of the displacement/strain, velocity and acceleration vectors as

$$\underline{y}(t)=L_a\underline{\ddot{u}}(t)+L_v\underline{\dot{u}}(t)+L_d\underline{u}(t) \tag{5.14}$$

where L_a, L_v and $L_d\in R^{N_{meas}\times N}$ are selection matrices for accelerations, velocities and displacements/strains, respectively. These measurements are generally collected from sensors such as accelerometers, strain gauges, etc.

Introducing the state vector $\underline{x}^T=[\underline{u}^T\ \ \underline{\dot{u}}^T]\in R^{1\times 2N}$, the equation of motion can be written in the state space form

$$\dot{\underline{x}} = A_c \underline{x} + B_c \underline{p}(t) \tag{5.15}$$

while the measured output vector $\underline{y}(t)$ is given by the observation equation

$$\underline{y}(t) = G_c \underline{x} + J_c \underline{p}(t) \tag{5.16}$$

where

$$A_c = \begin{bmatrix} 0 & I \\ -M^{-1}K & -M^{-1}C \end{bmatrix} \in R^{2N \times 2N} \tag{5.17}$$

is the state transition matrix,

$$B_c = \begin{bmatrix} 0 \\ M^{-1}L_p \end{bmatrix} \in R^{2N \times N_{in}} \tag{5.18}$$

$$G_c = [L_d - L_a M^{-1}K \quad L_v - L_a M^{-1}C] \in R^{N_{meas} \times 2N} \tag{5.19}$$

is the output influence matrix, and

$$J = L_a M^{-1} L_p \in R^{N_{meas} \times N_{in}} \tag{5.20}$$

is the direct transmission matrix.

Assuming that the structure is classically damped, and introducing the coordinate transformation $\underline{u}(t) = \Phi \underline{\xi}(t)$ the modal coordinate vector $\underline{\xi}(t) \in R^{m \times 1}$, the modeshape matrix $\Phi \in R^{N \times m}$ and the diagonal matrix $\Omega^2 = diag(\omega_r^2) \in R^{m \times m}$ of the eigenvalues ω_r^2, satisfying $K\Phi = M\Phi\Lambda$, the state vector $\underline{x} \in R^{2N}$ is given in terms of the modal state vector $\underline{z}^T = [\underline{\xi}^T \quad \dot{\underline{\xi}}^T] \in R^{1 \times 2m}$ in the form

$$\underline{x} = \begin{bmatrix} \Phi & 0 \\ 0 & \Phi \end{bmatrix} \underline{z} \in R^{2N \times 1} \tag{5.21}$$

where the modal state vector $\underline{z}$ and the measurement vector $\underline{y}(t)$ satisfy equations (7) and (8), respectively, with

$$A_c = \begin{bmatrix} 0 & I \\ -\Omega^2 & -\Gamma \end{bmatrix} \in R^{2m \times 2m} \tag{5.22}$$

$$B_c = \begin{bmatrix} 0 \\ \Phi^{-1}L_p \end{bmatrix} \in R^{2m \times N_{in}} \tag{5.23}$$

$$G_c = [L_d\Phi - L_a\Phi\Omega^2 \quad L_v\Phi - L_a\Phi\Gamma] \in R^{N_{meas} \times 2m} \tag{5.24}$$

$$J = L_a \Phi \Phi^T L_p \in R^{N_{meas} \times N_{in}} \tag{5.25}$$

$\Gamma = diag(2\zeta_r\omega_r) \in R^{m\times m}$ and ζ_r is the damping ration of the r mode, where L_a, L_v and $L_d \in R^{N_{meas}\times N}$ are selection matrices for accelerations, velocities and displacements/strains, respectively. These measurements are generally collected from sensors such as accelerometers, strain gauges, etc.

Depending on whether the objective is to predict the power spectra densities or the full time histories of the strains, the following techniques can be applied.

5.3.2 Stationary Stochastic Excitations

A first attempt to compute the fatigue at the entire body of a structure using vibration measurements at a limited number of locations has been presented in (Papadimitriou et al., 2011), assuming that the excitation can be represented by a stationary stochastic process and the system is linear, thus meaning that the response is a stationary stochastic process. The power spectral densities $S_\sigma(\omega)$ of the strains at different locations where measurements are not available can be computed with respect to the cross power spectra densities $\hat{S}_y(\omega)$ of the responses at measured locations. A Kalman filter approach, integrating information from the finite element model of the structure and the measurements, was presented to estimate the power spectral densities $S_\sigma(\omega)$. The cross power spectra densities $\hat{S}_y(\omega)$ of the measured response are obtained by analyzing adequately long measured time histories. The PSD $S_\sigma(\omega)$ of the stresses are obtained by using the linear stress strain relationships for linear elastic material. Given the PSD $S_\sigma(\omega)$ of the stresses, the moments λ_i required in the stochastic fatigue prediction formulas are readily computed and used to provide an estimate of the damage accumulation using the formulation in Section 5.2.2. The whole formulation was presented for a single stochastic excitation but it can be readily extended to cover the case of several stochastic excitations applied at different points in a structure.

Another method that is applicable in the case of stochastic excitation and linear systems is the kriging technique (Papadimitriou, 2009) which, under stationarity conditions, can be used to predict the strain time histories at unmeasured locations in a structure in terms of the strain time histories measured at optimally selected locations (Papadimitriou et al., 2011). An alternative Kalman filter-type method for wind-induced strain estimation and fatigue from output only vibration measurements that explicitly account for spatial correlation and for the colored nature of the excitation and fatigue predictions have also been presented (Hermandez al., 2013).

5.3.3 Non-Stationary Deterministic Excitations

The previous formulation assumes that the response can be considered to be stationary. However, for a number of applications the nonstationarity dominates the features of the excitation and the response, such as in civil engineering problems involving, for example, the passage of trains or heavy trucks over metallic bridges. The damage accumulation prediction proposed in (Papadimitriou et al., 2011) is not applicable in such nonstationary cases. New estimation methods capable of predicting the full acceleration and strain response time histories, applicable to the case of non-stationary excitations, have been developed in (Lourens, Papadimitriou et al., 2012). Specifically, a joint input-state estimation filter proposed in (Lourens, Papadimitriou et al., 2012) was adopted and extended to estimate strain response time histories in the entire body of the structure using output-only vibration measurements collected from the sensor network.

5.3.3.1 Modal Expansion Technique

A class of techniques that can be used in the case of deterministic non-stationary excitation and linear systems is the modal expansion method. The displacement, acceleration and strain response of a structure at various locations can be represented as $\underline{u}(t) = \Phi \underline{\xi}(t)$, $\underline{\ddot{u}}(t) = \Phi \underline{\ddot{\xi}}(t)$, $\underline{\varepsilon}(t) = L_{\varepsilon} \Phi \underline{\xi}(t) = \Phi_{\varepsilon} \underline{\xi}(t)$, where $\underline{\xi}(t)$ are the modal coordinate vector, while Φ and Φ_{ε} are the modeshape matrices for displacements and strains respectively. Using this expansion for the case of measured strain responses $\underline{\hat{\varepsilon}}(t)$, one can in principle obtain the modal coordinates from

$$\underline{\xi}(t) = (\Phi_{\varepsilon}^{T} \Phi_{\varepsilon})^{-1} \Phi_{\varepsilon}^{T} \underline{\hat{\varepsilon}}(t) \tag{5.26}$$

where for a nonsingular matrix $(\Phi_{\varepsilon}^{T} \Phi_{\varepsilon})^{-1}$ the number of sensors should be at least equal to the number of contributing modes. Once these modal coordinates have been identified, then the strain responses $\underline{\varepsilon}_{pr}(t)$ at unmeasured locations can be obtained from equation

$$\underline{\varepsilon}_{pr}(t) = \Phi_{\varepsilon, pr} \underline{\xi}(t) \tag{5.27}$$

where the modeshape component values $\Phi_{\varepsilon, pr}$ in (5.26) are based on those predicted by a finite element model of the structure. The modeshape components Φ_{ε} can be replaced by the ones identified by a modal identification method. It is worth noting that assuming that the response and the excitation can be represented by stationary processes, the PSD of the strain responses at unmeasured locations

can also be predicted from the CPSD of the responses obtained from vibration measurements so that the stochastic fatigue techniques can also be applied.

It should be noted that optimal sensor location methods are already available to use for improving the accuracy of the estimates. The problem of optimizing the sensor locations is formulated as a problem of finding the sensor locations that provide the best estimates of the modal coordinates $\underline{\xi}(t)$. This problem has first been addressed in (Papadimitriou, 2004) and efficient computational techniques have been provided (Giagopoulos and Natsiavas, 2007) based on the modeshapes of a finite element model. A drawback of the formulation based on modal expansion is that the predictions are sensitive to model and measurement errors. Also, the predictions make efficient use of strain or displacement measurements which are less frequently employed in monitoring systems. For acceleration measurements one can derive $\ddot{\underline{\xi}}(t)$ and use double integration to estimate $\underline{\xi}(t)$. However, such double integration is a source of extra processing errors which are expected to affect the predictions of strains.

5.4 State of the Art Algorithms for Joint Input-State Estimation

Although the state identification has been a task that is frequently addressed in recent years, the joint identification of state and input information is a topic less treated so far in the literature. It is widely recognized that structural systems are inherently characterized by uncertainty, relating to measurement errors, sensor noise, and inefficacy of the numerical models and lack of a priori knowledge on the system and loading conditions. In practice, one common approach is to assume the unknown input as a zero mean white Gaussian process and make use of the aforementioned Bayesian techniques for state estimation. However, in many cases this assumption is violated and therefore it may lead to major adverse effects on the accuracy of the estimations. To address this issue, a number of optimal filtering techniques in the presence of unknown input have been proposed.

In a pioneering work, Kitanidis developed an unbiased minimum-variance recursive filter for input and state estimation of linear systems without direct transmission; his algorithm did not make any a-priori assumption on the input (Kitanidis, 1987). Gillijns and De Moor proposed a new filter for joint input and state estimation for linear systems without direct transmission (Gillijns and De Moor, 2007). Their filter is globally optimal in the minimum-variance unbiased sense. Later Gillijns and De Moor developed a new formulation of the

aforementioned filter which included a direct transmission term in its structure (Gillijns and De Moor, 2007).

In more recent years, Lourens (Lourens, Papadimitriou et al., 2012) has proposed an extension of the method developed in (Gillijns and De Moor, 2007) to deal with the numerical instabilities that arise when the number of sensors surpasses the order of the model, i.e. when a large number of sensors is used in combination with a reduced-order model assembled from a relatively small number of modes. It was reported that, although the algorithm provides a reasonable prediction of the accelerations, the input force and displacement estimates are affected by spurious low frequency components that must be filtered out in this case. This approach is developed in Section 5.4.1. Moreover, Lourens, Reynders et al. (2012) have proposed an augmented Kalman filter (AKF) for unknown force identification in structural systems, and concluded that the AKF is prone to numerical instabilities due to un-observability issues of the augmented system matrix. Details about the augmented state-space model and the Kalman Filter equations used are given in Section 5.4.2

It is worth noting, that in dealing with the drift that appears in displacements Chatzi (Chatzi and Fuggini, 2015) and later Naets (Naets et al., 2015) have proposed a technique that avoids drift effect in the estimated displacements by introducing artificial dummy displacement measurements into the observation vector. This technique, known as augmented Kalman filter with dummy measurements is presented in Section 5.4.3.

Moreover, a dual implementation of the Kalman filter is proposed by Eftekhar Azam et al. (2015) to estimate the unknown input and state of a discrete-time state space model. Eftekhar Azam et al. (2015) have shown that the expert guess on the covariance of the unknown input provides a tool for avoiding the so-called drift effect in the estimated input force and displacements, since the drift is linked to the integral nature of these quantities in the presence of acceleration information. The dual Kaman filter approach is presented in Section 5.4.4.

Finally, we should mention that although all the above mentioned state of the art techniques are proposed for joint input and state estimation, the current chapter is interested in the accurate estimation of the displacements strains and stresses in order to obtain a robust prediction of fatigue that is the objective of this chapter and the input estimation itself is a secondary goal compared to state estimation.

5.4.1 Joint Input – State Estimation Technique

The approach is based on a filter that has the structure of the Kalman filter, which is used to jointly estimate the inputs and the full state of a linear system using a limited number of vibration measurements. This filter extends Gillijns and De Moor's (Gillijns and Moor, 2007) joint input-state estimation algorithms to handle structural dynamics applications. In contrast to the method proposed in (Papadimitriou et al., 2011), no assumptions are made on the spatial and temporal characteristics of the applied loads, as well as the number and location of the excitations on the structure.

The proposed methodology was validated using simulated data from a laboratory beam structure subjected to impulse-type and stochastic excitations as well simulated measurements from a railway bridge (Papadimitriou et al., 2012). The proposed Kalman-type filters were demonstrated to be accurate for estimating acceleration time histories at unmeasured locations in the structure. For displacement and strain time histories, the filter estimates were inaccurate due to low frequency shift manifested in the time histories. Such inaccuracies were corrected by applying a high frequency filter to the modal estimates provided by the joint input-state estimation filter technique. The main steps of the joint input-state estimation algorithm based on combined acceleration and strain measurements (Lourens et al., 2012) are next presented.

5.4.1.1 Formulation of discrete-time State-Space Model

Using the sampling rate $1/\Delta t$ the discrete-time state space model corresponding to (5.15) and (5.16) is

$$\underline{x}_{k+1} = A\underline{x}_k + B\underline{p}_k + \underline{w}_k \tag{5.28}$$

$$\underline{y}_k = G\underline{x}_k + J\underline{p}_k + \underline{v}_k \tag{5.29}$$

where $\underline{x}_k = \underline{x}(k\Delta t)$, $\underline{p}_k = \underline{p}(k\Delta t)$ and $\underline{y}_k = \underline{y}(k\Delta t), k = 1,...,N_s$, are the digitized state, load and output vectors, $A = e^{A_c \Delta t}$ is the state transition matrix for the discrete formulation, $B = (A - I)A_c^{-1}B_c$, $G = G_c$ and $J = J_c$. It is noteworthy that, in this approach the G and J matrices are converted from continuous time to discrete via a zero-order-hold (ZOH) assumption, which assumes a constant inter-sample behavior for the input. It should be noted at this point, that Bernal (Bernal and Ussia, 2015) has carried out a thorough study of other more realistic assumptions on the inter-sample behaviors of the input for dynamic systems and concluded that a Dirac comb impulse assumption can significantly improve the discretization accuracy. A further analysis of this issue lies beyond the scope of

this thesis The ZOH assumption is adopted here in for the further purpose of allowing the direct cross-comparison of this methodology with the methodologies presented in next sections.

The discrete-time state space equations (5.28) and (5.29) have been supplemented with the random vectors $\underline{w}_k$ and $\underline{\upsilon}_k$ to account for the stochastic system and measurement noise, respectively. It is assumed that $\underline{w}_k$ and $\underline{\upsilon}_k$ are mutually uncorrelated, zero mean, white noise processes with known covariance matrices $Q = E[\underline{w}_k \underline{w}_k^T] \in R^{2m \times 2m}$ and $R = E[\underline{\upsilon}_k \underline{\upsilon}_k^T] \in R^{N_{meas} \times N_{meas}}$.

5.4.1.2 Gillijns and De Moor's Joint Input – State Estimation Algorithm

Let $\hat{x}_{k|l}$ be the estimate of the state x_k given the load $\{y_n\}_{n=0}^{l}$ and let $P_{k|l} = E[(x_k - \hat{x}_{k|l})(x_k - \hat{x}_{k|l})^T]$ be the error covariance matrix. Based on the filter proposed in Lourens et al. (2012) the force and the state estimates are computed recursively in three steps: the input estimation

$$\begin{aligned} \tilde{R}_k &= G P_{k|k-1} G^T + R \in R^{N_{meas} \times N_{meas}} \\ M_k &= (J^T \tilde{R}_k^{-1} J)^{-1} J^T \tilde{R}_k^{-1} \in R^{N_{in} \times N_{meas}} \\ \hat{p}_{k|k} &= M_k (d_k - G \hat{x}_{k|k-1}) \in R^{N_{in} \times 1} \end{aligned} \tag{5.30}$$

the measurement update

$$\begin{aligned} L_k &= P_{k|k-1} G^T \tilde{R}_k^{-1} \in R^{2m \times N_{meas}} \\ \hat{x}_{k|k} &= \hat{x}_{k|k-1} + L_k (d_k - G \hat{x}_{k|k-1} - J \hat{p}_{k|k}) \in R^{2m \times 1} \\ P_{k|k} &= P_{k|k-1} - L_k (\tilde{R}_k - J P_{p[k|k]} J^T) L_k^T \in R^{2m \times 2m} \\ P_{xp[k|k]} &= P_{xp[k|k]}^T = -L_k J P_{p[k|k]} \in R^{2m \times Nin} \end{aligned} \tag{5.31}$$

and the time update

$$\begin{aligned} x_{k+1|k} &= A \hat{x}_{k|k} + \hat{p}_{k|k} \in R^{2m \times 1} \\ P_{k+!|k} &= [A \;\; B] \begin{bmatrix} P_{k|k} & P_{xp[k|k]} \\ P_{px[k|k]} & P_{p[k|k]} \end{bmatrix} \begin{bmatrix} A^T \\ B^T \end{bmatrix} + Q \in R^{2m \times 2m} \end{aligned} \tag{5.32}$$

The initial unbiased state estimate $\hat{x}_{0-1}$ and its error covariance matrix P_{0-1} are assumed known.

In structural dynamics applications, numerical instabilities may arise when the number of contributing structural modes is less than the number of sensors or the number of loads applied to the structure. These instabilities are due to numerical

deficiencies of the inverse of the matrices $\tilde{R}_k$, $J^T\tilde{R}_k^{-1}J$ and $JP_{p[k|k]}J^T$. To avoid these numerical deficiencies, the inverses of the aforementioned matrices are computed by truncating the expansion obtained by a singular value decomposition, keeping only the terms associated with the dominant singular values. The proposed technique is shown to avoid the numerical rank deficiency of the aforementioned matrices in (Lourens et al., 2012).

It has been demonstrated (Lourens et al., 2012). that the best estimates are obtained by assuming the location of the forces to be unknown. This is a realistic situation encountered in all practical applications with operational vibrations. The forces are spatially distributed over the boundary of the structure. However, using the fact that there is a correlation between the spatially distributed forces, one can replace the forces by a number of independent forces acting on the structure. In the joint input-state estimation algorithm, a set of equivalent forces is thus assumed to act at a number of arbitrarily chosen locations. These locations are chosen to correspond to the locations of the measurements used in the filter for the estimation. In this case, the filter was demonstrated to provide improved estimates of the states. It should be noted that the estimates of the equivalent forces do not correspond to any estimates of the unknown input forces.

In the context of this thesis, this work has also been extended for the case where the measured quantities are only strains by modifying the approach presented in Gillijns and De Moor's (Gillijns and Moor, 2007) for input-state estimation of systems to handle structural dynamics applications. In this case, the discrete-time state space model corresponding to (5.15) and (5.16) is

$$\underline{x}_{k+1} = A\underline{x}_k + B\underline{p}_k + \underline{w}_k \tag{5.33}$$

$$\underline{y}_k = G\underline{x}_k + \underline{\upsilon}_k \tag{5.34}$$

where matrices A and B have been defined in (5.28),the output influence matrix G is

$$G = [L_d \quad 0] \in R^{N_{meas}\times 2m} \tag{5.35}$$

and the direct transmission matrix J is given by the equation

$$J = GB \in R^{N_{meas}\times 2N_{in}} \tag{5.36}$$

The main steps of this extended joint input-state estimation algorithm are next presented in three steps the input estimation

$$\begin{aligned}
\tilde{R}_k &= GP_{k|k-1}G^T + R \in R^{N_{meas}\times N_{meas}} \\
M_k &= (J^T\tilde{R}_k^{-1}J)^{-1}J^T\tilde{R}_k^{-1} \in R^{N_{in}\times N_{meas}} \\
\hat{p}_{k|k} &= M_k(d_k - G\hat{x}_{k|k-1}) \in R^{N_{in}\times 1}
\end{aligned} \tag{5.37}$$

the measurement update

$$\begin{aligned}
L_k &= P_{k|k-1}G^T\tilde{R}_k^{-1} \in R^{2m\times N_{meas}} \\
\hat{x}^*_{k|k} &= \hat{x}_{k|k-1} + B\hat{p}_{k|k} \in R^{2m\times 1} \\
\hat{x}_{k|k} &= \hat{x}^*_{k|k} + L_k(d_k - G\hat{x}^*_{k|k}) \in R^{2m\times 1} \\
N_k &= BM_k \in R^{2m\times Nmeas} \\
H_k &= I - N_kG \in R^{2m\times 2m} \\
S_k &= -N_k\tilde{R}_k \in R^{2m\times Nmeas} \\
P^*_{k|k} &= H_kP_{k|k-1}H_k^T + N_k\tilde{R}_kN_k^T \in R^{2m\times 2m} \\
P_{k|k} &= P^*_{k|k} - L_k(P^*_{k|k}G^T + S_k^T) \in R^{2m\times 2m}
\end{aligned} \tag{5.38}$$

and the time update

$$\begin{aligned}
x_{k+1|k} &= A\hat{x}_{k|k} \in R^{2m\times 1} \\
P_{k+!|k} &= AP_{k|k}A^T + Q \in R^{2m\times 2m}
\end{aligned} \tag{5.39}$$

The stress time histories at a point of a structure are obtained by using the linear stress strain relationships for linear elastic material. Given the stress time histories, the damage accumulation due to fatigue are obtained by cycle count methods, S-N fatigue curves and the linear fatigue damage accumulation laws presented in Section 5.2.1.

5.4.2 Augmented Kalman Filter

The proposed technique essentially consists of a standard Kalman filter (Kalman, 1960) applied to an augmented state-space model (Lourens et al. 2012) in which the forces are added to the unknown state vector. In Section 5.4.2.1 the augmented model is developed first, followed by a presentation of the filter equations in Section 5.4.2.2.

5.4.2.1 Augmented State-Space Model

The augmented state-space model is derived starting from the classical discrete-time state equation (5.33), which is supplemented with an equation which directly relates the force vectors at times k and $k+1$

$$\underline{p}_{k+1} = \underline{p}_k + \underline{\eta}_k \tag{5.40}$$

where $\underline{\eta}_k$ is assumed to be a mutually uncorrelated, zero mean, white noise process with known covariance matrix $S = E[\underline{\eta}_k \underline{\eta}_k^T]$.

By combining (5.33) and (5.40) and redefining the state vector $\underline{x}^a \in R^{(2m+N_{in})\times 1}$, where the superscript a refers to augmented

$$\underline{x}_k^a = \begin{bmatrix} \underline{x}_k \\ \underline{p}_k \end{bmatrix} \tag{5.41}$$

an augmented state equation is obtained

$$\underline{x}_{k+1}^a = A_a \underline{x}_k^a + \underline{\zeta}_k \tag{5.42}$$

The matrix $A_a \in R^{(2m+Nin)\times(2m+Nin)}$ is defined as:

$$A_a = \begin{bmatrix} A & B \\ 0 & I \end{bmatrix} \tag{5.43}$$

where the system matrices A and B have been defined in (5.28) and the noise vector $\underline{\zeta}_k \in R^{m+Nin}$, again assumed unknown, accounts for the modelling errors $\underline{w}_k \in R^{2m}$ as well as the force increment $\underline{\eta}_k \in R^{Nin}$ and is defined as

$$\underline{\zeta}_k = \begin{bmatrix} \underline{w}_k \\ \underline{\eta}_k \end{bmatrix} \tag{5.44}$$

The classical discrete time observation equation (5.29) with unknown noise vector $\underline{\upsilon}_k \in R^{N_{meas}}$, becomes in the augmented model

$$\underline{y}_k = G_a \underline{x}_k^a + \underline{\upsilon}_k \tag{5.45}$$

where $\underline{y}_k \in R^{N_{meas}}$ represents the measured data vector and the matrix $G_a \in R^{N_{meas}\times(2m+N_{in})}$ is assembled from the output influence and direct transmission matrices G and J as follows:

$$G_a = [G \;\; J] \tag{5.46}$$

The output influence matrix $G = G_c$ has been defined in (5.24) and the direct transmission matrix $J = J_c$ has been defined in (5.25).

To summarize, the state and observation equation defining the augmented state-space model are formulated by equations (5.42) and (5.45).

5.4.2.2 Kalman Filter Equations for the Augmented State-Space Model

Before presenting the filter expressions, it is useful to give some definitions and clarify the underlying assumptions. Firstly, the discrete-time state space equations (5.42) and (5.45) have been supplemented with the random vectors $\underline{w}_k \in R^m$, $\underline{\eta}_k \in R^{Nin}$ and $\underline{\upsilon}_k \in R^{N_{meas}}$ to account for noise, that are assumed to be a mutually uncorrelated, zero mean, white noise process with known covariance matrix $Q = E[\underline{w}_k \underline{w}_k^T] \in R^{2m \times 2m}$, $S = E[\underline{\eta}_k \underline{\eta}_k^T] \in R^{Nin \times Nin}$ and $R = E[\underline{\upsilon}_k \underline{\upsilon}_k^T] \in R^{N_{meas} \times N_{meas}}$ respectively.

Moreover, let make the convention that $\underline{\hat{x}}_{k|l}^a$ is the estimate of the state $\underline{x}_k^a$ given the load $\{y_n\}_{n=0}^l$ and $P_{k|l} = E[(\underline{x}_k^a - \underline{\hat{x}}_{k|l}^a)(\underline{x}_k^a - \underline{\hat{x}}_{k|l}^a)^T] \in R^{(2m+N_{in}) \times (2m+N_{in})}$ is the error covariance matrix. According to this convention, $\underline{\hat{x}}_{0|-1}^a$ refers to an initial estimate of $\underline{x}^a$ at time $k = 0$. Both the initial state estimate $\underline{\hat{x}}_{0|-1}^a$ and its error covariance matrix P_{0-1} are assumed known.

Based on the filter proposed in (Lourens, Reynders et al., 2012) the Kalman filter equations for the discrete-time state-space system of equations (5.42) and (5.45) are now presented in terms of the measurement update, where the previously predicted state estimate is updated with the new observation, and the time update, where the state is advanced based on the model equations:

The measurement update

$$\begin{aligned} L_k &= P_{k|k-1} G_a{}^T (G_a P_{k|k-1} G_a{}^T + R)^{-1} \in R^{(2m+N_{in}) \times N_{meas}} \\ \underline{\hat{x}}_{k|k}^a &= \underline{\hat{x}}_{k|k-1}^a + L_k (y_k - G_a \underline{\hat{x}}_{k|k-1}^a) \in R^{(2m+N_{in}) \times 1} \\ P_{k|k} &= P_{k|k-1} - L_k G_a P_{k|k-1} \in R^{(2m+N_{in}) \times (2m+N_{in})} \end{aligned} \tag{5.47}$$

and the time update

$$\begin{aligned} \underline{\hat{x}}_{k+1|k}^a &= A_a \underline{\hat{x}}_{k|k}^a \in R^{(2m+N_{in}) \times 1} \\ P_{k+1k|k} &= A_a P_{k|k} A_a{}^T + Q_a \in R^{(2m+N_{in}) \times (2m+N_{in})} \end{aligned} \tag{5.48}$$

where $Q_a \in R^{(2m+N_{in}) \times (2m+N_{in})}$,in conjunction with the augmented noise vector $\underline{\zeta}_k \in R^{m+Nin}$ from (5.44), is the augmented covariance matrix and is given by:

$$Q_a = \begin{bmatrix} Q & 0 \\ 0 & S \end{bmatrix} \tag{5.49}$$

5.4.3 Augmented Kalman Filter with dummy measurements

In Section 5.4.2, it was shown that in order to obtain a coupled estimation of both the states and the forces, the regular state vector is augmented with the unknown forces and these are estimated in the same fashion as the other states by providing a basic model for the forces.

However, Naets (Naets, 2015) has shown that the case where the estimation is performed based on acceleration measurements is not observable, which leads to unreliable estimates and that only in the case of a full position measurement full observability can be guaranteed. In order to circumvent the observability issues, Naets proposes the addition of dummy measurements on the position of all the degrees of freedom in order to prevent drift. In this approach, the acceleration measurements take care for the transient behavior while the dummy measurements provide long-term stability.

In Section 5.4.3.1 the augmented model, in the case that dummy measurements are used, is developed first, followed by a presentation of the filter equations in Section 5.4.3.2.

5.4.3.1 State-Space Model for the Augmented Kalman Filter with dummy measurements

In order to obtain a stable simulation, dummy measurements (Naets et al., 2015) are proposed to be added for the positions. This approach is similar to the one proposed by Chatzi (Chatzi and Fuggini, 2015) for stabilizing tracking for civil structure monitoring purposes. In structural systems the deformation of the structure is bounded and an order of magnitude for the deformation can typically be estimated apriori (possibly based on a simulation). These bounds for the deformation can then be considered as the uncertainty on a dummy measurement which indicates that the deformation is zero. The dummy measurements have measurement equations

$$G_{dm}\underline{x}^{a} + \underline{\upsilon}_{dm} = 0 \tag{5.50}$$

where

$$G_{dm} = [L_d \quad 0 \quad 0] \in R^{N_{meas}\times(2m+N_{in})} \tag{5.51}$$

This equation states that the position of the DOFs is zero with an uncertainty $\underline{\upsilon}_{dm}$ with covariance $R_{dm} = E[\underline{\upsilon}_{dm}\underline{\upsilon}_{dm}^{T}] \in R^{N_{meas}\times N_{meas}}$. The entries of this covariance matrix R_{dm} can be used for the tuning of the final Kalman filter in order to generate desirable results. The covariance R_{dm} should be chosen an order of

magnitude higher than the actual motion of the system, because a smaller covariance will constrain the estimates too much and lead to erroneous results. On the other hand, if the covariance is chosen to high, the dummy measurement will not be capable to properly restrict the drift on the estimates, which is not desirable in the context of this thesis since the main objective of this chapter is the accurate prediction of the displacements of the system in order to get accurate estimates of the fatigue prediction. Within an order of magnitude change, the results of the estimator are relatively insensitive to the exact value of R_{dm}.

Due to the relatively large uncertainty on these dummy measurements they will not contribute considerably to the fast estimation typically required for force estimation. They will however prevent the long term drift created by the acceleration measurements and allow an effective means to stabilize the estimated covariance of the filter. Finally, if the steady-state position of the system is known to not be the zero-state, the dummy measurements should be adjusted in order to take this behavior in to account.

5.4.3.2 Kalman Filter Equations for the Augmented State-Space Model with dummy measurements

Based on the filter proposed in (Naets et al., 2015) the Kalman filter equations for the discrete-time augmented state-space system are now presented. The discrete time Kalman filtering equations are typically split into two steps. In the first step, we get the equations presented in (5.48). In the second step, these estimates are corrected through the following equations:

The correction step

$$\begin{aligned} K_{k+1} &= P_{k+1|k}\begin{bmatrix} G_a \\ G_{dm} \end{bmatrix}^T \left(\begin{bmatrix} G_a \\ G_{dm} \end{bmatrix} P_{k+1|k} \begin{bmatrix} G_a \\ G_{dm} \end{bmatrix}^T + \begin{bmatrix} R & 0 \\ 0 & R_{dm} \end{bmatrix} \right)^{-1} \in R^{2N_{meas}\times 2N_{meas}} \\ \underline{\hat{x}}^a_{k+1|k+1} &= \underline{\hat{x}}^a_{k+1|k} + K_{k+1}\left(\begin{bmatrix} y_k \\ 0 \end{bmatrix} - \begin{bmatrix} G_a \\ G_{dm} \end{bmatrix}^T \underline{\hat{x}}^a_{k+1|k} \right) \in R^{(2m+N_{in})\times 1} \\ P_{k+1|k+1} &= P_{k+1|k} - K_{k+1}\begin{bmatrix} G_a \\ G_{dm} \end{bmatrix} P_{k+1|k} \in R^{(2m+N_{in})\times(2m+N_{in})} \end{aligned} \tag{5.52}$$

Using the correction step (5.52), the fictitious dummy measurements dictate the estimator to return to an undeformed state and lead to a stable estimation approach.

5.4.4 Dual Kalman Filter

A dual implementation (Eftekhar Azam et al., 2015) of the Kalman filter is proposed to estimate the unknown input and states of a state-space model. However, the input estimation itself is a secondary goal compared to state estimation, as the objective of this thesis is to estimate the fatigue damage accumulation. In this approach, it is assumed that a limited number of noisy acceleration measurements are available. The successive structure of the suggested filter prevents numerical problems attributed to un-observability and rank deficiency of the Augmented Kalman Filter. Additionally, it is shown that the expert guess on the covariance of the unknown input provides a tool for avoiding the so-called drift effect in the estimated input force and displacements. The drift is linked to the integral nature of these quantities in the presence of acceleration information.

In Section 5.4.4.1 the state –space model that is used in this approach is presented. The Kalman Filter equations that are used in the context of Dual Kalman Filter are given in Section 5.4.4.2.

5.4.4.1 State-Space Model for Dual Kalman Filter

Starting from the discrete time state-space equations (5.28) and (5.29), the problem is to estimate the unknown input $\underline{p}_k$ and the hidden or partially observed state $\underline{x}_k$ of the system using the noisy observations $\underline{y}_k$. In the context of this problem, a dual implementation of the Kalman filter is proposed in this section. The proposed solution could be divided in two stages, with the Kalman Filter pertaining to both stages. At each time iteration, the fictitious process equation (5.40) serving for calibration of the input force is introduced.

Then, it is assumed that an estimation of the state at time t_k is available. By using equations (5.29) and (5.40), a new state-space equation can be obtained, where the observed quantity is $\underline{y}_k$, the new state is $\underline{p}_k$ and the state $\underline{x}_k$ of the system plays the role of a known input to the system:

$$\begin{aligned} \underline{p}_{k+1} &= \underline{p}_k + \underline{\eta}_k \\ \underline{y}_k &= G\underline{x}_k + J\underline{p}_k + \underline{\upsilon}_k \end{aligned} \tag{5.53}$$

Through implementation of the Kalman filter, an online estimation of $\underline{p}_{k+1}$ can be obtained. Then, once the estimation of $\underline{p}_{k+1}$ is performed, it can in a next step be substituted in equations (5.28) and (5.29), and a subsequent Kalman filter implementation could be used for estimating $\underline{x}_{k+1}$.

At this point, it is worth noting that, the procedure needs a-priori information on expected value and covariance of the state and input at time t_0. Moreover, similar to the Augmented Kalman Filter, the value of the process noise $S = E[\underline{\eta}_k \underline{\eta}_k^T] \in R^{Nin \times Nin}$ for equation (5.48) must be properly chosen so that an accurate estimate of the unobserved state and the unknown input could be achieved. The proper choice of the value of the covariance noise is sometimes called the tuning knob of the system, and methods relying on the use of Bayesian techniques, maximizing the likelihood of measurements with respect to the noise parameters, have recently been proposed for a proper adjustment (Yuen et al., 2007). Also, it is very helpful to clarify the nature of the influence of the covariance matrices $Q = E[\underline{w}_k \underline{w}_k^T] \in R^{2m \times 2m}$, $S = E[\underline{\eta}_k \underline{\eta}_k^T] \in R^{Nin \times Nin}$ and $R = E[\underline{\upsilon}_k \underline{\upsilon}_k^T] \in R^{N_{meas} \times N_{meas}}$. The process noise covariance matrices Q and S reveal the confidence put on the utilized model of the system. The lower this is, the more accurate the model is considered to be. The observation noise covariance R reveals the confidence put in the acquired measurements. The lower this is, the tighter the estimator is forced to fit the recorded data.

5.4.4.2 Dual Kalman Filter Equations

The Dual Kalman Filter is initialized using the initial state $\hat{\underline{x}}_{0|-1}$ and its variance $P_{0|-1}$ and the initial input force $\hat{\underline{p}}_{0|-1}$ and its variance $P^p_{0|-1}$. Hereafter, it computes the force and state estimates recursively in three stages for each one: the input estimation, the measurement update and the time update:

Initialization of the filter at time t_0:

$$\begin{aligned} \hat{\underline{x}}_{0|-1} &= E[\underline{x}_0] \\ P_{0|-1} &= E[(\underline{x}_0 - \hat{\underline{x}}_{0|-1})(\underline{x}_0 - \hat{\underline{x}}_{0|-1})^T] \end{aligned} \tag{5.54}$$

$$\begin{aligned} \hat{\underline{p}}_{0|-1} &= E[\underline{p}_0] \\ P^p_{0|-1} &= E[(\underline{p}_0 - \hat{\underline{p}}_{0|-1})(\underline{p}_0 - \hat{\underline{p}}_{0|-1})^T] \end{aligned} \tag{5.55}$$

Prediction and update stage for the input:

1. Evolution of the input and prediction of covariance of input:

$$\begin{aligned} \underline{p}_k^- &= \underline{p}_{k|k-1} \in R^{N_{in} \times 1} \\ P_k^{p-} &= P^p_{k|k-1} + S \in R^{N_{in} \times N_{in}} \end{aligned} \tag{5.56}$$

2. Calculation of Kalman gain for input:

$$M_k^p = P_k^{p-} J^T (J P_k^{p-} J^T + R)^{-1} \in R^{N_{in} \times Nmeas} \tag{5.57}$$

3. Time update of the prediction for input:

$$\begin{aligned} \underline{\hat{p}}_{k|k} &= \underline{p}_k^- + M_k^p (\underline{y}_k - G\underline{\hat{x}}_{k|k-1} - J\underline{p}_k^-) \in R^{N_{in} \times 1} \\ P_{k|k}^p &= P_k^{p-} - M_k^p J P_k^{p-} \in R^{N_{in} \times N_{in}} \end{aligned} \tag{5.58}$$

Prediction and update stage for the state:

1. Evolution of the input and prediction of covariance of state:

$$\begin{aligned} \underline{x}_k^- &= A\underline{\hat{x}}_{k|k-1} + B\underline{\hat{p}}_{k|k} \in R^{2m \times 1} \\ P_k^- &= AP_{k|k-1}A^T + Q \in R^{2m \times 2m} \end{aligned} \tag{5.59}$$

2. Calculation of Kalman gain for state:

$$M_k = P_k^- G^T (G P_k^- G^T + R)^{-1} \in R^{2m \times N_{meas}} \tag{5.60}$$

3. Time update of the prediction for state:

$$\begin{aligned} \underline{\hat{x}}_{k|k} &= \underline{x}_k^- + M_k (\underline{y}_k - G\underline{x}_k^- - J\underline{\hat{p}}_{k|k}) \in R^{2m \times 1} \\ P_{k|k} &= P_k^- - M_k G P_k^- \in R^{2m \times 2m} \end{aligned} \tag{5.61}$$

Using the above presented equations and by fine-tuning the covariance of the fictitious process noise of the unknown input, a reasonable estimate of the state is obtained. The expert guess on the covariance of the unknown input is of great importance, since it provides a tool for avoiding the so-called drift in the estimated displacements, that are useful for an accurate fatigue damage estimation.

5.5 Applications

5.5.1 N-DOF Spring – Mass Chain- Like Model

A 30-DOF spring-mass chain like model, shown in Figure 5.1, is used to demonstrate the effectiveness of the proposed methodologies. The model is comprised of two substructures. The first substructure contains the first body, with mass m_1, in the chain and the two springs k_1 and k_2 attached to this mass, while the second substructure consists of the rest of the 29-DOF. This sub-structuring approach allows us to isolate the large components of the structure that behave linearly from the isolated parts that may behave nonlinearly. Thus, the proposed methodologies can be applied to the linear substructures. It is assumed herein that

the second 29-DOF substructure behaves linearly, while the first substructure may consist of nonlinear springs as shown in Figure 5.2.

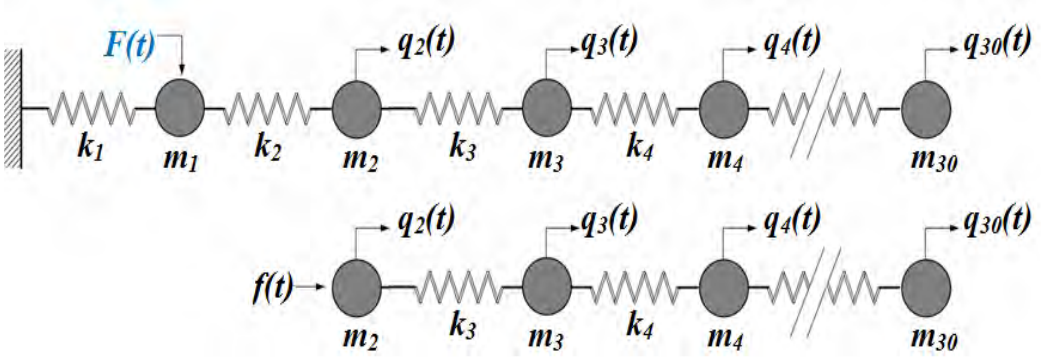

Figure 5.1: 30-DOF spring mass chain-like model.

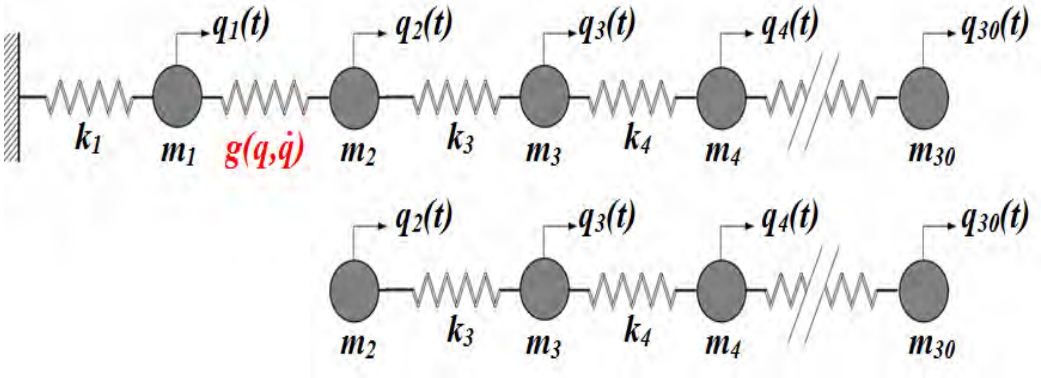

Figure 5.2: 30-DOF spring mass chain-like model with the first substructure including nonlinear spring

More specifically, the first substructure includes the first body in the chain, with mass m_1, that is attached through a linear spring with stiffness k_1 to the ground and through a nonlinear spring k_2 to mass m_2. As a result, a nonlinear restoring force f_k is developed in this substructure and is selected to have the following specific form:

$$f_k = k_s \cdot x + \mu_k \cdot x^3 \tag{5.62}$$

where $x = x_2 - x_1$, $k_s = 10^5$ and $\mu_k = 1{,}1 \cdot 10^7$. Then, the second subsystem includes the remaining 29-DOF spring-mass system, as shown in Figure 5.2. The value of each mass of the 29-DOF model system is $m_2 = m_3 = \cdots = m_{30} = 0.3 \ \ kg$ and the stiffness value of each spring is set to be $k_3 = \cdots = k_{29} = 15 \times 10^4 \ \ N/m$.

This substructure is linear and is assumed to exhibit classical damping properties, with a common damping ratio $\zeta = 0.005$ in all of its modes. The undamped natural frequencies of the system are reported in Table 5.1 .

Due to the presence of the interconnecting nonlinear spring in the first substructure, the equations of motion of this example system are strongly nonlinear, since the value of the nonlinear term in (5.62) is not restricted to be small compared to the value of the corresponding linear term. Therefore, the equations of motion are solved numerically by applying a variable step Runge-Kutta Method. Here, this was done in place of performing an experiment for determining the acceleration, velocity and displacement time histories of the 30-DOF model. More specifically, the full 30-DOF nonlinear model is first solved in the time domain by numerical differentiation, after applying a selected displacement base excitation $x_g(t)$ to the nonlinear substructure. The form of the applied excitation is presented in Figure 5.3, while the time history of the force $F(t)$ applied to mass m_1 is illustrated in Figure 5.4.

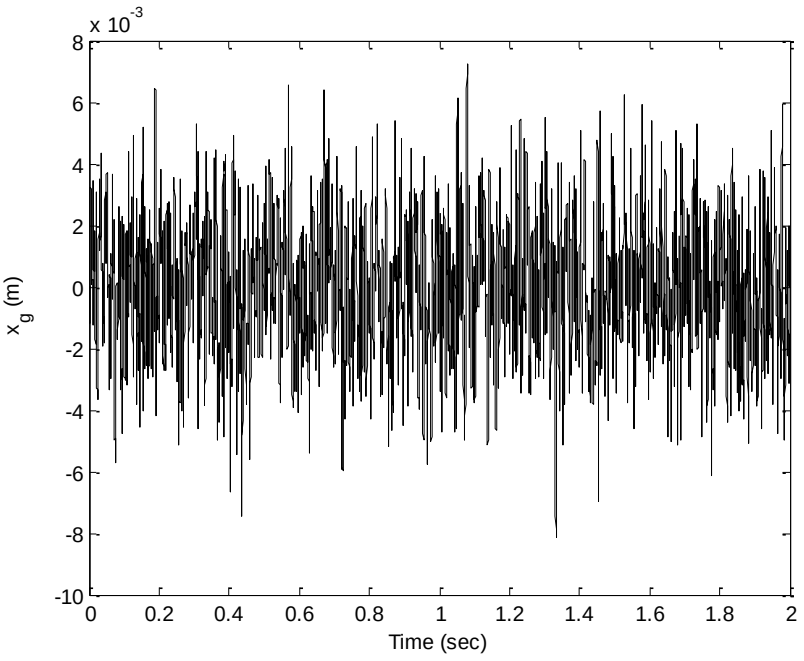

Figure 5.3: Displacement Time History selected as base excitation.

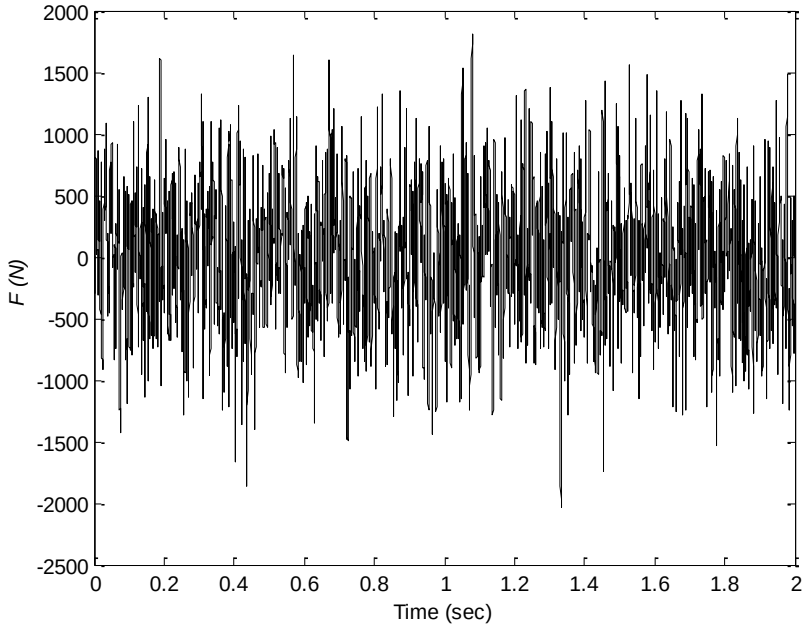

Figure 5.4: Time History of force $F(t)$ applied to mass m_1.

The force $F(t)$ is given from the following specific form:

$$F(t) = k_w \cdot x_g(t) + c_w \cdot \dot{x}_g(t) \tag{5.63}$$

where $k_w = 2,5 \cdot 10^5$ and $c_w = 0$. Simulated, noise contaminated, response time histories are generated from the 30-DOF model by applying the force $F(t)$ to the mass m_1. Displacements, velocities, accelerations and strains are recorded and are used as the exact estimates against which comparisons of predictions from the 29-DOF model will be made. The calculated displacement and velocity time histories at mass m_2 are presented in Figure 5.5 and Figure 5.6 respectively. Then, these calculated displacement and velocity time histories are used as a base excitation to the second linear substructure, as shown in Figure 5.2. The force $f(t)$ from the nonlinear spring to mass m_2 is graphically depicted in Figure 5.7. Finally, the solution of this 29-DOF model provides predictions for the dynamic response of the linear substructure.

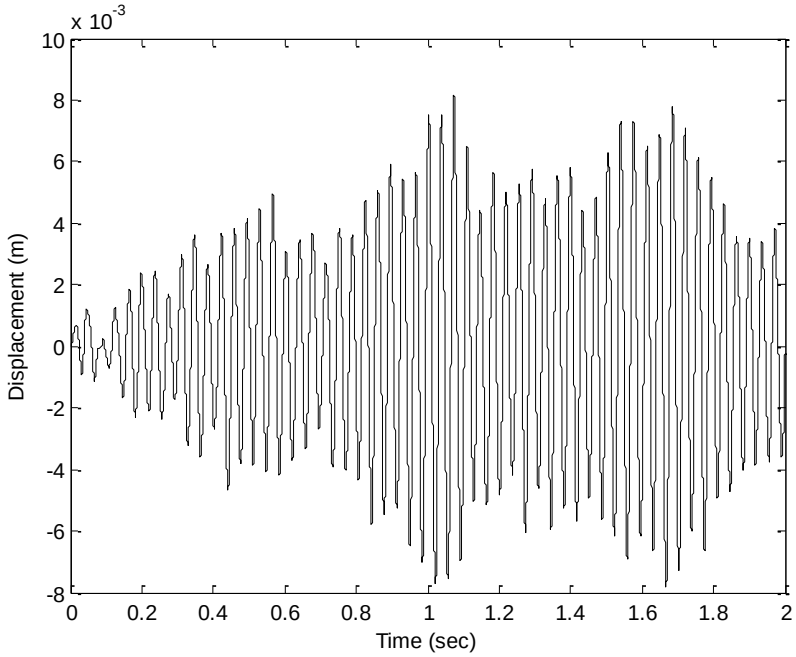

Figure 5.5: Experimental Displacement Time History at DOF 2 of the 30-DOF system.

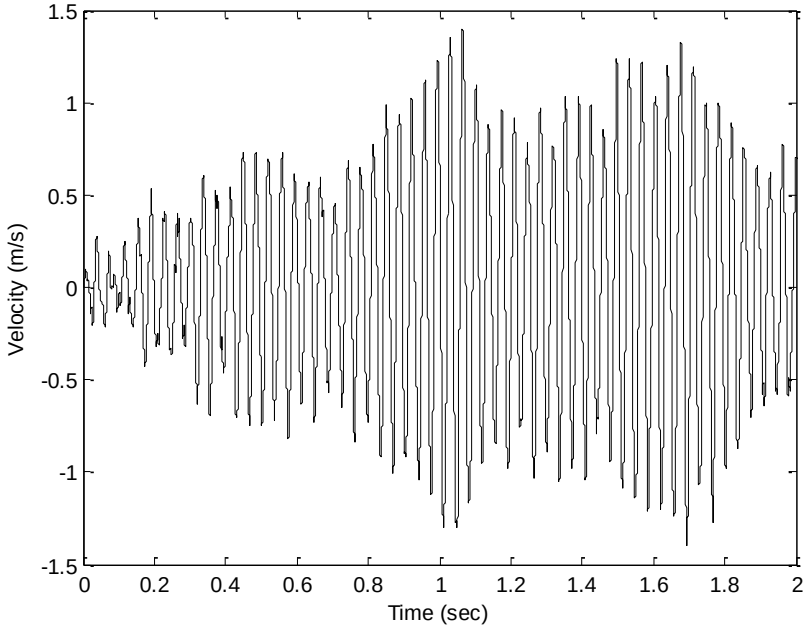

Figure 5.6: Experimental Velocity Time History at DOF 2 of the 30-DOF system.

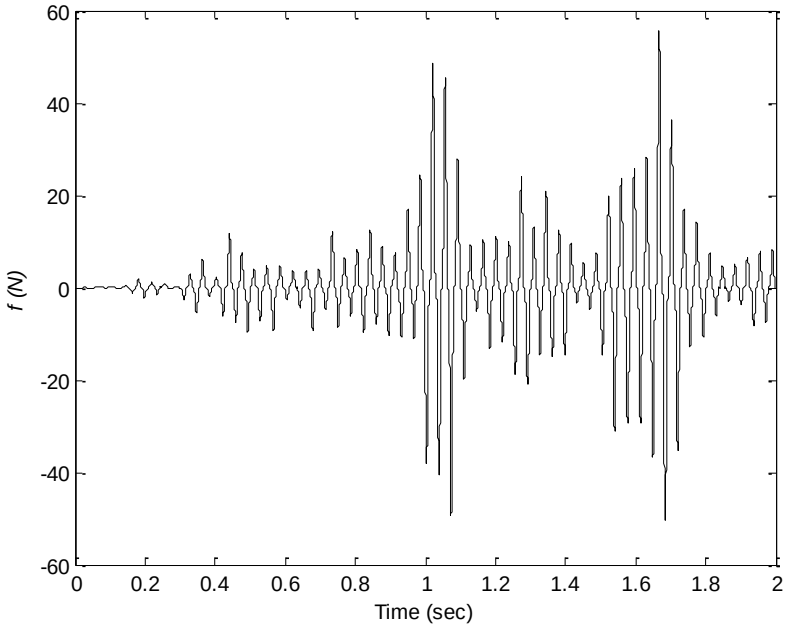

Figure 5.7: Time History of force $f(t)$ applied from nonlinear spring as input to the linear substructure

Specifically, predictions of displacement, accelerations and strains are obtained from the proposed methods using the 29-DOF model. The input $f(t)$ at the connection of the 29-DOF model with the other structure, that is graphically illustrated in Figure 5.7, is considered unknown. Moreover, it should be noted that the values of the masses and the springs of the 29-DOF model are the same as the ones used to simulate the measurements.

Throughout the numerical analysis, it is assumed that only acceleration measurements of the response of the structure at the masses are available. This is the common case in structural dynamics; in practice, the displacements and velocities are difficult, or even sometimes impossible to measure. Therefore, the problem lies in estimating the displacements of all masses of the system by using noisy observations acquired from acceleration sensors. Specifically, nine acceleration sensors are placed at DOFs 1, 6, 11, 16, 18, 21, 24, 26 and 29 of the model. Moreover, in order to represent measurement error in the simulated data, a

Table 5.1: The undamped natural frequencies of the 29-DOF model

No of Mode	Frequency (Hz)
1	5.9917
2	17.9582
3	29.8737
4	41.7046
5	53.4173
6	64.9785
7	76.3556
8	87.5162
9	98.4287
10	109.0623
11	119.3866
12	129.3726
13	138.9919
14	148.2171
15	157.0223
16	165.3823
17	173.2735
18	180.6736
19	187.5615
20	193.9178
21	199.7244
22	204.9648
23	209.6243
24	213.6895
25	217.1491
26	219.9931
27	222.2135
28	223.8040
29	224.7601

zero mean white Gaussian noise is added to the simulated acceleration time histories of the system. A choice was made to relate the level of added noise to the standard deviation of the signal as follows:

$$\underline{\tilde{y}} = \underline{y} + \gamma\sigma r \tag{5.64}$$

where $\underline{\tilde{y}}$ and $\underline{y} \in R^N$ represent, respectively, the polluted and unpolluted time histories at a given sensor location, γ is the noise level, σ signifies the standard

deviation of the considered data time history, and $r \in R^N$ is a vector of random values drawn independently from a normal distribution with zero mean and unit standard deviation. The influence of the level of the covariance of noise of the acceleration sensors $R_a = (\gamma\sigma)^2$ on the accuracy of the predicted estimates is also examined in the context of this thesis.

First of all, the nine acceleration time histories polluted with $\gamma = 5\%$ Gaussian white noise, that is added to the simulated data to account for modeling and measurement errors, are used to identify the state (displacements and velocities) of the system at all DOFs following the Kalman-type filter that is proposed in Section 5.4.1. The initial state $\underline{x}_0$ is assumed zero and the covariance matrix of the process noise Q and the covariance matrix of the observation noise R are assigned values of 10^{-15} and 10^{-1} on the diagonal, respectively. In accordance with what they represent, these values are chosen so as to have the order of the square roots of the diagonal elements of Q and R corresponding to a small percentage of the highest peaks in the measured state and response, respectively. It is also worth noting to report that the estimated displacements are filtered using a 3rd order Chebyshev high-pass filter. The low cut-off frequency in the high pass filter is chosen to be 0.3 times the modal frequency value of the lowest contributing mode of the structure. Then the filtered displacements predicted by this method are used to estimate the strains at the springs.

Moreover, the modal expansion method, proposed in Section 5.3.3.1, is also used to estimate the strains in the structure at all springs using simulated displacement measurements at the above nine DOFs. Results for strain predictions obtained from the Gillijns and De Moor's filter and the modal expansion method are presented in Figure 5.8 for the 19 spring of the 29-DOF model and in Figure 5.9 for the 25 spring. The predictions are compared with the simulated measurements. From the Figure 5.8 and Figure 5.9, it is clear that the comparisons show that strain predictions from both methods are very close to the exact ones. Specifically, the error between the measured and predicted strain time histories is estimated to be 18% for DOF 19 and 19% for DOF 25 in the case that the extension of Gillijns and De Moor's filter proposed by Lourens et al. (2012) is used. On the other hand, when modal expansion method is used, the error between the measured and predicted stress time histories is estimated to be 0.12% for DOF 19 and 0.13% for DOF 25. It is obvious that the modal expansion method gives more accurate predictions of the stress time histories at all DOFs for the spring mass chain system than the extension of Gillijns and De Moor's filter proposed by Lourens et

al. (2012) but the main disadvantage of this method is that cannot be implemented conveniently in practice since in the most cases we have

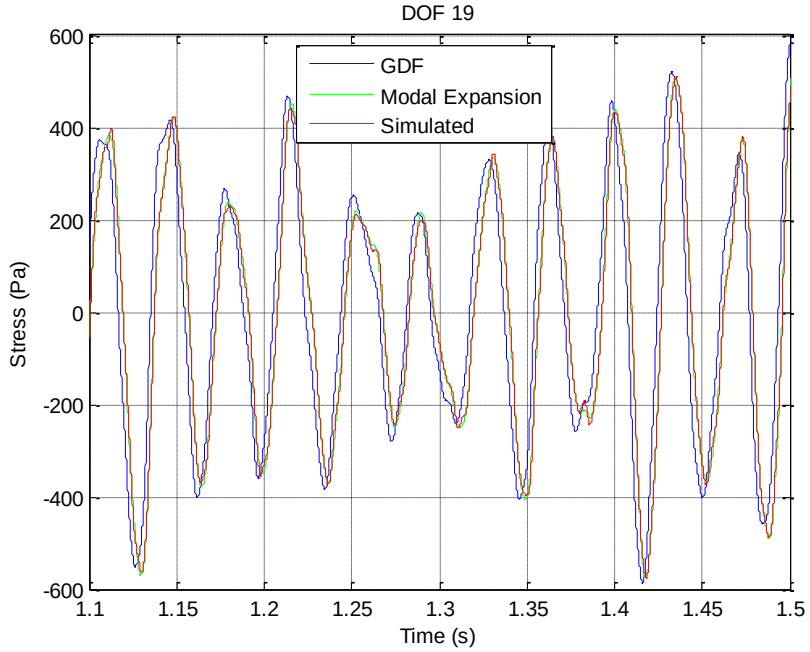

Figure 5.8: Estimated and simulated stress time histories at DOF 19.

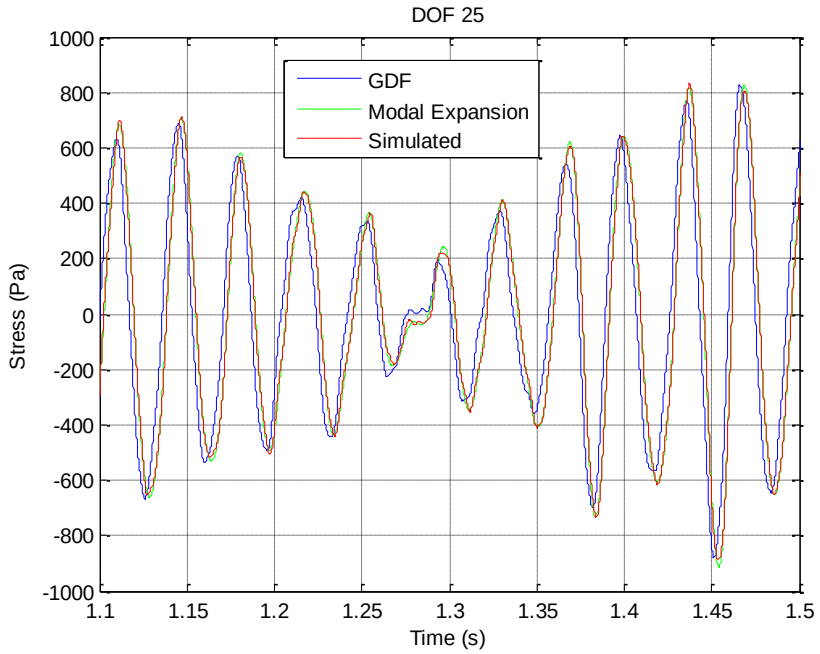

Figure 5.9: Estimated and simulated stress time histories at DOF 25.

acceleration measurements and not displacement or strain measurements that modal expansion method uses in order to predict the strain response of a system.

For this purpose, the accuracy of the other two proposed filters, Dual Kalman Filter and the Augmented Kalman Filter, for the prediction of the displacement and stress time histories of the 29-DOF system at all DOFs will be examined in order to get more accurate estimates of displacement and stress predictions and use them for the accurate prediction of fatigue damage accumulation.

For the implementation of Dual Kalman Filter for the prediction of displacements and stresses at all DOFs of the 29-DOF model, in the case that we have the nine polluted with Gaussian white noise acceleration time histories, the selection of the appropriate values for covariance parameters was necessary. The covariance matric of the process noise Q, the covariance matric of the observation noise R and the covariance matric of the input noise S are assigned values of 10^{-15} , 10^{-1} and 10^{1} on the diagonal, respectively. In all the simulations the model deployed in the algorithms is assumed to be accurate, hence the process noise is set to a small value $Q=10^{-15}\times I$; henceforth I is an identity matrix of appropriate dimension. In other words, the process noise covariance matrix reveals the confidence put on the utilized model of the system. Since a low value is chosen, the model is considered to be very accurate. Moreover, the value that is chosen for the observation noise covariance reveals the fact that there is measurement error in the acquired measurements and the estimator is not tightly forced to fit the recorded data. In Figure 5.10 and in Figure 5.11 the estimated and simulated stress time histories for DOF 19 and DOF 25 respectively are presented and compared to those predicted by the extension of Gillijns and De Moor's filter proposed by Lourens et al. (2012). It is obvious that estimates of higher accuracy are obtained when Dual Kalman Filter is utilized. Specifically, the error between the measured and predicted stress time histories is estimated to be 0.07% for DOF 19 and 0.08% for DOF 25, even much lower than those in the case of modal expansion method.

Finally, the Augmented Kalman Filter is utilized for the prediction of displacements selecting the above presented values for covariance matrices. The estimated and simulated stress time histories for DOF 19 and DOF 25 respectively are presented and compared to those predicted by the extension of Gillijns and De Moor's filter proposed by Lourens et al. (2012) and Dual Kalman Filter in Figure 5.12 and Figure 5.13 respectively. The error between the measured and predicted stress time histories is estimated to be 32% for DOF 19 and 37% for DOF 25, and is much higher than those estimated in the other methods. The low levels of accuracy in predicting the stress time histories at all DOFs of the 29-DOF model,

was expected since we used only acceleration measurements and has already been proven that we must use both acceleration

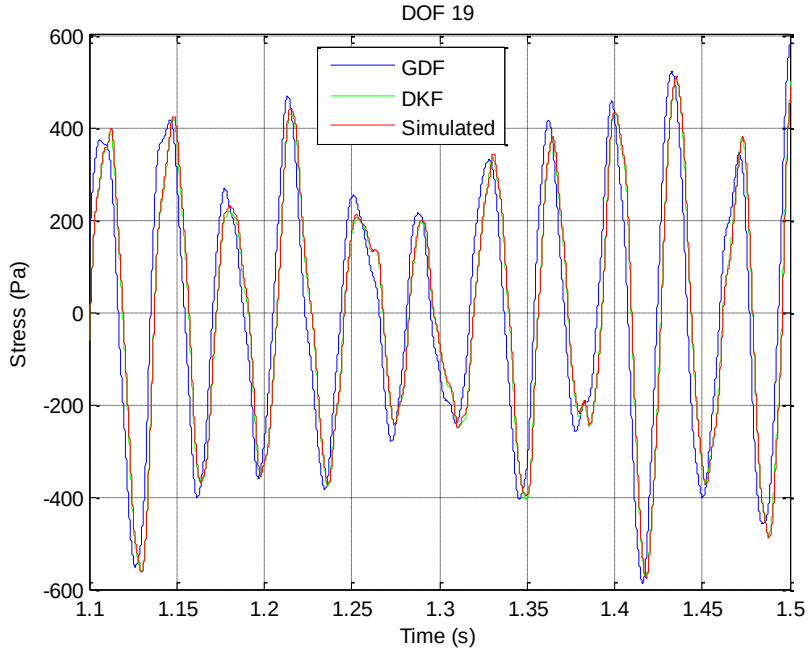

Figure 5.10: Estimated and simulated stress time histories at DOF 19.

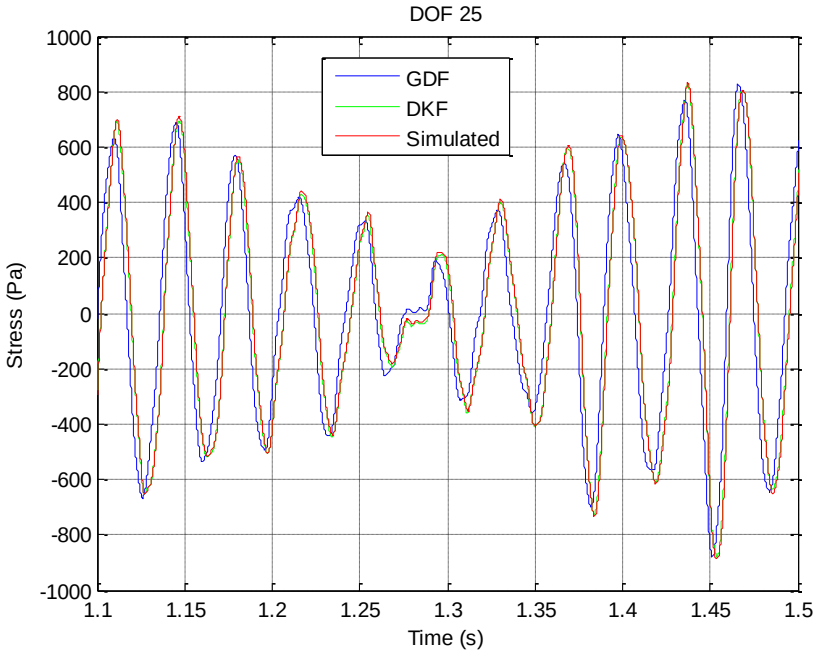

Figure 5.11: Estimated and simulated stress time histories at DOF 25.

and displacement measurements in order to get accurate estimates of displacements and stresses in the case of Augmented Kalman Filter.

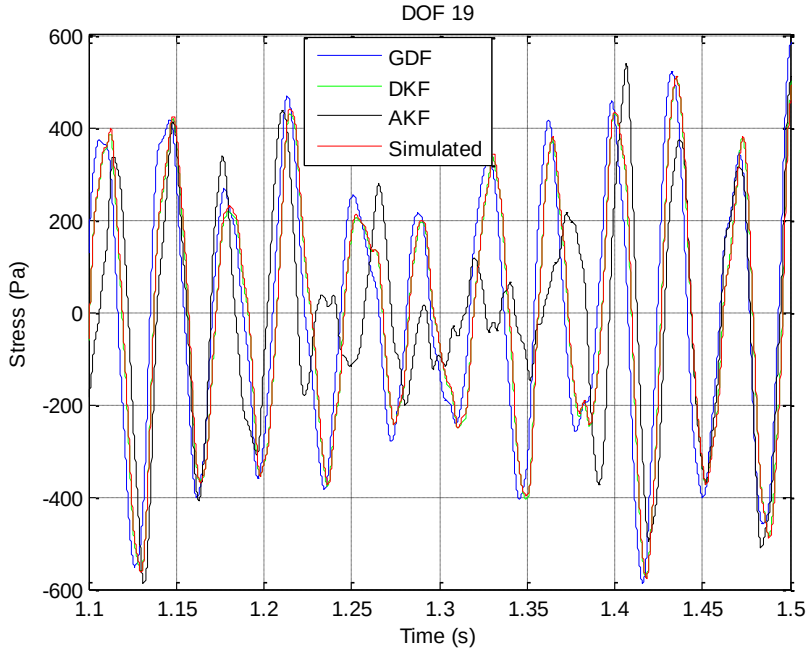

Figure 5.12: Estimated and simulated stress time histories at DOF 19.

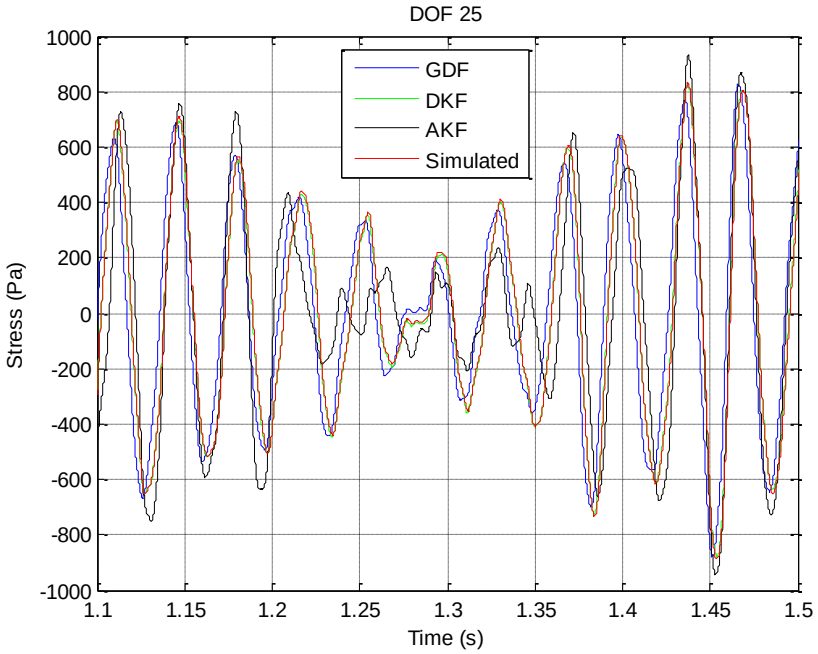

Figure 5.13: Estimated and simulated stress time histories at DOF 25.

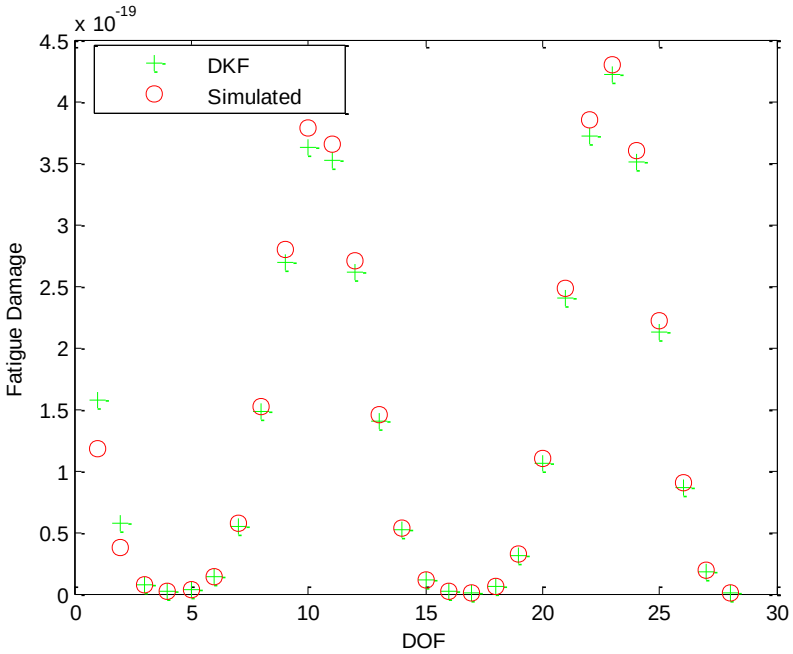

Figure 5.14: Fatigue Damage accumulation of the 29 DOF model.

Finally, using the predicted stress time histories at all DOFs predicted using the Dual Kalman Filter and utilizing the available S-N fatigue curves as described in Section 5.2.2, the Miner's rule is applied to estimate the fatigue damage accumulation for all DOFs of the 29 DOF model. The spring mass chain system is made of steel and the fatigue detail category 36 is adopted to illustrate the method. The static strength of steel is assigned the value $\sigma_u = 440$ MPa. According to Eurocode 3 for detail category 36, the following values of the parameters of the design S-N curves are recommended: $m = 3$, $\Delta\sigma_{\mathrm{D}} = 26.5\,\mathrm{MPa}$ and $\Delta\sigma_L = 14.5$ MPa. In Figure 5.14 the fatigue damage accumulation estimates for all DOFs using the stress time histories predicted by the Dual Kalman Filter are compared to those estimated by using the simulated stress time histories. From Figure 5.14 is clear that fatigue damage accumulation is estimated with very high accuracy, a fact that reveals that the methodology for estimating damage due to fatigue on the entire body of a structure by combining linear damage accumulation laws, S-N fatigue curves, rainflow cycle-counting algorithms, and acceleration measurements at a limited number of locations is a valuable tool for designing optimal fatigue-based maintenance strategies in a wide variety of structures.

5.5.2 Small Scale Vehicle-like Frame Structure

The accuracy and effectiveness of the new methodology was also demonstrated by applying it to a more complex mechanical system. Specifically, the framework is also demonstrated using the experimental small scale vehicle-like body, presented in Chapter 4 and shown in Figure 5.15. The vehicle structure is designed to simulate the frame substructure of a vehicle in a small scale of length 2m, width 1m and height 1.4 m. The frame substructure is made of steel with Young's modulus $E = 210GPa$, Poison's ratio $v = 0.3$ and density $\rho = 7850\,kg/m^3$. Figure 5.15 presents details of the geometrical dimensions of the frame and the sensor instrumentation that was used in order to produce simulated experimental data at 36 selected locations for the case of the vehicle. Details of material and geometrical dimensions of the frame can be found in Giagopoulos and Natsiavas (2007).

The basic idea in the case of the vehicle is the following: the selected frame structure comprises a frame structure with predominantly linear response and high modal density plus four substructures - supporting systems with strongly nonlinear action. These supporting systems consist of a lower set of linear discrete spring-damper units, connected to a concentrated mass, simulating the wheel subsystems, as well as of an upper set of a nonlinear discrete spring-damper (bushings) units connected to the frame and simulating the action of the vehicle suspension. More specifically, the nonlinear restoring and damping forces in the suspensions were selected to have the same form as those of the 30-DOF spring-mass chain model, which was presented in Section 5.51. The measurement points, indicated by points 3, 4, 28 and 29 in Figure 5.15, correspond to connection points between the frame and its supporting structures, while the rest 34 measurement points shown in Figure 5.15 were chosen on the frame. This sub-structuring approach allows us, based on the framework proposed in the case of the 30-DOF spring mass model, to isolate the large component of the frame of the vehicle that behaves linearly from the four isolated supporting subsystems that behave nonlinearly. Thus, the proposed methodologies can be applied to the linear vehicle frame.

Next, the procedure followed in the previous application was applied to this system. Namely, a nonlinear transient response analysis of the full vehicle model (frame and supports) was performed first, by applying four different stochastic road excitations to the wheel subsystems.

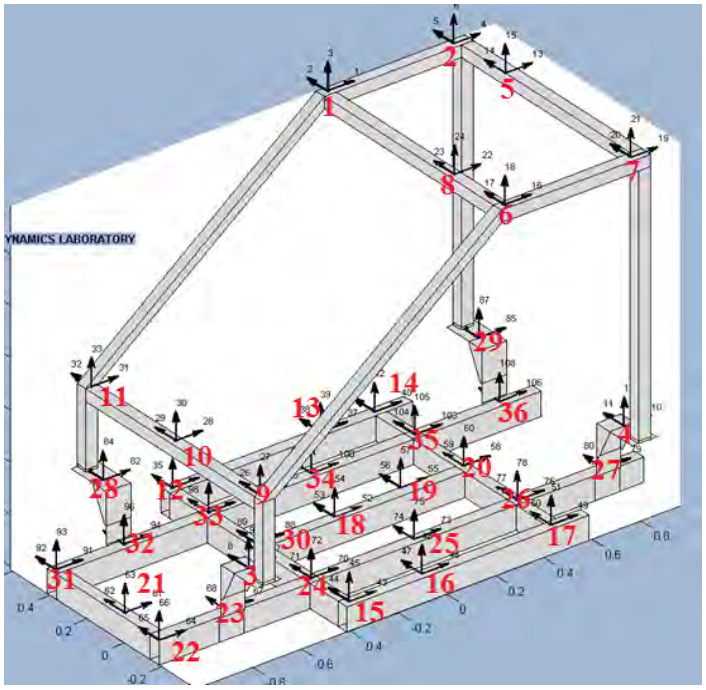

Figure 5.15: Sensor Instrumentation of vehicle frame.

Then, instead of performing experiments, the model was solved by using direct integration method. Specifically, a numerical method belonging to the well-known class of Newmark's methods (with parameters $\beta = 1/4$ and $\gamma = 1/2$) was applied for determining the acceleration and displacement time histories for the 36 points in three directions, graphically depicted in Figure 5.15. At this point, we should mention that the model that was numerically solved instead of performing experiments exhibits some differences in the meshing from the finite element model that will be used for performing the proposed methodologies. These differences yield in a maximum 8% difference in the eigenfrequencies between the two models, importing a kind of measurement error.

Displacement and acceleration time histories are recorded and are used as the exact estimates against which comparisons of predictions from the vehicle model will be made. The "measured" histories of the acceleration at boundary location 3, in the three directions (X-longitudinal, Y-transverse, Z-vertical), are presented in Figure 5.16, Figure 5.17 and Figure 5.18, respectively.

The finite element model, consisting of 15,202 finite elements and having 45,564 DOF, is used, after keeping only the first 30 modes, with the proposed methods to estimate the state of the structure at all DOFs. Then the strain predictions are then

obtained from the state estimates and the material properties. The excitations applied at the connections of the frame structure with the vehicle suspension are considered unknown.

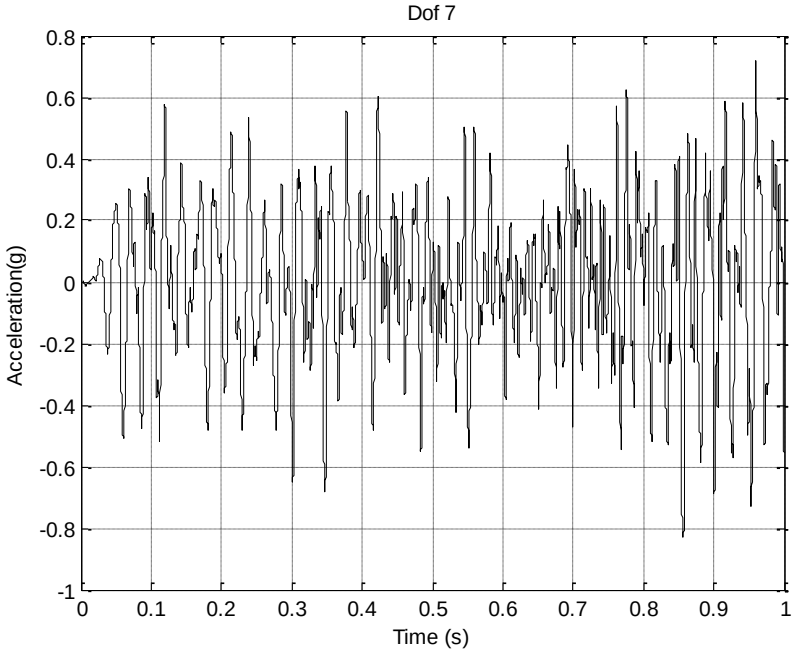

Figure 5.16: Acceleration time history at boundary location 3 in X direction.

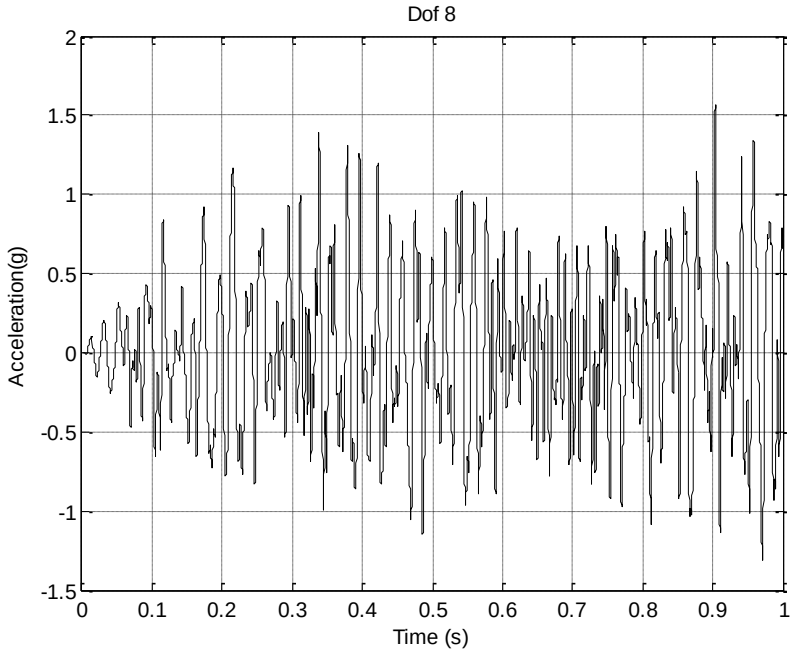

Figure 5.17: Acceleration time history at boundary location 3 in Y direction.

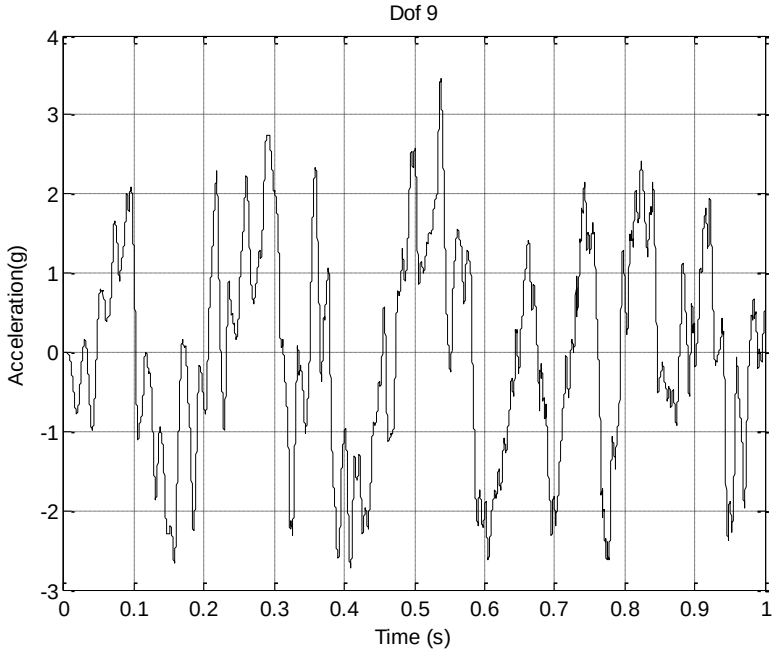

Figure 5.18: Acceleration time history at boundary location 3 in Z direction.

Fourteen acceleration sensors are used at DOFs 1, 3, 4, 7, 12, 14, 15, 17, 22, 27, 28, 29, 31, 36 of the model. The sensor locations are shown in Figure 5.15. The Kalman-type filter and the modal expansion method are used to estimate the state of the structure at all DOFs using the acceleration sensors, respectively. Moreover, a 5% noise is added to the simulated data to account for modeling and measurement errors. In the Kalman Filter, the initial state $\underline{x}_0$ is assumed zero and the covariance matrice of the process noise Q and the covariance matrice of the observation noise R are assigned values of 10^{-15} and 10^{-4} on the diagonal, respectively. Moreover, the estimated displacements are filtered using a 3rd order Chebyshev high-pass filter. The low cut-off frequency in the high pass filter is chosen to be 0.3 times the modal frequency value of the lowest contributing mode of the structure. The modal expansion method is also used to estimate the displacements in the structure using simulated displacement measurements at the above fourteen points. Results for displacement predictions obtained from the Kalman-type filter and the modal expansion method are presented in Figure 5.19-Figure 5.21 for the Point 2 of the top of the frame in three directions and in Figure 5.22-Figure 5.27 for Point 16 and Point 23 at the bottom of the frame in three directions. The predictions are compared with the simulated measurements.

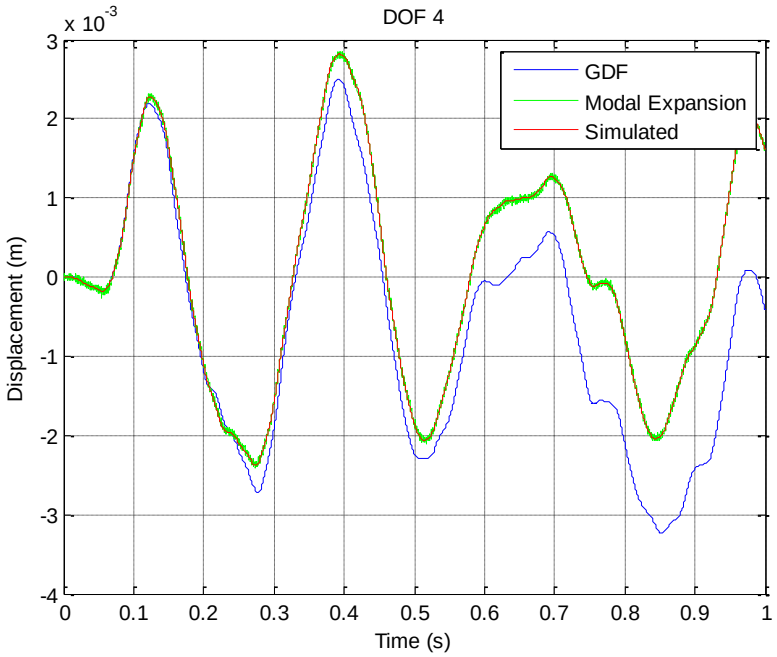

Figure 5.19: Displacement time history at Point 2 in X direction.

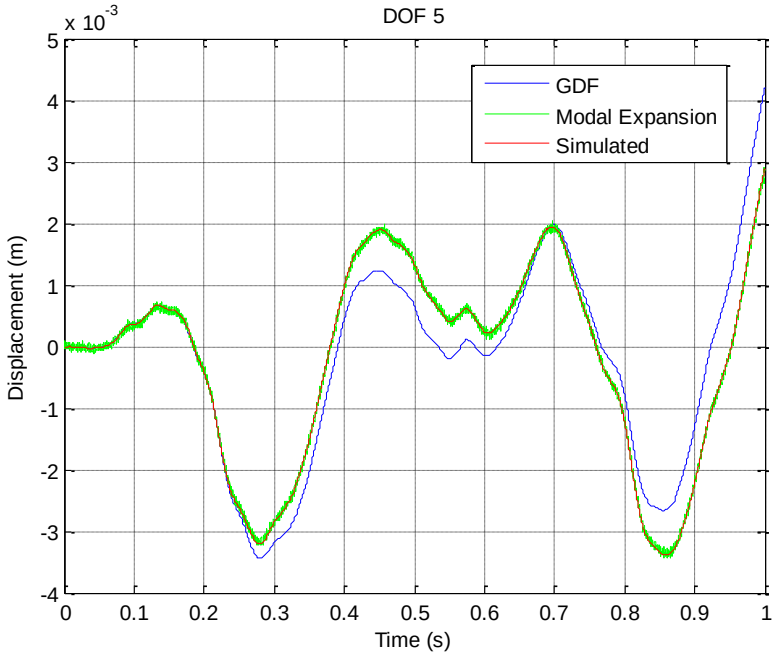

Figure 5.20: Displacement time history at Point 2 in Y direction.

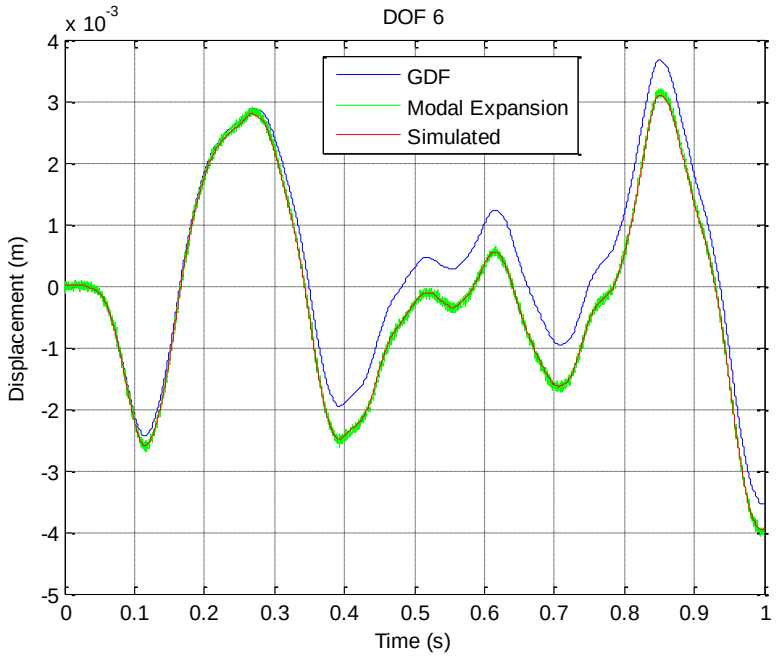

Figure 5.21: Displacement time history at Point 2 in Z direction.

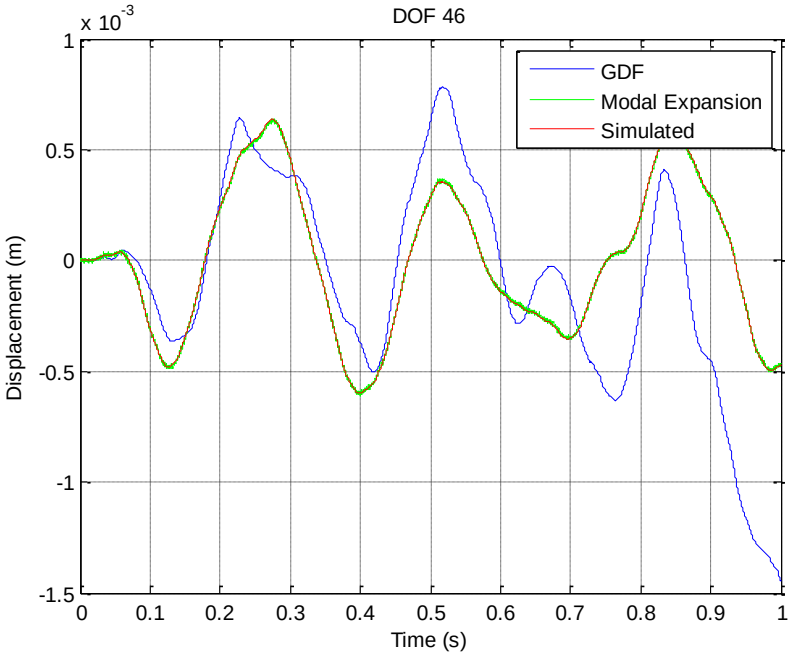

Figure 5.22: Displacement time history at Point 16 in X direction.

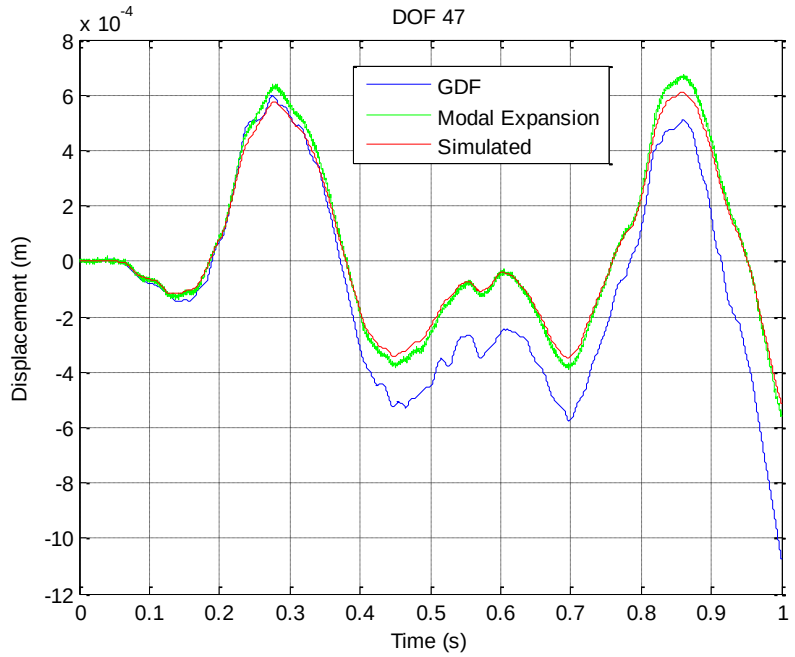

Figure 5.23: Displacement time history at Point 16 in Y direction.

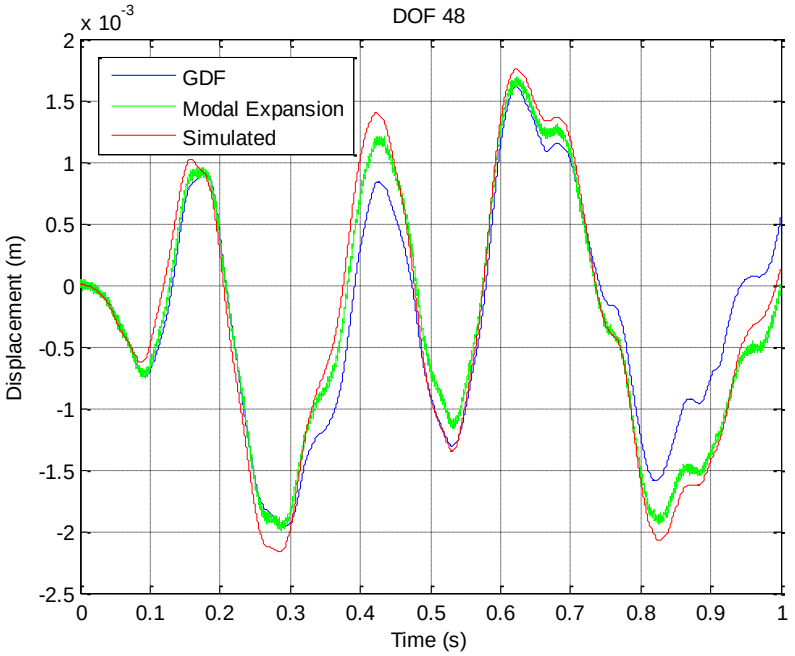

Figure 5.24: Displacement time history at Point 16 in Z direction.

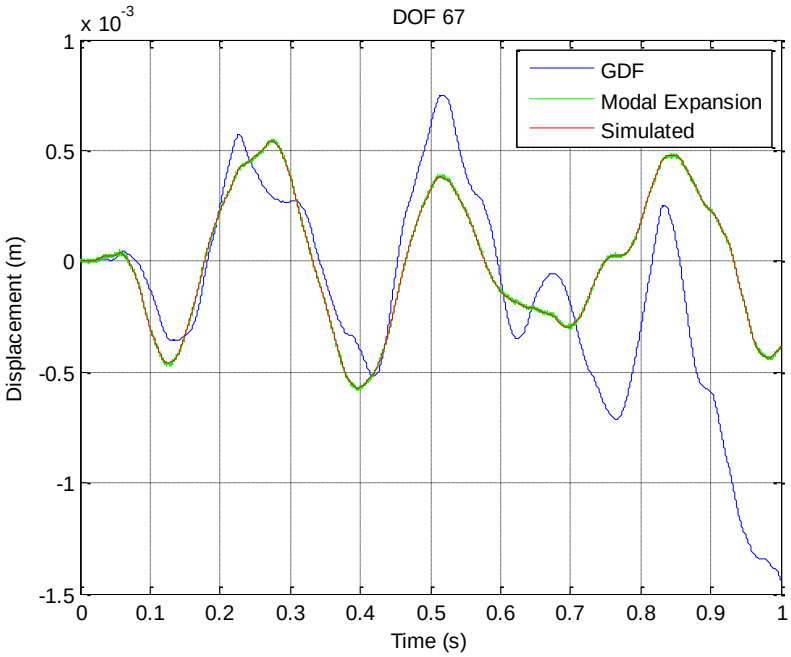

Figure 5.25: Displacement time history at Point 23 in X direction.

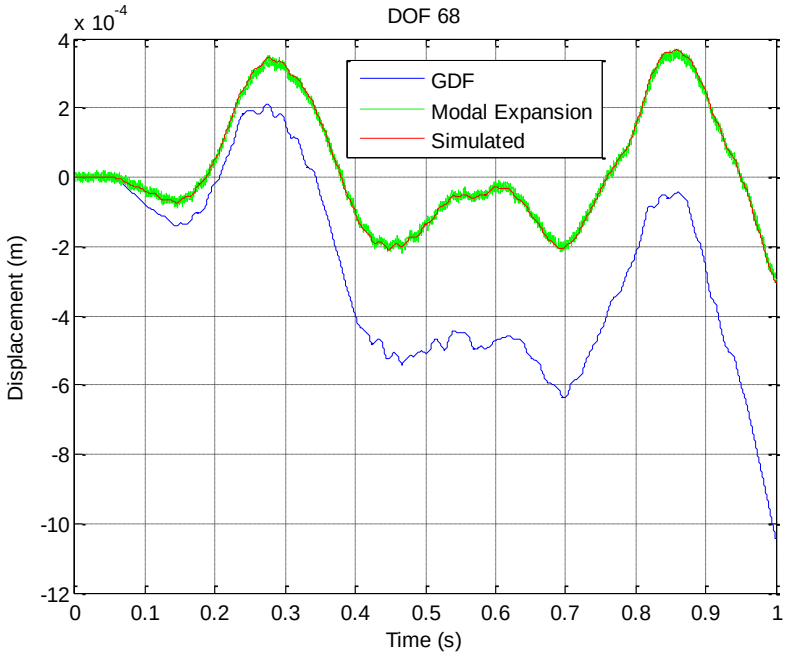

Figure 5.26: Displacement time history at Point 23 in Y direction.

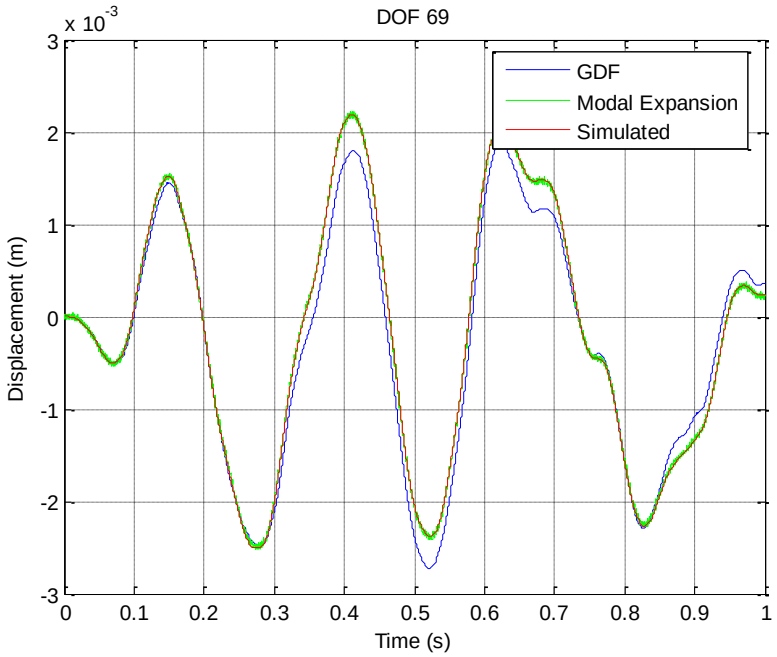

Figure 5.27: Displacement time history at Point 23 in Z direction.

From the comparison, it is clear that that the modal expansion method gives more accurate predictions of the displacement time histories than the extension of Gillijns and De Moor's filter proposed by Lourens et al. (2012), where a low-frequency drift is observed in all figures. For this purpose, the Dual Kalman Filter will be implemented in order to predict displacement time histories at all DOFs of the vehicle and use them for the accurate prediction of fatigue damage accumulation.

For the implementation of Dual Kalman Filter for the prediction of displacements at all DOFs of the vehicle, in the case that we have the fourteen polluted with Gaussian white noise acceleration time histories, the selection of the appropriate values for covariance parameters was necessary. The covariance matric of the process noise Q, the covariance matric of the observation noise R and the covariance matric of the input noise S are assigned values of 10^{-15} , 10^{-4} and 10^{1} on the diagonal, respectively. Results for displacement predictions obtained from the Kalman-type filter and the Dual Kalman Filter are presented in Figure 5.28-Figure 5.30 for the Point 2 of the top of the frame in three directions and in Figure 5.31-Figure 5.36 for Point 16 and Point 23 at the bottom of the frame in three

directions. The predictions are compared with the simulated measurements. It is obvious that estimates of higher accuracy are obtained when Dual Kalman Filter

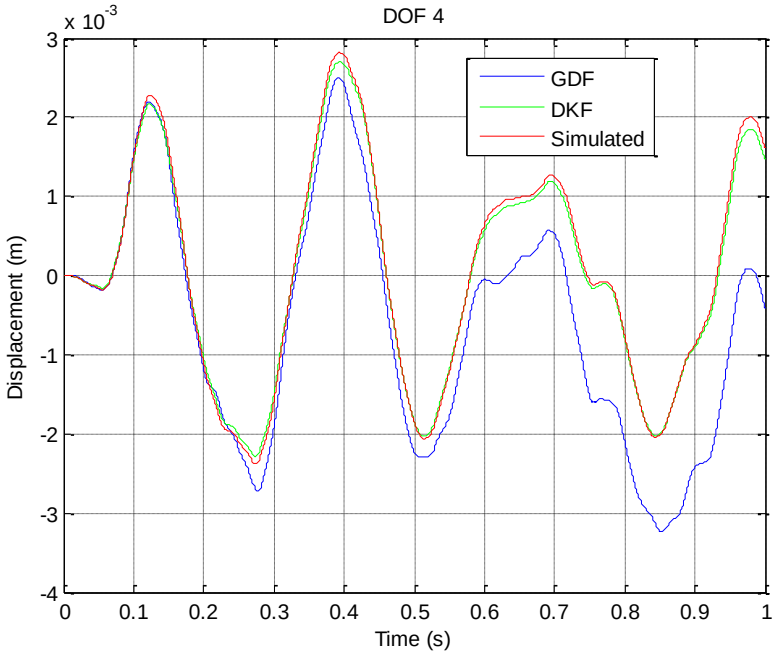

Figure 5.28: Displacement time history at Point 2 in X direction.

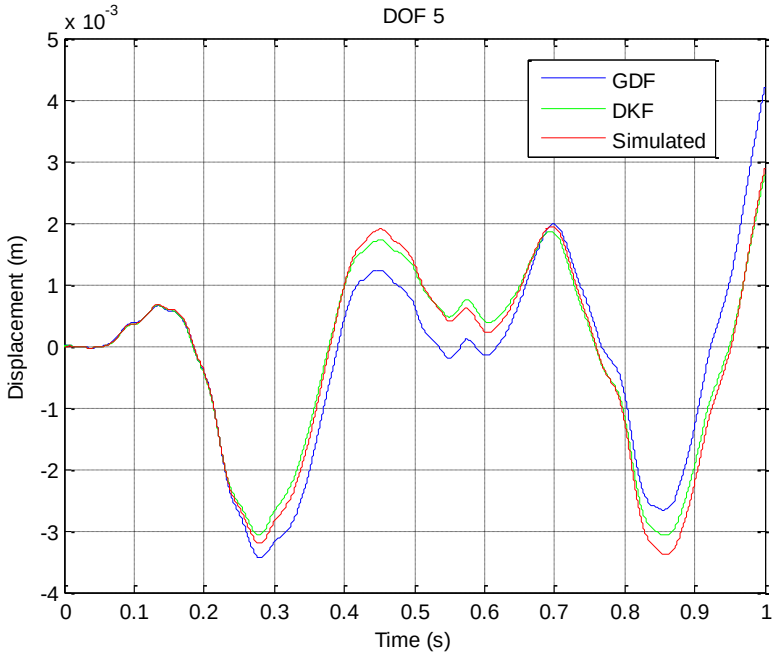

Figure 5.29: Displacement time history at Point 2 in Y direction.

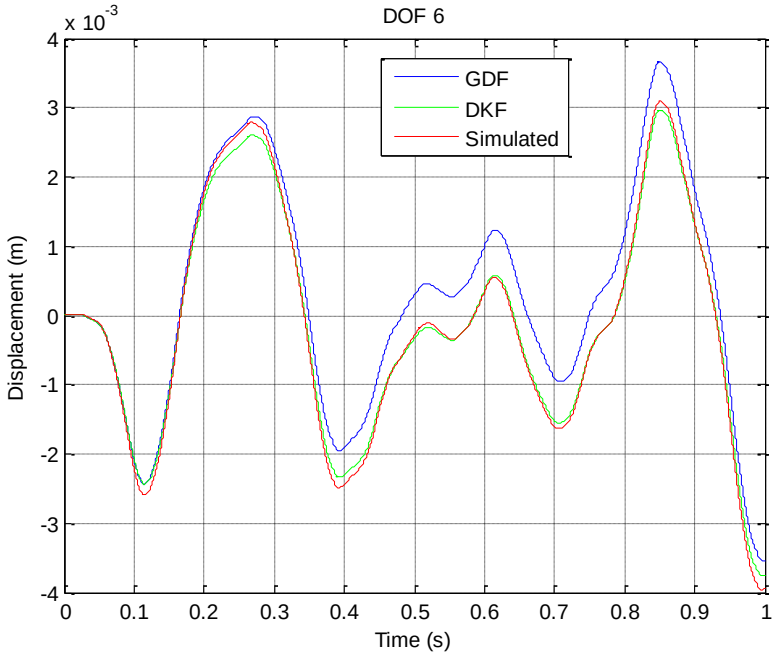

Figure 5.30: Displacement time history at Point 2 in Z direction.

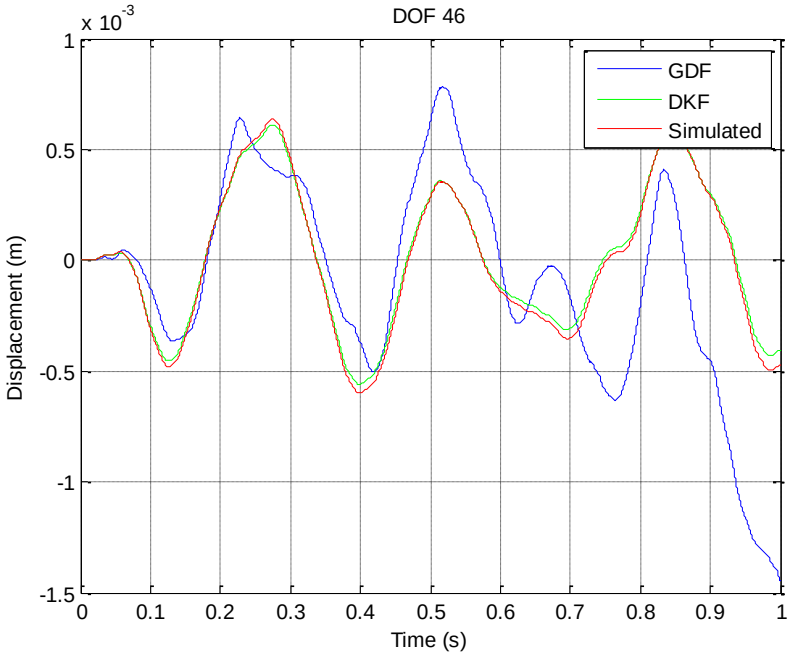

Figure 5.31: Displacement time history at Point 16 in X direction.

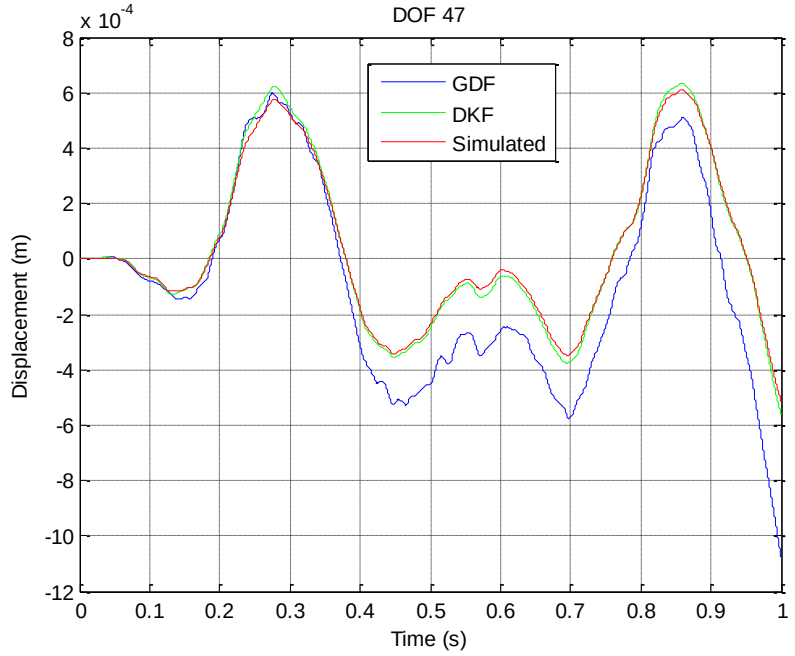

Figure 5.32: Displacement time history at Point 16 in Y direction.

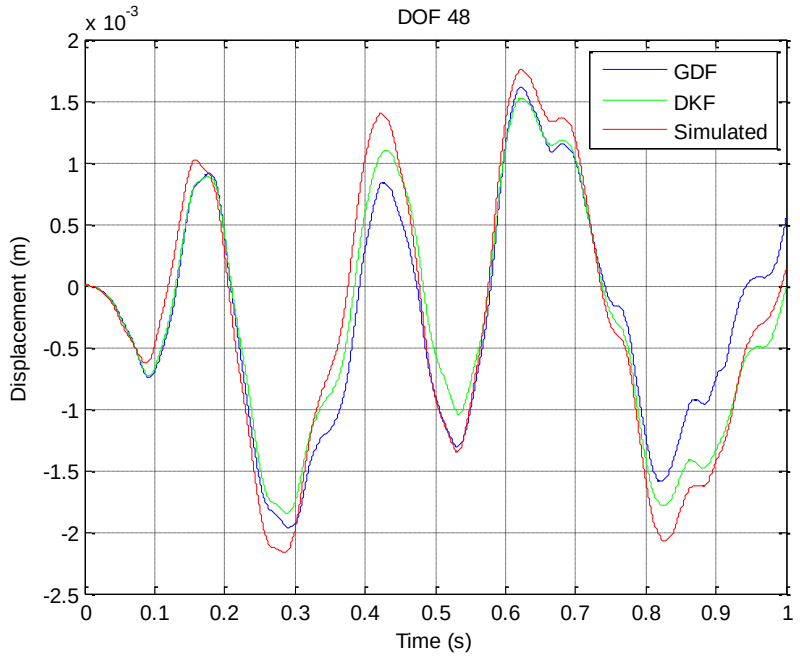

Figure 5.33: Displacement time history at Point 16 in Z direction.

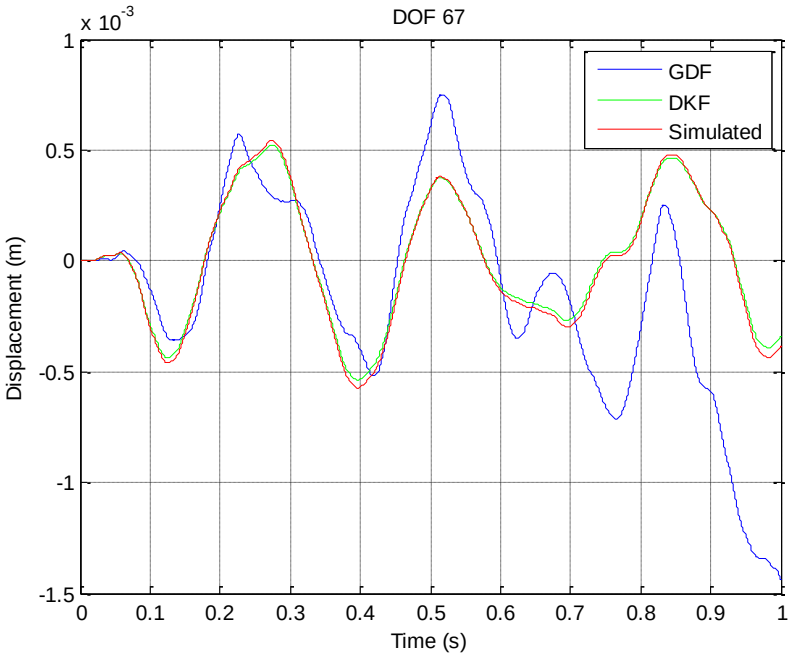

Figure 5.34: Displacement time history at Point 23 in X direction.

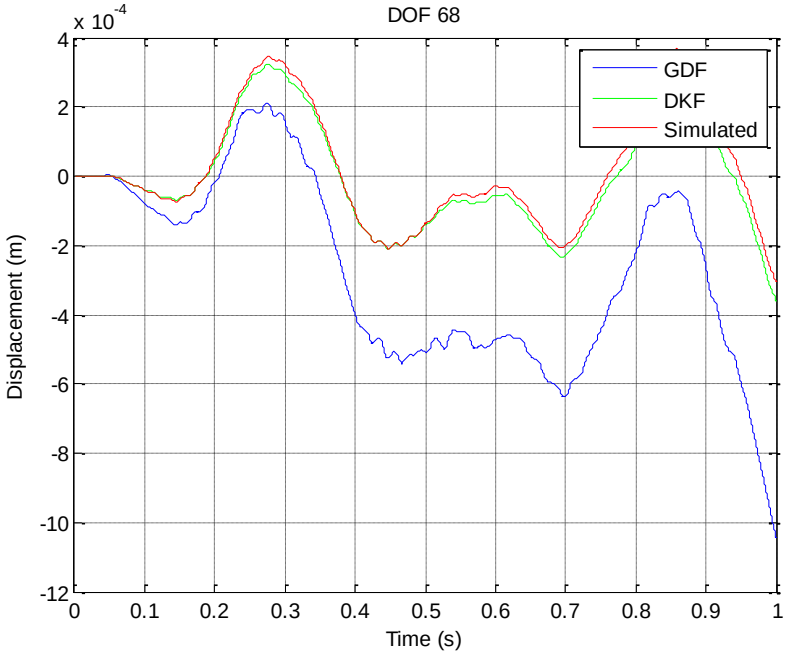

Figure 5.35: Displacement time history at Point 23 in Y direction.

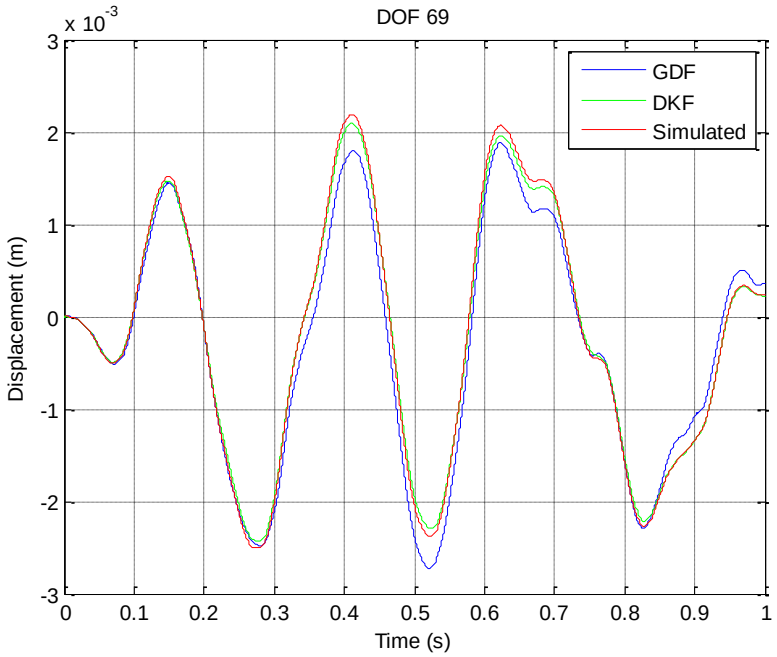

Figure 5.36: Displacement time history at Point 23 in Z direction.

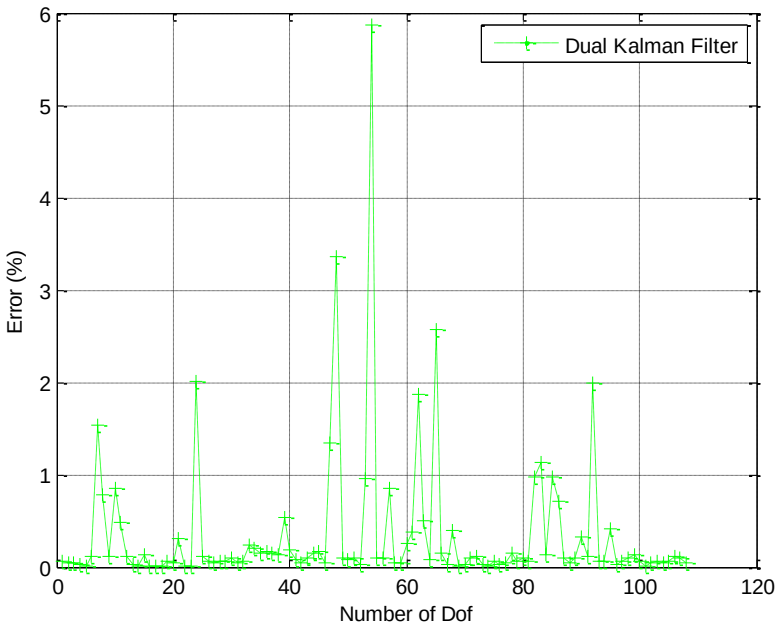

Figure 5.37: Error between predicted by DKF and simulated displacement time histories for all DOFs of the 36 points.

is utilized. Specifically, the error between the measured and predicted displacement time histories is estimated to be lower than 6%, as shown in Figure 5.37.

The strain and stress time histories are obtained for all finite elements of the vehicle, using the displacement time histories predicted by DKF at all DOFs and the relationships between stains and displacements that are given in Section 5.2.2. The predicted stress time histories in all three directions are presented in Figure 5.38 for Point 2, in Figure 5.39 for Point 16 and in Figure 5.40 for Point 23. Moreover, the predicted strain time histories in all three directions are presented in Figure 5.41 for Point 2, in Figure 5.42 for Point 16 and in Figure 5.43 for Point 23.

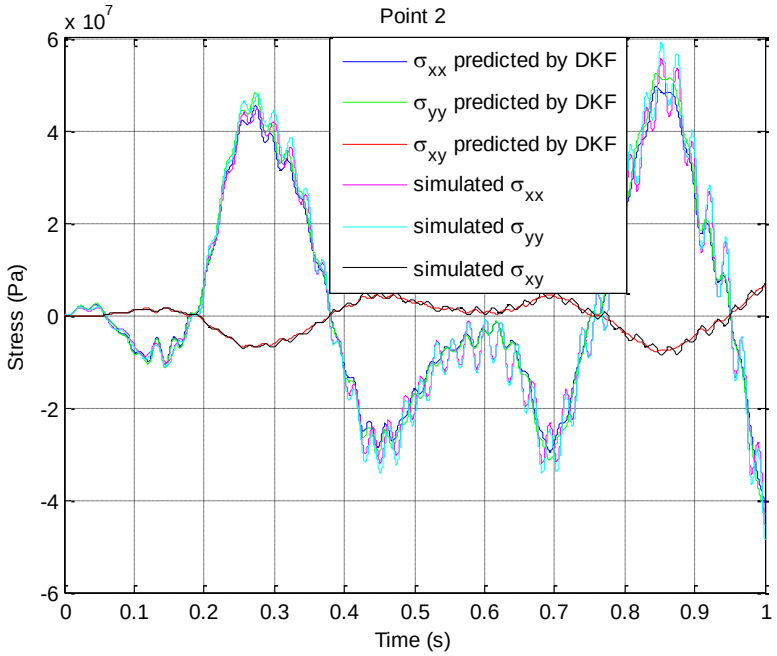

Figure 5.38: Stress time history at Point 2.

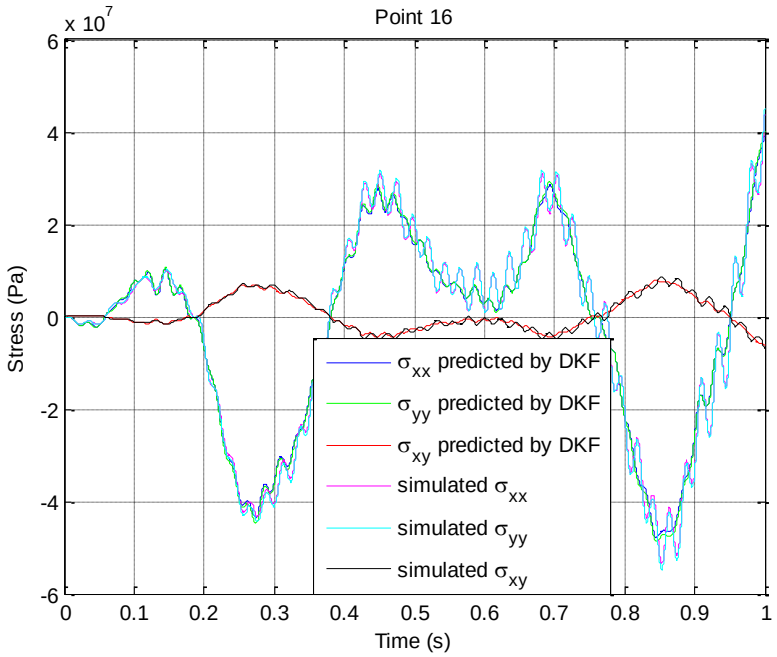

Figure 5.39: Stress time history at Point 16.

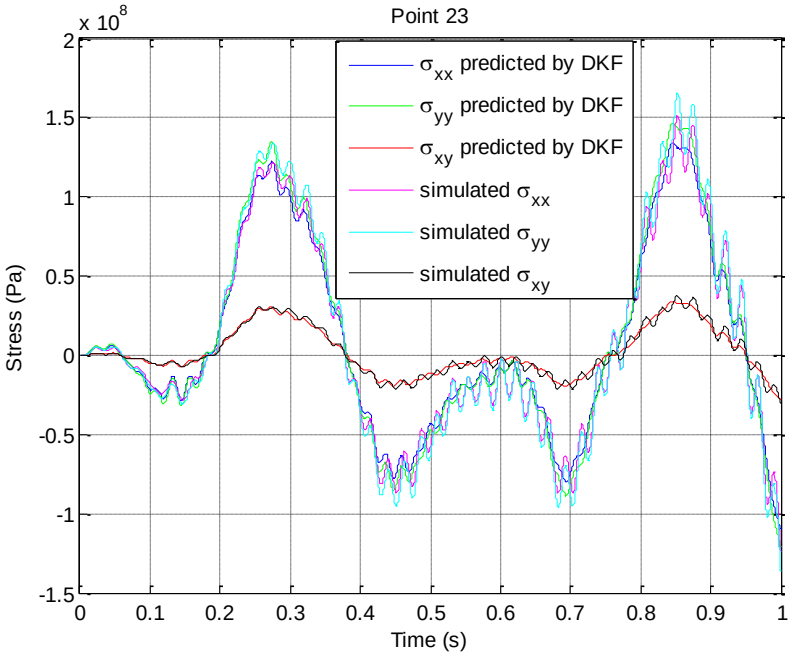

Figure 5.40: Stress time history at Point 23.

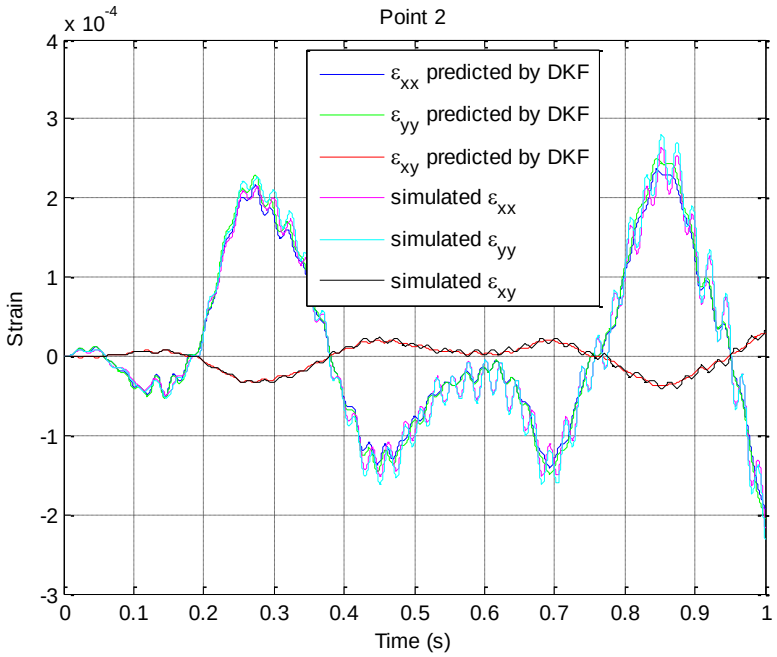

Figure 5.41: Strain time history at Point 2.

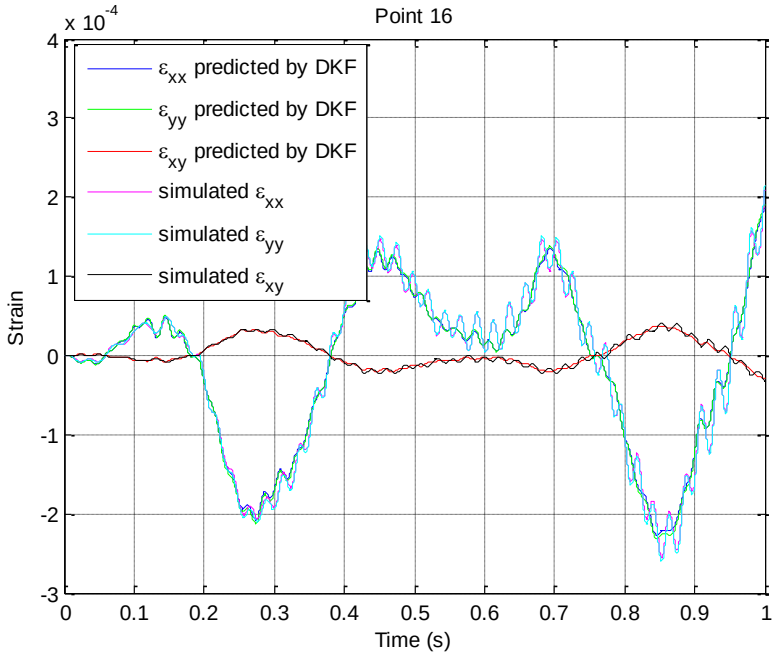

Figure 5.42: Strain time history at Point 16.

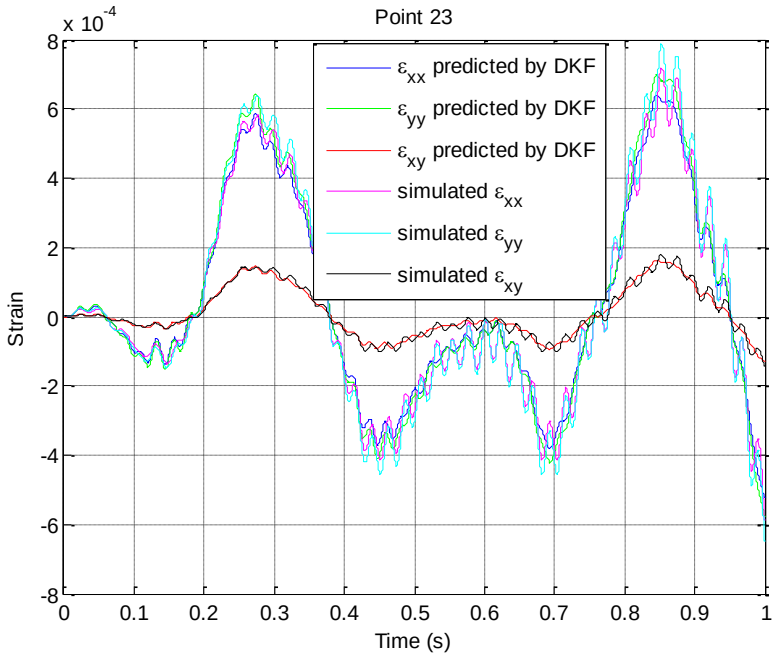

Figure 5.43: Strain time history at Point 23.

Finally, using the predicted stress time histories at all DOFs predicted by using the Dual Kalman Filter and utilizing the available S-N fatigue curves as described in Section 5.2.2, the Miner's rule is applied to estimate the fatigue damage accumulation for four points on the vehicle frame that we have uniaxial tension. The four points, for which fatigue damage is estimated are presented in Figure 5.44. For the estimation of fatigue damage, the static strength of steel is assigned the value $\sigma_u = 440$ MPa . Moreover, according to Eurocode 3 for detail category 36, the following values of the parameters of the design S-N curves are recommended: $m = 3$, $\Delta\sigma_{\mathrm{D}} = 26.5\,\mathrm{MPa}$ and $\Delta\sigma_L = 14.5$ MPa. We should also note that in the case of the vehicle fatigue is estimated only for some points on the bottom of the vehicle frame where we have mainly uniaxial tension while on the rest part of the vehicle severe shear stresses are imposed. However, it is worth noting that in the case of a structure that only uniaxial stresses are imposed on it, there is the potential of plotting the fatigue map since the code that has been developed in Matlab with cooperation with the interaction of Comsol gives as output plots like those presented for the plot of strains on the vehicle frame.

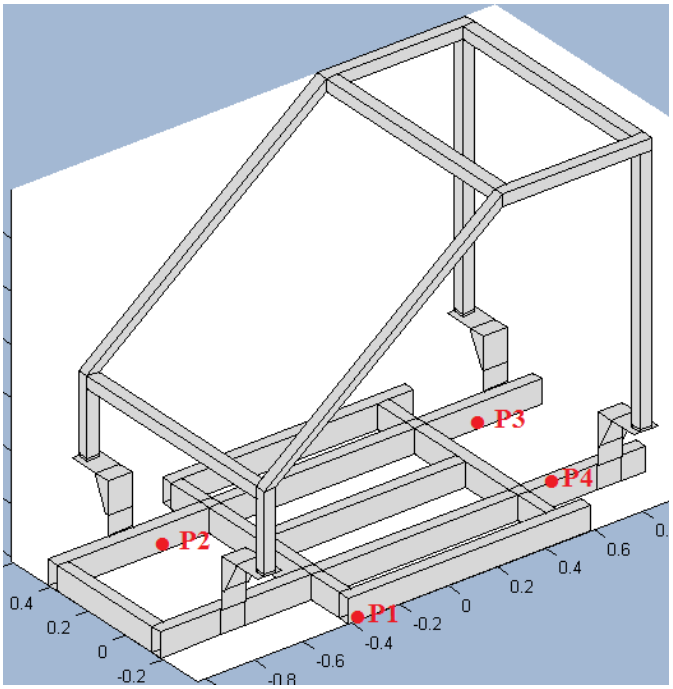

Figure 5.44: Points with uniaxial tension for fatigue calculation.

Table 5.2: Fatigue Damage accumulation for points on the vehicle

Point	Prediction of Fatigue Damage due to					
	σ_{xx} by DKF	simulated σ_{xx}	σ_{yy} by DKF	simulated σ_{yy}	σ_{xy} by DKF	simulated σ_{xy}
P1	2.5569×10^{-5}	2.5222×10^{-5}	0.0844	0.0823	6.2161×10^{-4}	6.0857×10^{-4}
P2	5.7142×10^{-4}	5.3388×10^{-4}	0.0122	0.0103	7.7101×10^{-5}	7.1322×10^{-5}
P3	4.4954×10^{-4}	4.0748×10^{-4}	0.0059	0.0051	8.6952×10^{-5}	8.5413×10^{-5}
P4	1.1972×10^{-4}	1.143×10^{-4}	0.0010	0.0009	2.3108×10^{-4}	2.2964×10^{-4}

The creation of fatigue maps on the vehicle are useful for designing optimal fatigue-based maintenance strategies for protecting structures like vehicles against failure due to fatigue.

5.6 Conclusions

A novel use of monitoring information for estimating fatigue damage accumulation in the entire body of metallic structures is outlined in this work. This is accomplished by combining fatigue damage accumulation laws with stress/strain predictions based on output only vibration measurements collected from a limited number of sensors. Methods for estimating strains by integrating high fidelity finite element model and estimation techniques were summarized. The predictions are currently based on linear model of structures. The accuracy of the proposed methods for fatigue predictions in the entire body of the structure depends on the number and location of sensors in the structures, the number of modes contributing in the dynamics of the structure, and the size of the model error and measurement error.

The proposed methodologies have also been extended to cover nonlinear models of structures. Applications cover a large variety of metallic structures, including ground and air vehicles, civil engineering structures such as steel buildings, high towers and railway/motorway bridges, industrial structures, wind turbine blades and supporting structures/masts, offshore structures, etc. The proposed methodology can be used to construct fatigue damage accumulation and lifetime prediction maps consistent with the actual operational conditions provided by a monitoring system. Such fatigue maps are useful for designing optimal fatigue-based maintenance strategies for metallic structures using structural vibration information collected from a sensor network.

CHAPTER 6 Conclusions – Future Work

6.1 Conclusions

The research work presented in the thesis deals with the management of uncertainties in structural response and reliability simulations using measured data. In the context of this thesis, it was shown that uncertainties play an important role in the prediction of the performance and safety of structural systems. Uncertainties arise in the process of simulating the behavior of these systems. Uncertainties are manifested from the assumptions and compromises that enter into the development of mathematical models of structural systems as well as the applied loads. Such uncertainties lead to significant uncertainties in the predictions made using simulations. Since simulations constitute the basis for design and maintenance decisions in order to meet desirable system performance and safety requirements, uncertainties affect these decisions and have to be accounted for in simulations. For this, stochastic/probabilistic models offer suitable mathematical tools for quantifying and propagating uncertainties in structural engineering simulations.

A specific focus of this thesis is the management of uncertainties that appear in model updating problem of structural systems. Structural model updating is an inverse problem according to which a model of a structure, usually a finite element model, is adjusted so that either the calculated time histories, frequency response functions, or modal parameters best match the corresponding quantities measured or identified from the test data. This inverse process aims at providing

updated models and their corresponding uncertainties based on the data. These updated models are expected to give more accurate response predictions to future loadings, as well as allow for an estimation of the uncertainties associated with such response predictions. In practice, the inverse problem of model updating is usually ill-conditioned due to insensitivity of the response to changes in the model parameters, and non-unique because of insufficient available data relative to the large number of model parameter needed to describe the desired model

The widely used deterministic methods for solving the structural model updating problem formulated both as single-objective and multi-objective optimization problem are reviewed in Chapter 2. The main theme of this chapter was to present a Bayesian statistical framework for structural model parameter identification that is used to identify the values of the weights that appear in structural model updting. Using Bayes theorem, the probability distribution of the weight values based on the data is formulated as a probability integral over the structural model parameters. Bayesian techniques are also proposed to quantify the uncertainty in the parameters of a FE model, select the best model class from a family of competitive model classes, as well as propagate uncertainties for robust response and reliability predictions. Posterior probability density functions (PDFs) are derived that quantify the uncertainty in the model parameters based on the data. These PDFs are formulated in terms of the modal residuals involved in the aforementioned single and multi-objectives deterministic methods. The Bayesian tools for identifying uncertainty models as well as performing robust prediction analyses are presented. These include Laplace methods of asymptotic approximation and more accurate stochastic simulation algorithms (SSA) such as Markov Chain Monte Carlo (MCMC), Transitional MCMC and Delayed Rejection Adaptive Metropolis. Similar to the deterministic FE model updating techniques, the asymptotic approximations in the Bayesian framework involve solving an optimization problem for finding the most probable model, as well as estimating the Hessian of the logarithm of the posterior PDF at the most probable model for describing the uncertainty in the model parameters. The SSA algorithms involve generating samples for tracing and then populating the important uncertainty region in the parameter space, as well as evaluating integrals over high-dimensional spaces of the uncertain model parameters.

The optimal structural models and their uncertainties resulting from model updating methods can be used for improving the model response and reliability predictions, for assessing structural health and identifying structural damage and for improving effectiveness of structural control devices. Engineers in practice are frequently requested to implement the above model updating methods in complex engineering systems including hundreds of thousands or even million degrees of freedom. Chapter 2 proposes methods for drastically reducing the computational

demands at the system, algorithm and hardware levels involved in the implementation of Bayesian tools. At the system level, model reduction techniques can be applied to reduce the order of the model selected to simulate the behavior of the system.

The importance of these reduction techniques was demonstrated in Chapter 3. In this chapter, a framework was presented for integrating the Craig-Bampton CMS technique into existing FE model updating formulations in order to reduce the time consuming operations involved in reanalyses of large-order models of hundreds of thousands or millions degrees of freedom. The proposed method exploits the fact that in FE model parameterization schemes the stiffness matrix of the structure often depends linearly on the parameters of the model and also that a parameter usually represents a global property (e.g. the modulus of elasticity) of a substructure. The division of the structure into components is then guided by the FE parameterization scheme so that the stiffness matrix that arise for each one of the introduced components to depend linearly on only one of the parameters to be estimated. In this case the fixed-interface and constraint modes of the components for any value of the model parameters can be obtained exactly from the fixed-interface and constraint modes corresponding to a single reference FE model, avoiding re-analyses at component level. Additional substantial reductions in computational effort are also proposed by reducing the number of interface DOF using characteristic interface modes through a Ritz coordinate transformation. The repeated solutions of the component and interface eigen-problems are avoided, reducing drastically the computational demands in FE formulations, without compromising the solution accuracy. It is also shown that the linear expansions of the original mass and stiffness matrices in terms of the structural parameters are preserved for the reduced mass and stiffness matrices. Thus, the reassembling of the reduced system matrices from the original matrices is also avoided in the execution of the system re-analyses. The only time consuming operation left is the re-analysis of the eigenproblem of the reduced-order model. It is finally demonstrated that the new developments are readily accommodated in existing FE model updating formulations and software with minimal modifications. The effectiveness of the proposed algorithms, in terms of computational efficiency and accuracy, was demonstrated with application on model updating and damage identification of a bridge using simulated data and a high fidelity model with hundreds of thousands of DOF.

In Chapter 4, a Bayesian uncertainty quantification and propagation (UQ&P) framework was presented for identifying nonlinear models of dynamic systems using vibration measurements of their components. The accuracy of the Bayesian UQ&P framework to identify models of linear and nonlinear components of a system was shown through the application on a small scale experimental model of

a vehicle. The identification of the uncertainty models of the nonlinear wheel and suspension components is investigated using the experimentally obtained response spectra. The uncertainty models for the vehicle frame are also obtained using experimental data. The uncertainty is propagated to output quantities of interest for the combined wheel-suspension-frame system. The computational challenges and efficiency of the Bayesian UQ&P framework are outlined. The effectiveness of the framework on the specific example structure is discussed.

In Chapter 5, the problem of estimating the full strain time histories characteristics at critical locations of the structure using operational vibration measurements from a limited number of sensors is presented. The measurements may consist of response time histories such as e.g. strain, acceleration, velocity, displacement, etc. Moreover, this chapter deals with the use of such estimates to predict fatigue damage accumulation in the entire body of a metallic structure and lays out the formulation for estimating fatigue using output-only vibration measurements and outlines methods for estimating the stress response history characteristics required in deterministic and stochastic fatigue theories. Similar estimation techniques can be used to estimate other important response characteristics in the entire body of the structure, such as displacements, velocities, accelerations, etc. The analyses in this study are first implemented to the case of linear structures and then have been extended to cover nonlinear models of structures. The stress response quantities are predicted at locations subjected to uni-axial stress states. The measured quantities are considered to be accelerations, displacements or strains or a combination of accelerations, displacements and strains. The objective of this chapter is to formulate the fatigue prediction problem, illustrate the methodology and point out its use in evaluating the damage accumulation in the entire structure from a limited number of vibration measurements. For this, the analyses in this study are restricted to the case of stress response predictions at locations subjected to uni-axial stress states for both linear and nonlinear structures.

Summarizing the current thesis contributes to the following three interrelated research areas of management of uncertainties using vibration measurements: (1) development of component mode synthesis techniques that are integrated with model updating methods (2) development of Bayesian uncertainty and quantification framework for both linear and nonlinear systems and (3) fatigue-based damage accumulation predictions in the entire body of metallic structures using a limited number of vibration sensors. Finally, the novel contributions in this thesis are as follows.

- Iterative optimization algorithms and stochastic simulation algorithms involved in both deterministic and Bayesian FE model updating formulations require a moderate to large number of FE model re-analyses.

For large size FE models with hundreds of thousands or even million DOF, the computational demands may be excessive. Exploiting certain stiffness-related parameterization schemes, often encountered in FE model updating formulations, to guide the division of the structure into components results in exact linear representations of the Craig-Bampton reduced stiffness matrix as a function of the model parameters with coefficient matrices computed and assembled once from a single CMS analysis of a reference structure. Further significant reductions in the size of the reduced system are shown to be possible using characteristic interface modes estimated for each interface between components. Re-analyses required in FE model updating formulations are associated with the solution of the eigenproblem of the reduced-order system, completely avoiding the re-analyses of the component fixed-interface and characteristic interface modes as well as the re-assembling of the reduced system matrices. FE model updating and damage identification results using a solid model of a bridge demonstrated the implementation, computational efficiency and accuracy of the proposed model reduction methodology. The computational effort was reduced drastically by more than three orders of magnitude. In particular, for the application in damage identification the computational time was reduced from approximately one month to several minutes. Further computational savings can be obtained by adopting surrogate modes to drastically reduce the number of reduced-order system re-analyses and parallel computing algorithms to efficiently distribute the computations in available multi-core CPUs .

- A Bayesian UQ&P framework was presented for identifying nonlinear models of dynamic systems using vibration measurements of their components. The use of Bayesian tools, such as stochastic simulation algorithms (e.g., TMCMC algorithm), may often result in excessive computational demands. Drastic reduction in computational effort to manageable levels is achieved using component mode synthesis, surrogate models and parallel computing algorithms. The framework was demonstrated by identifying the linear and nonlinear components of a small-scale laboratory vehicle model using experimental response spectra available separately for each component. Such model uncertainty analyses for each component resulted in building a high fidelity model for the combined system to be used for performing reliable robust response predictions that properly take into account model uncertainties. The theoretical and computational developments in this work can be used to identify and propagate uncertainties in large order nonlinear dynamic systems that consist of a number of linear and nonlinear components.

- A novel use of monitoring information for estimating fatigue damage accumulation in the entire body of metallic structures is outlined in this work. This is accomplished by combining fatigue damage accumulation laws with stress/strain predictions based on output only vibration measurements collected from a limited number of sensors. Methods for estimating strains by integrating high fidelity finite element model and estimation techniques were summarized. The predictions are currently based on linear model of structures. The accuracy of the proposed methods for fatigue predictions in the entire body of the structure depends on the number and location of sensors in the structures, the number of modes contributing in the dynamics of the structure, and the size of the model error and measurement error. The proposed methodologies have also been extended to cover nonlinear models of structures. Applications cover a large variety of metallic structures, including ground and air vehicles, civil engineering structures such as steel buildings, high towers and railway/motorway bridges, industrial structures, wind turbine blades and supporting structures/masts, offshore structures, etc. The proposed methodology can be used to construct fatigue damage accumulation and lifetime prediction maps consistent with the actual operational conditions provided by a monitoring system. Such fatigue maps are useful for designing optimal fatigue-based maintenance strategies for metallic structures using structural vibration information collected from a sensor network.

6.2 Future Work

The developed strategies of this thesis certainly open the door for future research activities. This concerns especially the application of stochastic updating algorithms for large and complex FE models. While a successful implementation of the Bayesian updating algorithms in the FE model of Metsovo bridge was shown in this thesis, there are several possibilities for improvements in further applications. More specifically, in the current application the physical parameters have been grouped into various categories and these categories have been updated. The next interesting step would consist in splitting the groups down to the level of physical parameters. This however requires an additional step, namely the application of sensitivity analysis in order to identify the most important parameters since an independent treatment of all structural parameters of a real FE model, which might amount up to several thousands, is not feasible.

Furthermore, another recommendation for future work relates to the deterministic model updating problem. Over the last years, a substantial amount of research has

been performed in the context of efficient vibration-based FE model updating techniques for effective damage assessment. Many authors advocate that it is beneficial to use other residual definitions such as modal strain energy or modal flexibilities, other types of experimental data such as frequency response functions or modal strains, or combining several types of data in multi-objective optimization schemes. Therefore, it is suggested to extend the methods proposed to FE model updating schemes which make use of these alternative objective function configurations.

Another interesting issue that is not investigated in the context of this thesis is the application of Bayesian inference in robust optimal experimental design and specifically in a civil engineering context often referred to as optimal sensor placement (OSP). The relation between OSP and Bayesian model updating is briefly summarized in the following: a sensor configuration can be determined such that the information obtained from the data regarding the model parameters is maximized. For instance, in the context of damage assessment by FE model updating, it can be verified that OSP leads to configurations where more sensors are situated in arreas attaining high modal curvature. Moreover, all current research related to OSP remains mostly limited to optimality with respect to parameter inference; this could be extended to OSP for optimal predictive response. Moreover, in view of the recommendation made above, it is suggested to assess OSP for heterogeneous sensor networks, i.e where various types of experimental data are combined.

Finally, related to suggested future work, it is suggested to thoroughly investigate the accuracy of implementing asymptotic approximations as Bayesian tools in real structures instead of implementing the stochastic simulation algorithms that were used in the context of this thesis. The use of asymptotic expressions reduces the computational demand for the determination of the full posterior pdfs to a single deterministic optimization routine. The accuracy of the implementation of stochastic simulation algorithms as a tool for identifying uncertainty models and performing robust prediction analyses in the Bayesian framework was demonstrated in the context of this thesis. But the investigation of the accuracy of asymptotic approximation expressions still remains a challenge to be investigated for future work.

References

Alvin K.F., (1997), "Finite element model update via Bayesian estimation and minimization of dynamic residuals," *AIAA Journal*, Vol. 35, pp. 879-886.

Angelikopoulos P., Papadimitriou C., Koumoutsakos P., (2012), "Bayesian uncertainty quantification and propagation in molecular dynamics simulations: A high performance computing framework.", *Journal of Chemical Physics*, Vol. 137(14).

Angelikopoulos P., Papadimitriou C., Koumoutsakos P., (2015), "X-TMCMC: Adaptive Kriging for Bayesian inverse modelling", *Mechanical Systems and Signal Processing*, Vol. 289, pp. 409-428.

Eftekhar Azam S., Chatzi E., Papadimitriou C., (2015), "A dual Kalman filter approach for state estimation via output-only acceleration measurements", *Computer Methods in Applied Mechanics and Engineering*, Vol. 60-61, pp. 866-886.

Barbato M., Conte J.P., (2005), "Finite element response sensitivity analysis: a comparison between force-based and displacement-based frame element models." *Computer Methods in Applied Mechanics and Engineering*, Vol. 194(12-16), pp. 1479-1512.

Barbato M., Zona A., Conte J.P., (2007), "Finite element response sensitivity analysis using three-field mixed formulation: General theory and application to frame structures", *International Journal for Numerical Methods in Engineering*, Vol. 69(1), pp. 114-161.

Balmes E., (1996), "Parametric families of reduced finite element models. Theory and applications.", *Mechanical Systems and Signal Processing*, Vol. 10(4), pp. 381-394.

Bathe K.J., Wilson E.L., (1976), "Numerical methods in finite element analysis", Prentice Hall.

Bathe K.J., (1996), "Finite Element Procedures", Prentice Hall.

Batou A., Soize C., Corus M., (2011), "Experimental Identification of an uncertain computational dynamical model representing a family of structures". *Computers and Structures*, Vol.89, pp.1440-1448.

Beck J.L., (1989), "Statistical System Identification of Structures", *Proceedings of the 5th International Conference on Structural Safety and Reliability (ASCE),* San Francisco, pp.1395-1402.

Beck J.L., May B.S., Polidori D.C. (1994), "Determination of modal parameters from ambient vibration data for structural health monitoring", *Proceedings of the 1st World Conference on Structural Control*, Los Angeles, USA, pp. 1395-1402.

Beck J.L., Katafygiotis L.S., (1998), "Updating models and their uncertainties- I: Bayesian statistical framework", *Journal of Engineering Mechanics (ASCE),* Vol. 124, pp. 455-461.

Beck J.L., Au S.K., (2002), "Bayesian updating of structural models and reliability using Markov chain Monte Carlo simulation", *ASCE Journal of Engineering Mechanics,* Vol.128(4), pp. 380-391.

Beck J.L., Yuen K.V. (2004), "Model selection using response measurements: Bayesian probabilistic approach", *ASCE Journal of Engineering Mechanics*, Vol. 130(2), pp. 192-203.

Beck J.L., (2010), "Bayesian system identification based on probability logic", *Structural Control and Health Monitoring*, Vol. 17(7), pp. 825–847.

Benasciutti D, Tovo R., (2006), "Comparison of spectral methods for fatigue analysis of broad-band Gaussian random processes", *Probabilistic Engineering Mechanics*, Vol. 21, pp. 287–299.

Bernal D., Ussia A., (2015), "Sequential deconvolution input reconstruction", *Mechanical Systems and Signal Processing,* Vol. 50-51, pp. 41-55, 2015.

Bohle K., Fritzen C.-P., (2003), "Results obtained by minimizing natural frequency and mac-value errors of a plate model" *Mechanical Systems and Signal Processing,* Vol. 17(1), pp. 55-64.

Castanier M.P., Tan Y.-C., Pierre C., (2001), "Characteristic constraint modes for component mode synthesis", *AIAA Journal*, Vol. 39(6), pp. 1182-1187.

Chatzi E.N., Smyth A.W., (2009) "The unscented Kalman filter and particle filter methods for nonlinear structural system identification with non-collocated heterogeneous sensing", *Structural Control and Health Monitoring,* Vol. 16, pp. 99–123.

Chatzi E.N., Fuggini C., (2015) "Online Correction of Drift in Structural Identification Using Artificial White Noise Observations and an

Unscented Kalman Filter,", *Special Volume of Smart Structures and Systems on Errors/uncertainties in sensors for Structural Health Monitoring*, in press.

Ching, J., Beck, J.L., Porter, K.A.,(2006), " Bayesian state and parameter estimation if uncertain dynamical systems", *Probabilistic Engineering Mechanics*, Vol. 21, pp. 81-96.

Ching J., Chen Y.C., (2007), "Transitional Markov Chain Monte Carlo method for Bayesian updating, model class selection, and model averaging", *ASCE Journal of Engineering Mechanics*, Vol. 133, pp. 816–832.

Christodoulou K., Papadimitriou C., (2007), "Structural identification based on optimally weighted modal residuals", *Mechanical Systems and Signal Processing*, Vol. 21, pp. 4-23.

Christodoulou K., Ntotsios E., Papadimitriou C., Panetsos P., (2008), "Structural model updating and prediction variability using Pareto optimal models", *Computer Methods in Applied Mechanics and Engineering*, Vol. 198 (1), pp. 138-149.

COMSOL AB COMSOL Multiphysics User's Guide, 2005 [http://www.comsol.com/].

Cox R.T., (1946), "Probability, frequency and reasonable expectation", *American Journal of Physics*, Vol. 14 (1), pp. 1-13.

Craig Jr R.R.., Bampton M.C.C., (1968), "Coupling of substructures for dynamic analysis.", *AIAA Journal* , Vol. 6(7), pp. 1313-1319.

Craig Jr. R.R., (1981), "Structural Dynamics - An Introduction to Computer Methods", John Wiley & Sons, New York.

Das I., Dennis J.E. Jr., (1998), "Normal-boundary intersection: A new method for generating the Pareto surface in nonlinear multi-criteria optimization problems", *SIAM Journal of Optimization*, Vol.8, pp. 631-657.

Dirlik T., (1985), "Applications of Computers to Fatigue Analysis", PhD Thesis, Warwick University.

Fan W., Qiao P., (2011), "Vibration-based damage identification methods: a review and comparative study", *Structural Health Monitoring*, Vol. 10(1), pp. 83-111.

Felber A.J. (1993), "Development of a hybrid bridge evaluation system", PhD Thesis, University of British Columbia, Vancouver, Canada.

Fonseca J., Friswell M.I, Mottershead J., Lees A. (2005), "Uncertainty identification by the maximum likelihood method" *Journal of Sound and Vibration*, Vol. 288, pp. 587-599.

Friswell M.I., Mottershead J.E. (1995), "Finite Element Model Updating in Structural Dynamics", Kluwer Academic Publishers.

Friswell M.I., Mottershead J.E., (2001), "Inverse methods in structural health monitoring", *Key Engineering Materials*, Vol. 4, pp. 201-210.

Fritzen C.P., Jennewein D., Kiefer T., (1998), "Damage detection based on model updating methods", *Mechanical Systems and Signal Processing*, Vol. 12(1), pp. 163-186.

Giagopoulos, D., Natsiavas, S., Hybrid, (2007), "(Numerical-Experimental) Modeling of Complex Structures with Linear and Nonlinear Components", *Nonlinear Dynamics*, Vol. 47, pp. 193-217.

Giagopoulos D., Papadioti D.-C. Papdimitriou C., Natsiavas S. (2013), "Bayesian Uncertainty Quantification and Propagation in Nonlinear Structural Dynamics." *in International Modal Analysis Conference (IMAC)*, California.

Gillijns, S., De Moor, B., (2007), "Unbiased minimum-variance input and state estimation for linear discrete-time systems", *Automatica*, Vol. 43(1), pp. 111–116.

Gillijns, S., De Moor, B., (2007), "Unbiased minimum-variance input and state estimation for linear discrete-time systems with direct feedthrough", *Automatica*, Vol. 43(5), pp. 934–937.

Ghanem R.G., Spanos P., (1991), "Stochastic Finite Elements: A spectral approach", Springer.

Goller B., Broggi M., Calvi A., Schueller G.I, (2011), "A stochastic model updating technique for complex aerospace structures', *Finite Elements in Analysis and Design*, Vol. 47, pp. 739-752.

Goller B., Pradlwarter H.J., Schueller G.I., (2011), "An interpolation scheme for the approximation of dynamical systems", *Computer Methods in Applied Mechanics and Engineering*, Vol. 200, pp. 414-423.

Goller B., (2011), "Stochastic Model Validation of Structural Systems", Ph.D. Dissertation, University of Innsbruck.

Haario H., Laine M., Mira A., Saksman E., (2006), "DRAM: Efficient adaptive MCMC", *Statistics and Computing*, Vol.16, pp. 339-354.

Hansen N., Muller S.D., Koumoutsakos P., (2003), "Reducing the time complexity of the derandomized evolution strategy with covariance matrix adaptation (CMA-ES)." *Evolutionary Computation*, Vol. 11(1), pp. 1-18.

Haralampidis Y., Papadimitriou C., Pavlidou M., (2005), "Multi-objective framework for structural model identification", *Earthquake Engineering and Structural Dynamics*, Vol.34 (6), pp. 665-685.

Hastings, W. K., (1970), "Monte Carlo sampling methods using Markov chains and their applications", *Biometrika*, Vol. 57(1), pp. 97-109.

Hadjidoukas P.E., Angelikopoulos P., Papadimitriou C., Koumoutsakos P., (2015), "Π4U: A high performance computing framework for Bayesian uncertainty quantification of complex models", *Journal of Computational Physics*, Vol. 284, pp. 1-21.

Hernandez E.M., Bernal D., (2008), "State estimation in structural systems with model uncertainties", *ASCE Journal of Engineering Mechanics*, Vol. 134(3), pp. 252–257.

Hernandez E.M., Bernal D., Caracoglia L.,(2013), "On-line monitoring of wind-induced stresses and fatigue damage in instrumented structures", *Structural Control and Health Monitoring*, Vol. 20(10), pp. 1291-1302.

Hinke L., Dohnal F., Mace B., Waters T., Ferguson N., (2009), "Component mode synthesis as a framework for uncertainty analysis", *Journal of Sound and Vibration*, Vol. 324(1–2), pp. 161–178.

Hong S.K., (2011), "Parametric reduced-order models for predicting the vibration response of complex structures with component damage and uncertainties", *Journal of Sound and Vibration*, Vol. 330(6), pp. 1091-1110.

Hong S.K., Epureanu B.I., Castanier M.P., Gorsich D.J., (2011), "Parametric reduced-order models for predicting the vibration response of complex structures with component damage and uncertainties", *Journal of Sound and Vibration*, Vol. 330, pp. 1091-1110.

Hurty W., (1965), "Dynamic analysis of structural systems using component modes.", *AIAA Journal*, Vol. 3(4), pp. 678–685.

Jaynes E.T., (2003), "Probability Theory: The Logic of Science", Cambridge University Press.

Jensen H.A., Vergara C., Papadimitriou C., Millas A. , (2013), " The use of updated robust reliability measures in stochastic dynamical systems." *Computer Methods in Applied Mechanics and Engineering*, Vol. 267, pp. 293-317.

Jensen H.A., Millas A., Kusanovic D., Papadimitriou C., , (2014), "Model-Reduction Techniques for Bayesian Finite Element Model Updating Using Dynamic Response Data" *Computers and Structures*, Vol. 279, pp. 301-324.

Kalman R., (1960), "A new approach to linear filtering and prediction problems", *Basic Eng. Trans. ASME*, Vol. 82D, pp. 35–45.

Kammer D.C., (1991), "Sensor placements for on orbit modal identification and correlation of large space structures", *Journal of Guidance, Control and Dynamics*, Vol. 14, pp. 251-259.

Katafygiotis L.S., Papadimitriou C., Lam H.F., (1998), "A probabilistic approach to structural model updating", *International Journal of Soil Dynamics and Earthquake Engineering*, Vol. 17, pp. 495-507.

Katafygiotis L.S., Beck J.L., (1998), "Updating models and their uncertainties. II: Model identifiability", *Journal of Engineering Mechanics (ASCE)*, Vol. 124 (4), pp. 463-467.

Katafygiotis L.S, Lam H.F. (2002), "Tangential-projection algorithm for manifold representation in unidentifiable model updating problems.", *Earthquake Engineering & Structural Dynamics*, Vol. 31(4), pp. 791-812.

Kitanidis P.K., (1987), "Unbiased minimum-variance linear state estimation", *Automatica*, Vol. 23, pp. 775-778.

Lopez I., Sarigul-Klijn N., (2010), "A review of uncertainty in flight vehicle structural damage monitoring, diagnosis and control", *Challenges and opportunities, Progress in Aerospace Sciences*, Vol. 46(7), pp. 247-273.

Lophaven S.N., Nielsen H.B., Søndergaard J., (2002), "DACE,A MATLAB Kriging Toolbox", DTU: DK-2800 Kgs. Lyngby - Denmark.

Lourens, E., Papadimitriou, C., Gillijns, S., Reynders, E., De Roeck, G., Lombaert, G., (2012), "Joint input-response estimation for structural systems based on reduced-order models and vibration data from a limited number of sensors", *Mechanical Systems and Signal Processing*, Vol.29, pp. 310–327.

Lourens, E., Reynders, E., De Roeck, G., Degrande, G., Lombaert, G., (2012), "An augmented Kalman filter for force identification in structural dynamics", *Mechanical Systems and Signal Processing*, Vol. 27(1), pp. 446-460.

Lutes LD, Larsen CE., (1990), "Improved spectral method for variable amplitude fatigue prediction", *Journal of Structural Engineering (ASCE)*, Vol. 116(4), pp. 1149-1164.

Lutes LD., Sarkani S., (2004), "Random Vibrations: Analysis of Structural and Mechanical Systems", Elsevier Butterworth-Heinemann.

Lyness J.N., Moler C.B., (1969), "Generalized Romberg Methods for Integrals of Derivatives.", *Numerische Mathematik*, Vol. 14(1), pp. 1-12.

Marwala T., (2010), "Finite Element Model Updating Using Computational Intelligence Techniques: Applications to Structural Dynamics", Springer.

Mace B., Shorter P., (2001), "A local modal/perturbational method for estimating frequency response statistics of built-up structures with uncertain properties", *Journal of Sound and Vibration*, Vol. 242(5), pp. 793–811.

Metha M. L., (2004), "Random Matrices". Elsevier.

Metallidis, P., Verros, G., Natsiavas, S. & Papadimitriou, C, (2003), "Fault detection and optimal sensor location in vehicle suspensions.", *Journal of Vibration and Control*, 2003. Vol. 9(3-4), pp. 337-359.

Metallidis P., Stavrakis I., Natsiavas S., (2008), "Parametric identification and health monitoring of complex ground vehicle models.", *Journal of Vibration and Control*, Vol. 14(7), pp. 1021-1036.

Metropolis N., Rosenbluth A.W., Rosenbluth M.N., Teller A.H., Teller E., (1953), "Equation of state calculations by fast computing machines", *The Journal of Chemical Physics*, Vol. 21(6), pp. 1087-1092.

Miner M.A.,(1945), "Cumulative damage in fatigue", *Applied Mechanics Transactions (ASME)*, Vol.12(3), pp. 159-164.

Moaveni B., He X, Conte J.P., De Callafon R.A., (2008), "Damage identification of a composite beam using finite element model updating", *Computer-Aided Civil and Infrastructure Engineering*, Vol. 23(5), pp. 339-359.

Moaveni B., He X, Conte J.P., De Callafon R.A., (2010), "Damage identification study of a seven-story full-scale building slice tested on the UCSD-NEES shake table", *Structural Safety*, Vol. 32(5), pp. 347-356.

Mottershead J.E., Friswell M.I, (1993), "Model updating in structural dynamics: A survey." *Jounal of Sound and Vibration*, Vol. 167, pp. 347-375.

Mottershead J., Mares C., James S., Friswell M.I., (2006), "Stochastic model updating: Part 2 – application to a set of physical structures." *Mechanical Systems and Signal Processing*, Vol. 20(8), pp. 2171-2185.

Muto M., Beck J.L., (2008) "Bayesian updating and model class selection using stochastic simulation", *Journal of Vibration and Control*, Vol. 14, pp. 7–34.

Naets F., Cuadrado J., Desmet W., (2015), "Stable force identification in structural dynamics using Kalman filtering and dummymeasurements", *Mechanical Systems and Signal Processing*, Vol. 50-51, pp. 235-248, 2015.

Ntotsios E., Papadimitriou C., (2008), "Multi-objective optimization algorithms for finite element model updating." *Proceedings of Isma 2008: International Conference on Noise and Vibration Engineering*, Vol. 1-8, pp. 1895-1909.

Ntotsios E., Papadimitriou C., Panetsos P., Karaiskos G., Perros K., Perdikaris Ph., (2009), "Bridge health monitoring system based on vibration measurements", *Bulletin of Earthquake Engineering*, Vol.7(2), pp. 469-483.

Ntotsios E., (2009), "Experimental Modal Analysis using Ambient and Earthquake Vibrations: Theory, Software and Applications", Master Thesis, Department of Mechanical Engineering, University of Thessaly.

Palmgren A.,(1924), " Die Lebensdauer von Kugallagern", *VDI-Zeitschrift*, Vol. 68(14), pp. 339-341.

Papadimitriou C., Katafygiotis L.S., (2001), "A Bayesian Methodology for Structural Integrity and Reliability Assessment.", *International Journal of Advanced Manufacturing Systems*, Vol. 4(1), pp. 93-100.

Papadimitriou C., Beck J.L., Katafygiotis L.S., (2001), "Updating robust reliability using structural test data", *Probabilistic Engineering Mechanics*, Vol. 16, pp. 103-113.

Papadimitriou C.,(2004), "Optimal sensor placement methodology for parametric identification of structural systems", *Journal of Sound and Vibration*, Vol. 278(4), pp. 923-947.

Papadimitriou C., Haralampidis G., Sobczyk K., (2005), "Optimal experimental design in stochastic structural dynamics", *Probabilistic Engineering Mechanics*, Vol. 20, pp. 67-78.

Papadimitriou C., (2009), "Fatigue Lifetime Predictions in Metallic Structures using Limited Number of Vibration Measurements", *SMIM2009, R. Iwankiewicz and Z. Kotulski (Eds)*, Warsaw, Poland.

Papadimitriou C., Fritzen C.-P., Kraemer P., Ntotsios E., (2011), "Fatigue predictions in entire body of metallic structures from a limited number of vibration measurements using Kalman filtering", Structural Control and Health Monitoring, Vol.18, pp. 554-573.

Papadimitriou C., Ntotsios E., Giagopoulos D., Natsiavas S., (2012), "Variability of Updated Finite Element Models and their Predictions Consistent with Vibration Measurements", *Structural Control and Health Monitoring*, Vol. 19(5), pp. 630-654.

Papadimitriou C., Lourens E.-M., Lombaert G., De Roeck G., Liu K. (2012), "Predictions of Fatigue Damage Accumulation in the Entire Body of Metallic Bridges by Analysing Operational Vibrations", *3rd International Symposium on Life-Cycle Civil Engineering*, Oct. 2012, Vienna, Austria.

Papadimitriou D.I., Papadimitriou C., (2013), "Bayesian Estimation of Turbulence Model Parameters Using High-Order Sensitivity Analysis.", *Proceedings of FEMTEC 2013 Conference.* , Las Vegas, USA.

Peeters B., De Roeck G. (1999), "Reference-based stochastic subspace identification for output-only modal analysis", *Mechanical Systems and Signal Processing*, Vol. 13 (6), pp. 855-878.

Peeters B., De Roeck G., (2001), "One-year monitoring of the z24-bridge: environmental effects versus damage events", *Earthquake Engineering and Structural Dynamics*, Vol. 30 (2), pp. 149-171.

Pitoiset X., Preumont A.,(2000), "Spectral methods for multiaxial random fatigue analysis of metallic structures", *International Journal of Fatigue*, Vol. 22, pp. 541–50.

Pradlwarter H., Schueller G., Szıkely G., (2002), "Random eigenvalue problems for large systems", *Computers and Structures*, Vol. 80, pp. 2415–2424.

Reynders E., De Roeck G., (2008), "Reference-based combined deterministic-stochastic subspace identification for experimental and operational modal analysis", *Mechanical Systems and Signal Processing*, Vol. 22 (3), pp. 617-637.

Reynders E., (2009), "System Identification and modal analysis in structural mechanics.", PhD Thesis, Department of Civil Engineering, KU Leuven.

Schueller G., (2001), "Computational stochastic mechanics – recent advances", *Computers and Structures*, Vol. 79, pp. 2225-2234.

Schueller G., (2006), "Developments in stochastic structural mechanics", *Archive of Applied Mechanics*, Vol. 75, pp. 755-773

Schueller G., Pradlwarter H., (2009), "Uncertainty analysis of complex structural systems", *International Journal for Numerical Methods in Engineering*, Vol. 80(6), pp. 881-913

Shannon C. E, (1948), "A mathematical theory of communication". *Bell System Technical Journal*, Vol.27, pp. 379-423.

Sohn H, Law K.H., (1997), "Bayesian probabilistic approach for structural damage detection", *Earthquake Engineering and Structural Dynamics*, Vol. 26, pp. 1259-1281.

Soize C., (2000), "A nonparametric model of random uncertainties for reduced matrix models in structural dynamics", *Probabilistic Engineering Mechanics*, Vol. 15, pp. 277-294

Soize C., (2001), "Maximum entropy approach for modeling random uncertainties in transient elastodynamics", *Journal of the Acoustical Society of America*, Vol. 109(5), pp. 1979-1996

Soize C., (2005), "A comprehensive overview of a non-parametric probabilistic approach of model uncertainties for predictive models in structural dynamics", *Journal of Sound and Vibration*, Vol. 288, pp. 623-652

Soize C., (2008), "Construction of probability distributions in high dimensions using the maximum entropy principle: applications to stochastic processes, random fields and random matrices,", International *Journal for Numerical Methods in Engineering,* Vol. 75, pp. 1583-1611

Soize C., (2010), "Generalized probabilistic approach of uncertainties in computational dynamics using random matrices and polynomial chaos decompositions,", *International Journal for Numerical Methods in Engineering,* Vol. 81(8), pp. 939-970

Soize C., (2013), "Stochastic modeling of uncertainties in computational structural dynamics - Recent theoretical advances". *Journal of Sound and Vibration*, Vol.332 (10), pp.2379-2395

Teughels A., Roeck G. De,. Suykens J.A.K, (2003), "Global optimization by coupled local minimizers and its application to FE model updating", *Computers and Structures*, Vol. 81(24-25), pp. 2337-2351.

Teughels A., (2003), "Inverse modelling of civil engineering structures based on operational modal data", PhD Thesis, Department of Civil Engineering, KU Leuven.

Teughels A., Roeck G. De, (2005), "Damage detection and parameter identification by finite element model updating", *Archives of Computational Methods in Engineering*, Vol.12 (2), pp. 123-164.

Tunna J.M., (1986), "Fatigue life prediction for Gaussian random loads at the design stage", *Fatigue and Fracture of Engineering Materials and Structures,* Vol.9, pp. 169–184.

Tierney L., Kadane J.B., (1986), "Accurate Approximations for Posterior Moments and Marginal Densities.", *Journal of the American Statistical Association,* Vol. 81(393), pp. 82-86.

Vanik M.W., Beck J.L., Au S.K.,(2000), "Bayesian probabilistic approach to structural health monitoring", *ASCE Journal of Engineering Mechanics*, Vol.126, pp. 738-745.

Wu M., Smyth A.W., (2007), "Application of the unscented Kalman filter for real-time nonlinear structural system identification", *Structural Control and Health Monitoring*, Vol. 14, pp. 971–990.

Yuen K.V., Beck J.L., (2003), "Reliability-based robust control for uncertain dynamical systems using feedback of incomplete noisy response

measurements", *Earthquake Engineering and Structural Dynamics*, Vol. 32(5), pp. 751-770.

Yuen K.V., Katafygiotis L.S., (2003), "Bayesian Fast Fourier Transform Approach for Modal Updating Using Ambient Data", *Advanced Structural Engineering*, Vol. 6(8), pp. 81-95.

Yuen K.V., Au S.K., Beck J.L., (2004), "Structural damage detection and assessment using adaptive Markov Chain Monte Carlo simulation", *Journal of Structural Control and Health Monitoring*, Vol. 11, pp. 327–347.

Yuen K.V., Beck J.L., Katafygiotis L.S., (2006), "Efficient model updating and health monitoring methodology using incomplete modal data without mode matching", *Structural Control and Health Monitoring*, Vol.13, pp. 91–107.

Yuen K.V., Hoi K.I., Mok K.M, (2007), "Selection of noise parameters for Kalman filter", *Earthquake Engineering and Engineering Vibrations*, Vol. 6,pp. 49–56.

Yuen K.V., (2010), "Recent developments of Bayesian model class selection and applications in civil engineering", *Structural Safety*, Vol. 32(5), pp. 338-346.

Yuen K.V, Kuok S.C., (2011), "Bayesian methods for updating dynamic models", *Applied Mechanics Reviews*, Vol. 64 (1).

Verboven P. (2002), "Frequency domain system identification for modal analysis", PhD Thesis, Department of Mechanical Engineering, Vrije Universiteit Brussel, Belgium.